Recent advances in visible light-activated radical coupling reactions triggered by (i) ruthenium, (ii) iridium and (iii) organic photoredox agents

Jonathan D. Bell [ID] and John A. Murphy [ID]

Photoredox chemistry with organic or transition metal agents has been reviewed in earlier years, but such is the pace of progress that we will overlap very little with earlier comprehensive reviews. This review first presents an overview of the area of research and then examines recent examples of C–C, C–N, C–O and C–S bond formations *via* radical intermediates with transition metal and organic radical promoters. Recent successes with Birch reductions are also included. The transition metal chemistry will be restricted to photocatalysts based on the most widely used metals, Ru and Ir, but includes coupling chemistries that take advantage of low-valent nickel, or occasionally copper, complexes to process the radicals that are formed. Our focus is on developments in the past 10 years (2011–2021). This period has also seen great advances in the chemistry of organic photoredox reagents and the review covers this area. The review is intended to present highlights and is not comprehensive.

1 Introduction

Radical coupling reactions have a rich history with many prominent examples such as the Meerwein arylation reaction,[1] the Minisci reaction,[2,3] and the Giese addition of radicals to unsaturated substrates.[4] Recently, there has been a surge in interest in radical-mediated coupling reactions due to the emergence of

Department of Pure and Applied Chemistry, University of Strathclyde, 295 Cathedral Street, Glasgow, G1 1XL, UK. E-mail: john.murphy@strath.ac.uk, jonathan.bell@strath.ac.uk

new catalysts and reagents. New transformations have emerged that take advantage of photoinduced electron transfer (PET), hydrogen atom transfer (HAT) and energy transfer processes, and these three processes have their own selectivity criteria. PET selectivity is governed by redox potentials and electron transfer kinetics of the functional groups present upon the substrate.[5] HAT processes are principally determined by bond energies,[6] and energy transfers are regulated by triplet energy values of the species involved.[7] The area of photoredox chemistry has become vast. The area has moved rapidly since landmark general reviews;[8] many of the recent reviews represent very specific areas.

Dr Jonathan D. Bell graduated with a MChem honours from the University of St Andrews in 2014, which included a research project with Dr Euan Kay. He completed his PhD at the University of Glasgow under the supervision of Prof. Andrew Sutherland and Dr Chris Wellaway, where he investigated the stereoselective synthesis of fluorescent amino acids, natural products, and biomolecules. In 2019 he joined the Prof. John Murphy group at the University of Strathclyde for postdoctoral studies into C–H functionalisation of drug-like compounds.

Jonathan D. Bell

John Murphy was educated at the University of Dublin (TCD) and the University of Cambridge. After Fellowships at Alberta and Oxford, he was appointed as Lecturer, then Reader, at the University of Nottingham. Since 1995, he has held the Merck–Pauson Professorship at the University of Strathclyde. His interests are in reactivity, reaction mechanisms and synthesis.

John A. Murphy

Our aim here is to provide an overview of some of the areas of rapid development that deploy (i) transition metal photoredox reagents based on ruthenium and iridium complexes or (ii) organic photoredox catalysts.[9]

Photophysics

As a compound is excited with a photon of light, an electron is transferred from the ground state, (usually S_0), to a higher energy orbital (Fig. 1). An indication that a compound is an effective photocatalyst is that it is strongly photoluminescent as it signifies that non-productive deactivation pathways are minimised.[8a]

Kasha's rule states that in photoemissive processes, the emitting electronic level of a given multiplicity (usually singlet or triplet) is the lowest excited state of that multiplicity (in these cases S_1 or T_1). To date, azulene which has a large energy gap between the first and second singlet excited states ($\Delta E_{S2 \rightarrow S1} = 14\,000\ \mathrm{cm}^{-1}$) was reported in 2019 as the only compound that breaks Kasha's rule.[10] Recently it was suggested that "breaking" Kasha's rule may lead to more effective photochemistry.[11]

Intersystem crossing (ISC)

The multiplicity of an excited state has a major influence upon the photophysical properties of a compound. Triplet states are long-lived and this is due to the $T_1 \rightarrow S_0$ electronic transition being spin–forbidden. Therefore, the excited state lifetimes of these triplet states are much greater than for the corresponding singlet states. It can be envisioned that longer lifetimes may result in more successful photochemical processes due to more favourable kinetics.[5] However, it has been stated that efficient photoinduced SET only requires an excited state lifetime of 1 ns. Intersystem crossing (ISC) is the process through which a compound changes multiplicity, typically from the lowest excited singlet state to the lowest excited triplet state.[12] This process is formally forbidden within nonrelativistic quantum theory, and therefore access to the long-lived triplet states is limited.[8,13] However, efficient ISC is achieved with the inclusion of heavy atoms, paramagnetic atoms or the change of orbital character with the change in multiplicity.[12–16]

El-Sayed's rules

Processes where the total angular momentum is conserved are non-forbidden. Hence, if a change of electron spin coincides with a change in angular momentum, then efficient ISC is viable.[13–16] Therefore, highly efficient ISC is found with compounds such as benzophenone,[17] xanthone[15] and benzaldehyde,[18] with the ϕ_{ISC} of benzaldehyde being close to unity in the vapour phase.[19,20]

Heavy atom effect

The inclusion of heavy atoms increases ISC efficiency and this is demonstrated with naphthalene analogues **1a–1e** (Fig. 2); when successively heavier halogen atoms are added, the ϕ_{ISC} increases. The heavy atom effect can operate intermolecularly and through the chemically impermeable walls of molecular cages.[21] The presence of heavy atoms has a significant impact upon the characteristics of photocatalysts. For a photocatalyst without heavy atoms, such as 9,10-dicyanoanthracene DCA (**2**), low efficiency for ISC is observed ($\phi_{ISC} = 0.02$) and its photophysical behaviour is dominated by its S_1 state, which has a lifetime of 15.9 ns.[8a] However, the photocatalyst Ru(bpy)$_3^{2+}$ (**3**) has a heavy ruthenium atom and therefore its ISC is almost quantitative; its triplet state is long-lived.[22] The effect of heavy atom inclusion is also displayed with the xanthene dyes, fluorescein (**4**), Eosin Y (**5**) and Rose Bengal (**6**). Fluorescein has no heavy halogen atoms and has a ϕ_{ISC} of 0.03 but Eosin Y and Rose Bengal contain bromine and iodine atoms respectively and this results in higher ϕ_{ISC} with values of 0.32 and 0.77 respectively.[8a] This results in **4** having a short excited state lifetime (4.2 ns) while catalyst **6** has a much longer excited lifetime (2.4 μs).[8a,23]

Photochemical processes

Once a compound is promoted to an excited state, it can go through a number of different processes such as single electron transfer (SET, commonly described as photoinduced electron transfer, PET),[24] HAT (hydrogen atom transfer),[25] and energy transfer.[7]

Electron transfer

Single-electron transfer (SET) is a transfer of an electron from an electron donor (D) to an electron acceptor (A).[26–28] SET can
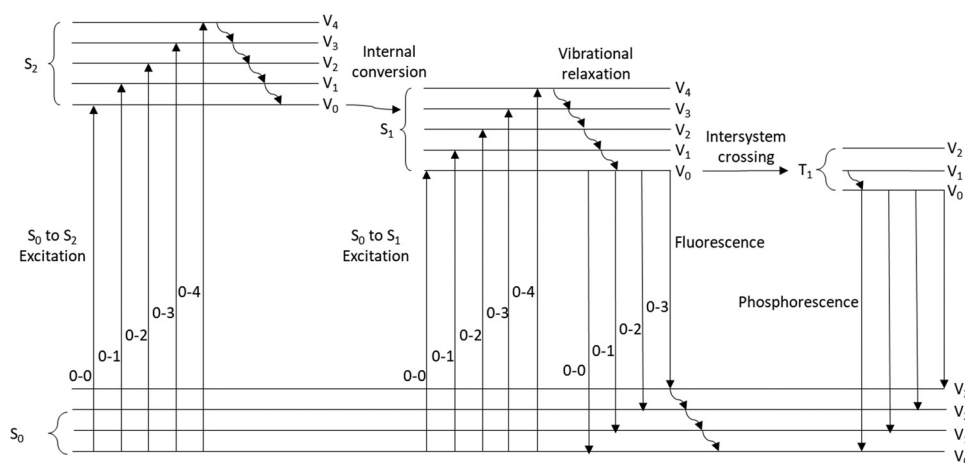

Fig. 1   Jablonski–Perrin diagram representing electron transitions between ground and excited states.

1a	X = H	Φ_F = 0.55	Φ_P = 0.051
1b	X = F	Φ_F = 0.84	Φ_P = 0.056
1c	X = Cl	Φ_F = 0.058	Φ_P = 0.30
1d	X = Br	Φ_F = 0.0016	Φ_P = 0.27
1e	X = I	Φ_F = 0.0005	Φ_P = 0.38

DCA, **2**
Φ_F = 0.87; Φ_{ISC} = 0.02
τ_F = 15.9 ns (MeCN)

Ru(bpy)$_3{}^{2+}$, **3**
$\Phi_{ISC} \approx 1.00$
τ_p = 650 ns (H$_2$O)

fluorescein^{2-} (**4**)
Φ_F = 0.93, Φ_{ISC} = 0.03
τ_F = 4.2 ns

Eosin Y^{2-} (**5**)
Φ_F = 0.48; Φ_{ISC} = 0.32
τ_F = 2.1 ns, τ_p = 190 μs

Rose Bengal^{2-} (**6**)
Φ_F = 0.09; Φ_{ISC} = 0.77
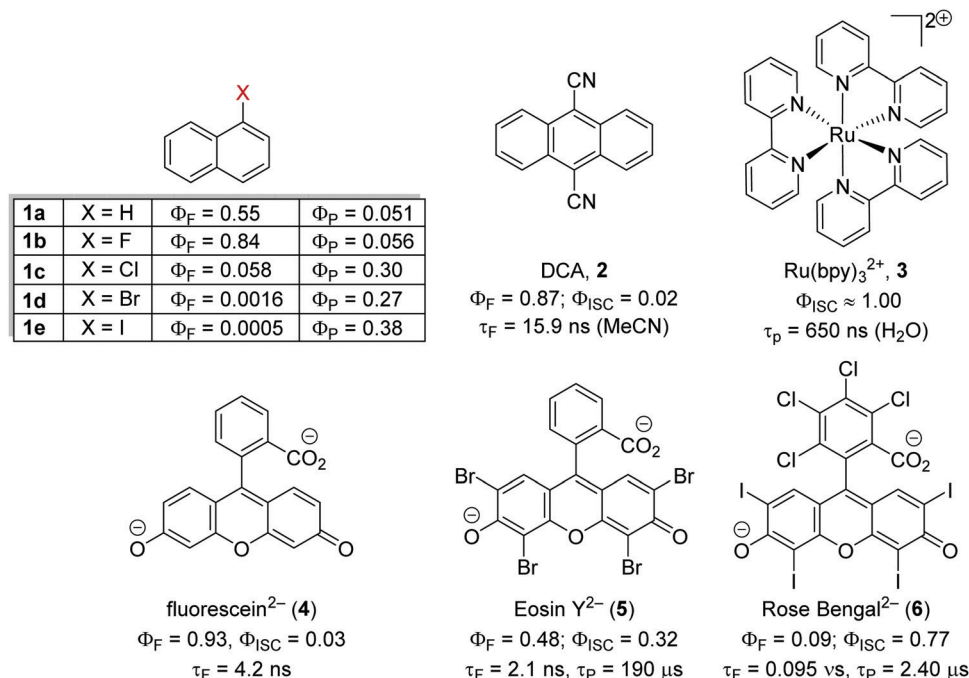τ_F = 0.095 vs, τ_p = 2.40 μs

Fig. 2 The effect of heavy atoms upon photophysical properties.

proceed *via* a transition state where the donor and acceptor molecules interact strongly (binding energy >4.8 kcal mol^{-1}) and this is referred to as inner-sphere electron transfer (ISET). Electron transfer events between species that are weakly interacting (1.0–3.8 kcal mol^{-1}) or non-bonded organic compounds are known as outer-sphere electron transfer (OSET). Marcus theory was developed so that rates of OSET between donor and acceptor species could be calculated (Scheme 1).

Photocatalysts are excellent species for SET as the excitation of an electron results in (i) a low energy electron–hole and (ii) a high-energy electron (Scheme 2). The electron–hole left by the transition can be filled with an electron from a donor molecule and thus the photocatalyst becomes a powerful SET oxidant. Alternatively, the high energy electron can be lost to an acceptor molecule and the photocatalyst is a strong SET reductant. The feasibility of SET processes can be evaluated with consideration
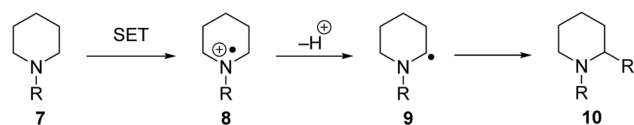
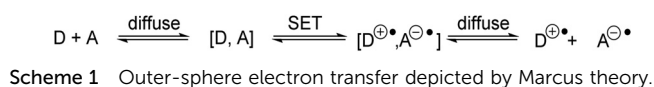**Scheme 3** C–H activation *via* SET.

of redox potentials and a comprehensive list of various functional groups has been reported.[30]

C–H functionalisation can be achieved *via* a SET process (Scheme 3). If an amine **7** is oxidised by electron transfer to the amine radical cation **8**, this can result in proton loss and formation of carbon-centred radical **9**. Numerous radical-based reactions can then take place and radical **9** is converted to functionalised product **10**.
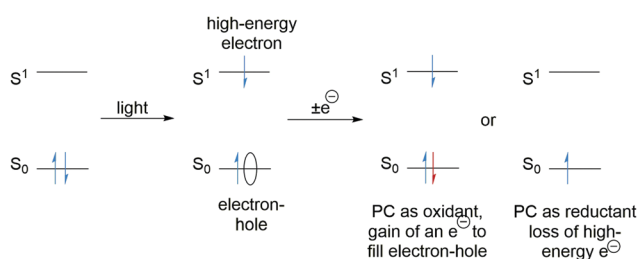
Photoredox catalysts

There is a vast array of metal[9,31] and organic[8] photoredox catalysts with different excited state redox potentials. The redox potential of metal catalysts can be altered with the selection of ligands around the metal centre, with more electron-poor ligands resulting in more oxidising catalysts and more electron-rich ligands giving better reducing catalysts. The photoexcited metal complex Ru(bpy)$_3{}^{2+}$ (**3**) is a weak oxidant but a strong reductant. When the more electron-poor bipyrazine are used as ligands, the resulting catalyst **11** becomes a strong oxidant but weak reductant. A similar observation is found with iridium catalysts; the photoactivated catalyst Ir(ppy)$_3$ **12** is an excellent reductant but weak oxidant whereas **13** is a very strong oxidant but weak reductant (Fig. 3).

The excited state redox potentials of organic catalysts are determined by the electronic properties of the compound,

D + A $\overset{\text{diffuse}}{\rightleftharpoons}$ [D, A] $\overset{\text{SET}}{\rightleftharpoons}$ [D$^{\oplus\bullet}$,A$^{\ominus\bullet}$] $\overset{\text{diffuse}}{\rightleftharpoons}$ D$^{\oplus\bullet}$ + A$^{\ominus\bullet}$

Scheme 1 Outer-sphere electron transfer depicted by Marcus theory.

Scheme 2 Photoredox processes.
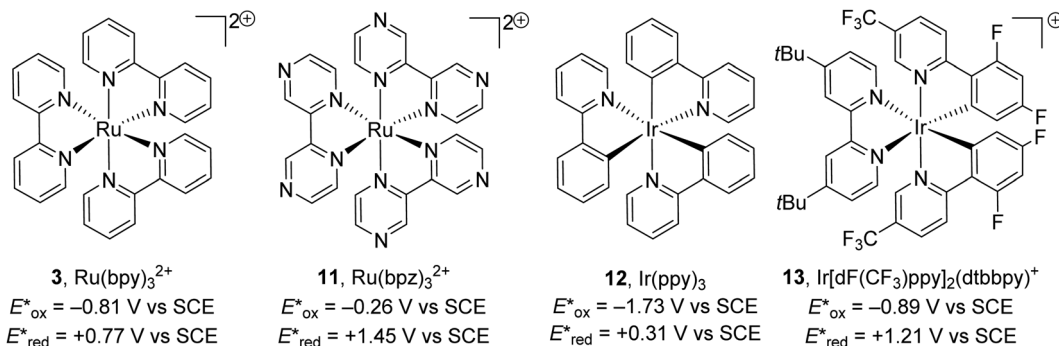
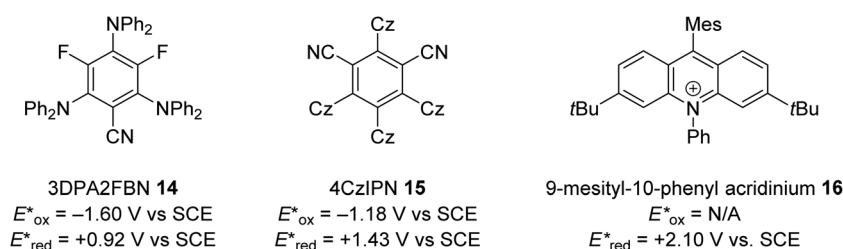**Fig. 3** Excited state redox potentials of metal photoredox catalysts.

3, Ru(bpy)$_3^{2+}$
E^*_{ox} = −0.81 V vs SCE
E^*_{red} = +0.77 V vs SCE

11, Ru(bpz)$_3^{2+}$
E^*_{ox} = −0.26 V vs SCE
E^*_{red} = +1.45 V vs SCE

12, Ir(ppy)$_3$
E^*_{ox} = −1.73 V vs SCE
E^*_{red} = +0.31 V vs SCE

13, Ir[dF(CF$_3$)ppy]$_2$(dtbbpy)$^+$
E^*_{ox} = −0.89 V vs SCE
E^*_{red} = +1.21 V vs SCE

3DPA2FBN **14**
E^*_{ox} = −1.60 V vs SCE
E^*_{red} = +0.92 V vs SCE

4CzIPN **15**
E^*_{ox} = −1.18 V vs SCE
E^*_{red} = +1.43 V vs SCE

9-mesityl-10-phenyl acridinium **16**
E^*_{ox} = N/A
E^*_{red} = +2.10 V vs. SCE

Fig. 4 Excited state redox potentials of non-metal photoredox catalysts.

with more electron-poor compounds being greater oxidants and more prone to reduction. The relationship between excited state reduction potentials and the electronic effects of substituents is demonstrated with the following compounds (Fig. 4). The most electron-rich compound 3PDA2FBN **14** has the lowest excited state reduction potential (+0.92 V *vs.* SCE). If the electron-rich diphenylamine groups of **14** are replaced with carbazole groups and an additional nitrile group is introduced, a more oxidising catalyst is obtained 4CzIPN **15** (+1.43 V *vs.* SCE).[32,33] Due to the presence of a formal positive charge, acridinium salts (**16**) make extremely strong photooxidants (+2.10 V *vs.* SCE).[32]
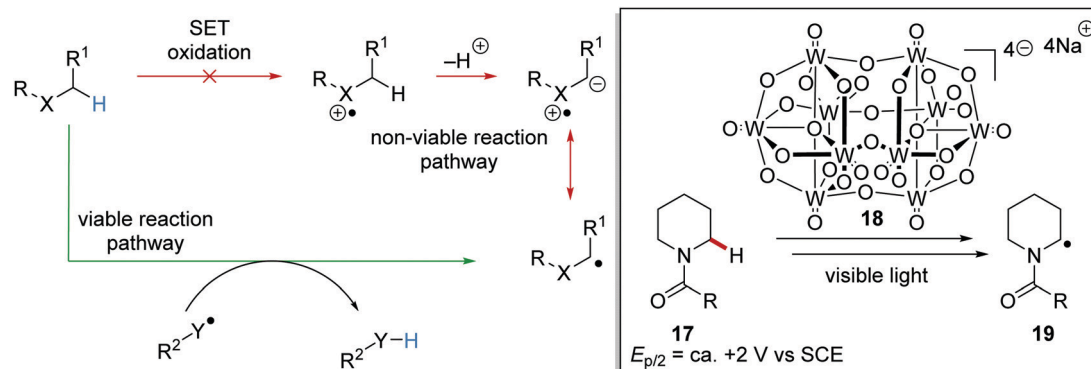
Hydrogen atom transfer

HAT is the transfer of an H-atom from one species to another. A wide range of HAT reagents (and catalysts) exists and they can be used in direct and indirect processes.[34] A direct HAT process is where the excited photocatalyst can abstract a hydrogen atom from the substrate. Sodium decatungstate **18** (Schemes 4 and 5) is a prominent example of a direct HAT catalyst. Indirect processes involve the activation of a HAT catalyst with another catalyst or reagent; a topical example of this process is the combination of an iridium photocatalyst with quinuclidine (Scheme 4).

HAT has one distinct advantage over SET processes in radical coupling.[34] Hard-to-oxidise functional groups (amides, ethers, alkanes) can be functionalised with a HAT approach, as HAT reagents have the advantage that the substrate does not need to be oxidised through loss of an electron for radical formation. Therefore, for hard-to-oxidise substrates, radical formation is achievable through an atom abstraction process for which a SET oxidation process is not feasible (Scheme 5).
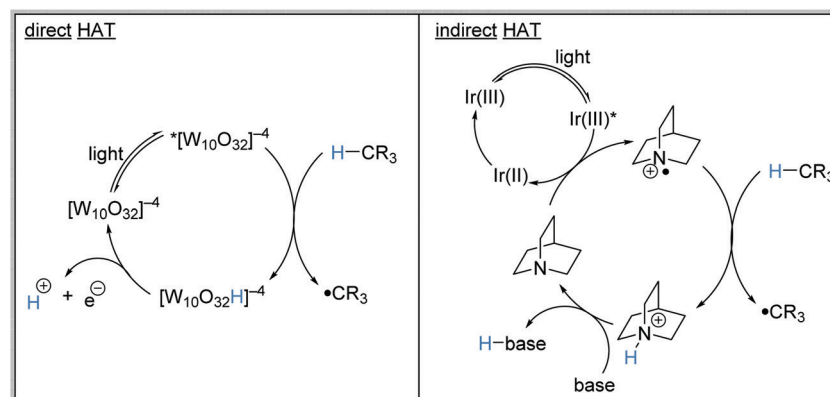
Scheme 4 Catalytic direct HAT *vs.* catalytic indirect HAT approaches.

This journal is © The Royal Society of Chemistry 2021

Chem. Soc. Rev., 2021, **50**, 9540–9685 | 9543

Scheme 5 HAT strategy *vs.* SET strategy.

For example, *N*-Boc-piperidine **17**, (R = O*t*Bu) has an oxidation potential of +1.96 V *vs.* SCE so commercial photoredox catalysts such as Ru(bpy)$_3$(PF$_6$)$_2$ (E_{red}^* = +0.77 V *vs.* SCE) and Ir[dF(CF$_3$)ppy]$_2$(dtbbpy)PF$_6$ (E_{red}^* = 1.21 V *vs.* SCE) are unable to oxidise this substrate.[35] However, decatungstate HAT catalyst **18** was able to functionalise **17** *via* α-amido hydrogen atom transfer after activation with visible light, and this gave radical **19**.[36] Hence, the use of HAT processes allows for radical formation on substrates that are unable to be easily oxidised with a photoredox catalyst.

On occasion, HAT processes are more regioselective than SET processes in radical coupling reactions (Scheme 6). For example, it has been shown that amines, such as *N*-methylmorpholine **20**, are oxidised *via* SET processes by an iridium photocatalyst and this generates amine radical cation **20⁺•**.[37] Proton loss showed little or no selectivity in forming two regioisomeric carbon-centred radicals **20•**. Radical addition of **20•** to an electron-poor alkene resulted in a 1:1 mixture of regioisomers of compound **21a**. However, when a DABCO-based HAT reagent was used, due to steric factors, hydrogen abstraction took place from the *N*-CH$_3$ position essentially exclusively and this gave a >30:1 mixture of regioisomers of **22**.[38]

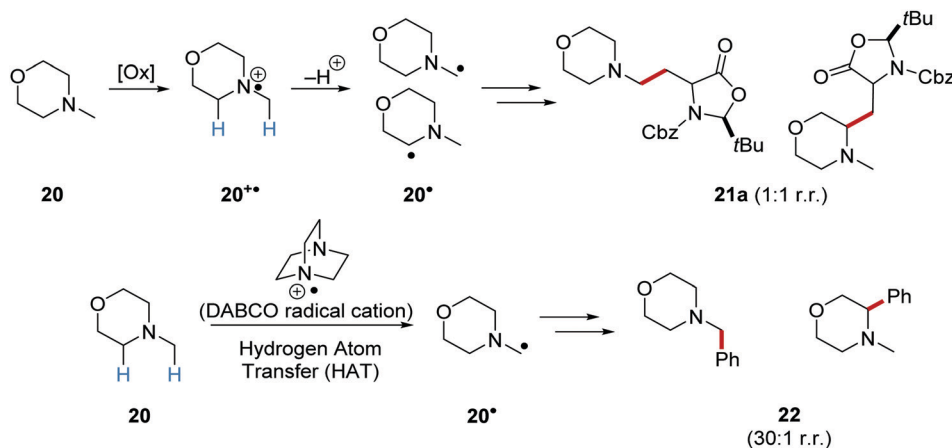In some instances, substrate control results in regiocontrol, even with transformations that involve sequential oxidation and loss of a proton. This was demonstrated when dextromethorphan (inset, Scheme 7) and *N*-methyldicyclohexylamine were used as substrates; only single regioisomers of compounds **21b** and **21c** were produced, unlike for **21a**.[37]

HAT reagents

Both direct HAT and indirect HAT catalysts (and reagents) have been well-reviewed.[34] Sodium decatungstate **18**, benzophenone **22** and uranyl cation **23** are all direct HAT species as, upon their excitation, they can abstract a hydrogen atom from the substrate (Fig. 5). The compounds **24–29** are all indirect HAT compounds as they require an additional reagent or catalyst for their formation. As discussed below, the rate of hydrogen abstraction can be calculated with consideration of bond energies and polarities. Therefore, different hydrogen atoms can be targeted for abstraction, depending upon the nature of the HAT catalyst.
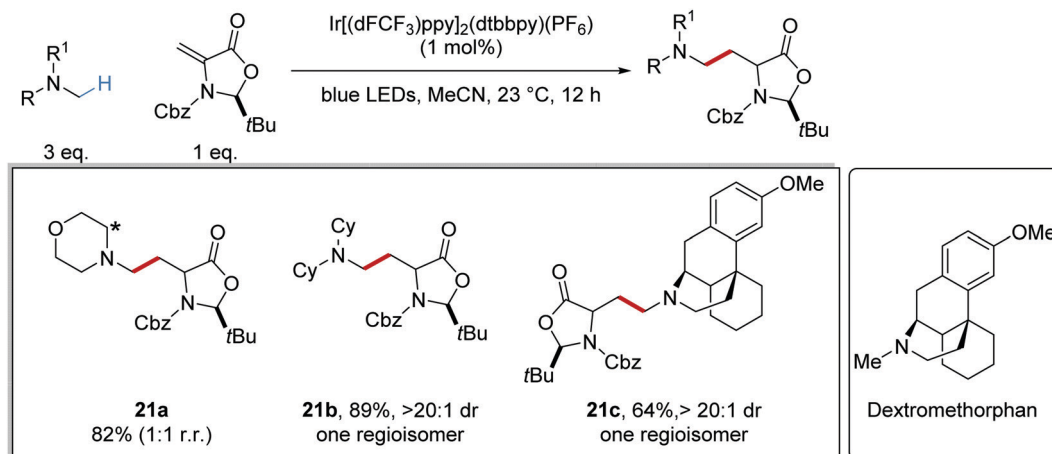
Kinetics of HAhT

As mentioned above, the rate of hydrogen-atom abstraction can be predicted from the ground-state properties of the reactants and products.[6] The rate constant (k_1) for a reaction can be determined with the Arrhenius equation (eqn (1)) in terms of activation energy (E_a) and pre-exponential factor (A). Therefore, the rate

Scheme 6 Regioselectivity of SET and HAT processes.

9544 | *Chem. Soc. Rev.*, 2021, **50**, 9540–9685

This journal is © The Royal Society of Chemistry 2021

Scheme 7 Substrate regiocontrol of SET processes. [Asterisk denotes alternative connectivity for another regioisomer.]
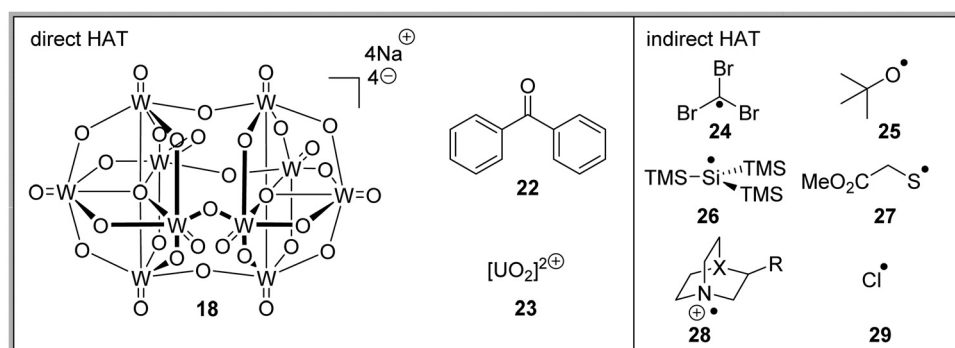

Fig. 5 Direct and indirect HAT species.

of a reaction could be predicted if a value of E_a could be calculated.

$$k_1 = A e^{\frac{-E_a}{RT}} \qquad (1)$$

The E_a of a HAT process (eqn (2)) is determined with the following equation (eqn (3)).[6] The term f is defined in eqn (4), where D_{AH}, D_{BH} and D_{H2} correspond to the bond dissociation energy (BDE) for AH, BH and H$_2$ respectively. Data tables for BDE are abundant in the literature,[39–43] but it has been suggested that free energies should be used instead.[44] The term $\Delta_{\chi AB^2}$ is the difference in electronegativity between the radicals A$^\bullet$ and B$^\bullet$. The S-factors (S_A and S_B) relate to structural parameters of the radicals A$^\bullet$ and B$^\bullet$ taking into account structural changes during the reaction. Small S factors are obtained if little structural changes occur during the reaction, for example if A$^\bullet$ and B$^\bullet$ both represent atoms. Large values are obtained if significant structural changes occur such as conversion of a tetrahedral structure to trigonal planar for the formation of the methyl radical from methane. To account for the non-linearity in stabilisation of the newly formed radical B$^\bullet$ by conjugative delocalisation of the unpaired electron, the term d is included into the equation. The constants E_0, α, β and γ are determined from multiple regression analysis of experimental data. This approach was successful in reproducing the activation

energies for 65 reactions. Therefore, it can be concluded that bond energies, polarities, structural changes and radical stabilisation with delocalisation of the unpaired electron must all be considered in evaluating whether a HAT process is viable. However, most attention should be spent considering the strengths of the bonds involved in the process; as stated by Roberts "the activation energy for an endothermic reaction cannot be less than ($\Delta H^\circ + RT$), no matter how favourable are the polar factors!"[45]

$$A^\bullet + B\text{–}H \rightarrow A\text{–}H + B^\bullet \qquad (2)$$
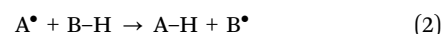
$$E_a = E_0 f + \alpha \Delta H^\circ (1 - d) + \beta \Delta_{\chi AB^2} + \gamma (S_A + S_B) \qquad (3)$$

$$f = \left(\frac{D_{AH} D_{BH}}{D_{H_2}^2} \right) \qquad (4)$$

Bond energies of HAT catalysts and substrates

The resulting bond between the HAT catalyst and the sequestered hydrogen atom is a key driving force in propagating a HAT process. The bond strength between H atoms and HAT catalysts vary and the strength of this bond dictates which substrates a HAT catalyst can be used upon. For example, thiol **30** has an S–H bond energy of 87.2 kcal mol^{-1}.[46] Therefore, a thiyl radical is unsuitable for breaking strong C–H bonds but it could break
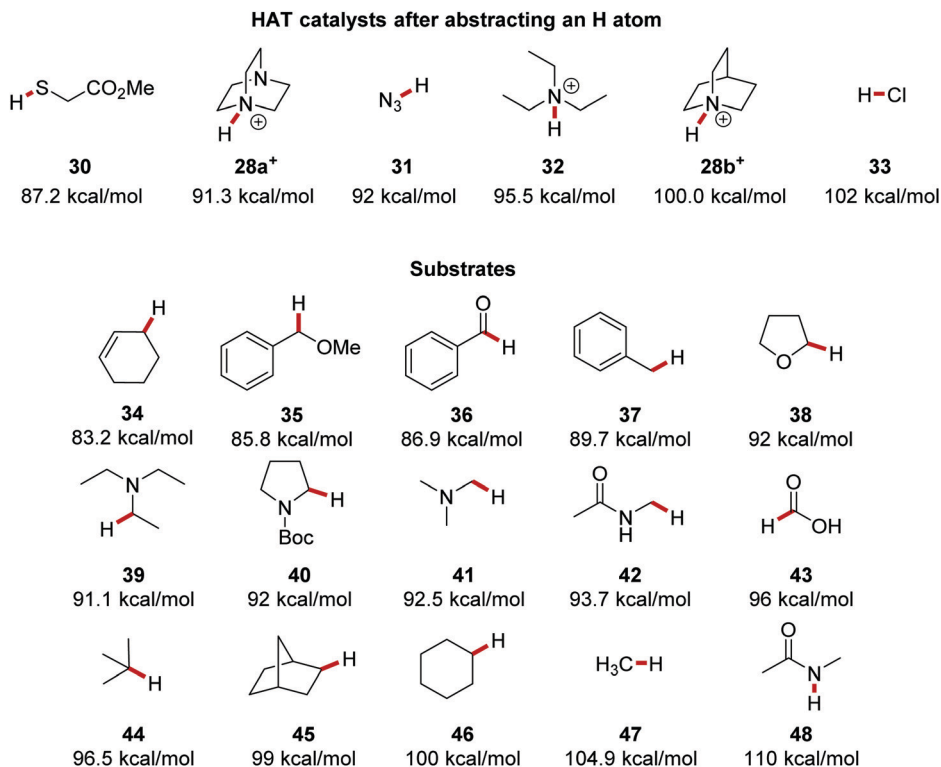
This journal is © The Royal Society of Chemistry 2021

Chem. Soc. Rev., 2021, 50, 9540–9685 | 9545

HAT catalysts after abstracting an H atom

30	**28a⁺**	**31**	**32**	**28b⁺**	**33**
87.2 kcal/mol	91.3 kcal/mol	92 kcal/mol	95.5 kcal/mol	100.0 kcal/mol	102 kcal/mol

Substrates

34	**35**	**36**	**37**	**38**
83.2 kcal/mol	85.8 kcal/mol	86.9 kcal/mol	89.7 kcal/mol	92 kcal/mol

39	**40**	**41**	**42**	**43**
91.1 kcal/mol	92 kcal/mol	92.5 kcal/mol	93.7 kcal/mol	96 kcal/mol

44	**45**	**46**	**47**	**48**
96.5 kcal/mol	99 kcal/mol	100 kcal/mol	104.9 kcal/mol	110 kcal/mol

Fig. 6 BDE of N⁺–H bonds and BDE of selected organic substrates.

weak C–H bonds of benzyl ethers, such as **35**, which has a bond strength of 85.8 kcal mol⁻¹ (Fig. 6). The chlorine atom forms a strong bond to a hydrogen atom with the formation of HCl **33** (BDE = 102 kcal mol⁻¹) and thus it can abstract hydrogen atoms from stronger C–H bonds. A well-reported HAT catalyst, the quinuclidine radical cation **28b** forms a strong N–H bond (BDE = 100 kcal mol⁻¹) in HAT processes.[43] Triethylamine radical cation forms a weaker bond to hydrogen in **32** than quinuclidine as cleavage of the N–H bond of **32** results in strain relief which is not possible due to the rigid structure of **28b**. The additional nitrogen atom present in DABCO **28a** stabilises the corresponding radical cation with a 1-spin-4-non-bonded-electron orbital interaction.[47] Therefore, the N–H bond in **28a⁺** (91.3 kcal mol⁻¹) is weaker than in **28b⁺** as homolytic N–H bond cleavage results in a more stable radical cation. Quinuclidine radical cation can functionalise α-amido C–H bonds (92 kcal mol⁻¹) whereas its DABCO counterpart cannot due to its resulting weaker bond to the hydrogen atom.[38,48] The BDE of C–H bonds are well reported in the literature and thus by comparing bond energies, feasible HAT processes can be designed. Methane has the strongest C–H bond of alkanes (BDE = 104.9 kcal mol⁻¹) as there is no radical stabilisation for the methyl radical after H-atom abstraction. Carbon atoms with greater substitution have weaker C–H bonds, such as cyclohexane **46** (100 kcal mol⁻¹) and norbornane **45** (99 kcal mol⁻¹ for C–H in the methylene group shown) due to hyperconjugation effects.[36] Due to the high stability of tertiary radicals, isobutane has a BDE of 96.5 kcal mol⁻¹ for its methine C–H bond.[40]

The C–H bonds adjacent to heteroatoms bearing one or more electron pairs are weak; for example, triethylamine has an α-amino C–H BDE of 91.1 kcal mol⁻¹.[39] The radical formed from triethylamine is stabilised with the sharing of π electrons between the C and N atoms. Benzylic and other α-heteroatom C–H bonds are suitable substrates for HAT due to their weak bonds.[36,39,49,50] Other appropriate HAT substrates are aldehydes,[40,51] benzylic ethers,[52] and allylic C–H bonds.[53] However, unlike C–H bonds, heteroatom–H bonds can be much stronger, and N-methyl acetamide (**48**) has a BDFE of 110 kcal mol⁻¹ and is unable to be activated with HAT strategies.[54]

As mentioned above, polarity effects also have a significant effect on the feasibility of HAT reactions and thus various analogues of quinuclidine **28a′–28g′** have been used as HAT catalysts (Fig. 7). In one instance, it was demonstrated that the C–H abstraction of adamantane was only achievable with sulfonate HAT catalyst **28e′** due to its strong polarity.[55]
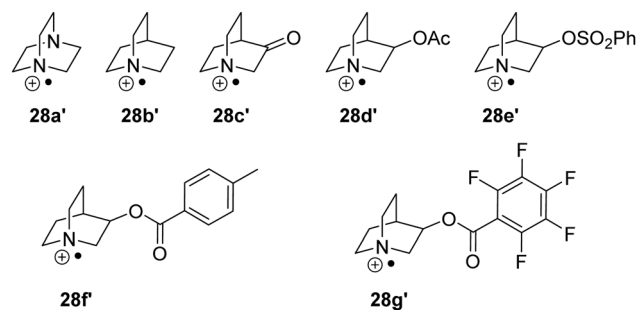
28a'	**28b'**	**28c'**	**28d'**	**28e'**

| **28f'**	**28g'**

Fig. 7 Nitrogen-based HAT catalysts.

PCET

Proton-coupled electron transfer (PCET) is closely related to HAT and there have been many conflicting definitions regarding HAT and PCET.[54–57] HAT is best defined as the concerted transfer of a proton and an electron from one species to another, while PCET is a concerted process, the proton and electron are transferred either to separate acceptors (oxidative PCET) or received from separate donors (reductive PCET). For example, for HAT, an electron and a proton from the α-amino C–H bond is transferred to the quinuclidine radical cation **28b'** and this gives the α-amido radical shown in Scheme 8. The oxidative PCET of amide **49** involves the simultaneous transfer of the N–H proton to a base and transfer of an electron to an electron acceptor, M. Reductive PCET of ketone **50** necessitates donation of a proton (from a suitable acid) and an electron from a donor M.

These are complementary transformations with PCET being able to abstract hydrogen atoms, typically from X–H bonds (where X = O and N), where HAT processes are not feasible due to the high bond energies. For example, the N–H bond present in *N*-methyl acetamide **48** has a bond dissociation free energy (BDFE) of 110 kcal mol^{-1}.[54] Common HAT catalysts such as quinuclidine radical cation and carbon-centred radicals resulted in the formation of N–H and C–H bonds that have BDE 98–100 kcal mol^{-1}. Therefore, for most HAT catalysts the removal of a hydrogen atom from the amide functional group is thermodynamically unfavourable. However, it is routinely observed that the PCET of amides is feasible with the use of a weak Brønsted base and a photoredox catalyst. PCET has also been demonstrated upon ketones and alcohols (Scheme 9).[54,58]
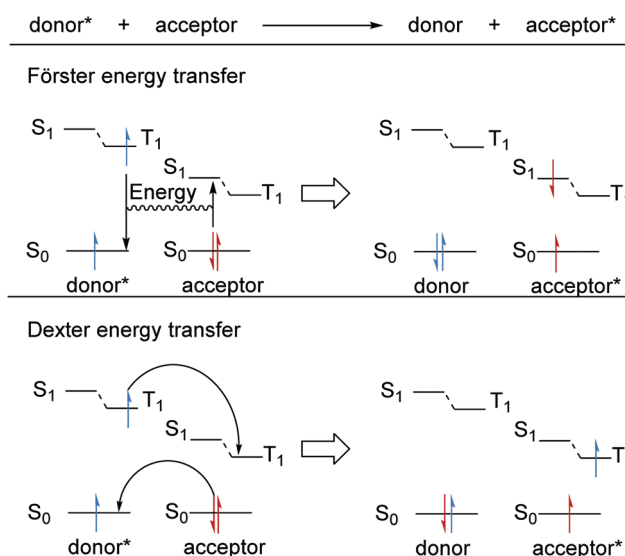
Energy transfer

Alongside PET and HAT, energy transfer is a complementary method that allows reactions that are not feasible in the ground-state to take place in an excited state.[59,60] For these transformations to take place, the substrate must access its excited triplet state. However, direct methods to access T_1 commonly require high-energy light which may result in potential degradation of the organic substrate and the required ISC crossing can be inefficient.[60]
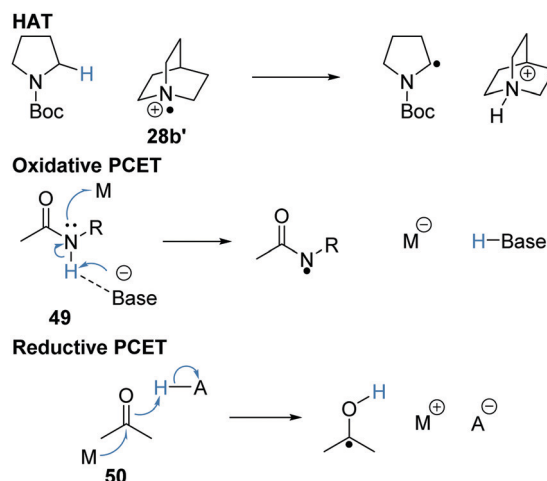
Scheme 8 HAT and PCET processes.
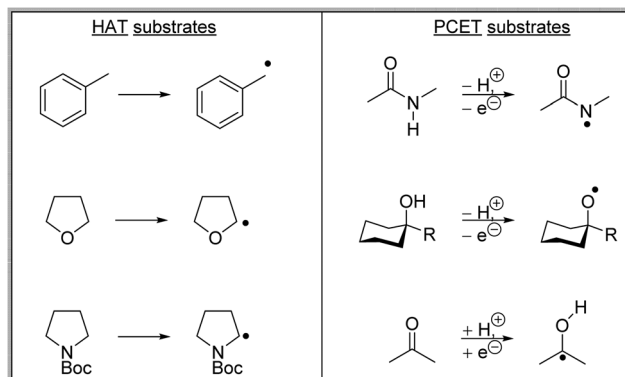
Scheme 9 HAT processes and PCET processes.

Scheme 10 Energy transfer processes.

Therefore, photocatalysts (sensitisers) have been employed as energy-transfer reagents so that organic substrates can access their T_1 state without the need for high-energy UV light. There are two energy transfer mechanisms, Förster resonance energy transfer (FRET) and Dexter energy transfer (Scheme 10).[61] In both cases, an excited donor molecule transfers its energy to an acceptor molecule and this becomes excited with the quenching of the original donor compound. For FRET, coulombic interactions between the electronic transitions gives rise to the transfer of energy.[61] After a FRET, the substrate molecule will be in its singlet excited state and will still require an ISC processes to populate its triplet state. On the other hand, Dexter energy transfer results from the exchange of electrons; for this, wave-function overlap is required and thus Dexter energy transfer can only take place over short distances (<10 Å). Here, triplet to triplet (TT) energy transfer operates as a Dexter process with two simultaneous electron transfers.[61]

Energy-transfer catalysts

Previously mentioned photoredox catalysts can also be used as energy-transfer catalysts. However, for energy-transfer, the triplet
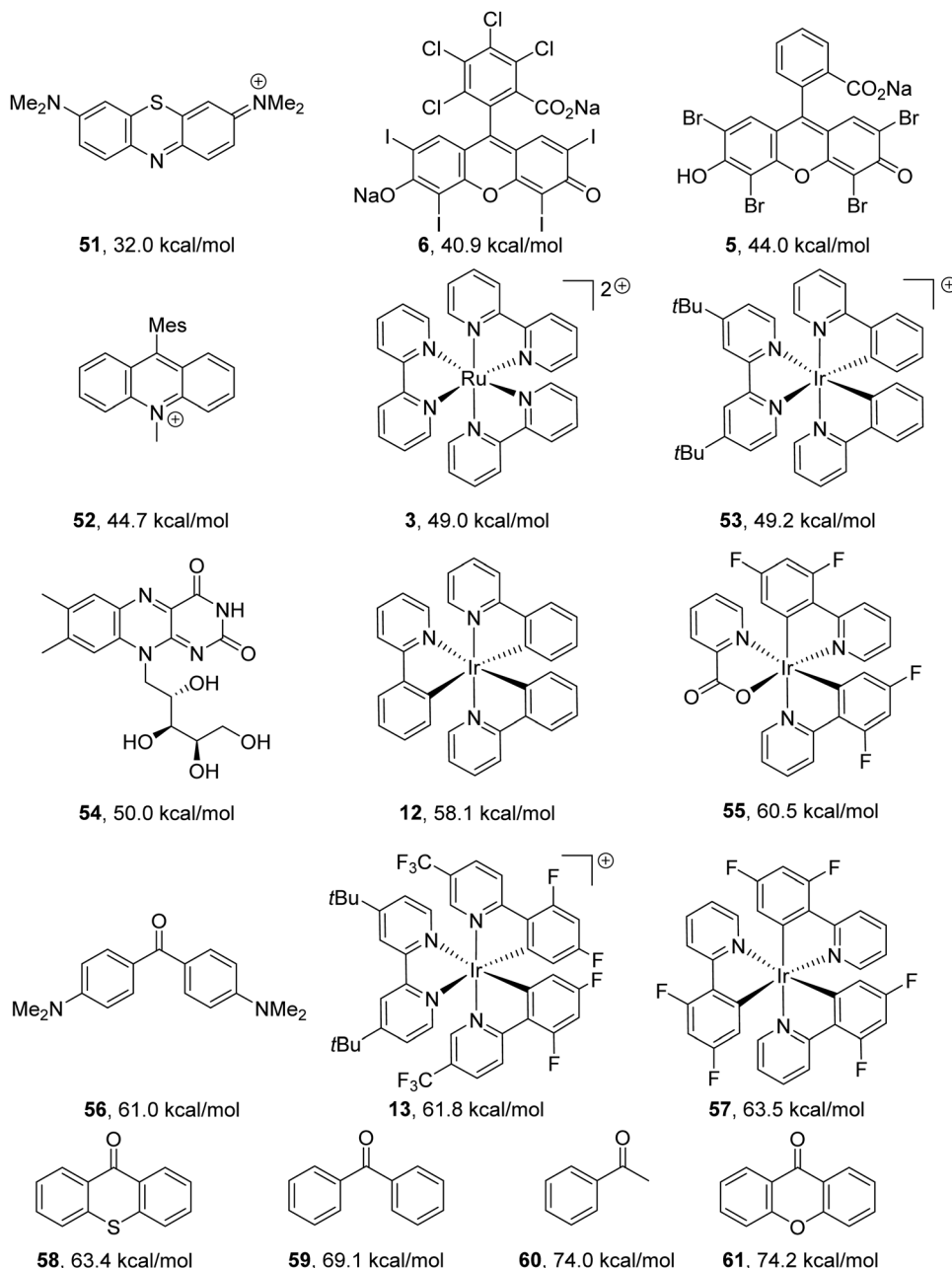
51, 32.0 kcal/mol   **6**, 40.9 kcal/mol   **5**, 44.0 kcal/mol

52, 44.7 kcal/mol   **3**, 49.0 kcal/mol   **53**, 49.2 kcal/mol

54, 50.0 kcal/mol   **12**, 58.1 kcal/mol   **55**, 60.5 kcal/mol

56, 61.0 kcal/mol   **13**, 61.8 kcal/mol   **57**, 63.5 kcal/mol

58, 63.4 kcal/mol   **59**, 69.1 kcal/mol   **60**, 74.0 kcal/mol   **61**, 74.2 kcal/mol

Fig. 8   Triplet energy values taken from the following sources.[7,8,60,62,63]

energy of the donor must be greater than the triplet energy of the acceptor.[7] Triplet energy values of catalysts can be found in the literature (Fig. 8).

Bicatalytic processes

Redox mediation. In some cases, a catalytic amount of redox mediator is required for PET processes which do not have favourable kinetics or suffer from rapid back-electron transfer (BET).[5] An example of redox mediation was the coupling of α-silyl ether **62** with electron-poor alkene **63** with catalytic quantities of DCA **2** (Scheme 11). Successful formation of ester **64** required the addition of biphenyl (10 mol%) as a redox

mediator to decrease BET, which has been reported as an issue with DCA.[64] (See later for further discussion.)

Auxiliary metal catalysis. The addition of a transition metal catalyst has vastly increased the scope of functionalisation that was achieved with PET, HAT, or energy transfer reactions. Nickel, in particular, has found extensive use in radical coupling chemistry and computational investigations into the mechanistic pathways of these reactions have been carried out.[65] Two mechanisms have been proposed for radical cross-coupling chemistry with a nickel catalyst (Scheme 12). It was thought that a radical could either add to a Ni(0) species or a Ni(II) complex and this was investigated computationally with the nickel cross-coupling reaction of benzylic radical **B** (derived from boronate salt **A**) with
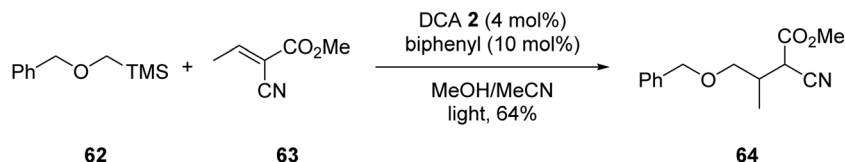
Scheme 11 DCA and BP mediated coupling of α-silyl ether **3** with electron-poor alkene **63**.
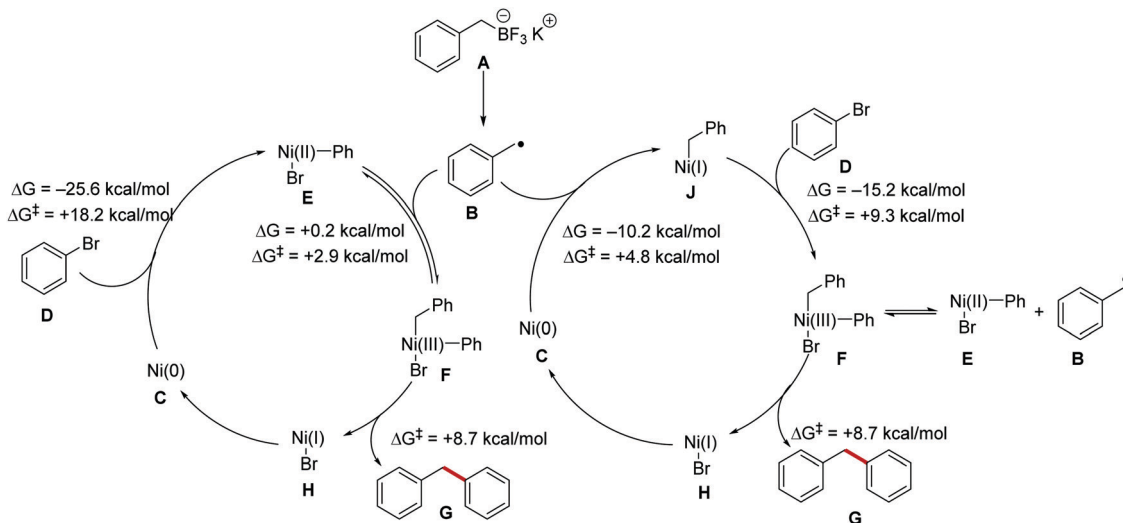
Scheme 12 Processing of radicals by nickel complexes.

bromobenzene **D** and this found that both mechanisms were feasible. Radical addition of **B** to Ni(II) complex **E** was only slightly endergonic (ΔG = +0.2 kcal mol^{-1}) and had a favourable transition state energy ($\Delta G^{\ddagger}$ = +2.9 kcal mol^{-1}). The addition of radical **B** to Ni(0) complex **C** was thermodynamically favoured (ΔG = −10.2 kcal mol^{-1}) and had a low transition state energy ($\Delta G^{\ddagger}$ = +4.8 kcal mol^{-1}). The highest energy barrier found for both mechanisms was the oxidative addition of aryl bromide **D** to Ni(0) complex **C** forming Ni(II) complex **E**, this had a transition state energy of +18.2 kcal mol^{-1} but was exergonic by −25.6 kcal mol^{-1}. Therefore, it can be concluded that both reaction pathways could be operative for radical nickel cross-coupling reactions. The transition state energy for reductive elimination from common complex **F** was +8.7 kcal mol^{-1}, meaning that radical dissociation happens more rapidly than reductive elimination leading to a reversible process between complexes **E** and **F**.

The intricacies of the role of nickel complexes in coupling reactions continue to be studied. In 2020, the MacMillan team studied[66] the mechanism of C–N bond formation in the presence of iridium(III) photoredox catalysts and DABCO. DABCO reduced the photoactivated Ir(III) to Ir(II), and this in turn reduced Ni(II) to Ni(I). Ni(I) and Ni(III) then operated a catalytic cycle transforming aryl halide to arylamine.

Examples of catalysts and reagents

Metal-based photoredox agents. It has been demonstrated that ruthenium and iridium complexes make effective photoredox

and energy transfer catalysts.[7,67] The inclusion of heavy metal atoms results in efficient ISC and long excited state lifetimes. Furthermore, excited state redox potentials and triplet energies can be finely tuned with the use of the right ligands, making them very attractive catalysts. However, there are issues regarding the sustainability of these metal catalysts.[68]

In the excited state, decatungstate salts (sodium and tetrabutylammonium salts have been reported)[69,71] make highly reactive direct HAT catalysts, which have been shown to remove hydrogen atoms from the strong C–H bonds present in cyclohexane (BDE up to 100 kcal mol^{-1}).[36,70,71] Decatungstate salts are also strong PET catalysts (E_{red}^{*} = +2.44 V $vs.$ SCE) and have an excited triplet state lifetime of 51.5 ± 5 ns.[72] Tetrabutylammonium decatungstate (TBADT, **18**) can be prepared in one step from tetrabutylammonium bromide and sodium tungstate (Scheme 13).[73] Alongside decatungstate catalyst, a manganese perchlorophthalocyanine catalyst has been used for C–H functionalisation.[74] These compounds will not be discussed in detail in this review.

Non-metal based photoredox agents. Due to sustainability issues with some transition-metal catalysts, non-metal-based catalysts can be used instead (Fig. 9), including DCA **2**, xanthene dyes (such as Eosin Y, **5**), cyanobenzene-derived photocatalysts (such as 4CzIPN, **15**), acridinium dyes **16**, triarylaminium radical cations **65** and persulfate salts **66**. An important advantage for non-metal based catalysts is the cost difference between TM and non-TM catalysts. In 2016, Ru(bpy)$_3$Cl$_2$ was $57.3 per g from Sigma-Aldrich, Ir(ppy)$_3$ cost $1078 per g purchased from

This journal is © The Royal Society of Chemistry 2021

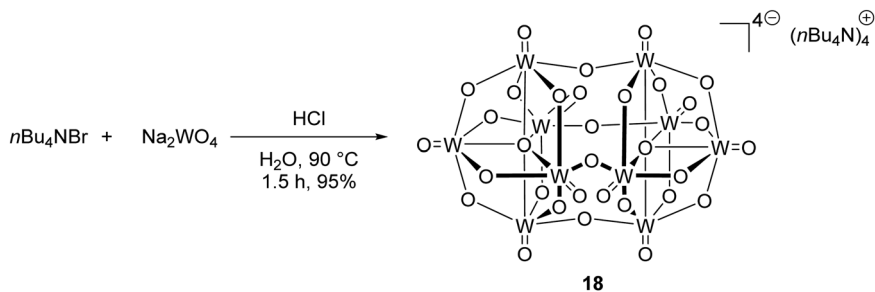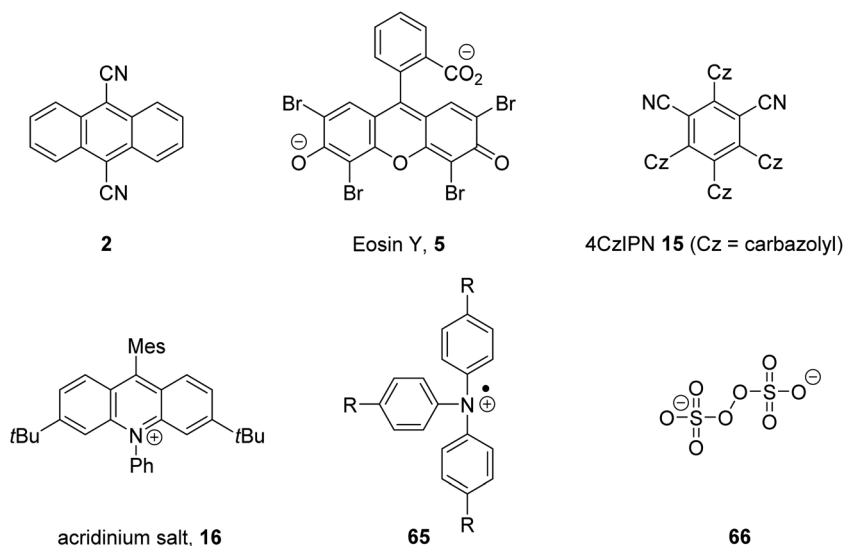Chem. Soc. Rev., 2021, **50**, 9540–9685 | 9549

Scheme 13   Synthesis of tetrabutylammonium decatungstate (**18**)

Fig. 9   Examples of sustainable radical promoters.

Sigma-Aldrich, $Ir[dF(CF_3)ppy]_2(dtbbpy)PF_6$ cost \$117.56 per g to synthesise, whereas non-TM were much less, for example, 4CzIPN cost \$6.01 per g to synthesise.[75] Another popular organic catalyst, 3,6-di-*tert*-butyl-9-mesityl-10-phenylacridin-10-ium tetrafluoroborate **16** (Fig. 11) can be purchased for \$871 per g but can be easily synthesised in three steps from 3-*tert*-butylbromobenzene and 3-*tert*-butylphenol.[32]

Acridinium dyes. Organic dye **68**, based upon the acridinium ring system **67** was first reported by Fukuzumi as a potent, long-lived photocatalyst (Fig. 10).[76] The presence of the mesityl aromatic ring present in acridinium **68** resulted in nucleophilic deactivation at the substituted 9-position while the fluorescence quantum yield and excited singlet state lifetime was increased as C–C bond rotation was blocked. While acridinium dye **67** had a long excited state lifetime and was a strong oxidant ($E_{red}^* = +2.32$ V *vs.* SCE), it was an unsuitable photocatalyst due to high levels of photobleaching.[8a] Acridinium dye **16** is a more stable photocatalyst; replacement of *N*-CH$_3$ with *N*-Ph prevented *N*-demethylation and the inclusion of *tert*-butyl groups inhibited nucleophilic attack.[77] It was also found that replacement of *N*-Ph with *N*-Bn, as in **69**, resulted in an extended excited state lifetime (25.7 ns) while still being a strong photooxidant.[32]
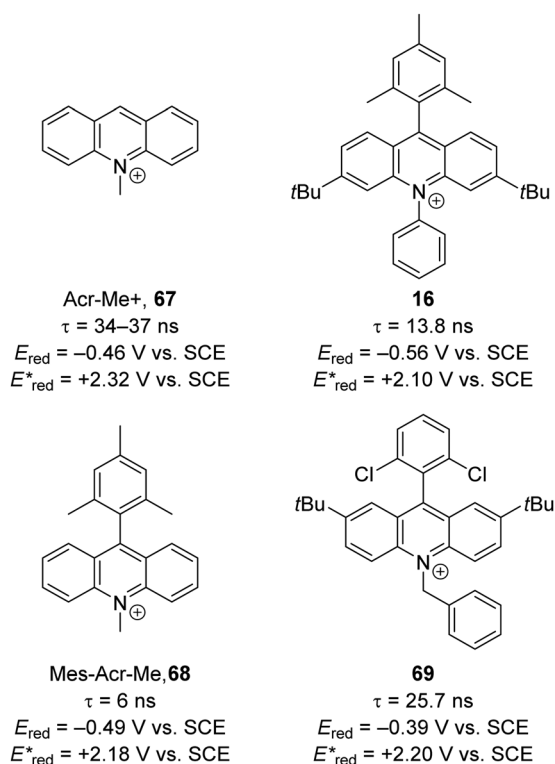

Acr-Me+, **67**
τ = 34–37 ns
E_{red} = −0.46 V vs. SCE
E_{red}^* = +2.32 V vs. SCE

16
τ = 13.8 ns
E_{red} = −0.56 V vs. SCE
E_{red}^* = +2.10 V vs. SCE

Mes-Acr-Me, **68**
τ = 6 ns
E_{red} = −0.49 V vs. SCE
E_{red}^* = +2.18 V vs. SCE

69
τ = 25.7 ns
E_{red} = −0.39 V vs. SCE
E_{red}^* = +2.20 V vs. SCE

Fig. 10   Examples of acridinium catalysts.

9550 | *Chem. Soc. Rev.*, 2021, **50**, 9540–9685

This journal is © The Royal Society of Chemistry 2021

3CzClIPN **70**
E^*_{red} = +1.56 V vs SCE
E^*_{ox} = −0.93 V vs SCE

4CzIPN **15**
E^*_{red} = +1.43 V vs SCE
E^*_{ox} = −1.18 V vs SCE

3DPA2FBN **14**
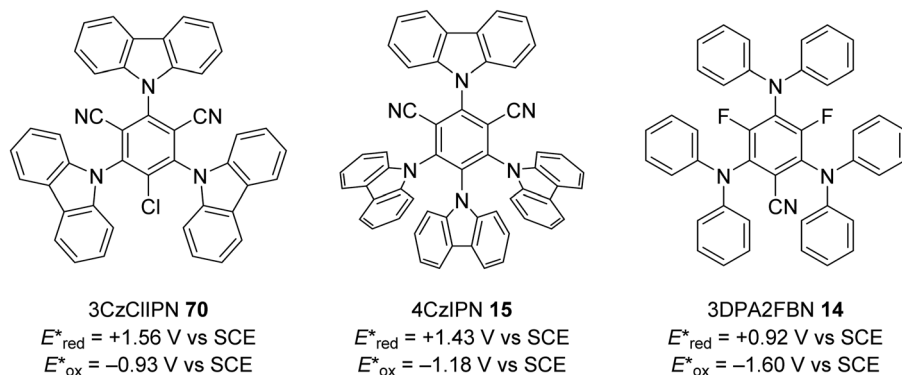E^*_{red} = +0.92 V vs SCE
E^*_{ox} = −1.60 V vs SCE

Fig. 11 Cyanobenzene derived photocatalysts and photoredox values.

Table 1 Maximum solubility of catalysts **72** and **13** in various organic solvents (molar)

2CzIPN **72**

Ir[dF(CF$_3$)ppy]$_2$(dtbbpy)$^+$ **13**

Solvent	2CzIPN 72 (M)	13 (M)
Toluene	1.3×10^{-2}	7.0×10^{-5}
1,4-Dioxane	1.6×10^{-2}	2.2×10^{-4}
Dichloromethane	8.3×10^{-2}	5.6×10^{-3}
Methyl tert-butyl ether	9.2×10^{-4}	7.0×10^{-5}
Dimethyl sulfoxide	1.6×10^{-2}	1.6×10^{-1}

Cyanobenzene-derived photocatalysts. Cyanobenzene-derived photocatalysts are highly flexible catalysts, due to their modular design.[33] For example, the photocatalyst 3CzClIPN (**70**) is a strongly oxidising photocatalyst with an E_{red}^* of +1.56 V vs. SCE. However, a similar catalyst 3DPA2FBN (**14**) is a strong reductant (E_{ox}^* = −1.60 V vs. SCE). The most commonly used cyanobenzene-derived photocatalyst is 4CzIPN (**15**) that is both a competent oxidant and reductant (Table 1).

The photocatalyst 4CzIPN (**15**) is accessed in one step from tetrafluoroisophthalonitrile (**71**) and carbazole with sodium hydride in 93% yield, rapidly and economically without column chromatography (Scheme 14).[78]

A key advantage of these cyanobenzene-derived photocatalysts over Ru and Ir photocatalysts is their high solubility in non-polar solvents.[79] For example, the catalyst 2CzIPN (**72**) has a much greater solubility in non-polar solvents than Ir[dF(CF$_3$)ppy$_2$](dtbbpy)PF$_6$, **13**. This was demonstrated with **72** having a maximum solubility in toluene of 1.3×10^{-2} M while **13** had a maximum solubility of 7.0×10^{-5} M. It has been recently highlighted that the majority of iridium and ruthenium photocatalysts have low solubility in non-polar organic solvents.[80]
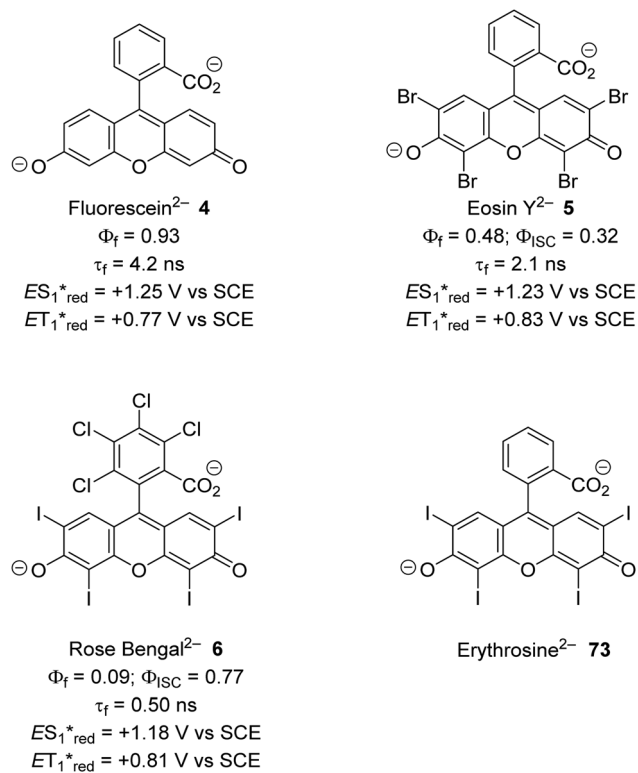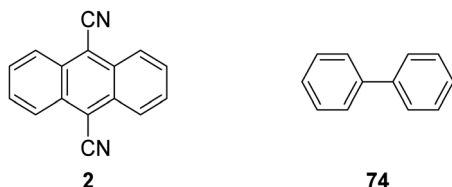

carbazole (5.0 eq.)
NaH (7.5 eq.)

THF (0.04 M)
rt, 24 h, 93%

71

15
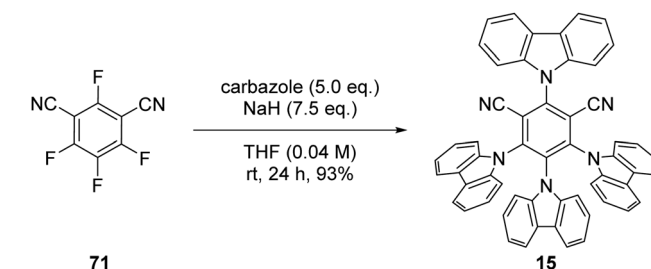
Scheme 14 Synthesis of 4CzIPN (**15**).

Xanthene dyes. The xanthene dyes fluorescein (**4**), Eosin Y (**5**), rose Bengal (**6**) and erythrosine (**73**) have remarkably similar photoredox values but very different photophysical properties due to the presence or absence of heavy halogen atoms (Fig. 12; for discussion, see 'Heavy atom effect').[8a]

DCA. A popular organic photocatalyst is 9,10-dicyanoanthracene (DCA, Fig. 13, **2**), due to its high absorption wavelength (>400 nm) so that it can be excited with visible light.[81] As mentioned, it has a low efficiency of ISC (ϕ_{ISC} = 0.0085), and therefore its excited triplet state is not easily accessible but its ^{1}S excited state is a strong oxidant (E_{red}^* = +1.99 V vs. SCE) with a high energy (66.9 kcal mol^{-1})[8a] However, due to back electron transfer (BET), the efficiency of DCA as a photoredox reagent is compromised, but this can be overcome with the inclusion of biphenyl.[5,62] Here, photoactivated DCA converts BP to its radical cation. As biphenyl undergoes BET more slowly than DCA, this allows the oxidised substrate to escape the solvent cage and thus proceed through a constructive reaction pathway.

Triarylaminium radical cations. Triarylaminium salts have found use as one-electron oxidation agents.[82] However, they have poor stability (Fig. 14). An oxygen-free solution of dichloromethane and tris-(p-bromophenyl)aminium perchlorate (**75**) was only stable for two days under vacuum and in the absence of light. When **75** was submitted to sunlight or a UV-lamp the reagent was fully decomposed within 1 h. It was also observed that **75** was unstable to protic solvents such as methanol. Greater stability was attained with-(p-bromophenyl)aminium hexachloro-antimonate (**76**, magic blue), with solutions in dichloromethane

This journal is © The Royal Society of Chemistry 2021

Chem. Soc. Rev., 2021, **50**, 9540–9685 | **9551**

Fluorescein^{2-} **4**
$\Phi_f = 0.93$
$\tau_f = 4.2$ ns
$ES_1^*{}_{red} = +1.25$ V vs SCE
$ET_1^*{}_{red} = +0.77$ V vs SCE

Eosin Y^{2-} **5**
$\Phi_f = 0.48$; $\Phi_{ISC} = 0.32$
$\tau_f = 2.1$ ns
$ES_1^*{}_{red} = +1.23$ V vs SCE
$ET_1^*{}_{red} = +0.83$ V vs SCE

Rose Bengal^{2-} **6**
$\Phi_f = 0.09$; $\Phi_{ISC} = 0.77$
$\tau_f = 0.50$ ns
$ES_1^*{}_{red} = +1.18$ V vs SCE
$ET_1^*{}_{red} = +0.81$ V vs SCE

Erythrosine^{2-} **73**

Fig. 12 Some photophysical properties of xanthene dyes.[8a]

2

74

Fig. 13 Structures of DCA (**2**) and biphenyl (**74**).

being stable for several days under ordinary laboratory lighting.[82] Therefore, the increased stability of **76**, and its strong SET oxidant properties ($E^0 = +0.70$ V vs. Fc) have allowed for **76** to have many applications and this has been reviewed.[83] However, **76** is still prone to decomposition via dimerisation reactions and these decomposition compounds are colloquially known as the "blues brothers."[84] From DFT calculations, NMR and optical spectroscopy and X-ray crystallography, the major decomposition product was found to be tetrakis-(4-bromophenyl)benzidine dimer **78**. The decomposition of magic blue **76** has been addressed with the design and successful synthesis of tris(2-bromo-4-tert-butylphenyl)-amine (**77**), which is known as "blues cousin" ($E_{red} = +0.78$ V vs. Fc). Recently, there has been much progress in designing new amine radical cations based upon this triarylamine.[85–87]

Persulfate salts. The anion of Marshall's acid (peroxydisulfuric acid, $H_2S_2O_8$) is a strong oxidising agent ($E_{red} = +1.76$ V vs. SCE).[88,88b] Therefore, its salts have found use in traditional chemical synthesis, with the Elbs persulfate oxidation and Boy-land–Sims oxidation being particular examples.[89] The O–O bond present within compound **66** undergoes homolytic cleavage and this generates the sulfate radical anion (SO$_4^{\bullet-}$, **79**, Scheme 15).[90] The counter-ion of the peroxydisulfate salt affects the decomposition temperature of the salt, with the sodium salt having a higher decomposition temperature than the potassium and ammonium salts.[88] As well as thermal decomposition, it has been shown that the sulfate radical anion is generated between
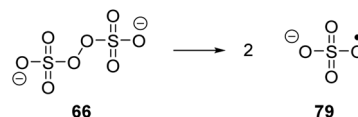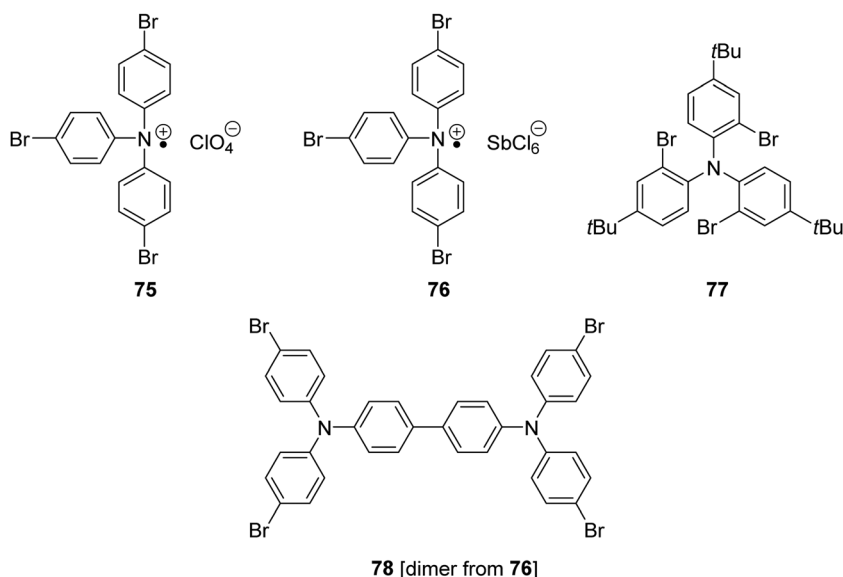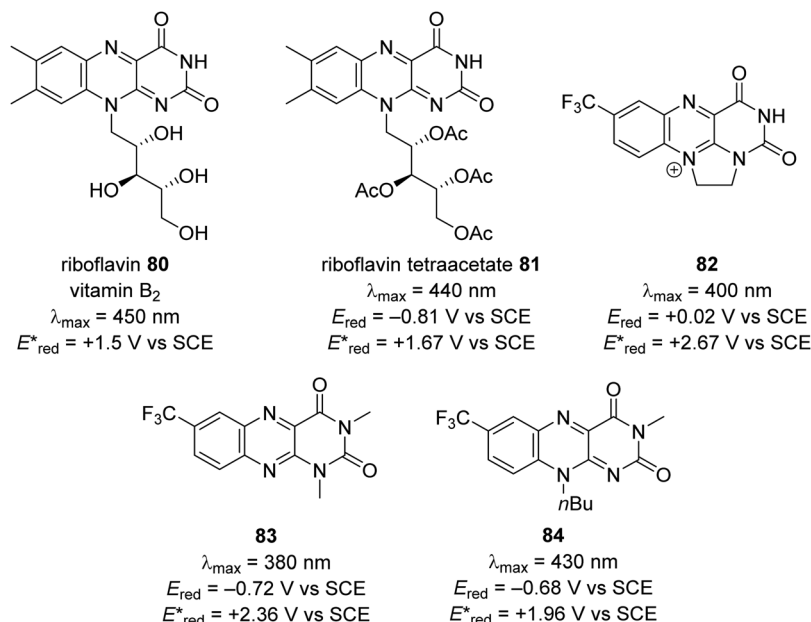

Scheme 15 Generation of sulfate radical anion **79**.

75

76

77

78 [dimer from **76**]

Fig. 14 Structures of triarylamine radical cations.

riboflavin **80**
vitamin B$_2$
$\lambda_{max} = 450$ nm
$E^*_{red} = +1.5$ V vs SCE

riboflavin tetraacetate **81**
$\lambda_{max} = 440$ nm
$E_{red} = -0.81$ V vs SCE
$E^*_{red} = +1.67$ V vs SCE

82
$\lambda_{max} = 400$ nm
$E_{red} = +0.02$ V vs SCE
$E^*_{red} = +2.67$ V vs SCE

83
$\lambda_{max} = 380$ nm
$E_{red} = -0.72$ V vs SCE
$E^*_{red} = +2.36$ V vs SCE

84
$\lambda_{max} = 430$ nm
$E_{red} = -0.68$ V vs SCE
$E^*_{red} = +1.96$ V vs SCE

Fig. 15 Redox values for flavin-based compounds.[95–99]

66 and an electron donor, such as Ru(ii)*,[91] and in ambient temperature DMSO solutions.[90,92] The sulfate radical anion can abstract hydrogen atoms[91] from activated C–H bonds and it can act as an oxidising agent.[90,92]

Flavins. Vitamin B$_2$ (riboflavin, **80**) has a tricyclic dimethyl-isoalloxazine ring system and this is commonly known as the flavin group.[93] About 1% of proteins are flavoproteins and they have a significant role in redox reactions in biology, undergoing one or two-electron transfer processes.[94] Recently, it has been shown that modification to the flavin ring system can impact the photoredox properties of these compounds. For example, **80** has an excited state reduction potential of +1.5 V *vs.* SCE,[95] and with the placement of electron-withdrawing groups onto the compound this was increased, as seen for **81–84** (Fig. 15).[96]

Summary of radical coupling reactions

A summary of the reactions discussed in this review is presented here. The reactions have been categorised, differentiating between reactions proceeding *via* a carbon-centred radical, reactions proceeding *via* a heteroatom-centred radical and energy transfer. Carbon-centred radicals **XV** can be accessed from many different substrates (Scheme 16). For example, carboxylates **I** were oxidised *via* a SET process and this resulted in a carboxyl radical, which after radical decarboxylation gave radical **XV**. Similar approaches have been developed to convert alcohols **II** to carbon-centred radicals **XV** *via* oxalate intermediates **III**. Carbon-centred radicals have also been prepared from alkyl halides **IV**, organosilanes **V** and boronates **VI**. The use of HAT allows carbon-centred radicals to be prepared from α-hetero-atom C–H bonds **VIII**, benzylic C–H bonds **IX**, allylic C–H bonds **X**, aldehyde C–H bonds **XI**, hydroxy C–H bonds and C–H bonds of silyl protected alcoholic compounds **XIII**. The use of PCET
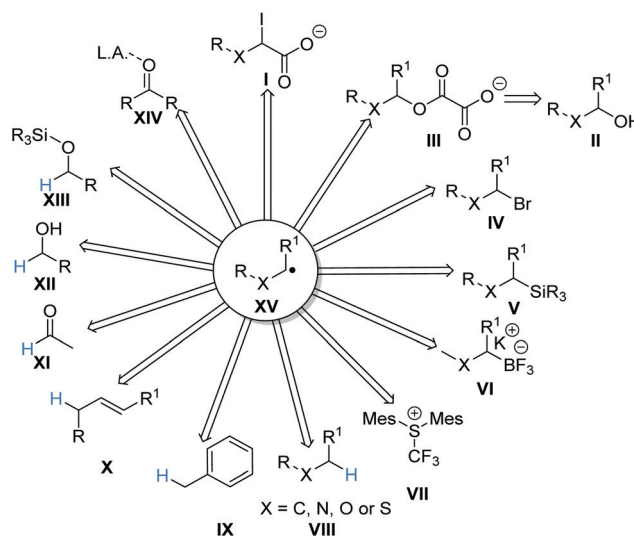

Scheme 16 Radical precursors.

allows for carbon-centred radical formation from carbonyl compounds **XIV**.

Once formed, the carbon-centred radical can take part in many different reactions (Scheme 17). A Giese reaction can be performed where the radical adds to an electron-poor alkene and this gives the alkylated compounds **85**.[99,100] The use of vinyl sulfones in combination with a carbon-centred radical led to the formation of vinyl compounds **86** (following loss of the sulfonyl radical)[101,102] The use of ethynyl-benziodoxolone (EBX) reagents allowed for the preparation of alkyne compounds **87** with carbon-centred radicals under mild conditions.[103] Carbon-centred radicals were used in the Minisci reaction, with function-alised heterocycles **88** being produced.[2] Tandem photoredox and
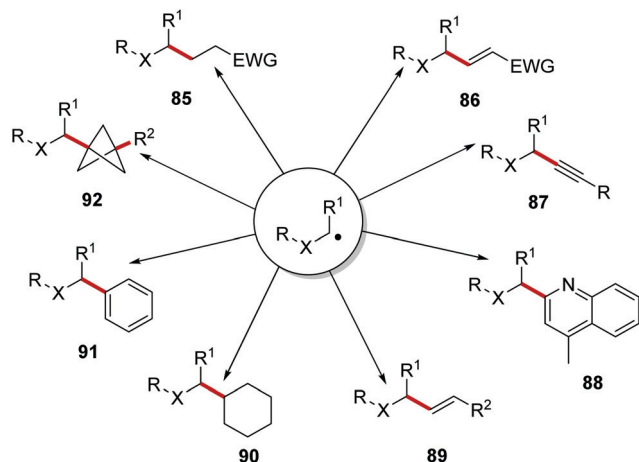
Scheme 17   Common radical reactions reported in the literature.

cross-coupling catalytic strategies have allowed for the formation of alkenes **89**, alkyl derivatives **90** and aryl products **91**. Reactions of [1.1.1]propellane with carbon-centred radicals have led to the formation of bicyclo[1.1.1]pentanes **92**, as potential isosteres of aromatic rings.[104]

As well as carbon-centred radicals, heteroatom-centred radicals can also be formed (Scheme 18). Sulfonyl radicals **93** are formed *via* SET oxidation of sulfinate salts **94**, whereas the oxygen-centred radical **95** is formed from a PCET from the alcohol **96**. Nitrogen-centred radicals **97** and **99** are formed under a similar process, where the cations **98** and **100** gain a single electron and the loss of an anion gives these radical cations. Primary aminyl radicals **101** were formed from the single electron reduction of azides **102** in the presence of a proton source. PCET can give rise to amidyl radicals **103** from amides **104** and a HAT process can give silyl radicals **105** from silanes **106**.

These heteroatom radicals can take part in a variety of reactions (Scheme 19). For example, the formation of oxygen-centred radical **107** results in ketone formation and C–C bond fragmentation leading to products such as **108**.[105] Incorporation of a nickel

Scheme 18   Heteroatom radical precursors.

catalyst facilitated cross-coupling reactions between sulfonyl radicals **109** and bromobenzene and this led to coupled products such as **110**.[106] Amidyl radicals **113** can partake in 5-*exo*-trig cyclisation, followed by further radical functionalisation and this gave lactams such as **114**. Additionally, amidyl radicals **115** also underwent 1,5-hydrogen atom transfer and this allowed for remote site-selective functionalisation giving amides such as **116**. Secondary amine radical cations **117** and pyridine radical cations **118** have both been used to form substituted aniline products **119**. It was also demonstrated that a Zincke reaction with piperidine could be performed on pyridinium adduct intermediate **120** and this generated unsubstituted anilines **121**.

Energy transfer processes facilitated complementary transformations (Scheme 20). Singlet oxygen generation can be accessible through energy transfer processes.[107,108] The [2+2] cycloadditions of alkenes are highly successful processes with energy transfer catalysis.[109,110] The application of quantum dots as energy transfer catalysts in organometallic cross-coupling reactions has increased the efficiency and selectivity of these transformations.[111] Energy transfer has also found use in the activation of azides and, from this, N-heterocycles have been formed, such as pyrazines.[112]

Summary of introduction

A considerable amount of progress in radical coupling has been achieved due to PET, HAT and energy transfer approaches. The reactivity and selectivity of these processes are dependent upon different factors. Photoredox approaches are dependent upon redox potentials, HAT approaches are dependent upon bond dissociation energies and energy transfer is dependent upon triplet energies. With these three different but complementary processes, a wide range of mild, non-hazardous transformations has been developed. Photocatalysts, in particular, have garnered considerable attention due to the enhanced reactivity of the excited state. The use of nickel and copper catalyst alongside a PET, HAT or energy transfer catalyst has resulted in a greatly expanded scope of feasible transformations.
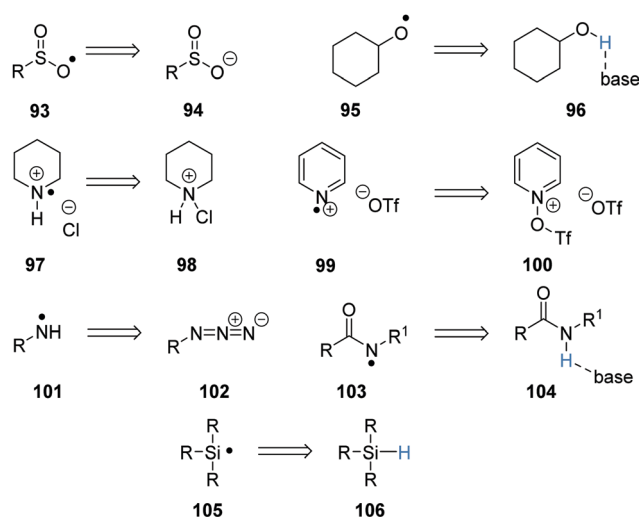
2 Metal-mediated bond formations

Ruthenium

Photoactivated ruthenium(II)* complexes can act as electron donors or as acceptors. This means that catalytic cycles can either involve Ru(I) and Ru(II), or Ru(II) and Ru(III). In addition, photoactivated Ru(II)* complexes can engage in energy transfer reactions. Examples of these roles are now described, based on proposals for mechanisms described in the original research papers. This section builds on extensive earlier discoveries on visible light photoredox catalysis with transition metal complexes, and the reader is referred there for further reading.[9]
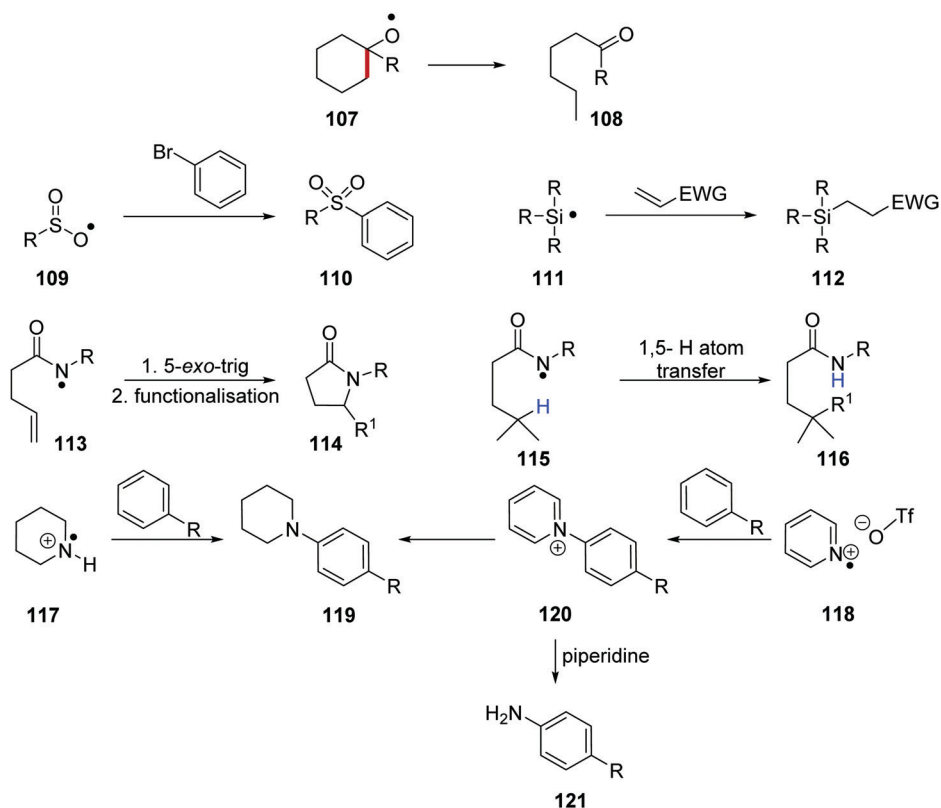
2.1   Catalytic cycles featuring Ru(II)/Ru(I)

Stephenson's team converted tetrahydroisoquinoline **122a** into the Henry product **123a** in the presence of nitromethane using Ru(bpy)Cl$_2$ in 81% yield or Ir(ppy)$_2$(dtbbpy)PF$_6$ in 92% yield (Scheme 21).[113]
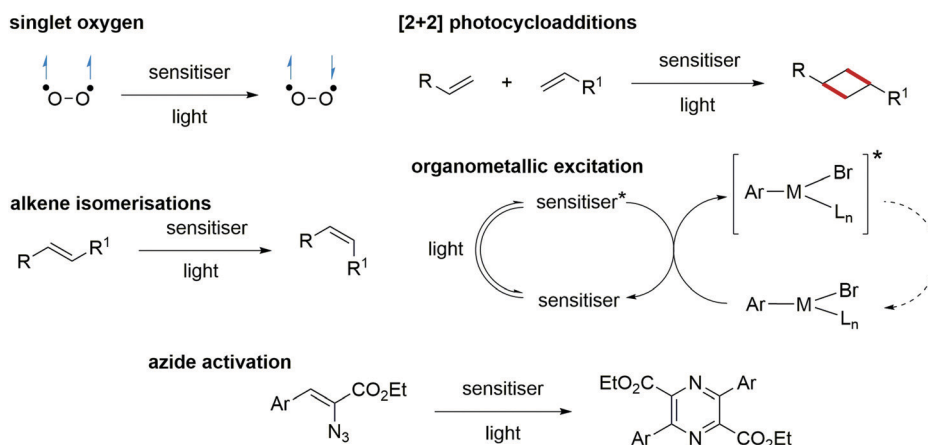
9554 | *Chem. Soc. Rev.*, 2021, **50**, 9540–9685

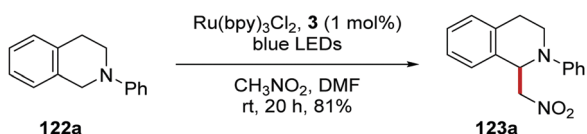This journal is © The Royal Society of Chemistry 2021

Scheme 19 Heteroatom radical reactions found in the literature.

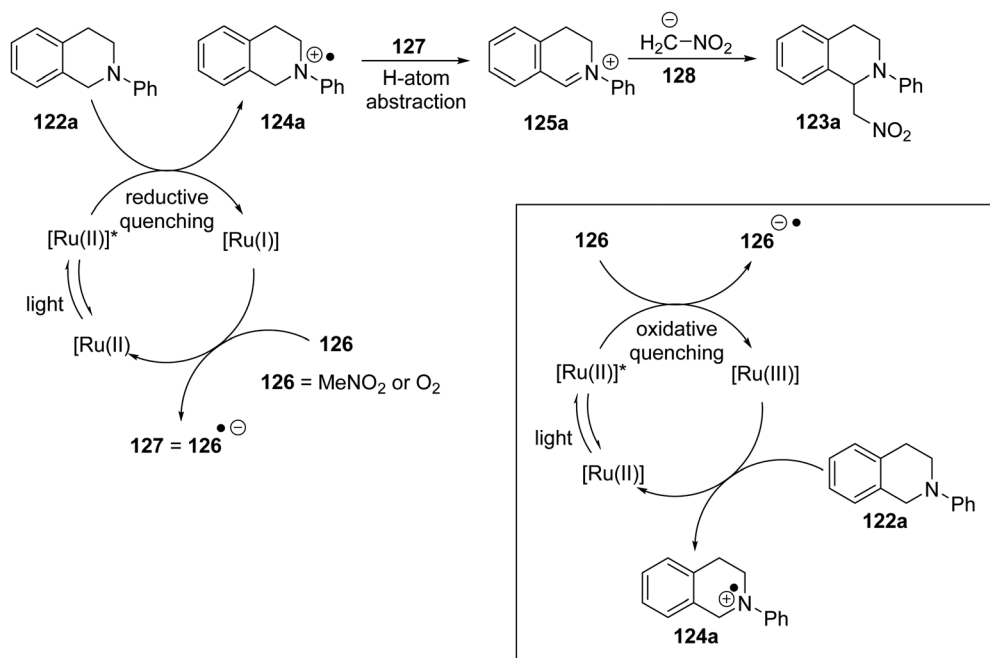**Scheme 20** Energy transfer reactions.

Scheme 21 C–H functionalisation of THIQ **122a** with nitromethane.

A specific mechanism is proposed for the Ir(III)-catalysed reaction, and may also be valid for the Ru(II) variant. Here, the photoactivated catalyst is reductively quenched by the amine substrate **122a** to form the radical cation **124** (Scheme 22). The reduced

form of the catalyst Ir(II) or Ru(I) is returned to its original oxidation state Ir(III)/Ru(II) through interaction with an oxidant **126** (MeNO$_2$ or O$_2$) which is converted to its radical anion **127**. The radical component of this radical anion abstracts an H atom from the amine radical cation, to form an iminium salt **125**, while the anionic component can deprotonate nitromethane to form the nitronate nucleophile **128**.

However, for the ruthenium pathway, an alternative mechanism may or may not be at play. It was reported that **122a** (+0.88 V *vs.* SCE)[113b] cannot be oxidised with photoactivated [Ru(bpy)$_3$$^{2+}$]* (+0.77 V *vs.* SCE[113b]) (+0.84 V is cited[113a]) but can be oxidised

This journal is © The Royal Society of Chemistry 2021

Chem. Soc. Rev., 2021, **50**, 9540–9685 | **9555**

Scheme 22

with $Ru(bpy)_3^{3+}$ (+1.29 V *vs.* SCE). This seems also to have been considered by Stephenson *et al.* who noted that $[Ru(bpy)_3^{2+}]^*$ can be oxidised by nitromethane (inset Scheme 22). The result would be that the same species, iminium salt **125** and nitronate anion **128**, would be produced in solution, but would involve an oxidative quenching of the photoactivated Ru catalyst and therefore involve a Ru(II)/Ru(III) cycle. Subsequent papers from Stephenson promote the Ru(I)/Ru(II) cycle for these Henry reactions, so we proceed on that basis.

The slow conversion observed in Scheme 21, was due to the slow re-oxidation of Ru(I) to Ru(II). Therefore, it was thought that a terminal oxidant could be added to accelerate the reaction.[114] It was found that bromotrichloromethane was the best terminal oxidant for this process. The inclusion of BrCCl₃ led to the formation of iminium salts **125** from THIQs **122** within 3 h (Scheme 23). Afterwards, a variety of different nucleophiles gave the products corresponding to **123**. Addition of the nucleophile

was best performed in the dark with an excess of triethylamine and the reactions were complete within 3 h. Under these conditions the aza-Henry reaction was feasible, and this gave **123a** in 95% yield. The use of methallyltrimethylsilane gave **123b** in 85% yield, whilst 2-(trimethylsilyloxy)propene gave ketone **123c** in 59% yield. When dimethyl malonate was used in the reaction with potassium carbonate, diester analogue **123d** was given in 69% yield. Alkynylation of iminium salt **125** was also achieved with phenylacetylene when a catalytic amount of Cu(I)Br was added and this gave alkyne derivative **123e** in 82% yield. Indole was another suitable nucleophile for this transformation when used with KOtBu, and this gave **123f** in 83% yield.

C–H functionalisation of THIQ was achieved asymmetrically (Scheme 24) with a thiourea catalyst **129**.[115] As previously discussed, iminium salt **124** was formed from **122**. During optimisation of the reaction conditions, it was found that iminium salt formation was most efficient in MeCN, whereas the asymmetric addition

Scheme 23 Iminium salt formation and subsequent nucleophile addition upon ring system **122**.
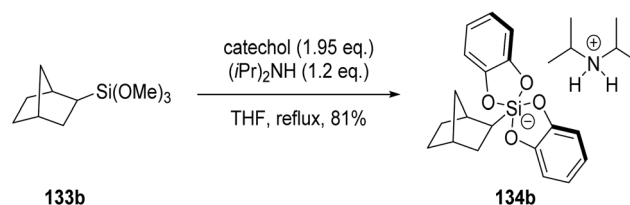
9556 | *Chem. Soc. Rev.*, 2021, **50**, 9540–9685

This journal is © The Royal Society of Chemistry 2021

Scheme 24 Asymmetric alkylation of THIQs **122**.

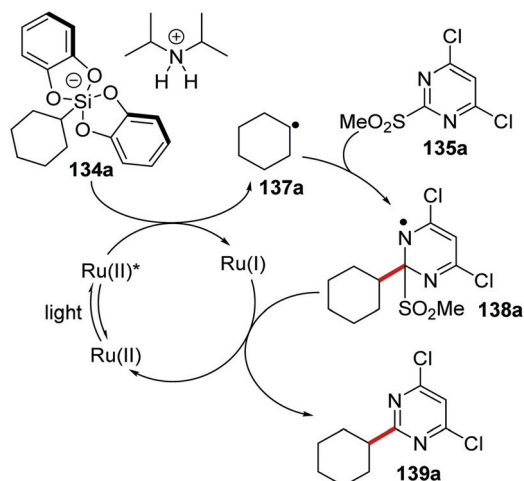**Scheme 25** Lewis acid-promoted coupling of α-silylamines to electron-poor alkenes.

of 1-(*tert*-butyldimethylsilyloxy)-1-methoxyethylene proceeded best in MTBE. Therefore, in preparing ester **123g**, a solvent swap was carried out between formation of intermediate iminium salt **125** and addition of the nucleophile, and this achieved the highest yields and highest ee for this compound. In investigating different terminal oxidants for iminium salt formation, it was discovered that the photocatalyst counterion and halogen atom source had significant effects on enantioselectivity. Higher ee values were obtained when CCl$_4$ was used as a terminal oxidant over BrCCl$_3$. Furthermore, the common counterion PF$_6$ also gave lower ee than the chloride counterion. Once optimisation of the reaction conditions was concluded, a small substrate scoping study was carried out. From this, it was observed that the enantioselectivity of the reaction was very sensitive to the electronic nature of the THIQ ring; electron-rich substituents gave lower yields and lower ee. For example, ester **123g** was isolated in 72% yield and 95% ee, whereas the more electron-rich analogue **123h** was isolated in 44% yield and 42% ee.

Silanes. α-Silylamines **130** were successful coupling partners for radical coupling reactions to electron-poor alkenes **131** (Scheme 25).[116] With consideration of redox potentials, SET between Ru(II)* and **130** was feasible (Ru$_{red}$* = +0.77 V *vs.* SCE, dimethylaniline has a redox potential of +0.74 V *vs.* SCE and the adjacent silyl group further lowers the oxidation potential)[30,117]

and this gave amine radical cation. Loss of $^+$SiMe$_3$ resulted in a carbon-centred α-aminoalkyl radical. Asymmetric radical addition to dicarbonyl compound **131** facilitated with scandium triflate as Lewis acid and chiral PyBox ligand **L1** gave coupled alkylated anilines **132**. These conditions allowed for the preparation of a library of 20 alkylated anilines **132**; for example, analogues **132a–c** were among a series of products all prepared with high ee (85–96%).

Silicate chemistry. Organosilicates **134** are excellent radical precursors due to their low oxidation potentials (E_{red} = +0.4 → +0.7 V *vs.* SCE).[118] These silicates were accessed by reacting the corresponding trimethoxysilane **133** with catechol and an amine base, such as diisopropylamine.[119] For example, the use of silane **133b** led to the formation of silicate **134b** in 81% yield (Scheme 26).
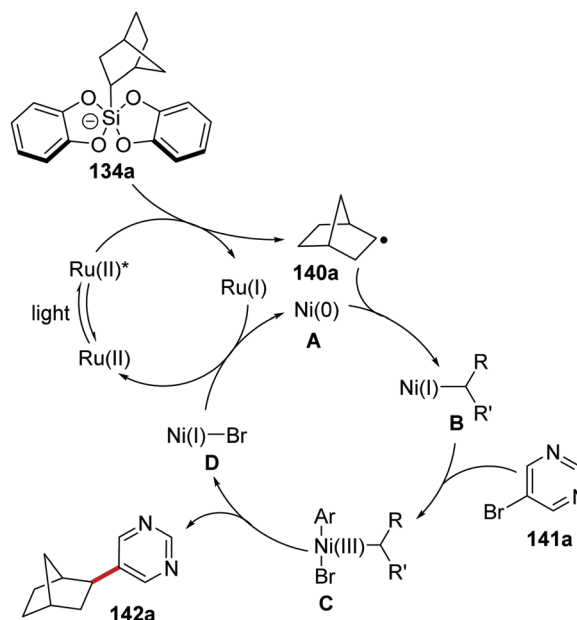
Scheme 26 Formation of silicate **134b**.

This journal is © The Royal Society of Chemistry 2021

Chem. Soc. Rev., 2021, **50**, 9540–9685 | 9557

Scheme 27 Formation of **139a** from **134a**.

The coupling of organosilanes **133** with electron-poor arenes, such as pyrimidine sulfones **135** (Schemes 27 and 28) and benzothiazole-sulfones **136** was realised *via* a silicate intermediate **134** under blue light and a Ru(bpy)$_3$(PF$_6$)$_2$ photoredox catalyst. Under the reaction conditions, the Ru(II) complex was excited to the Ru(II)* species (Scheme 27). SET to Ru(II)* complex (E_{red}^{*} = +0.77 V *vs.* SCE) from **134a** (*ca.* +0.40 V *vs.* SCE)[119] resulted in the formation of alkyl radical **137a** and Ru(I) complex. Addition of **137a** to electron-poor pyrimidine **135a** formed the key C–C bond with the generation of radical **138a**. The ruthenium catalytic cycle was closed with a SET to **138a** from Ru(I) species. This reformed the original Ru(II) complex and after the loss of sulfinate anion from **138a**, gave coupled compound **139a**.

The reaction worked better for pyrimidines than benzothiazoles. Low yields were recorded for benzothiazoles **140a** (36%) and **140b** (25%) (Scheme 28), whereas high yields were found for pyrimidine compounds **139a** (83%) and **139b** (81%).

The inclusion of a nickel catalyst permitted coupling between organosilicates **134** and aryl bromides **141**.[119] Irradiation of the reaction mixture with blue light resulted in the formation of

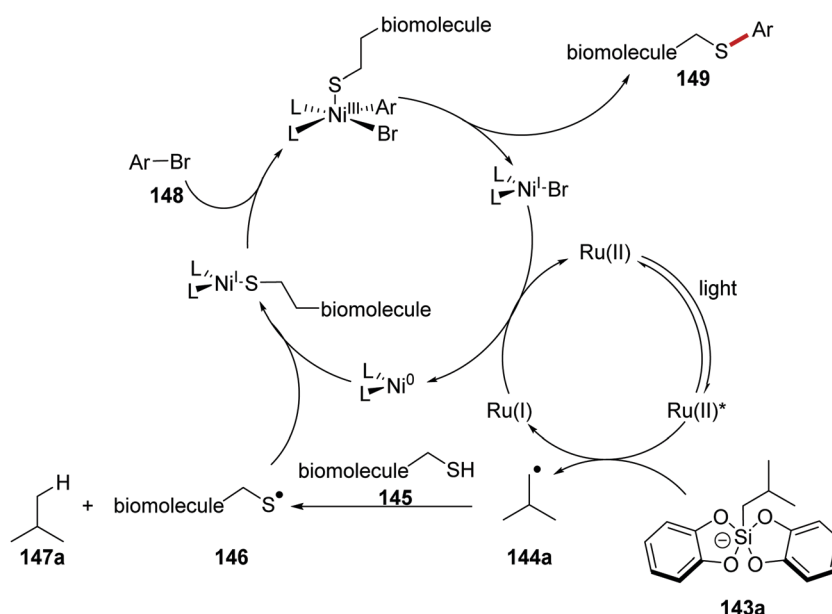Scheme 29 Mechanism of silicate coupling to aryl bromides.

Ru(II)* species from Ru(II) complex (Scheme 29). SET to Ru(II)* from silicate **134a** afforded Ru(I) complex and radical **140a**. Interception of **140a** with Ni(0) complex **A** gave Ni(I) complex **B**. Oxidative addition of complex **B** to aryl bromide **141a** resulted in Ni(III) complex **C**, which underwent reductive elimination and this yielded coupled product **142a** and Ni(I) complex **D**. The ruthenium and nickel catalytic cycles were closed with an outer-sphere SET between Ni(I) and Ru(I) complexes as both original Ni(0) and Ru(II) species were returned.

Coupled compound **142a** was also produced when the Ir[dF(CF$_3$)ppy](bpy)(PF$_6$) photocatalyst was used but similar yields of **142a** were obtained with the more economical Ru(bpy)$_3$(PF$_6$)$_2$ photocatalyst. These optimised conditions afforded bicyclic **142a**, *N*-Boc protected amine **142b** (53%) and heterocyclic **142c** (50%) (Scheme 30).

Scheme 28 Silicate coupling to pyrimidine sulfones **135** and benzothiazole sulfones **136** with Ru(bpy)$_3$(PF$_6$)$_2$.

9558 | *Chem. Soc. Rev.*, 2021, **50**, 9540–9685

This journal is © The Royal Society of Chemistry 2021

Scheme 30 Coupling of silicates to aryl bromides.

Scheme 31 Proposed mechanism for radical coupling to biomolecules with ammonium bis(catechol)silicate as a HAT reagent precursor.

The arylation of biomolecules (containing cysteine residues) **145** (Schemes 31 and 32) with aryl bromides **148** was achieved with a ruthenium/nickel and silicate strategy, using silicate **143a** as a HAT reagent precursor (Scheme 31).[120] Irradiation of the reaction mixture led to Ru(II)* formation from Ru(II) complex. SET from silicate **143a** to Ru(II)* afforded radical **144a**, and the Ru(I) complex. Radical **144a** abstracted a hydrogen atom from a cysteine residue present in **145** and this gave thiyl radical **146** and alkane **147a**. Radical **146** was intercepted with Ni(0) complex and a Ni(I) complex was formed. Oxidative addition of aryl bromide **148** generated Ni(III) complex and this underwent reductive elimination forming biomolecule **149** and Ni(I) complex. Both ruthenium and nickel catalytic cycles were closed with an electron transfer to Ni(I) from Ru(I).
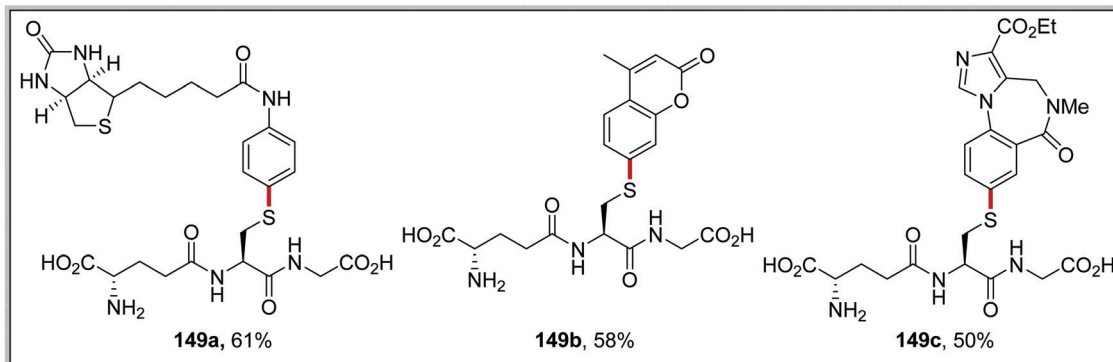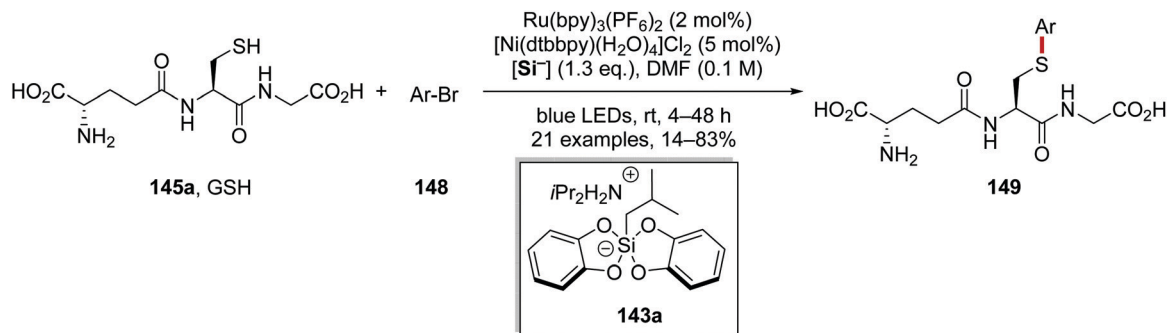
This transformation allowed for the functionalisation of tripeptide ʟ-glutathione (γ-Glu-Cys-Gly; GSH, **145a**). Both a biotin analogue **149a** and a fluorescent variant **149b** of GSH were prepared in 61% and 58% yield, respectively, using low loadings of both Ru and Ni catalyst. The drug molecule flumazenil was also coupled with GSH and this gave **149c** in 50% yield (Scheme 32).

Finally, this methodology was used to functionalise nonapeptide **145d** with 4-bromobenzonitrile **148d** and this gave full conversion to **149d** within 2 h.

Sulfinate oxidation to sulfonyl radicals. The formation of C–S bonds was achieved with a ruthenium/nickel catalytic strategy under blue light.[106] Here, sodium sulfinate salts **150** and aryl bromides/iodides **152** were coupled in high yields and this gave aryl sulfones **153** (Scheme 33). Under the reaction conditions, Ru(bpy)$_3$(PF$_6$)$_2$ catalyst is excited from exposure to light giving excited Ru(II)* complex. Electron transfer from sulfinate **150a** ($E_{1/2}$ = −0.37 V vs. SCE)[106] to Ru(II)* (+0.77 V vs. SCE) gave sulfonyl radical **151a** and Ru(I) complex. Ni(0) complex **B** intercepted the sulfonyl radical **151a** and Ni(I) complex **C** was formed. Oxidative addition of aryl bromide **152d** to Ni(I) complex **C** and then subsequent reductive elimination resulted in the generation of coupled product **153d** and restoration of the original Ni(I) complex **A**. Electron transfer to Ni(I) complex **A** from Ru(I) complex resulted in the formation of Ni(0) complex **B** and the original Ru(II) complex.

Both aryl iodides and aryl bromides were used with this Ru/Ni catalytic system and this afforded 40 examples of the coupled
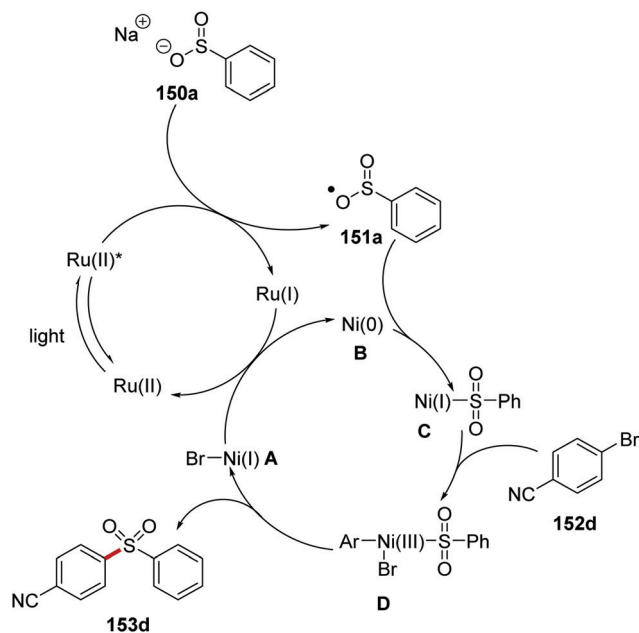
This journal is © The Royal Society of Chemistry 2021

Chem. Soc. Rev., 2021, **50**, 9540–9685 | **9559**

Scheme 32 Results of radical coupling to biomolecules.

sulfone products in 33–86% yields (Scheme 34 for selected examples). The reaction was functional group-tolerant; phenol **153a** was isolated in 74% yield and 1,3-benzodioxole derivative **153b** was given in 81% yield. Furthermore, lactone **153c** was prepared in 75% yield from the corresponding aryl bromide. When 4-bromobenzonitrile was used in this reaction, **153d** was formed in 83% yield. The presence of heterocycles did not impede this transformation with **153e** and **153f** isolated in 79% and 57% yield, respectively.

Lewis acid-activated ketones. The combination of Lewis acid catalysis, chiral ligands and ruthenium photoredox was also

employed in the asymmetric ring-expansion of cyclopropanes **154** with coupling to terminal alkenes **158** (Scheme 35).[121] In this case, gadolinium(III) triflate was employed as the Lewis acid in combination with a PyBox ligand and a Ru(bpy)₃X₂ photocatalyst. SET to Ru(II)* from the amine base, DIPEA (**161**), resulted in the formation of a Ru(I) complex and the DIPEA radical cation **161⁺•**. Donation of an electron from Ru(I) to gadolinium adduct **155a** resulted in carbon-centred radical **156a**. Direct reduction of ketone **154a** is not possible with the Ru(I) complex and this is supported by the reduction potential of acetophenone (-2.11 V $vs.$ SCE)[30] and the oxidation potential

9560 | Chem. Soc. Rev., 2021, **50**, 9540–9685

This journal is © The Royal Society of Chemistry 2021

Scheme 33 Reaction mechanism of coupling between sulfonyl radicals with aryl halides.

of Ru(bpy)$_3^+$ (−1.33 V *vs.* SCE).[8b] Electron donation from Ru(I) complex to the carbonyl group present in compound **155a**, formed from **154a**, generated cyclopropyl ketyl radical **156a**. Subsequent reversible endergonic radical ring-opening of the cyclopropane moiety resulted in alkyl radical **157a**.[122] Slow stepwise cycloaddition with alkene **158a** resulted in a [Gd]-ketyl radical **159a**. Chain-propagating electron transfer to another equivalent of the substrate or chain-terminating reduction of the amine radical cation **161**$^{+•}$ resulted in the formation of **160a**.

This reaction was applied to a wide range of different substrates generating a library of enantioenriched cyclopentanes **160** where the vast majority of yields and ee values were in the range 80–100% (Scheme 36). Terminal alkenes bearing two substituents were tolerated under the reaction conditions and this allowed for the preparation of compounds **160a** and **160b** in 80 and 95% yield, respectively. The use of a methyl-substituted cyclopropane substrate resulted in a lower 57% yield and only 50% ee for the corresponding cyclised product **160c**.

Ruthenium(I) behaved as an electron donor when it reduced alkyl C–Br bonds below and this led to cyclisation (Schemes 37 and 38).[123] Under the reaction conditions, the excited Ru(II)* complex received an electron from triethylamine (**163**), resulting in the formation of a Ru(I) complex and the amine radical cation **160**. Ru(I) then reduced the C–Br bond in **162a** which formed radical **165a** and the bromide anion. This SET was supported by the reduction potential of ethyl bromoacetate ($E = −1.08$ V *vs.* SCE)[30] which should be comfortably reduced by Ru(bpy)$^+$ ($E = −1.33$ V *vs.* SCE). Cyclisation of the electron-poor radical onto the electron-rich indole in **165a** gave **166a**. It was not determined whether the transformation of benzylic radical **166a** to indole compound **167a** operated *via* a radical chain mechanism (*via* bromine atom abstraction from **162a**) or through electron transfer to Ru(II)* complex followed by deprotonation.

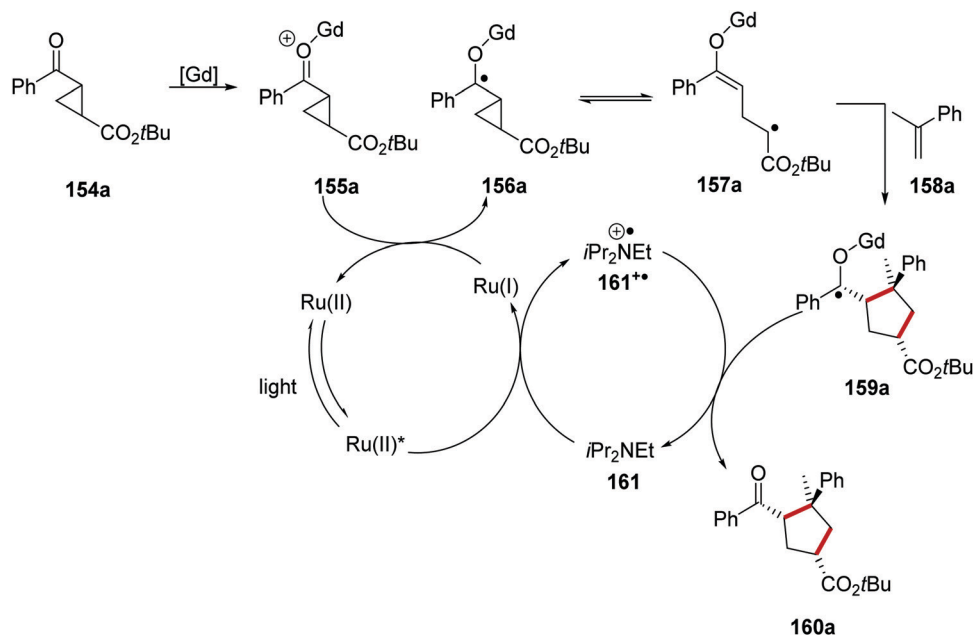An optimisation study was carried out where it was found that triethylamine was the optimal base to generate Ru(I) complex from Ru(II)*. Other bases tested such as DABCO and trimethylamine resulted in the loss of the bromine atom from the substrate but with no cyclisation. Under the optimised reaction conditions, tricycle **167a** was isolated in 60% yield (Scheme 38). Thirteen other cyclised products were also prepared with yields ranging from 40% to 90%. These conditions were also applied to a radical cascade cyclisation giving tetracycle **167d** in 79% yield.

The C–H functionalisation of furan, pyrroles and indoles was achieved *via* a radical coupling strategy with diethyl bromomalonate (**168a**) as coupling partner.[124] N,N-Diphenyl-4-methoxyaniline (**174**) reduced the excited Ru(II)* complex to Ru(I) species with **175** being formed (Scheme 39). The strongly reducing Ru(I) reduced **168a**,
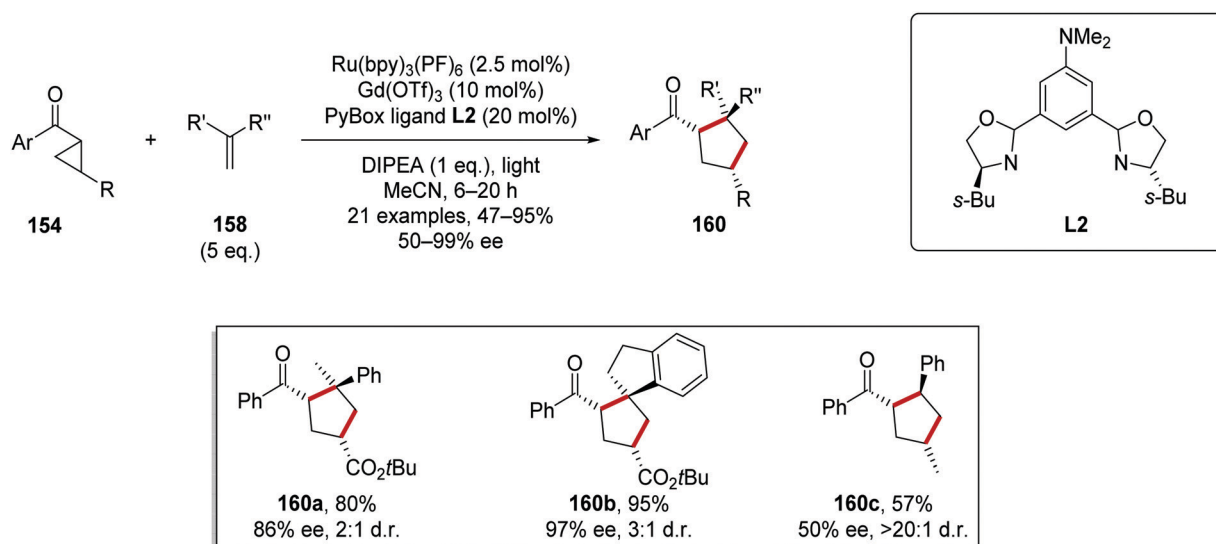

Scheme 34 Scope of the coupling reaction between sulfonyl radicals and aryl halides.

This journal is © The Royal Society of Chemistry 2021

Chem. Soc. Rev., 2021, **50**, 9540–9685 | **9561**

Scheme 35 Ruthenium and Lewis acid-promoted ring-expansion.

Scheme 36 Ru and Lewis acid-mediated cyclopropane ring expansion.

resulting in bromide loss and formation of alkyl radical **169a**. This electron-deficient malonate radical then underwent coupling with electron-rich indole **170a**, which provided benzylic radical **171a**. The loss of an electron from **171a** gave benzylic cation **172a**, which, after proton loss, afforded the coupled product **173a**.
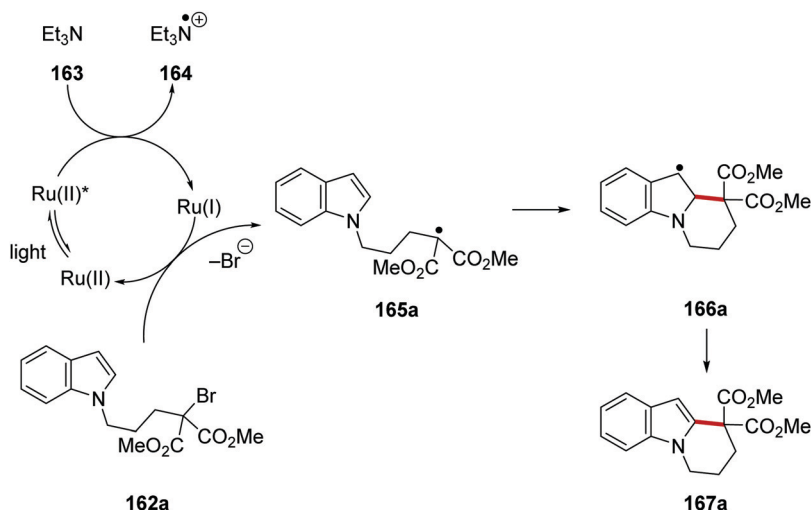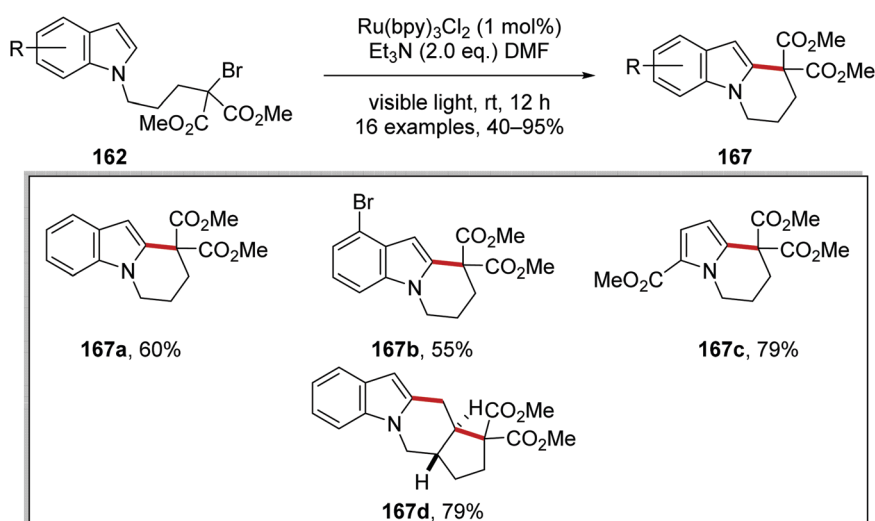
This reaction was used to prepare functionalised indoles **173a–e**, pyrroles **173f** and **173g** and furan **173h** analogues (Scheme 40). The reaction generally worked well although a low yield (40%) was obtained for tryptophan analogue **173c** when the reaction was conducted in water.

α-Functionalisation of aldehydes **180** with bromoacetonitrile (**176**) *via* C–H activation was an effective enantioselective transformation with a Ru photoredox and organocatalyst system.[125]

The reaction was proposed to go through the following reaction mechanism (Scheme 41). The reduced Ru(I) complex ($E = -1.33$ V *vs.* SCE) was able to donate an electron to nitrile **176** ($E_{1/2}^{\text{red}} = -0.69$ V *vs.* SCE)[124] and this gave alkyl radical **177** and Ru(II) complex. Coincidentally, aldehyde **180** and organocatalyst **183** formed chiral electron-rich enamine adduct **181**. Radical coupling between enamine **181** and radical **177** resulted in the formation of α-aminoalkyl radical **178**. Subsequent single-electron oxidation with Ru(II)* resulted in the reformation of Ru(I) complex and iminium compound **179**, hydrolysis of which gave enantioenriched product **182**.

These conditions were used to generate a library of 10 compounds in 68–97% yields and with 90–97% ee. Aliphatic **182a**,

9562 | Chem. Soc. Rev., 2021, 50, 9540–9685

This journal is © The Royal Society of Chemistry 2021

Scheme 37 Cyclisation onto indoles with Ru(bpy)$_3$Cl$_2$.

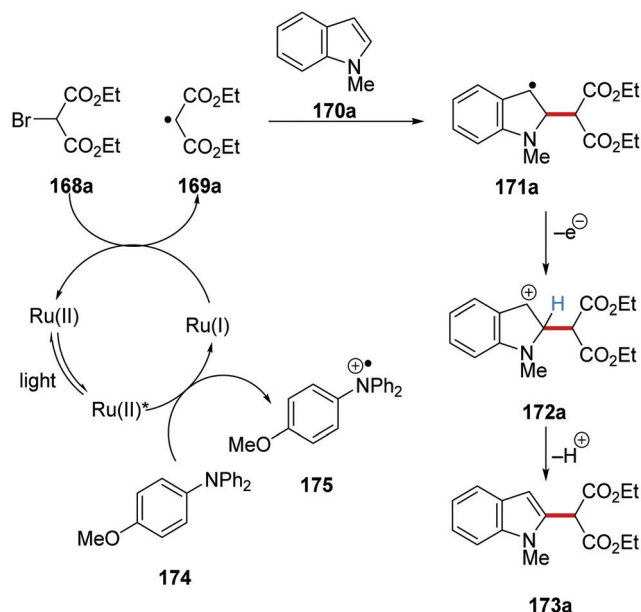**Scheme 38** Cyclisation of bromoalkylindoles and bromoalkylpyrroles.

aromatic **182b** and benzyl **182c–d** substituents were all tolerated in the reaction and with a high yield and enantiomeric excess in each case, as shown in Scheme 42.

Substituted α-bromonitriles **184** were also employed under similar reaction conditions to afford nitrile products **185** with organocatalyst **186** (Scheme 43).[125] Acetal **185a**, trifluoromethyl derivative **185b** and sulfonamide analogue **185c** were all prepared under the optimised reaction conditions. All-carbon quaternary stereocentres with excellent enantiocontrol were also prepared, as seen in the formation of **185d** with 98% ee.

The asymmetric α-functionalisation of ketones **187** with azides **189** (Schemes 44 and 45) or diazoacetates **193** (Scheme 45) was achieved with a Ru/Rh catalytic system.[126] Coordination of **187a** to the Rh catalyst **188** gave Rh complex **A** and this allowed for base-promoted deprotonation, which gave complex **B**. Stern–Volmer studies it was shown that only the Rh-enolate complex could quench the excited Ru(ɪɪ)* complex. Therefore, it was thought

that an outer-sphere SET between **B** and Ru(ɪɪ)* initiated the reaction with formation of the strongly reducing Ru(ɪ) species. The Ru(ɪ) complex reduced azide **189a** giving anilinyl radical **190a** after protonation. This mechanism was supported with cyclic voltammetry studies performed by the authors. Organic azide **189a** has an irreversible reduction peak at −1.82 V *vs.* Fc/Fc$^+$ which would not be reduced by the excited state of Ru(bpy)$_3$$^{2+}$ (−0.81 V *vs.* SCE) but could feasibly be reduced by Ru(bpy)$_3$$^+$ (−1.33 V *vs.* SCE). Addition of **190a** to electron-rich enolate **B** resulted in enantioselective C–N bond formation with ketyl radical **C** being formed. It was thought that the strongly reducing radical **C** could either participate in a radical-chain mechanism with reduction of **189a** or SET with Ru(ɪɪ)* complex. The loss of an electron from **C** resulted in cationic intermediate **D**. Dissociation of complex **D** gave the enantio-enriched amine product **191a** with the Rh catalyst being regenerated.
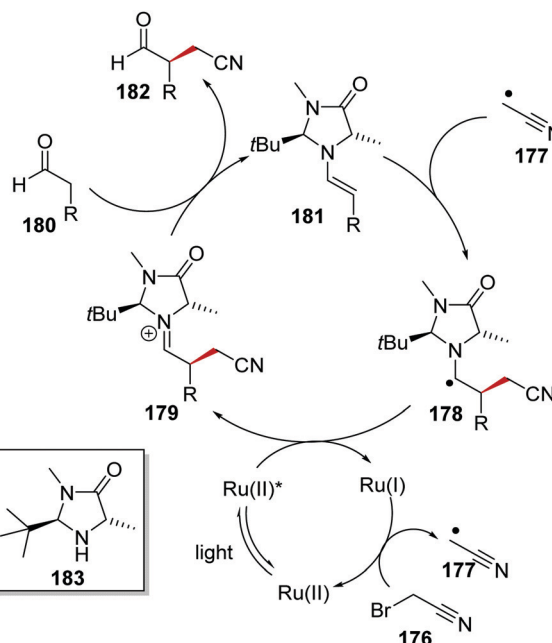
This journal is © The Royal Society of Chemistry 2021

Chem. Soc. Rev., 2021, **50**, 9540–9685 | **9563**

Scheme 39 Radical coupling of heterocycles with diethyl bromomalonate.

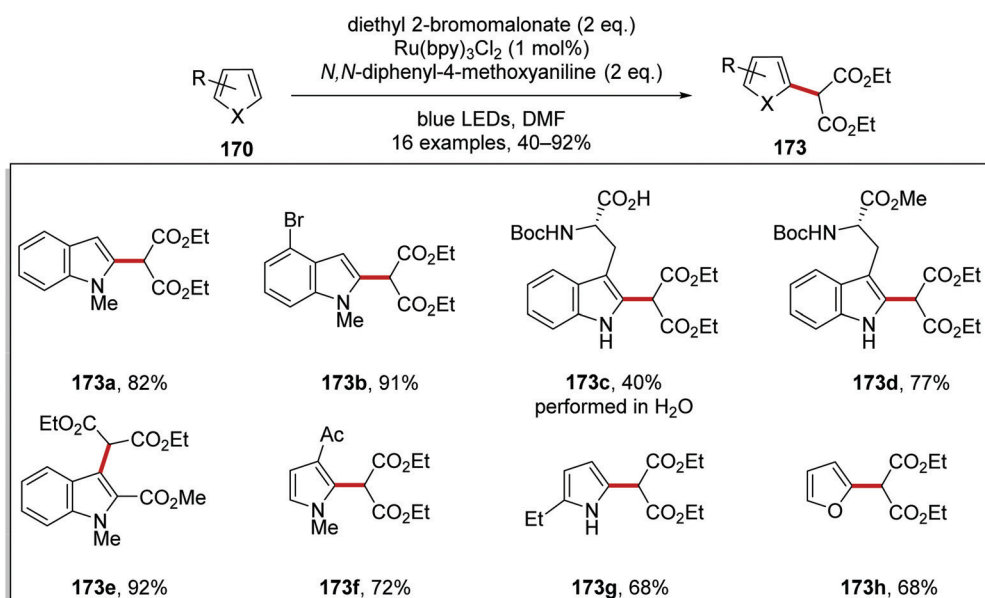Scheme 41 Reaction mechanism between bromoacetonitrile (**176**) and aldehyde **180**.

This methodology allowed for the preparation of 18 enantio-enriched anilines **191** (Scheme 45). High yields and ee were recorded for bromo **191a**, ester **191b** and nitrile **191c** analogues. The reaction was tolerant of heterocyclic motifs; for example, thiophene analogue **191d** was isolated in 42% yield.

Diazoacetates **193** were coupled to 2-acylimidazoles **192** using the same Ru/Rh catalytic system (Scheme 46). This was exemplified by the preparation of 16 coupled products. Ethyl ester **194a** was prepared in 99% yield and with 97% ee using this methodology. Additionally, a geraniol derivative **194b**, L-(−)-borneol derivative **194c** and a cholesterol derivative **194d** were all prepared in the yields stereoselectivities shown in Scheme 45.
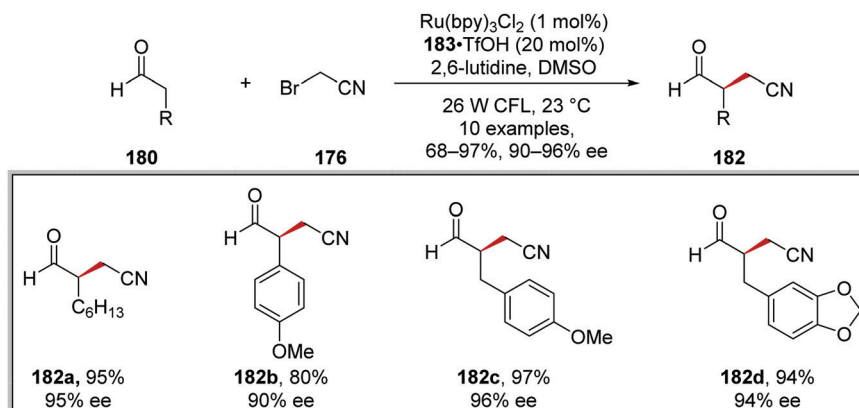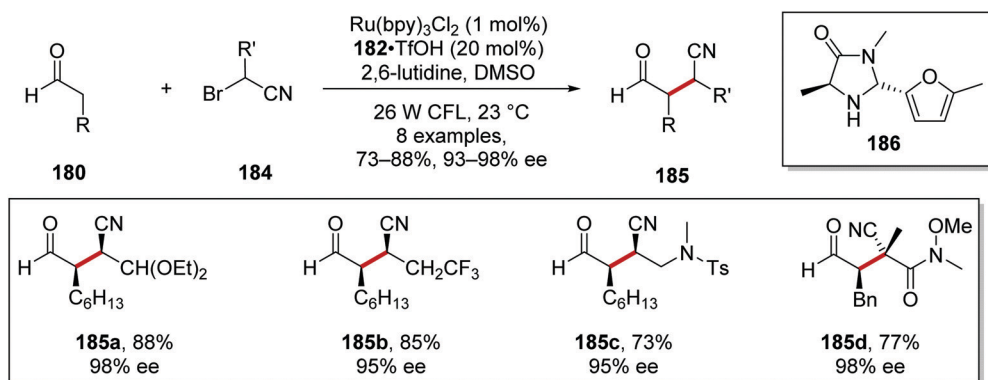
2.2 Catalytic cycles featuring Ru(ɪɪ)/Ru(ɪɪɪ)

The coupling of secondary amines to arenes was achieved with the ruthenium photocatalyst in an HLF-inspired reaction (Scheme 47).[127] The chlorination and protonation of amine **195** gave the compound **197**. This salt received an electron from excited $\text{Ru(ɪɪ)(bpy)}_3\text{(PF}_6)_2$* complex and this gave amine radical cation **198** and Ru(ɪɪɪ) complex. It was clearly demonstrated by the authors that SET would only occur with protonated salt **197** and not with N-chloropiperidine (**196**). Cyclic voltammetry studies found that **196** (E_{red} = −1.80 V vs. SCE, in MeCN) was

Scheme 40 Radical coupling of diethyl malonate to heteroarenes.

9564 | Chem. Soc. Rev., 2021, **50**, 9540–9685

This journal is © The Royal Society of Chemistry 2021

Scheme 42 Substrate scope for the coupling of aldehydes **180** and bromoacetonitrile (**176**).

Scheme 43 Scope of the α-bromonitriles **184**.

unable to be reduced by Ru(II)* (E_{ox}* = −0.81 vs. SCE) but SET was very feasible with **197** (E_{red} = +0.43 V vs. SCE). Addition of the electron-poor radical **198** to electron-rich arene **199b** resulted in para-substituted radical **200b**, which was oxidised by Ru(III) forming anilinium salt **201b** following loss of one proton.

N-Chloroamine salt **197** is well known to chlorinate nucleophiles through S_N2 attack at the Cl atom (i.e. a non-radical mechanism). Therefore, it was crucial to develop reaction conditions that would exclusively produce the desired C–N product **202** and not the unwanted C–Cl product **203** (Table 2 and Scheme 48). This would require that the species **197** is susceptible to rapid reduction to **198** by the photoredox agent and also that the radical **198** does not lose a proton to become a neutral aminyl radical (this would be far less reactive towards arenes). Therefore the acidity of the reaction medium is crucial. Successful amination also depends on the nucleophilicity of the arene. If this is too nucleophilic, then it may attack **197** before the transformation to **198** can occur.

To study the reaction, tert-butylbenzene **199a** and anisole **199b** were chosen as substrates of moderately and highly electron-rich arenes, respectively. A range of different acids and solvents was tested to ascertain the best conditions for the formation of **202**. Initially, the use of acetic acid (entry 1, Table 2) gave no aniline or aryl chloride products for both substrates. The use of TFA (entry 2) gave no product formation for **202b** but it did provide

4-chloroanisole **203b** in 17% yield. p-TsOH (entry 3) gave unwanted product **203b** in 90% yield. When the superacid, perchloric acid, was used (entry 4) this gave exclusive aniline formation for both substrates with **202a** in 71% yield and **202b** in 94% yield. Further investigation demonstrated that using HFIP as solvent (entry 5) showed interesting but complex results; thus it gave an increased yield of 98% for **202a** relative to MeCN. Furthermore, HFIP allowed for the more convenient acid, TFA, to be used as the acid for moderately electron-rich arene substrates, with **202a** being prepared in 88% yield.

The optimised reaction conditions were used to investigate the scope of the reaction. The reaction accommodated a wide range of substrates, with the preparation of 103 coupled amine compounds (Scheme 48 for selected examples). With piperidine as the amine, various functionalised aryl compounds were employed giving coupled compounds in 21–99% yields, e.g. **202c–f** in Scheme 48. An assorted selection of secondary amines provided successful substrates for this reaction giving products in 40–99% yields, e.g. **202g–k**. The reaction also found a use in late-stage functionalisation of complex compounds; this resulted in the isolation of bioactive derivatives **202l–n** in the yields shown.

N-Centred radicals were formed from reaction of N-sulfonamidopyridinium salts with Ru(bpy)₃Cl₂ photocatalyst.[128] These N-centred radicals were then used to functionalise arenes
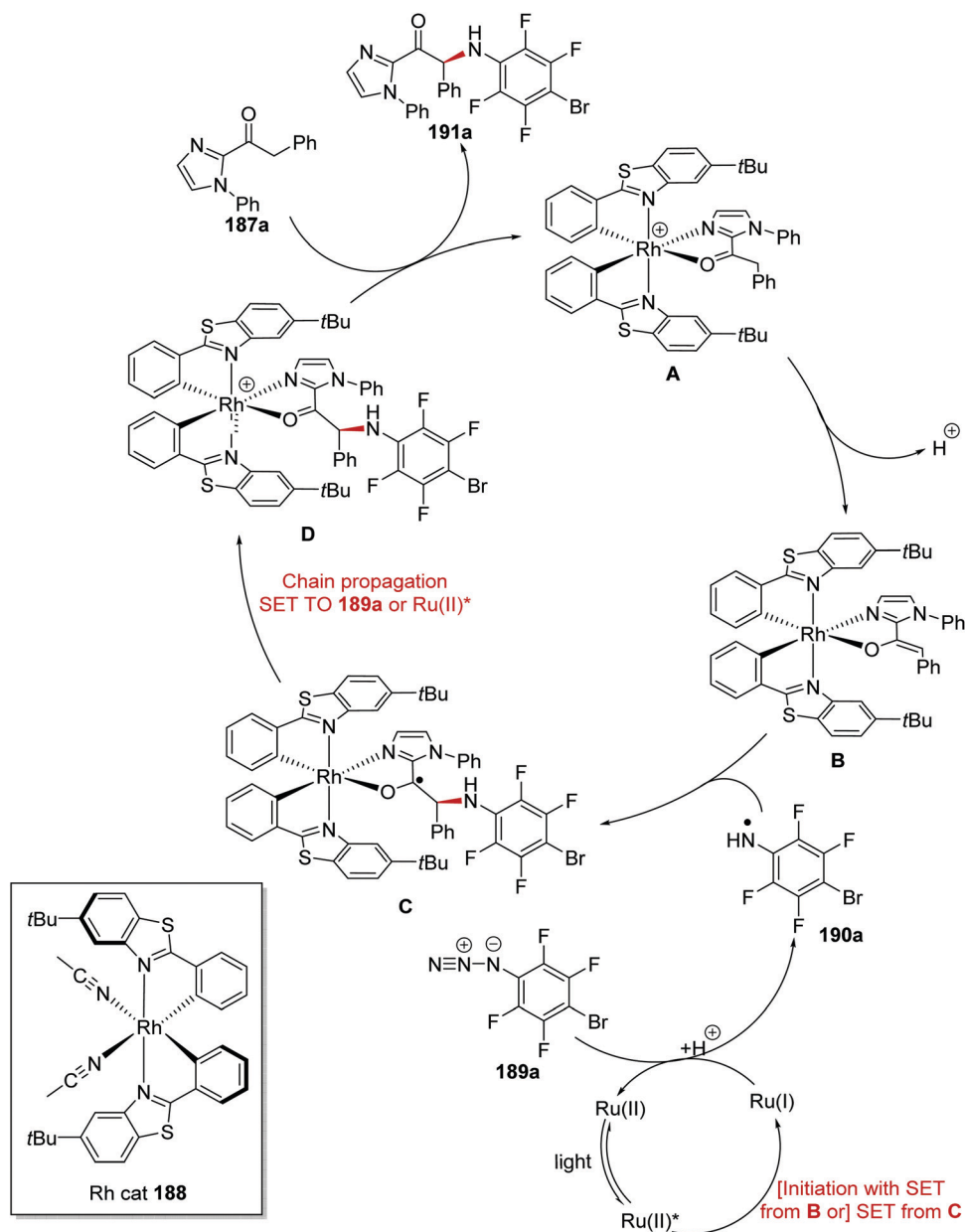
Scheme 44   Stereocontrolled coupling of azide **189a** to ketone **187a**.

and heterocycles without any pre-functionalisation. For example, *N*-sulfonamidopyridinium **204a** was used to functionalise *N*-methylindole **205a** and this produced sulfonamide **206a** (Scheme 49). Irradiation of the reaction mixture with blue light yielded excited Ru(II)* complex from the original Ru(bpy)$_3$Cl$_2$ complex. SET from Ru(II)* to **204a** resulted in N–N bond breakage which led to 2,4,6-collidine (**207a**) and nitrogen-centred radical **208a**. The excited photocatalyst Ru(bpy)$_3{}^{2+}$ ($E_{ox}{}^* = -0.81$ V *vs.* SCE)[8b] was able to reduce pyridinium salt **204a** ($E_{red} = -0.70$ V *vs.* Ag/Ag$^+$).[128] Regioselective addition of **208a** to *N*-methylindole (**205a**) resulted in carbon-centred radical **209a**. A second electron transfer to Ru(III) from **209a** closed the ruthenium catalytic cycle while cation **210a** was formed. Proton loss gave sulfonamide **206a** as the observed product.

Alongside sulfonamide **206a** which was isolated in 86% yield, 19 other functionalised compounds were prepared with this methodology (Scheme 50). A range of indole functionalised compounds was used as substrates and yielded sulfonamides **206b–d**. *N*-Aryl indoles were amenable under these conditions and aryl iodide **206e** was produced in 84% yield. When *N*-methylpyrrole was used in the reaction, compound **206f** was isolated in 71% yield. However, the substituent upon the nitrogen atom of the indole heterocycle had a significant influence upon the efficiency of the reaction. While ester **206g** was formed in 70% yield, the use of *N*-Boc and *N*-Ac indole gave no reaction, presumably due to ring deactivation. Finally, the synthetically useful *N*-Boc derivative **206j** was prepared in 61% yield when a Boc analogue of **204a** was used.
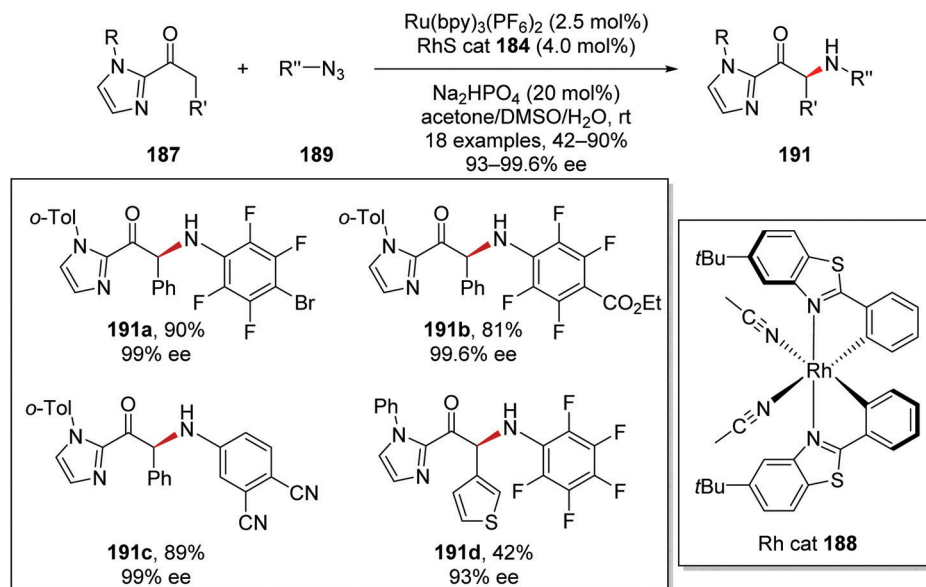
Scheme 45 Scope of products from Ru/Rh tandem catalytic coupling of ketones **187** with azides **189**.
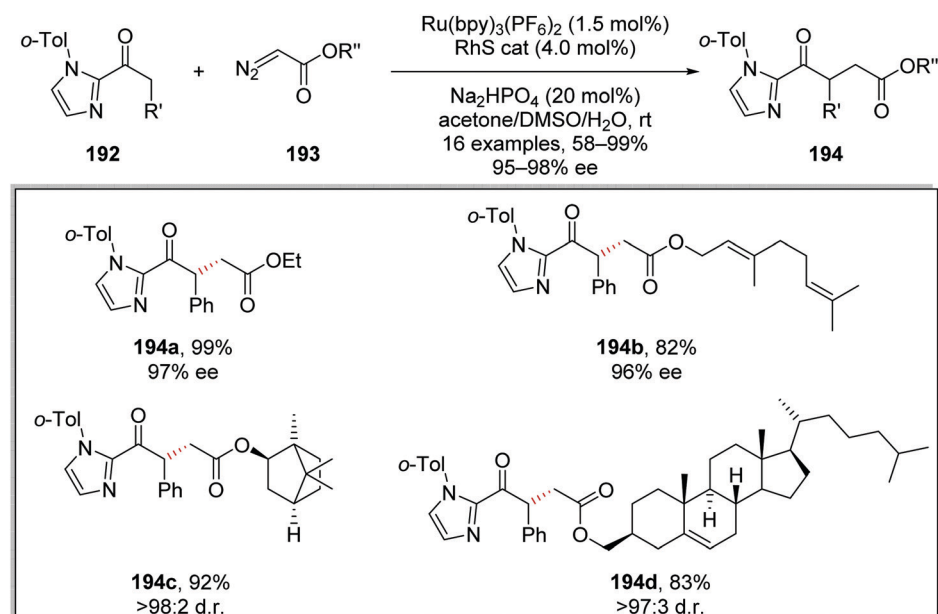
Scheme 46 Substrate scope of Ru/Rh tandem catalytic coupling of ketones **192** to diazoacetates **193**.
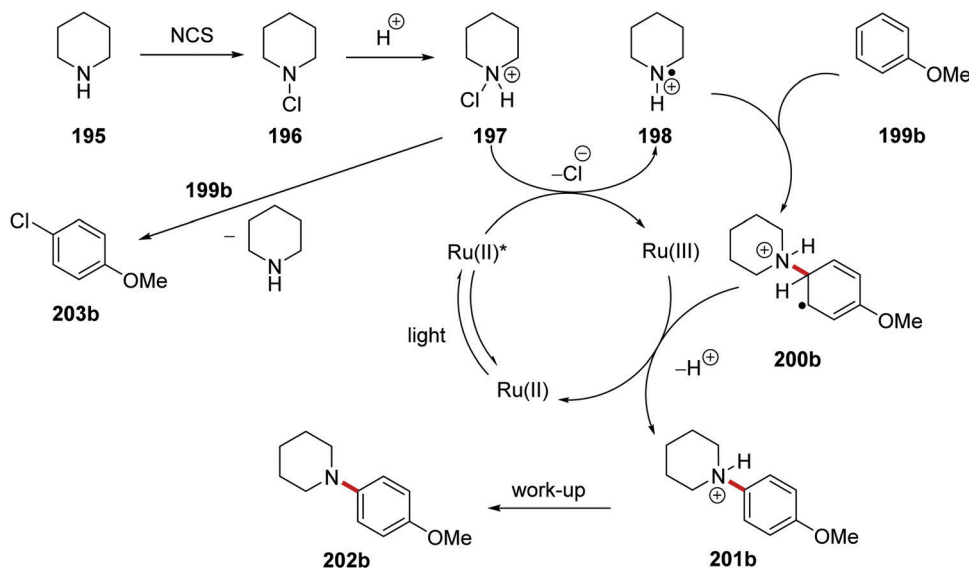
Furthermore, phthaloyl reagent **213** was used to prepare imides **212** from arenes **211** when used with Ru(bpy)$_3$Cl$_2$ (Scheme 51). The reaction was very successful with 12 imide compounds being prepared in 46–89% yield, although compounds **212b** and **212d** were isolated as a mixture of regioisomers. The reaction also tolerated heterocycles, and furan product **212h** was prepared in 46% yield.

The catalyst Ru(bpy)$_3$(PF$_6$)$_2$ was used as an electron donor in the generation of pyridyl radical cations **215** from *N*-(trifluoromethyl-sulfonyloxy)pyridinium salt **214**.[129,130] Irradiation of the reaction mixture with blue light led to excited Ru(II)* species (Scheme 52). SET gave pyridyl radical **215a** ($E_{red} = -0.14$ V *vs.* SCE)[130] and a Ru(III)

complex from Ru(II)* ($E_{ox}^* = -0.81$ V *vs.* SCE)[8b] species and triflate salt **214a**. Heterolytic N–O bond cleavage in **215a** formed triflate anion and pyridyl radical cation **216a**. Addition to arene **217a** formed the key C–C bond giving radical **218a**. The ruthenium catalytic cycle was closed with SET to Ru(III) complex from **218a**, this gave the original Ru(II) complex and, following proton loss, pyridinium **219a**.

The pyridinium salts **219** were utilised in a range of different reactions (Scheme 53).[129] Methylmagnesium chloride led to selective C2 alkylation and the combination of trichloroacetic anhydride and then sodium methoxide gave ester **220a** in 76% yield. Treatment of **219a** with piperidine resulted in aniline

This journal is © The Royal Society of Chemistry 2021

Chem. Soc. Rev., 2021, **50**, 9540–9685 | 9567

Scheme 47 Aryl coupling of secondary amines.

Table 2 Reaction optimisation, n.d. = not detected (where relevant, asterisk * indicates the alternative site of attachment of the amine)

			R = tBu		R = OMe	
Entry	Acid	Solvent	Ar-NR$_2$ ($p:o$)	Aryl-Cl	Ar-NR$_2$ ($p:o$)	Aryl-Cl
1	AcOH	MeCN	n.d.	n.d.	n.d.	n.d.
2	TFA	MeCN	n.d.	n.d.	n.d.	17%
3	p-TsOH	MeCN	n.d.	n.d.	n.d.	90%
4	HClO$_4$	MeCN	71% (3:1)	n.d.	94% (3:2)	n.d.
5	HClO$_4$	HFIP	98% (7:1)	n.d.	n.d.	79%
6	TFA	HFIP	88% (10:1)	n.d.	n.d.	55%

221a being isolated in 58% yield from triflate **214a** *via* a Zincke reaction. *N*-Arylated piperidine **222a** was produced in 74% yield after **219a** was exposed to hydrogenation conditions with Adam's catalyst (PtO$_2$). Diene **223a** was the product following treatment of **219a** with sodium borohydride in 86% yield.

Typical conditions for this transformation included the use of Ru(bpy)$_3$(PF$_6$)$_2$ (2 mol%) in MeCN and irradiation with blue light.[129] The pyridinium products were converted *in situ* to anilines with use of piperidine (10 eq.) and this allowed for the preparation of 14 anilines **221** in yields ranging from 28% to 59% (Scheme 54).

2.3 Ru energy transfer reactions

Formation of oxazolidinone **230** was achieved with an energy transfer strategy from carbamate **224** *via* nitrene intermediate under basic conditions.[131] Carbamate **224a** was deprotonated with potassium carbonate and this gave anion **225a** (Scheme 55). The Ru(bpy)$_3$(PF$_6$)$_2$ catalyst was excited with blue light. An energy

transfer to **225a** (E_T = 40.1 kcal mol^{-1}) from Ru(ɪɪ)* (E_T = 47.7 kcal mol^{-1}) resulted in N–O heterolytic bond cleavage and nitrene **226a** and carboxylate **227a** were formed. This bond cleavage was supported by DFT calculations. An intramolecular HAT to the nitrene in **226a** resulted in triplet diradical **228a**. ISC delivered singlet diradical **229a** from **230a**, and subsequent radical coupling gave lactam **230a**.

The reaction was initially trialled with azidoformate **231a** which had a triplet energy of 50.6 kcal mol^{-1} (Table 3). However, the use of commercial iridium and ruthenium photoredox catalysts resulted in either no formation of oxazolidinone **230a** or trace amounts (Table 3, entries 1–4), with carbamate **232a** being formed instead. It was postulated that the poor efficiency of this reaction was due to incompatible triplet sensitisation. Therefore, other nitrene precursors were examined, such as **224a**, which had triplet energy of 40.1 kcal mol^{-1} and a smaller singlet reorganisation energy. The combination of **224a** and the Ru(bpy)$_3$(PF$_6$) photocatalyst gave desired oxazolidine **230a** in 70% isolated yield.
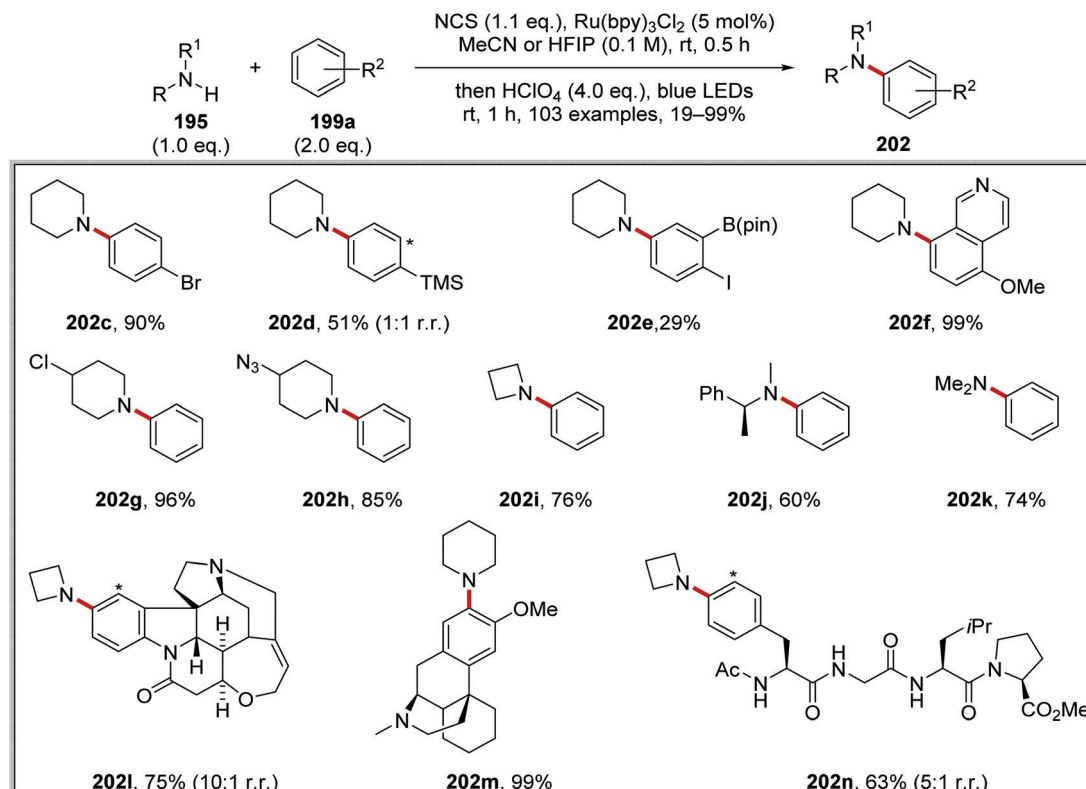
Scheme 48 Substrate scope for secondary amines coupling to arenes. (Asterisk * indicated alternative site for incoming group.)
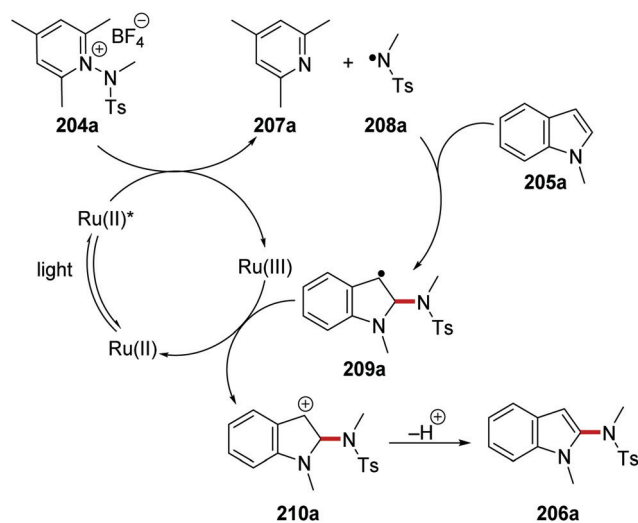
Scheme 49 Generation of sulfonamidyl radicals from pyridinium derivatives.

With optimised conditions in hand, the substrate scope of the reaction was investigated. A range of 33 oxazolidines and lactams **230** was prepared from **224** (Scheme 56). Functional groups like alkynes were also accommodated under the reaction conditions as seen with product **224h** and polycyclic compounds like **230e**, **230i** and **230j** were also prepared.

Iridium. As with ruthenium(ɪɪ) complexes, photoexcited iridium(ɪɪɪ) complexes can act as electron acceptors, in this case

resulting in a catalytic cycle that shuttles between Ir(ɪɪɪ) and Ir(ɪɪ), or as electron donors, leading to a cycle that incorporates Ir(ɪɪɪ) and Ir(ɪᴠ).
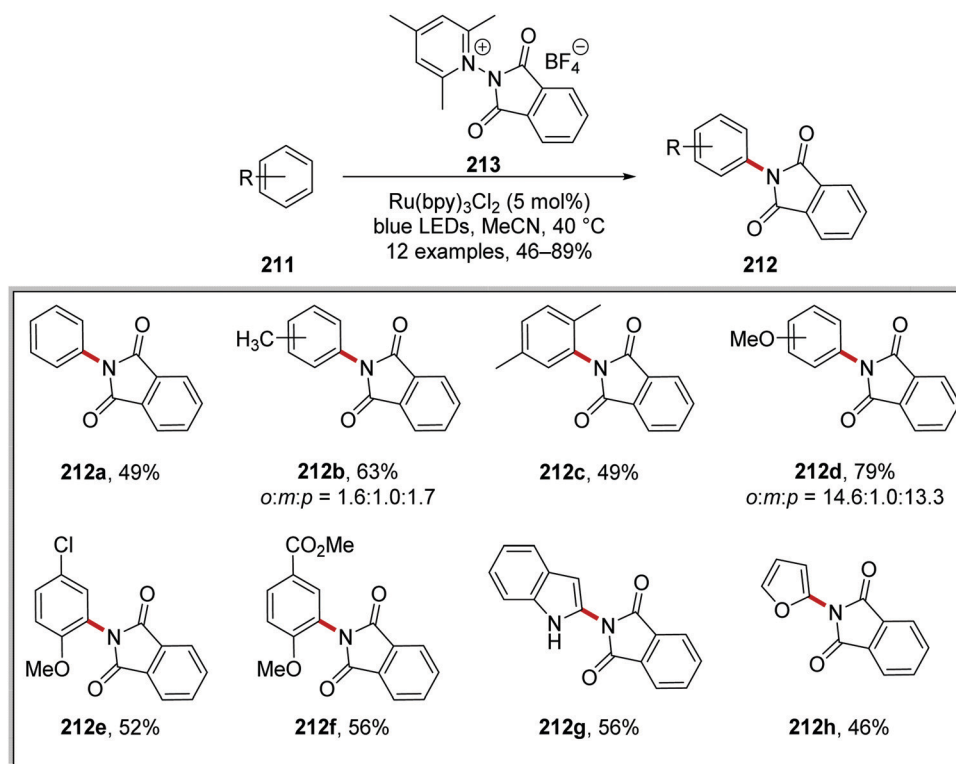
2.4 Catalytic cycles featuring Ir(ɪɪɪ)/Ir(ɪɪ)

Decarboxylation of carboxylic acids. The decarboxylation of aliphatic carboxylic acids with iridium photoredox catalysis is a very successful strategy at generating carbon-centred radicals. For example, a Giese coupling reaction of carboxylate-derived radicals with electron-poor alkenes has been reported (Scheme 57).[132] Under the reaction conditions, carboxylic acid **231a** was deprotonated with the phosphate base and this gave carboxylate **232a**. Carboxylates (Boc-Pro-OCs, E = +0.95 V $vs.$ SCE)[134] can be oxidised by the excited Ir(ɪɪɪ)* complex (E_{red}* = +1.21 V $vs.$ SCE) and thus carboxyl radical **233a** and reduced Ir(ɪɪ) species were formed SET. Decarboxylation of radical **233a** gave the electron-rich radical **234a** which added to the electron-poor alkene **235a** and this gave α-keto radical **236a**. The iridium catalytic cycle was closed with a SET between **236a** and Ir(ɪɪ) complex which regenerated the original Ir(ɪɪɪ) complex as well as anion **237a**. Protonation of **237a** led to the ketone **238a**.

As stated, this reaction allowed for the coupling of carboxylic acids **231** to electron-poor alkenes **235** and this resulted in the formation of C_{sp^3}–C_{sp^3} coupled products **238** (Scheme 58). The wide applicability of this reaction was proven with the synthesis of 35 compounds. Whilst the alkene had to be conjugated to an electron-withdrawing group, it was shown that ketones, esters, amides, and sulfones could all be utilised as electron-withdrawing

This journal is © The Royal Society of Chemistry 2021

Chem. Soc. Rev., 2021, **50**, 9540–9685 | 9569
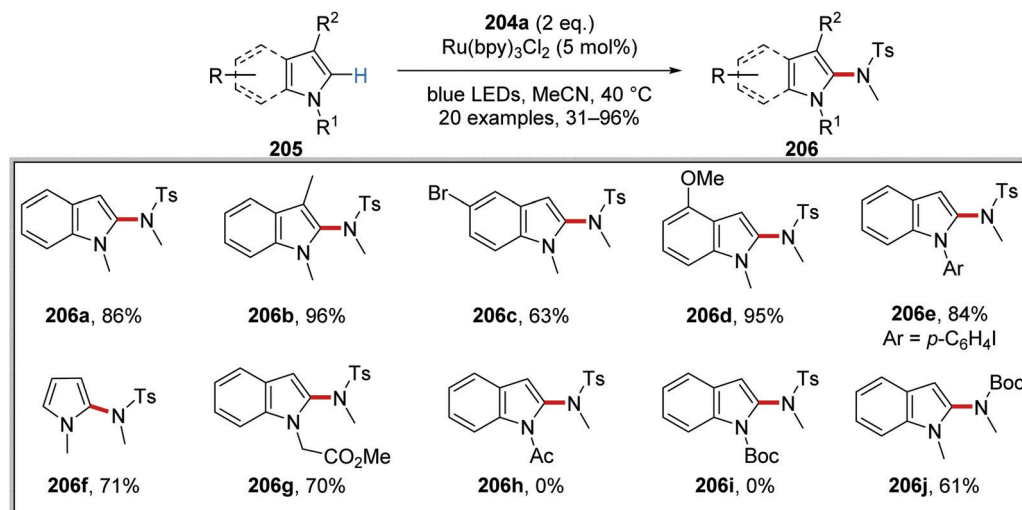
Scheme 50 Substitution of indoles and pyrroles.

Scheme 51 Phthalimidation of arenes.

groups (EWGs) with the preparations of **238a–d**. Different aliphatic carboxylic acids were also used in this reaction, as seen in the preparation of **238e–h** in 57–95% yields.
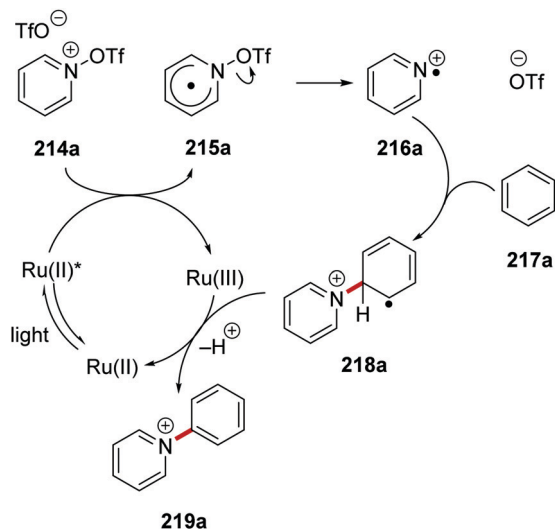
The synthetic utility of this reaction was demonstrated in the macrocyclisation of peptides (Scheme 59).[133] Treatment of alkene-derived peptide **239** with the optimised reaction conditions led to cyclised peptide **240** in 46% yield, using a commercially available iridium photocatalyst with catalytic loadings (20 mol%).

Carboxylic acids **241** were coupled to aryl halides **245** with use of an iridium and nickel catalytic system.[134] Akin to the

formation of radical **234** (Scheme 57), radical **244a** was formed from *N*-Boc amine **242a** (Scheme 60). A Ni(0) complex intercepted radical **244a** and a Ni(i) complex was formed. Oxidative addition of the Ni(i) complex to **245a** gave a Ni(iii) complex and this underwent reductive elimination, which gave the functionalised amine product **246a**. Both Ir and Ni catalytic cycles were closed with SET between Ir(ii) and Ni(i) complexes.

From this reaction, a wide range of coupled compounds was prepared in 60–93% yields, (Scheme 61 for **246a-I** as selected examples).[134] It should be noted that compounds **246a** and

9570 | *Chem. Soc. Rev.*, 2021, **50**, 9540–9685

This journal is © The Royal Society of Chemistry 2021

Scheme 52 Formation of pyridine radical cation from **214a**, and subsequent coupling.

246b were prepared from the aryl iodide, whereas compounds **246c–h** were prepared from the aryl bromides and compound **246i** was prepared from the aryl chloride.
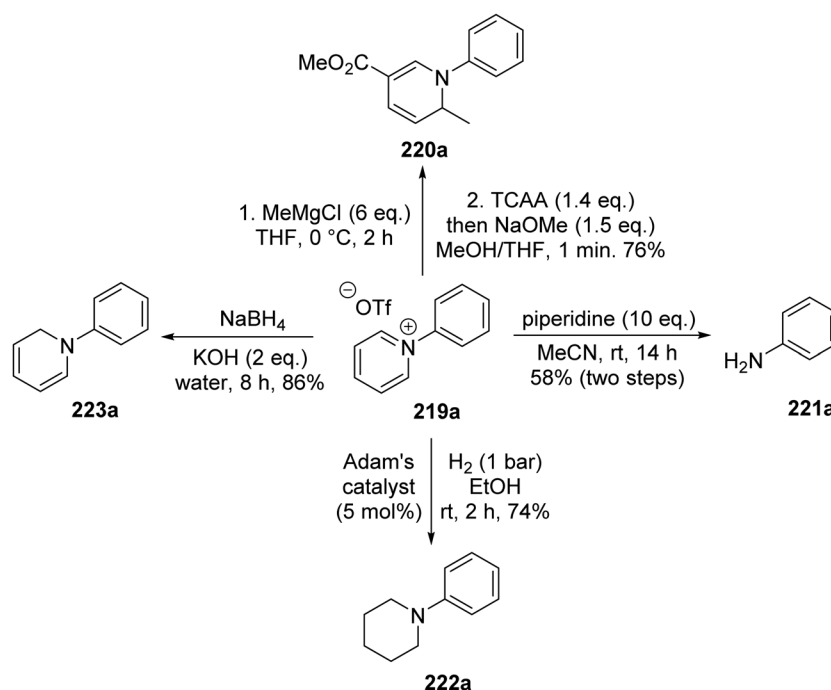
The coupling of carbon-centred radicals derived from carboxylic acids **247** with vinyl halides **251** was achieved with a similar nickel and iridium catalytic system and this gave alkene products **252** (Scheme 62).[135] Deprotonation of the acid to its carboxylate salt **248** (not shown) was followed by oxidation to the carboxyl radical **249** and decarboxylation to aliphatic radical **250**. The Ni-mediated coupling of vinyl halides **251** to these radicals was a very facile process and 22 alkenes **252** were

isolated in 60–96% yields. A vinyl bromide was used in the preparation of compound **252d**, whereas the other products were prepared from the vinyl iodide. This transformation was tolerant of functional groups **252b**, silyl groups **252d** and Boc-protected amines **252f** and **252g**.

Radical coupling to alkynes **253** was achieved using a similar iridium and nickel catalytic system (Scheme 63).[136] It was found that the use of 1,1,3,3-tetramethylguanidine (TMG) allowed for successful coupling and this produced alkenes **254**. The reaction allowed for the preparation of chloro **254b**, hydroxy **254c**, silyl **254d**, ketal **254g**, ester **254f** analogues. A diminished yield of secondary *N*-Boc amine was observed with **254h** (41% yield).

Enantioenriched amine derivatives **257** were prepared from the coupling of carboxylic acids **255** with aryl bromides **256** (Scheme 64).[137] The use of a chiral ligand **258** gave high yields and high levels of enantiopurity as exemplified with products **257a–h**.

An iridium- and nickel-mediated C_{sp^3}–C_{sp^3} coupling reaction between carboxylic acids **258** and alkyl bromides **259** was reported (Scheme 65).[138] This reaction was based upon the transformation discussed in Scheme 61. However, it was found that the reaction conditions had to be modified. The use of Cs_2CO_3 as base in DMF led to ester formation between carboxylic acid **258** and alkyl bromide **259**. After an extensive solvent screen, it was found that K_2CO_3 in MeCN allowed for the formation of **260a** in 68% GC yield. The use of the more electron-rich ligand 4,4′-dimethoxy-2,2′-bipyridine (4,4′-dMeO-bpy) increased the GC yield to 74% over dtbbpy ligand. The inclusion of water (20 eq.) in the reaction mixture, further suppressed ester formation, giving **260a** in 96% GC yield and 85% isolated yield. The synthetic utility of this reaction was seen with the preparation of alcohol **260d**,

Scheme 53 Transformations of pyridinium salt **219a**.

This journal is © The Royal Society of Chemistry 2021

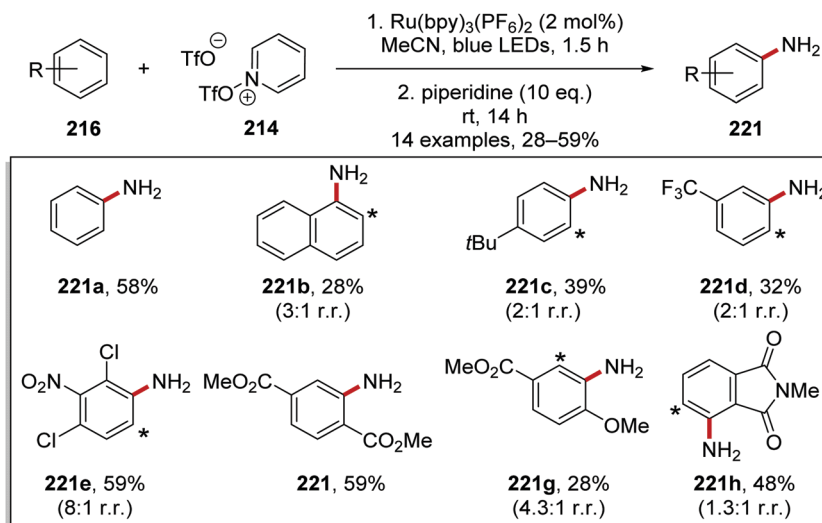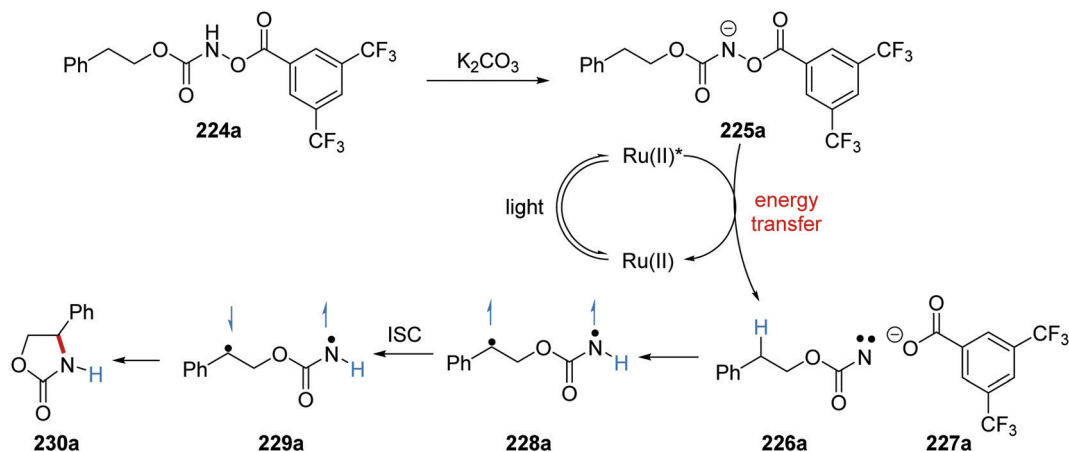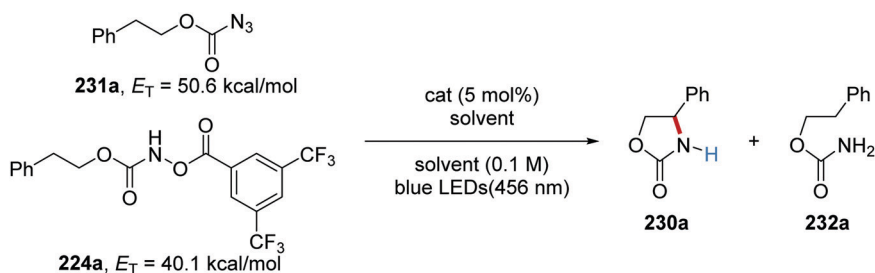*Chem. Soc. Rev.*, 2021, **50**, 9540–9685 | **9571**

Scheme 54 Synthesis of anilines **221** from arenes **216**. (Asterisk * marks alternative site of attachment.)

Scheme 55 Oxazolidinone ring formation from carbamate **224a**.

Table 3 Optimisation of oxazolidinone formation

Entry	Substrate	Catalyst	E_T, kcal mol^{-1}	Solvent	Yield of **230a** (%)	Yield of **232a** (%)
1	**231a**	Ru(bpy)$_3$(PF$_6$)$_2$	47.7	CH$_2$Cl$_2$	<5	<5
2	**231a**	Ir(ppy)$_2$(dtbbpy)(PF$_6$)	51.0	CH$_2$Cl$_2$	<5	18
3	**231a**	Ir(ppy)$_3$	55.4	CH$_2$Cl$_2$	5	16
4	**231a**	Ir[dF(CF$_3$)ppy]$_2$dtbbpy(PF$_6$)	61.0	CH$_2$Cl$_2$	<5	13
5	**224a**	Ru(bpy)$_3$(PF$_6$)$_2$	47.7	(CHCl$_2$)$_2$	70	N/A

9572 | *Chem. Soc. Rev.*, 2021, **50**, 9540–9685

This journal is © The Royal Society of Chemistry 2021
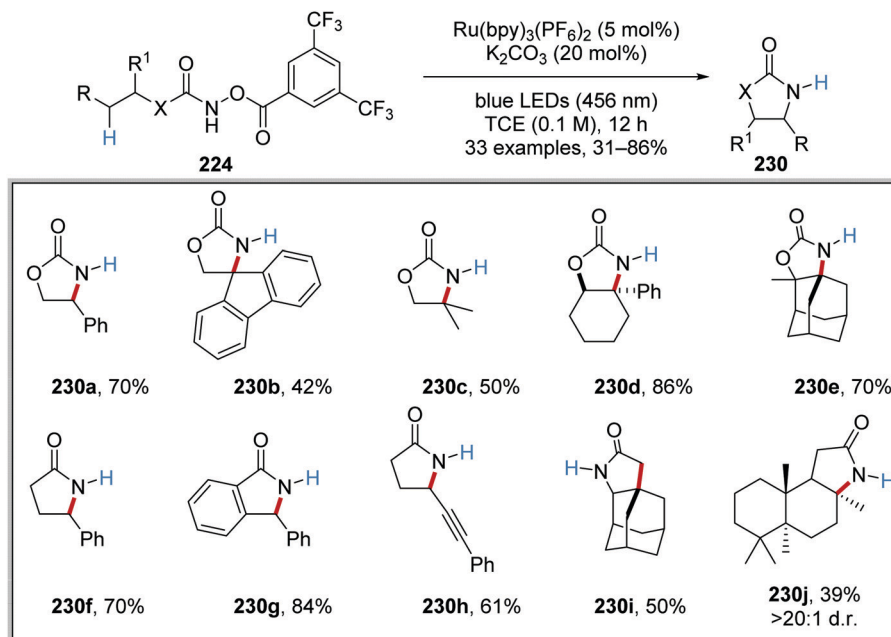
Scheme 56 Substrate scope for oxazolidinone synthesis.
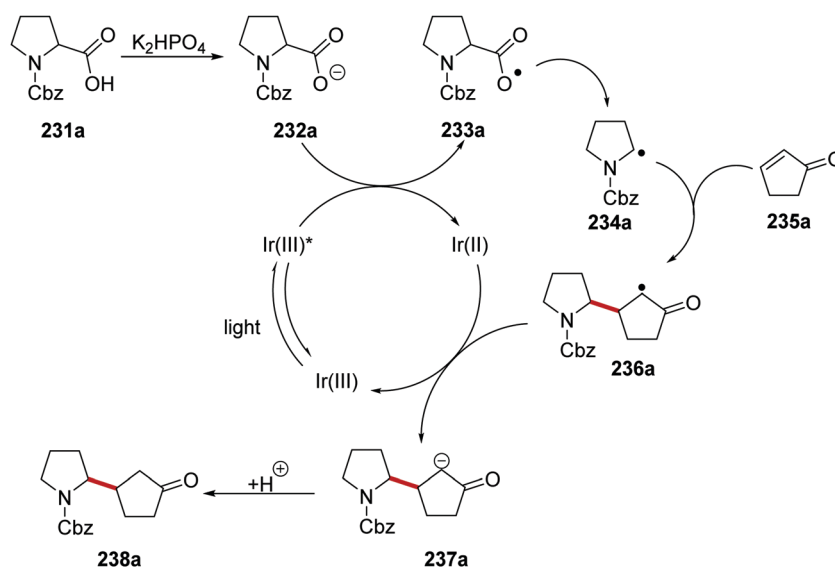
Scheme 57 Decarboxylative radical coupling to electron-poor alkenes.

aldehyde **260e**, ester **260f** and **260j**, epoxide **260g** and chloroalkane **260h** analogues.

The acylation of aryl halides **265** with α-oxo carboxylic acids **261** under an iridium and nickel catalytic system was developed.[139] Under the reactio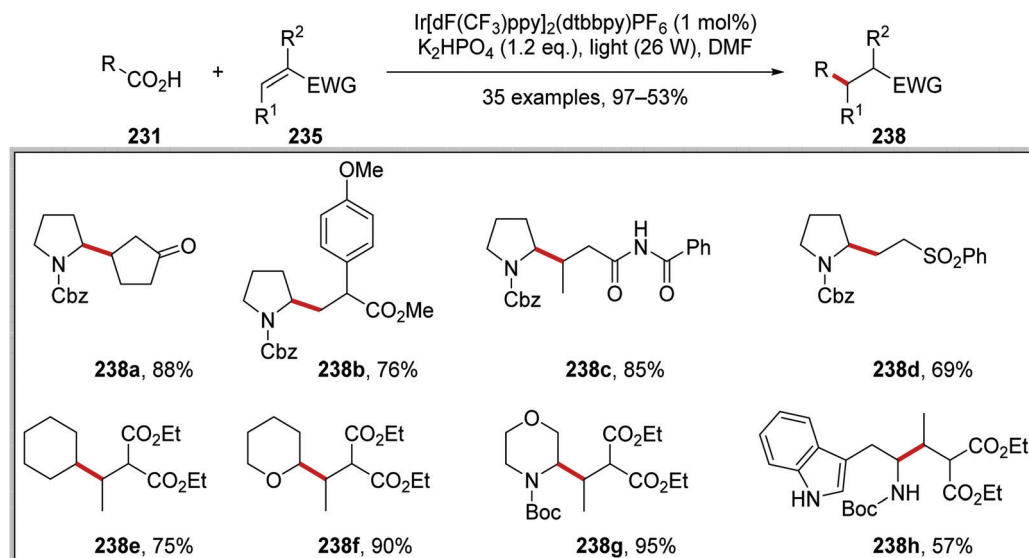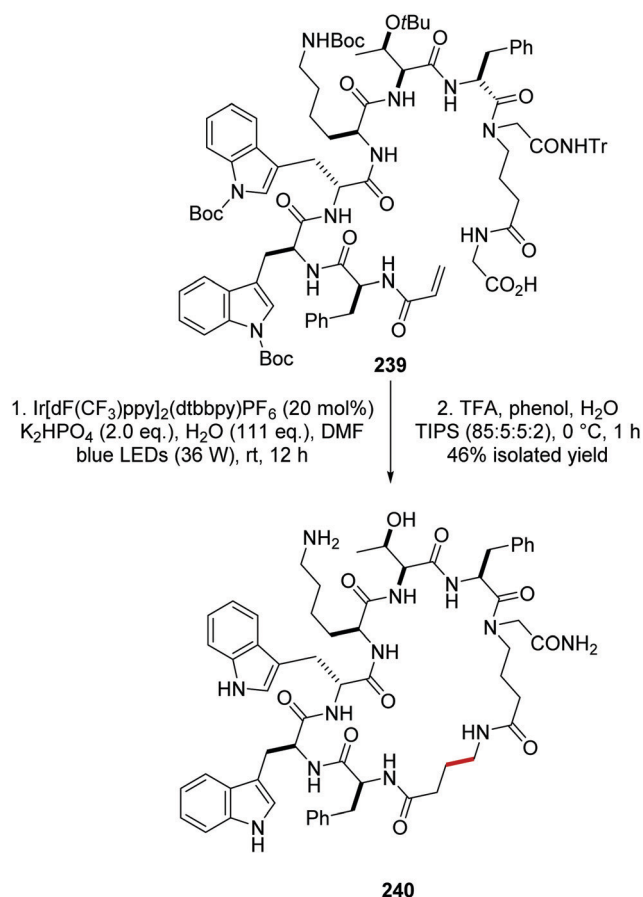n conditions, the carboxylate **262a** was formed from carboxylic acid **261a** and lithium carbonate (Scheme 66). SET between excited Ir(III)* complex (E_{red}^* = +1.21 V *vs.* SCE) and **262a** ($E_{1/2}$ = +1.03 V *vs.* SCE) resulted in carboxyl radical **263a** and the Ir(II) species. Decarboxylation of **263a** gave acyl radical **264a**. The presence of the nickel catalyst allowed for cross-coupling between **264a** and 4-bromotoluene (**265a**) and this gave ketone **266a**.

From optimisation studies, it was found that improved yields of **266** were obtained when lithium carbonate, rather than caesium carbonate, was used as base. Increased yields were also isolated when a more powerful blue light source was used, and so it was inferred that the reaction was photon-limited. The ^{1}H-NMR yield of **266c** was increased to 84% from 74% when 2 eq. of water were added to the reaction mixture. Higher loading of Ir[dF(CF$_3$)ppy]$_2$dtbby from 1 mol% to 2 mol% gave the optimal ^{1}H-NMR yield of **266c** (88%) and it was isolated in 80% yield (Scheme 67). Various α-oxoacids **261** and aryl halides could be used in this reaction giving ketones **266a–i**.

This journal is © The Royal Society of Chemistry 2021

Chem. Soc. Rev., 2021, **50**, 9540–9685 | 9573

Ir[dF(CF$_3$)ppy]$_2$(dtbbpy)PF$_6$ (1 mol%)
K$_2$HPO$_4$ (1.2 eq.), light (26 W), DMF

35 examples, 97–53%

Scheme 58 Products of decarboxylative radical coupling to electron-poor alkenes.

238a, 88% 238b, 76% 238c, 85% 238d, 69%

238e, 75% 238f, 90% 238g, 95% 238h, 57%

Scheme 59 Radical macrocyclisation of peptide **239**.

1. Ir[dF(CF$_3$)ppy]$_2$(dtbbpy)PF$_6$ (20 mol%)
K$_2$HPO$_4$ (2.0 eq.), H$_2$O (111 eq.), DMF
blue LEDs (36 W), rt, 12 h

2. TFA, phenol, H$_2$O
TIPS (85:5:5:2), 0 °C, 1 h
46% isolated yield

Ketones **270** were prepared with the combination of carboxylic acids **267**, DBU and acyl chlorides **268**, under an iridium and nickel catalytic system (Scheme 68).[140] The combination of **267a** and **268a** under basic conditions gave anhydride **269a**.

Interception of **269a** with a Ni(0) complex led to a Ni(II) complex. Loss of an electron, to an excited Ir(III)* complex, and carbon dioxide led to the formation of a Ni(II) complex. Reductive elimination of Ni complex led to ketone compound **270a** and a Ni(I) complex. An outer-sphere electron transfer between Ir(II) species and Ni(I) species closed both catalytic cycles as both the original Ni(0) and Ir(III) complexes were reformed.
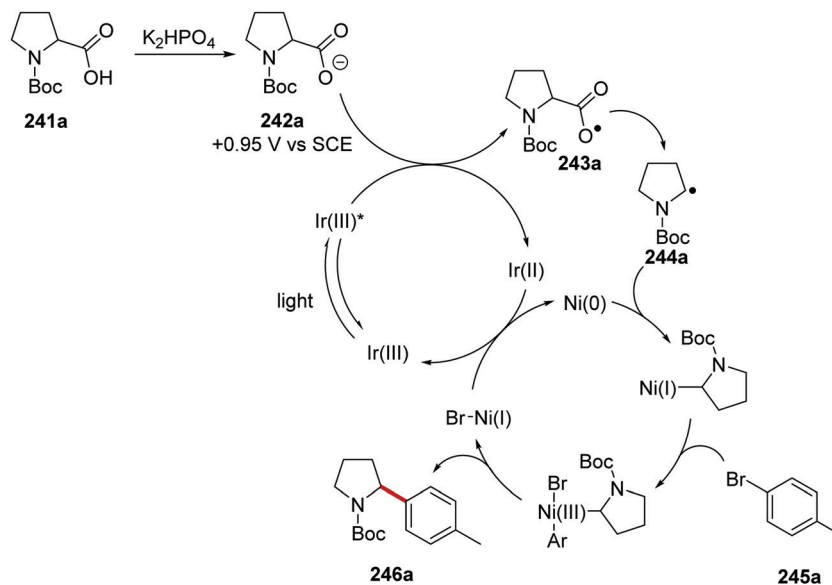
This transformation worked well as demonstrated with the preparation of 30 alkyl ketones **270** in yields ranging from 32% to 86%. (Scheme 69). The reaction was functional group-tolerant with nitrile **270b**, alkene **270c**, anisole **270d**, and *tert*-butyl **270e** analogues all being prepared. Various carboxyl radical precursors were used in this reaction and *N*-Boc tertiary amine **270j**, *N*-Boc secondary amine **270f**, tetrahydrofuran **270g**, alkyl **270h** and **270i** derivatives were all prepared.

Oxalate decarboxylation. Alcohols **271** were used as radical precursors *via* oxalate **272** *via* a radical decarboxylation reaction.[141,142] Oxalates such as **272a** were prepared by reacting alcohol **271a**, with oxalyl chloride and after quenching the reaction mixture with water, this gave compound **272a** in 99% yield (Scheme 70).

Coupling of oxalates **272** with aryl bromides **276** was accomplished with an iridium and nickel catalytic system.[142] Oxalate **272a** was deprotonated with caesium bicarbonate and this gave anion **273a** (Scheme 71). The iridium photocatalyst was excited with blue light and this afforded Ir(III)* species. A SET to Ir(III)* [Ir(dFppy)$_2$(ptbbpy)PF$_6$, E_{red}* = +1.1 V *vs.* SCE] from **273a** ($E_{p/2}$ = +1.26 V *vs.* SCE) gave Ir(II) species and radical **274a**, which underwent decarboxylation and alkyl radical **275a** was formed. The nickel catalyst intercepted radical **275a** and giving a Ni(I) complex. Oxidative addition of aryl bromide **276a** gave a Ni(III) species, which underwent reductive elimination giving coupled product **277a**.

The reaction of oxalates **272** with aryl bromides **276** was a highly facile reaction with the preparation of 33 coupled compounds **277** in yields of 37–91% (Scheme 72). A wide range

9574 | *Chem. Soc. Rev.*, 2021, **50**, 9540–9685

This journal is © The Royal Society of Chemistry 2021

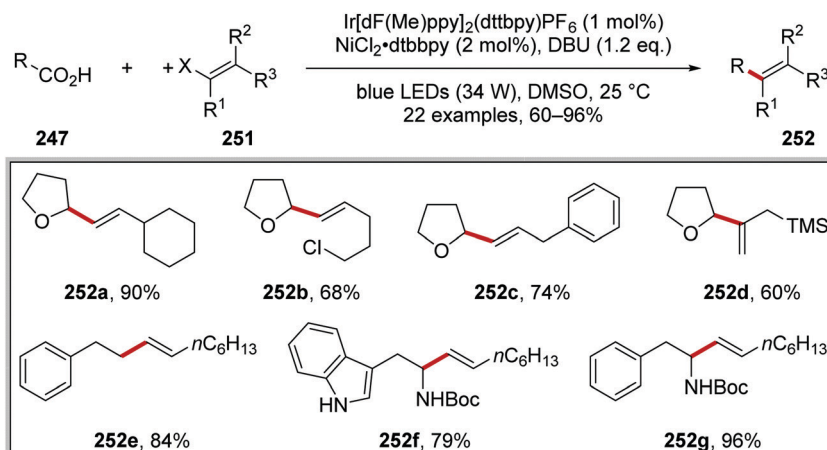**Scheme 60** Mechanism of radical coupling between carboxyl acid radical precursor **241a** and aryl halide **245a**.
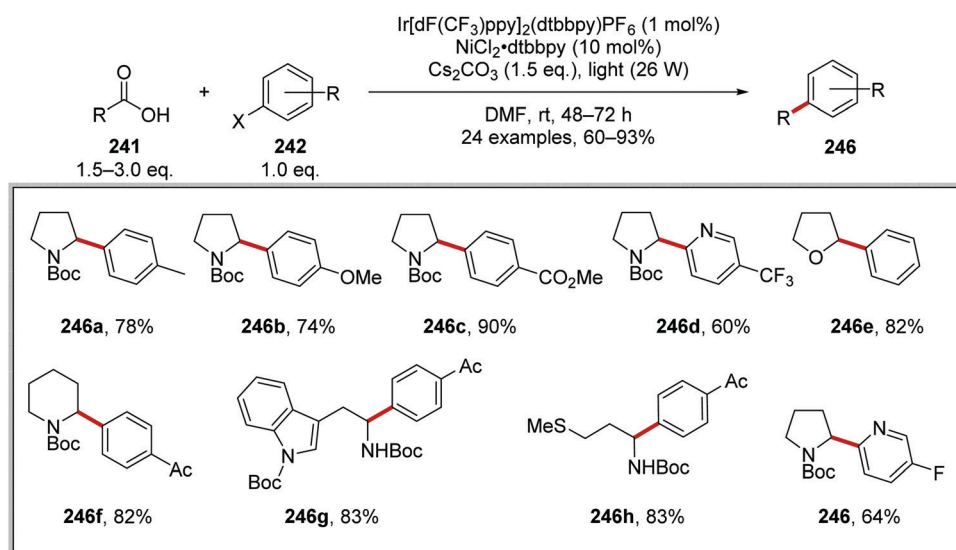
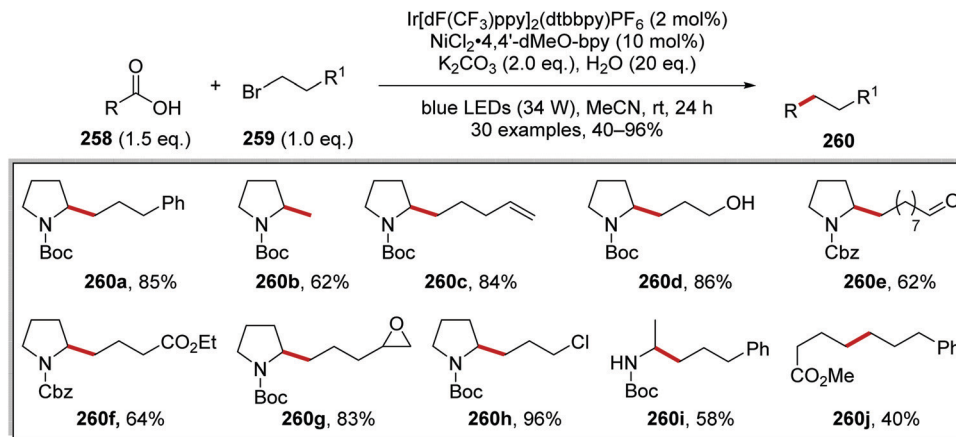**Scheme 61** Results of radical coupling between carboxyl acid **241** and aryl halide **242**.

Scheme 62 Results of decarboxylative radical coupling to vinyl halides.

This journal is © The Royal Society of Chemistry 2021

Chem. Soc. Rev., 2021, **50**, 9540–9685 | **9575**

Scheme 63 Decarboxylative radical coupling to alkynes.

Scheme 64 Asymmetric C–C bond formation.

of functional groups was tolerated, and this allowed for the preparation of functionalised derivatives **277a–f**. The synthetic utility of this reaction was demonstrated with the preparation of the bioactive steroid adduct **277g** in 51% yield.

The coupling of oxalates was also achieved with an iridium photocatalyst and radical decarboxylation strategy (Scheme 73).[141] A range of different electron-poor alkenes gave the products **280a–g** in yields of 67–95%. It was also shown that bioactive compounds were tolerated under the reaction conditions; for example, steroid-derived ester **280h** was prepared in 85% yield.
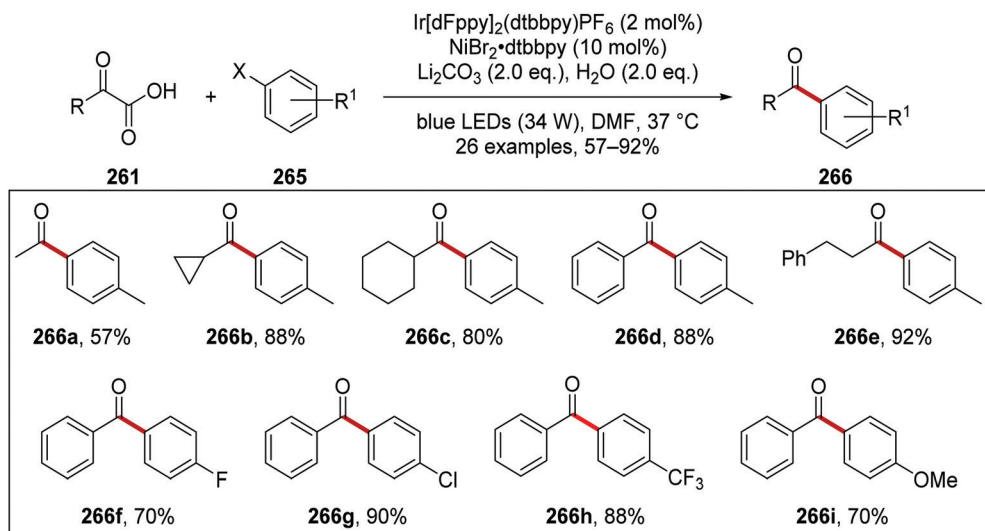
Other decarboxylative substrates. The inclusion of the bicyclopentane (BCP) bioisosteres into compounds was accomplished with a decarboxylative radical strategy.[143] SET oxidation of carboxylate **281** with Ir(III)* complex resulted in carboxyl radical **282** and Ir(II) species (Scheme 74). The cyclohexanecarboxylate anion has an electrochemical potential of +1.16 V vs. SCE[132] and therefore Ir[dF(CF$_3$)ppy$_2$]dtbpy(PF$_6$) (E_{red}^* = +1.21 V vs. SCE)[8b] is able to oxidise **281**. Radical decarboxylation led to amidyl radical **283**, which added to [1.1.1]propellane **284** and led to alkyl radical **285**. The inclusion of NCS (**286a**) led to compound
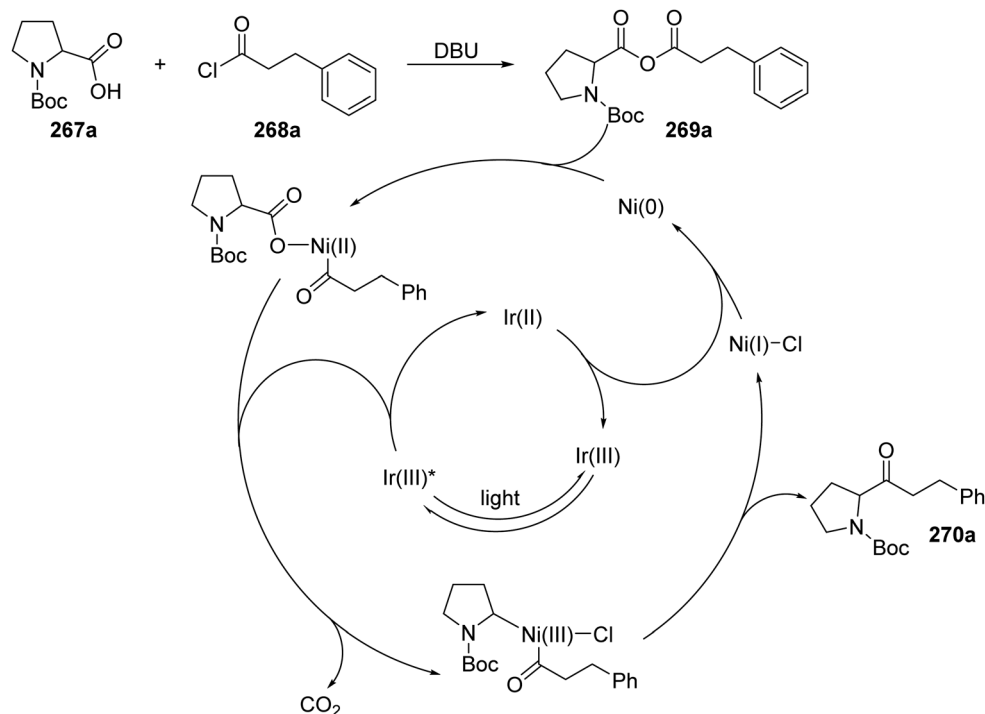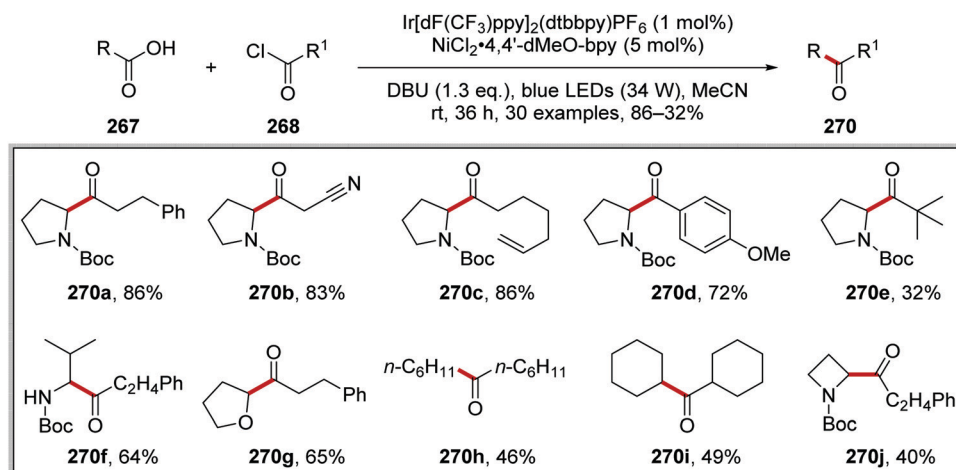
9576 | Chem. Soc. Rev., 2021, **50**, 9540–9685

This journal is © The Royal Society of Chemistry 2021

Ir[dF(CF$_3$)ppy]$_2$(dtbbpy)PF$_6$ (2 mol%)
NiCl$_2$•4,4'-dMeO-bpy (10 mol%)
K$_2$CO$_3$ (2.0 eq.), H$_2$O (20 eq.)

blue LEDs (34 W), MeCN, rt, 24 h
30 examples, 40–96%

258 (1.5 eq.)   **259** (1.0 eq.)   **260**

260a, 85%   **260b**, 62%   **260c**, 84%   **260d**, 86%   **260e**, 62%

260f, 64%   **260g**, 83%   **260h**, 96%   **260i**, 58%   **260j**, 40%

Scheme 65 Results of alkyl bromide **259** coupling to carboxylic acids **258** as radical precursors.

261a   **262a**   **263a**   **264a**

266a   **265a**
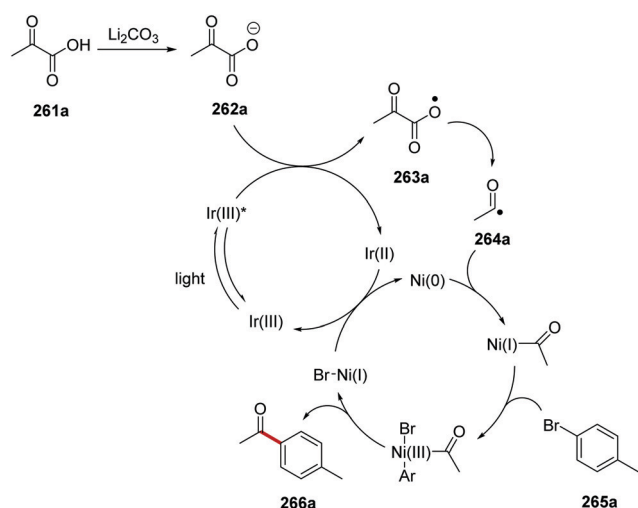
Scheme 66 Formation of ketone **266a** from α-oxo acid **261a** and aryl halide **265a**.

287 and succinimidyl radical **288a**. The iridium catalytic cycle was closed with a SET to **288a** from Ir(II) and this gave anion **289a** along with the original Ir(III) catalytic species.

This transformation worked well when N-chlorosuccinimide was used as **286** and this gave BCPs **287a–d** (Scheme 75). When bromotrichloromethane was used in the reaction as **286**, this gave **287e** in 20% yield. Trifluoromethylthio **287f**, thioether **287g** and selenyl ether **287h** derivatives were prepared from N-trifluoromethylthiophthalimide, N-phenylthiophthalimide and N-phenylselanylphthalimide.

Silanes. α-Aminosilanes **288** were used in a Giese coupling reaction with electron-poor alkenes **291** (Schemes 76 and 77).[144] Control reactions gave evidence for the mechanism for this transformation. The use of N-methyldiphenylamine gave no Giese coupled product but trimethylsilyl analogue **288a** with cyclohexenone gave coupled compound **294a** in 90% yield. Furthermore, when the reaction was performed with no aqueous work-up, silyl enol ether **293a** was isolated instead. Therefore, the following reaction mechanism was proposed. Irradiation of the

Ir[dFppy]$_2$(dtbbpy)PF$_6$ (2 mol%)
NiBr$_2$•dtbbpy (10 mol%)
Li$_2$CO$_3$ (2.0 eq.), H$_2$O (2.0 eq.)

blue LEDs (34 W), DMF, 37 °C
26 examples, 57–92%

261   **265**   **266**

266a, 57%   **266b**, 88%   **266c**, 80%   **266d**, 88%   **266e**, 92%

266f, 70%   **266g**, 90%   **266h**, 88%   **266i**, 70%

Scheme 67 Ketone formation from α-keto acids.

This journal is © The Royal Society of Chemistry 2021

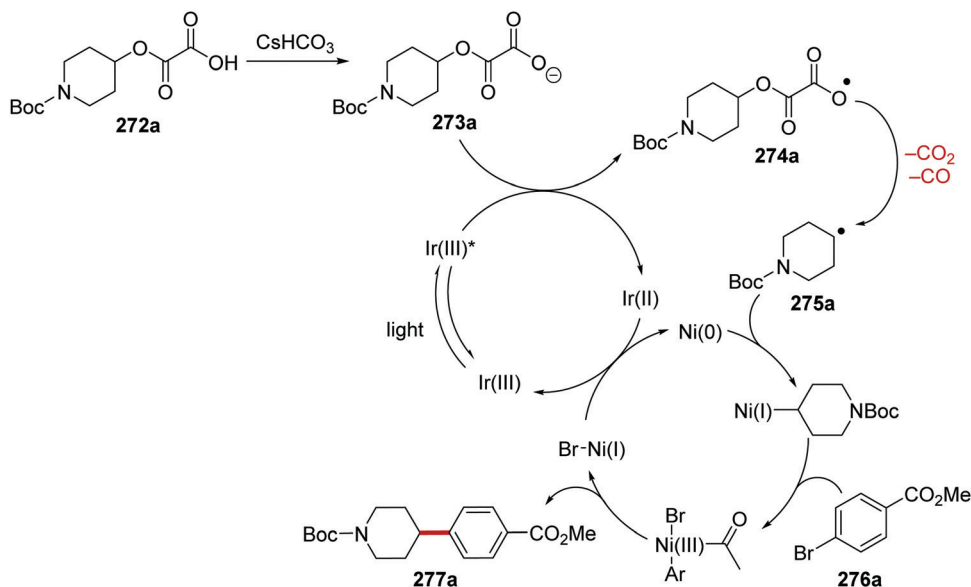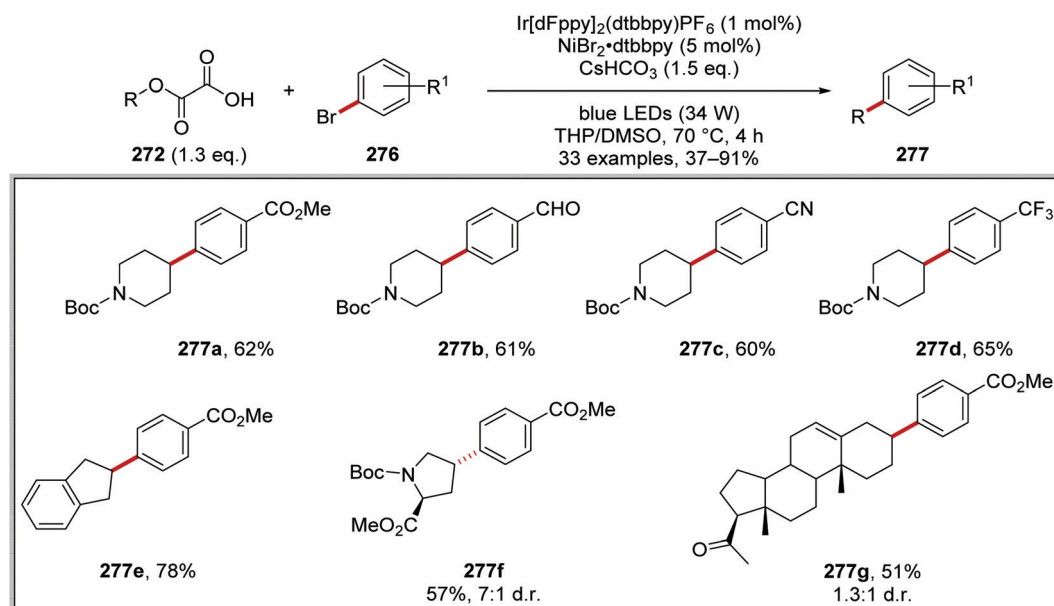*Chem. Soc. Rev.*, 2021, **50**, 9540–9685 | **9577**

Scheme 68 Formation of ketone **270a** from carboxylic acid **267a** and acyl chloride **268a**.

Scheme 69 Formation of ketone **270** from carboxylic acid **267** and acyl chloride **268**.
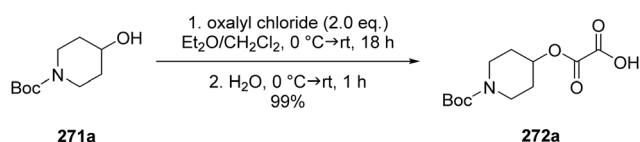
Scheme 70 Preparation of oxalate **272a** from alcohol **271a**.

reaction mixture with blue light gave the Ir(III)* complex from the iridium catalyst. Electron transfer from **288a** to Ir(III)* resulted in amine radical cation **289a** (Scheme 76). As previously mentioned, the presence the trimethylsilyl group decreases the oxidation potentials of substrates and thus **288a** has a very low oxidation

potential ($+0.41$ V *vs.* SCE;[144b] *N*-methyldiphenylamine $E_{ox} = 0.94$ V *vs.* SCE).[144c] Loss of trimethylsilyl cation gave carbon-centred radical **290a** which added to enone **291a**, forming radical **292a**. SET involving the Ir(II) complex, the TMS cation and **292a** gave silyl ether **292a**, which was detected in control experiments and this closed the iridium catalytic cycle.

Optimisation studies found that use of the Ir(dtbbpy)-(ppy)$_2$BF$_4$ catalyst gave coupled product **294a** in 90% yield. However, the use of Ru(bpy)$_3$(PF$_6$)$_2$ returned **294a** in 40% yield. The optimised reaction conditions were used to prepare a library of 13 coupled amine compounds **294**. Under the reaction conditions, silylaniline **288a** was coupled to a range of electron-poor alkenes

9578 | *Chem. Soc. Rev.*, 2021, **50**, 9540–9685

This journal is © The Royal Society of Chemistry 2021

Scheme 71 Coupling of oxalate **272a** with aryl bromide **276a**.

Scheme 72 Coupled products synthesised from corresponding alcohols.

and this products **294a–e** in 52–91% yield. Many different amines, including *N*-ethyl-2-trimethylsilylpyrrolidine, were compatible substrates and these gave products **294f–i**.
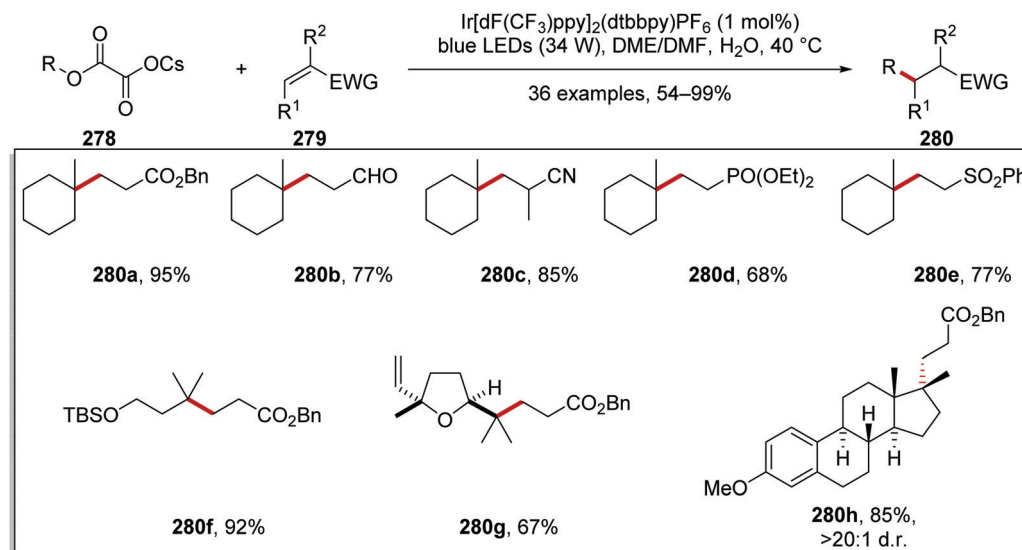
Use of α-aminosilanes **295** with electron-poor alkenes **298** (not shown in Scheme 78) and an Ir/Yb catalytic system allowed for the formation of tricyclic compounds **302**.[145] The reaction progressed with single-electron oxidation of indole **295a** (E_{ox} = +1.16 V *vs.* Ag/AgCl) with Ir(III)* complex and this gave radical cation **296a** and Ir(II) species (Scheme 78). The loss of TMS⁺ from **296a** resulted in carbon-centred radical **297a**. Addition of **297a** to ytterbium-activated enone **299a**, from alkene **298a**, gave α-keto radical **300a**. The electron-poor radical present in **300a** then added to the electron-rich heterocycle and this

formed **301a**. Oxidation and proton loss from **301a** resulted in the formation of **302a**.

Initially, the reaction was developed with a chiral oxazolidinone auxiliary **298** and this resulted in a highly diastereoselective transformation in combination with an ytterbium Lewis acid and a bipyridyl ligand (Scheme 79). Various indoles and electron-poor alkenes led to **302a–g** being isolated. However, the use of pyrroles led to the preparation of **302h** in 14% yield and a 93:3 d.r.

An enantioselective version of this reaction was developed with pro-chiral alkene **303** (Scheme 80).[145] The enantioenriched products **304a–d** were formed with modest ee using a Lewis acid/chiral ligand strategy with a PyBox ligand **305**.

This journal is © The Royal Society of Chemistry 2021

Chem. Soc. Rev., 2021, **50**, 9540–9685 | 9579

Scheme 73 Results of radical coupling between caesium carboxylates **278** and electron-poor alkenes **279**.
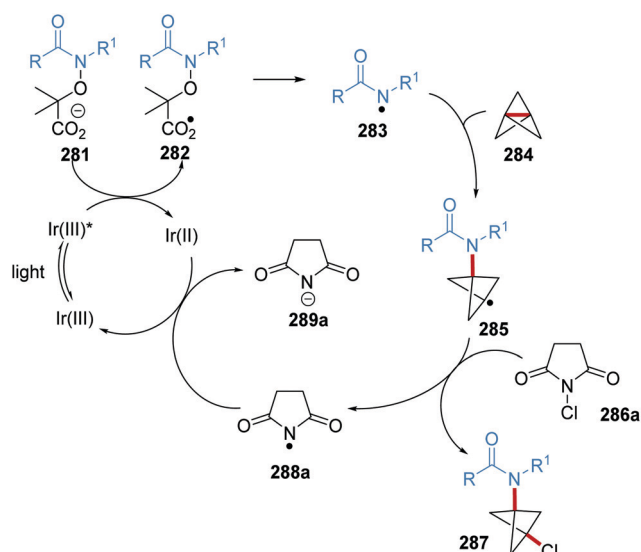
Scheme 74 Formation of bicyclopentane **287** from carboxylate **281**.

Boronates has radical precursors. The coupling of boronate-containing amino esters **306** to aryl bromides **276** under an iridium/nickel catalytic system was reported.[146] Under the reaction conditions, the Ir(III) complex was excited by blue light giving the Ir(III)* complex (Scheme 81). SET between Ir(III)* complex (E_{red}^* = +1.21 V *vs.* SCE) and boronate **306** (E_{ox} = +1.01 V *vs.* SCE) resulted in radical **307** and the Ir(II) complex. The iridium catalytic cycle was closed with a SET with Ni(I) complex **D** and this resulted in Ni(0) complex and the original Ir(III) species. Radical **307** was intercepted by Ni(0) complex **A** and this gave Ni(I) species **B**. Oxidative addition of aryl bromide **276** to **B** resulted in complex **C**, which underwent reductive elimination yielding coupled product **308** and Ni complex **D**.

This transformation allowed for a wide-range of α-amino esters **308** to be prepared from α-amino boronic salts **306** and
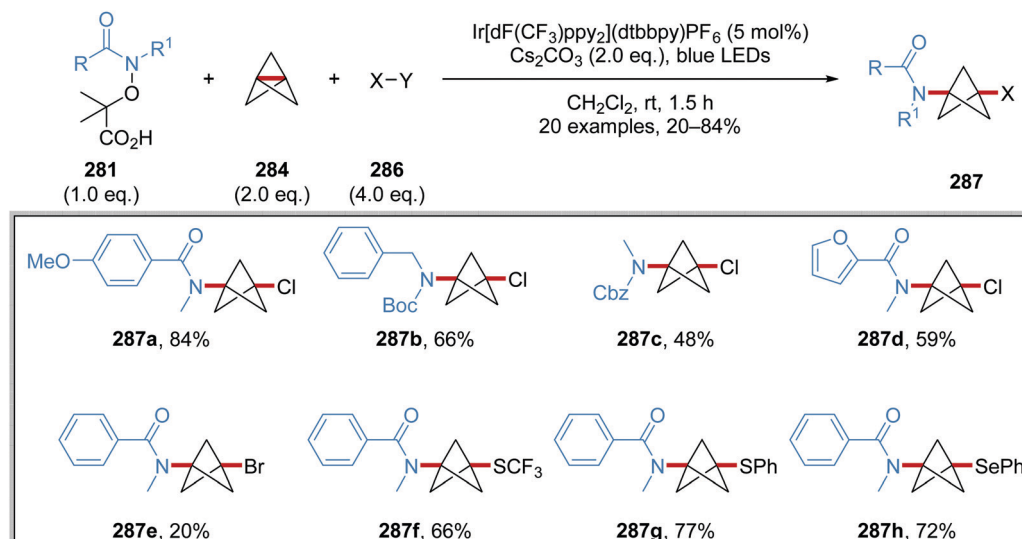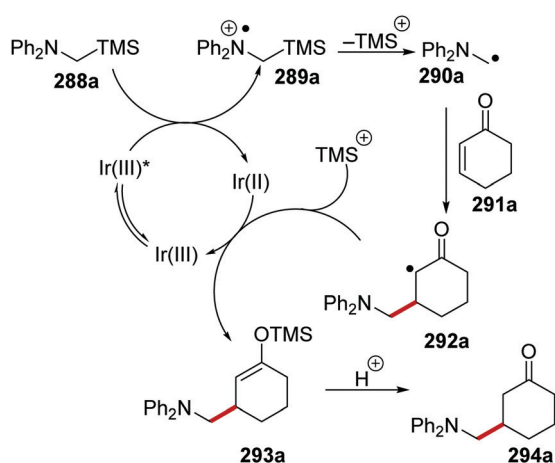
aryl bromides **276** (Scheme 82). Benzaldehyde **308a**, benzothiophene **308b**, sulfonamide **308c**, boronic ester **308d**, caffeine **308e**, oxadiazole **308f**, ketone **308g**, benzonitrile **308h** and pyrimidine **308i** analogues were all prepared in the yields shown. From chiral HPLC of two of the synthesised amino esters, the stereo-integrity of these compounds was not compromised.

All-carbon quaternary centres were prepared from organotrifluoroboronate salts (Scheme 83).[147] From optimisation studies, it was found that nickel-bipyridyl ligands were unsuitable for this transformation, as only starting material and protodehalogenation products were returned from the reaction mixture. Even with stoichiometric quantities of nickel catalyst and prolonged reaction times, no coupled compound was given with nickel bipyridyl complexes. Ligands for the nickel catalyst were screened, and it was found that only diketone-type ligands resulted in any significant product formation. The diketone, tetramethyl-heptanedione (TMHD) was the best ligand for the nickel complex for this transformation. The presence of inorganic bases, such as K_2HPO_4, decreased protodehalogenation and increased formation of **310a**. The inclusion of Lewis acid $ZnBr_2$ in the reaction mixture decreased the initial induction period and further increased the yield of **310a**. Under these optimal conditions, coupled product **310a** was prepared in a >95% HPLC yield and 90% isolated yield. The substrate scope of the reaction was examined with these optimised conditions. The *tert*-butyl group could be installed on electron-poor arene systems, such that ketone **310a**, and **310e**, aldehyde **310c**, sulfone **310b** and nitrile **310d** analogues were all synthesised.

Alkyltrifluoroborates derived from enones were also used in this reaction (Scheme 84). Therefore, compounds such as ketone **312a**, nitrile **312b** and 1,3,4-oxadiazole **312c** were all prepared. Electron-rich analogues such as dimethoxy **312d** were isolated in diminished yields. Other alkyltrifluoroborates allowed for the preparation of **312e–h**.
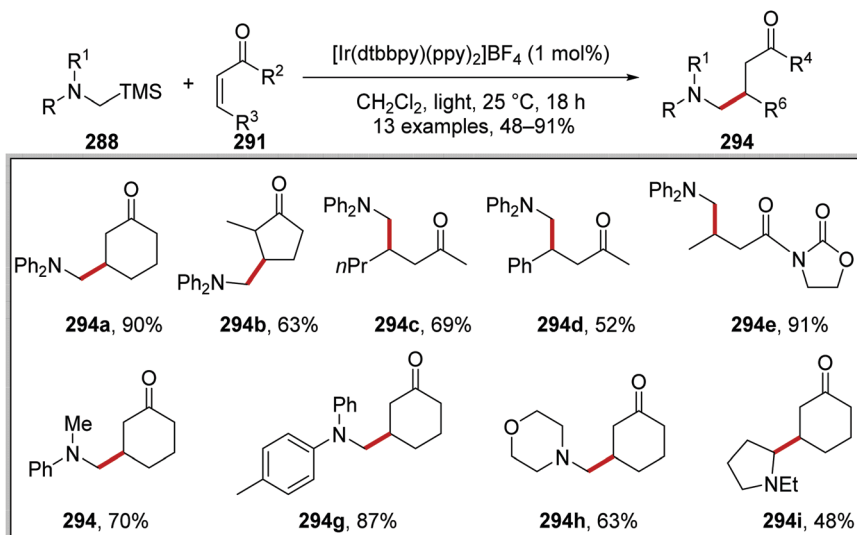
The preparation of allylic alcohols **316** was achieved from alkyltrifluoroboronates **313** *via* a radical Tsuji–Trost reaction
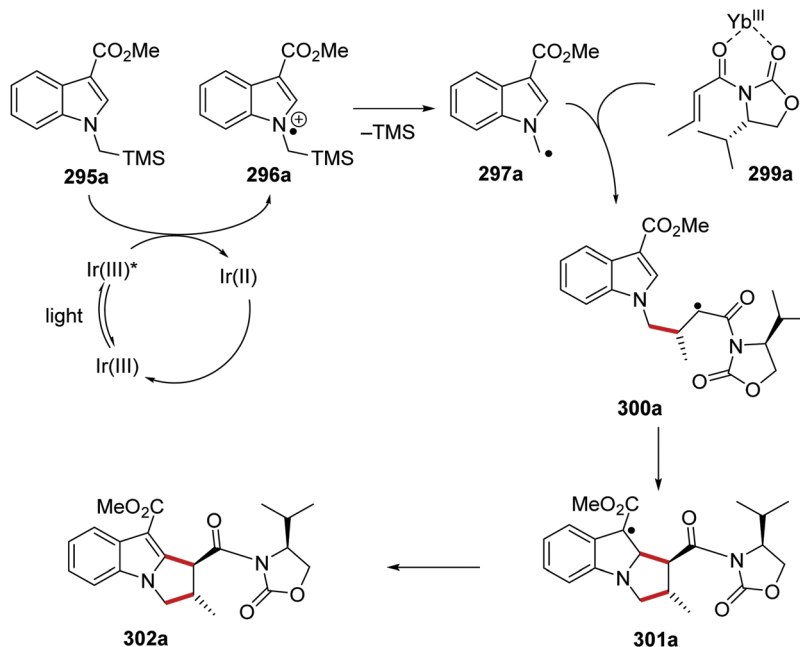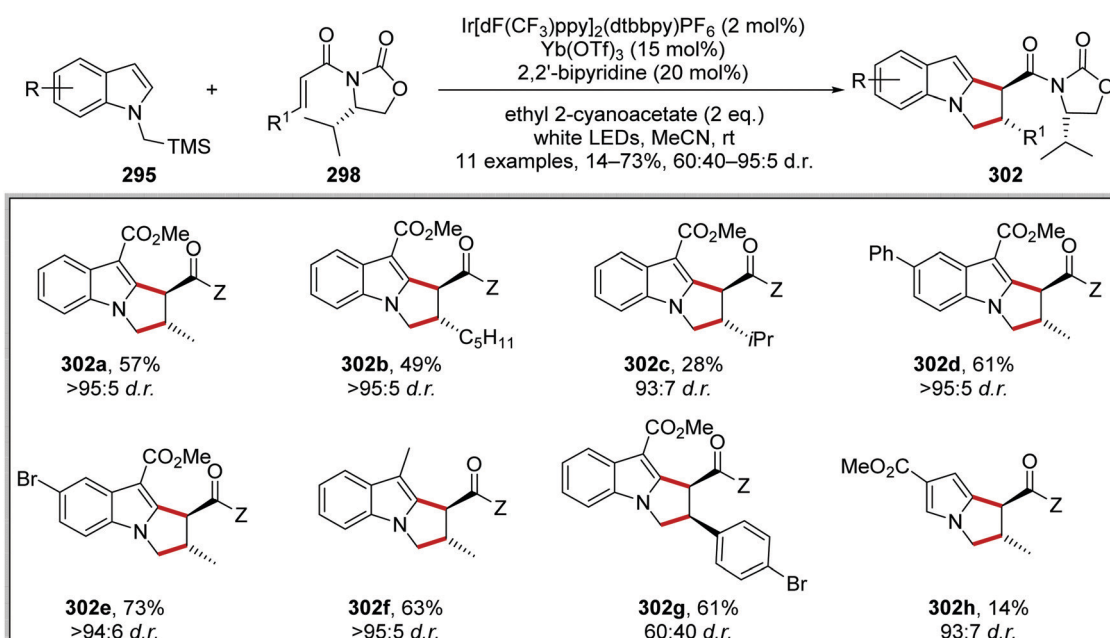
9580 | *Chem. Soc. Rev.*, 2021, **50**, 9540–9685

This journal is © The Royal Society of Chemistry 2021

Scheme 75 Synthesis of amide-functionalised BCPs **287**.

Scheme 76 Redox activation of silylamines.

under Ir photoredox conditions.[148] The transformation was investigated with DFT calculations and from this, a plausible mechanism was suggested (Scheme 85). Under the reaction conditions, benzylic radical **314a** was formed from boronate **313a** (E_{ox} = +0.93 V *vs.* SCE)[148b] and Ir(III)* complex (E_{red}^* = +1.21 V *vs.* SCE). The iridium catalytic cycle was closed with electron transfer to Ni(I) from Ir(II) and this reformed the original Ir(III) catalytic species and a Ni(0) complex. It was calculated that complex formation between Ni(0) and vinyl epoxide **315a** was favoured by 8.9 kcal mol^{-1} over the complexation between Ni(0) and benzyl radical **314a**; the former led to a Ni(II) π-allyl complex. Addition of benzylic radical **314a** to the Ni(II) complex resulted in a Ni(III) complex. Thereafter, C–C bond formation followed by reductive elimination was proposed to lead to the formation of allylic alcohol **316a** and Ni(I) complex.

Scheme 77 Results of iridium-mediated coupling of α-silylamines **288** to electron-poor alkenes **291**.
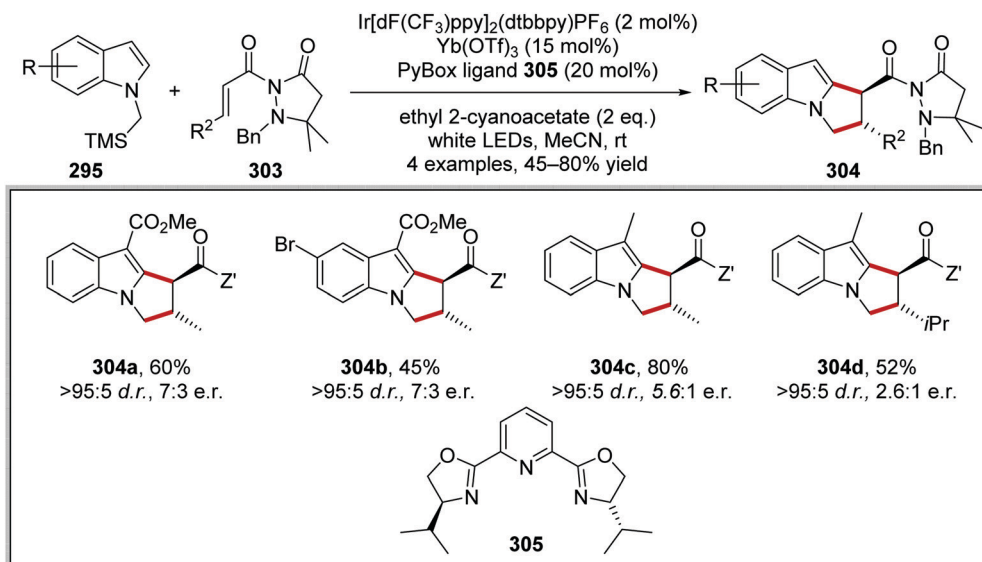
This journal is © The Royal Society of Chemistry 2021

Chem. Soc. Rev., 2021, **50**, 9540–9685 | **9581**

Scheme 78 Stereocontrolled coupling to activated alkene **299a**.

Scheme 79 Lewis acid-mediated diastereoselective radical ring formation of α-silyl amines and electron-poor alkenes.

The reaction was tolerant of both electron-rich aryl rings, giving allylic alcohols **316a–c** and electron-poor aryl rings affording **316d–f** (Scheme 86). However, higher yields and greater stereoselectivity were found for the electron-poor analogues. Alkyl-substituted products **316g–i** were also accessed.
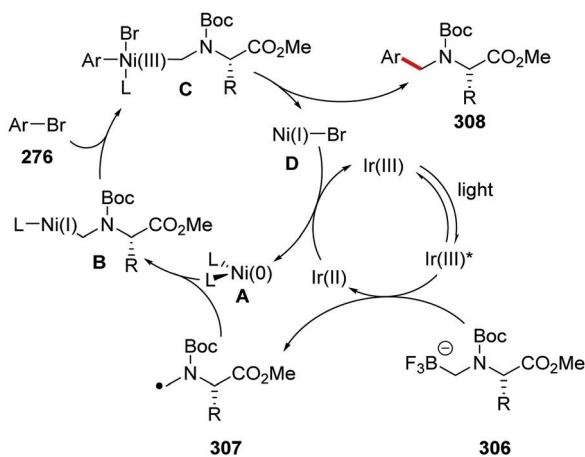
A three-component reaction involving boronate **317**, vinyl-boronic ester **319** and aryl bromide **321** under an Ir/Ni catalytic system resulted in saturated boronic ester products **322**.[149] Under the reaction conditions, boronate salt **317a** (E_{ox} = +1.26 V vs. SCE)[149] was oxidised by Ir(III)* and this gave a *tert*-alkyl radical

318a (Scheme 87). Addition of radical **318a** to alkene **319a** resulted in α-boronic ester radical **320a**. Radical **320a** was stabilised *via* overlap with the p-orbital situated on the boron atom; it was intercepted by a Ni(0) complex and this resulted in a Ni(I) complex. Oxidative addition of aryl bromide **321a** to the Ni(I) complex gave a Ni(III) complex. Reductive elimination of the Ni(III) complex resulted in boronate ester **322a** and a Ni(I) species. Both iridium and nickel catalytic cycles were closed with an outer-sphere SET from the Ir(II) to the Ni(I) complex.

9582 | Chem. Soc. Rev., 2021, **50**, 9540–9685

This journal is © The Royal Society of Chemistry 2021

Scheme 80 Lewis acid-mediated enantioselective radical ring formation of α-silyl amines and electron-poor alkenes.

Scheme 81 Mechanism of coupling with boronate salts as radical precursors.

This three-component reaction with an Ir/Ni catalytic system was highly facile, with the preparation of 57 analogues. As examples, analogues **322a–i** were prepared in 62–85% yields (Scheme 88).

Halide ions as radical precursors. Alkyl halides **324** were used as radical precursors for C–C bond formation with an iridium, nickel, silane catalytic system (Schemes 89 and 90).[150] Irradiation of the reaction mixture with blue light gave excited Ir(III)* complex from the Ir(III) complex (Scheme 89). Electron transfer from bromide ion (E_{ox} = +0.80 V vs. SCE) to Ir(III)* (E^*_{red} = +1.21 V vs. SCE) resulted in a bromine atom and an Ir(II) complex. H-atom abstraction from tris(trimethylsilyl)silane (TTMSS) by the bromine atom resulted in the formation of silyl radical **323** and hydrogen bromide. Bromine abstraction from alkyl bromide **324a** by silyl radical **323** gave alkyl radical **325a** and silyl bromide byproduct. Nickel cross-coupling reaction between alkyl radical **325a** and aryl bromide **321a** resulted in
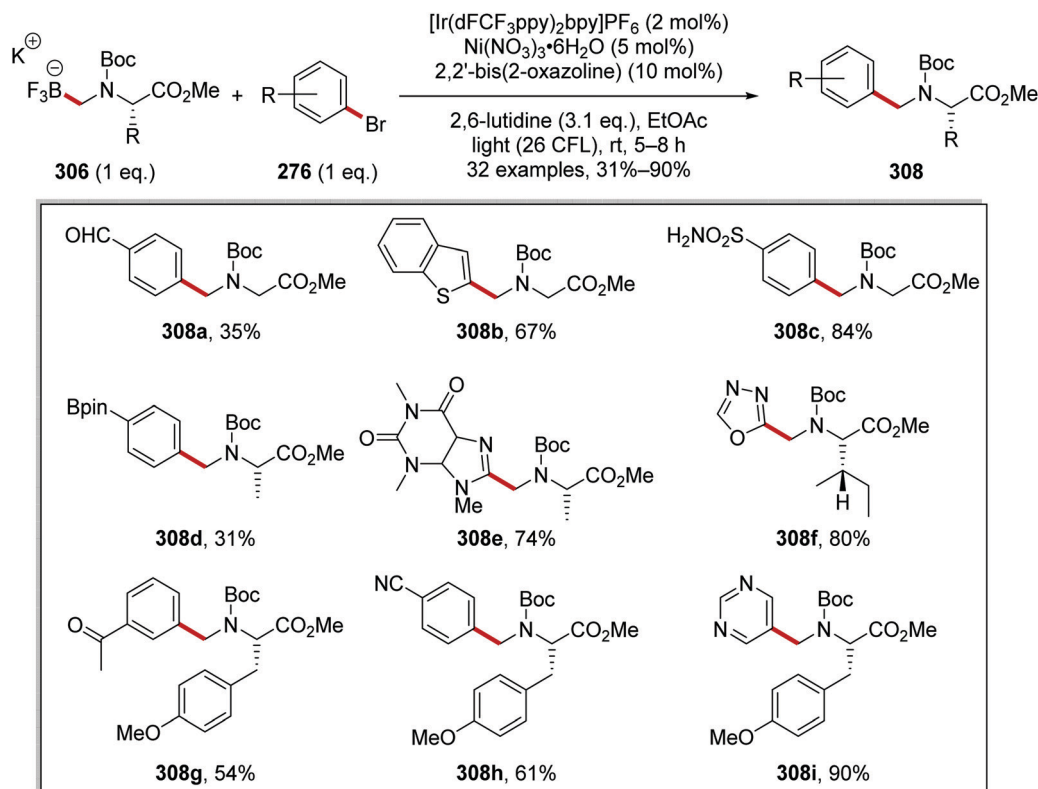
coupled product **326a**. The resulting Ni(I) complex accepted an electron from the Ir(II) complex to regenerate a Ni(0) complex and the original Ir(III) complex.

The combination of aryl bromides **321** and alkyl bromides **324** with iridium and nickel complexes and a silane was successful for the preparation of 39 coupled compounds **326** (Scheme 90). This transformation was effective in preparing coupled compound **326a** in 79% yield. Electron-rich anisole derivative **326b** was prepared in 77% yield and electron-poor analogues **326c–e** with yields ranging from 73% to 78%. Coupling to heterocycles as seen in **326f–j** was achieved. The transformation also accommodated Cbz and Boc protecting groups with N-Cbz **326k** and N-Boc **326l** derivatives being prepared in 80% and 92% yield, respectively. Coupling of tertiary carbon centres was achieved with the formation of **326m** and **326n**.
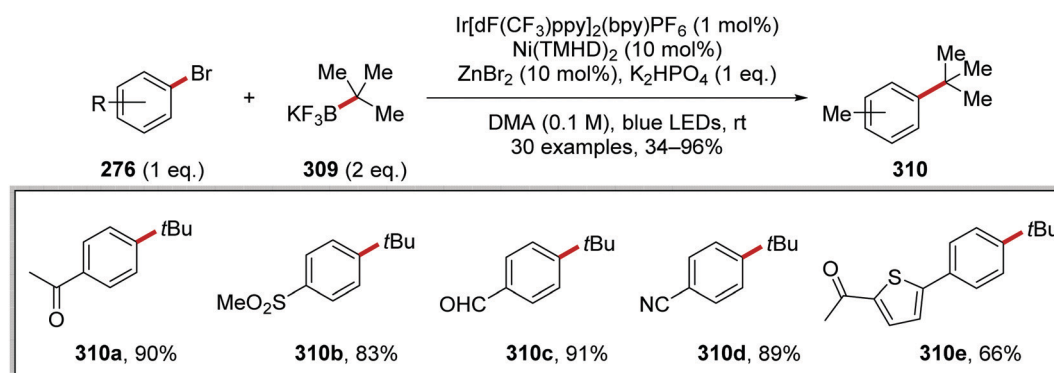
The difluoromethylation of aryl bromides was also achieved with the same iridium, nickel catalytic system-mediated with supersilane TTMSS, [which is (TMS)$_3$SiH] and 2,6-lutidine as base (Scheme 91).[151] The substrate scope for this reaction was explored and, for 36 examples, the reaction was found to be very accommodating, with yields obtained ranging from 45% to 86%. Esters **329a**, nitrile **329b**, N-Boc amines **329c**, methoxy **329d** aryl chlorides **329e**, boronic esters **329f** and alkynes **329g** analogues were all prepared. Furthermore, heterocycles were also functionalised, with pyridine **329h**, pyrimidine **329i**, pyrazole **329j**, thiazole **329k**, quinoline **329l**, quinoxaline **329m**, 1H-indazole **329n** and caffeine **329o** derivatives all being prepared. Four late-stage pharmaceutical agents also acted as substrates in this transformation.

The Ir/Ni/Si radical coupling strategy was then tested with the coupling of α-chlorocarbonyl compounds **331** with aryl bromides **333**.[152] Silyl radical **323** abstracted the chlorine atom present on **331a** and this led to α-keto radical **330a** (Scheme 92). Radical **330a** was intercepted by the Ni(II) complex and this resulted in coupling to aryl bromide **333a** with the formation of compound **334a**.

This journal is © The Royal Society of Chemistry 2021

Chem. Soc. Rev., 2021, **50**, 9540–9685 | **9583**

Scheme 82 Coupling of amino acid-derived boronic salts with aryl bromides.
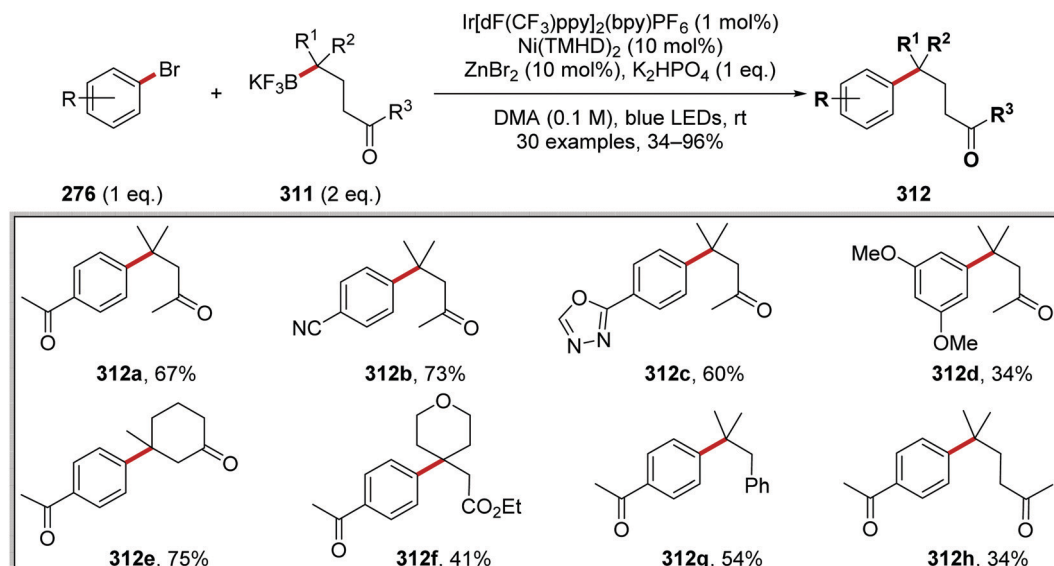

Scheme 83 Formation of all-carbon quaternary centres with boronates.

The use of the bulkier silane, tris(triethylsilyl)silane over tris(trimethylsilyl)silane **332** gave an increased yield of **334a** (from 65% to 80%) (Scheme 93). With these optimised conditions in hand, the substrate scope of the reaction was explored. Under the reaction conditions aryl esters **334a**, trifluoromethyl **334b**, Boc-protected amines **334c** and boronic ester **334d** derivatives were all prepared. It was also shown that 7-azaindazole **334e** and thiazole **334f** were accessed in 60% and in 45% yield, respectively. While the reaction worked well for aryl bromides **333**, it was observed that activated aryl chlorides could also be utilised in this reaction and this gave coupled compounds **334g** and **334h**. Alternatively, α-chloro carbonyl compounds were

also good substrates for this reaction and this allowed for the isolation of ketone **334i**, lactone **334j** and amide **334k** derivatives. It was also shown that 4-(trifluoromethyl)benzyl chloride was a successful substrate for this reaction and this allowed for the preparation of diaryl compound **334l** in 73% yield.

The generation of C_{sp^3}–C_{sp^3} bonds from alkyl-halogen compounds was achieved with the use of iridium, nickel catalysts and supersilanol **335** as a radical precursor (Scheme 94).[153] The reaction occurred with the oxidation of silanol **335** (E_{ox} = +1.54 V $vs.$ SCE)[154] with Ir(III)* complex (E_{red}^* = +1.21 V $vs.$ SCE)[8b] and after rearrangement, this gave silyl radical **336** and an Ir(II) species. Radical **336** abstracted a bromine atom from

9584 | Chem. Soc. Rev., 2021, 50, 9540–9685

This journal is © The Royal Society of Chemistry 2021

Scheme 84 Formation of all-carbon quaternary centres using a Ni/Ir mediated process.
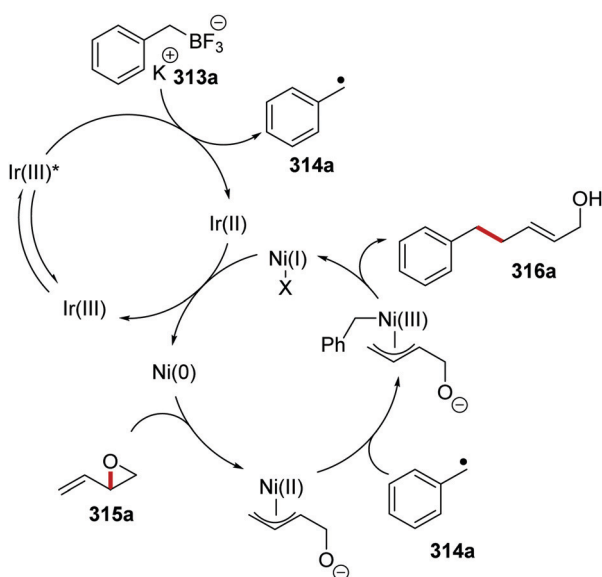
Scheme 85 Mechanism of 'radical Tsuji–Trost' reaction.

337 and this gave silyl bromide **339** and alkyl radical **338**. Interception of radical **338** with a Ni(0) complex resulted in a Ni(I) complex, which became a Ni(III) complex after oxidative addition of methyl bromide (**340**), formed from methyl tosylate (**342**) and tetrabutylammonium bromide. Reductive elimination from the Ni(III) complex gave methylated product **341** and a Ni(I) complex. Both catalytic cycles were closed with electron transfer to Ni(I) from the Ir(II) complex.

Initially, it was investigated whether methylation of alkyl bromides was feasible with tris(trimethylsilyl)silane (TTMSS, **332**). However, this resulted in a low yield (25%) of methylated product **341a** and large amounts of dehalogenated alkane product were produced instead. The presence of a Si–H bond in the silane reagent **332** led to deleterious HAT which
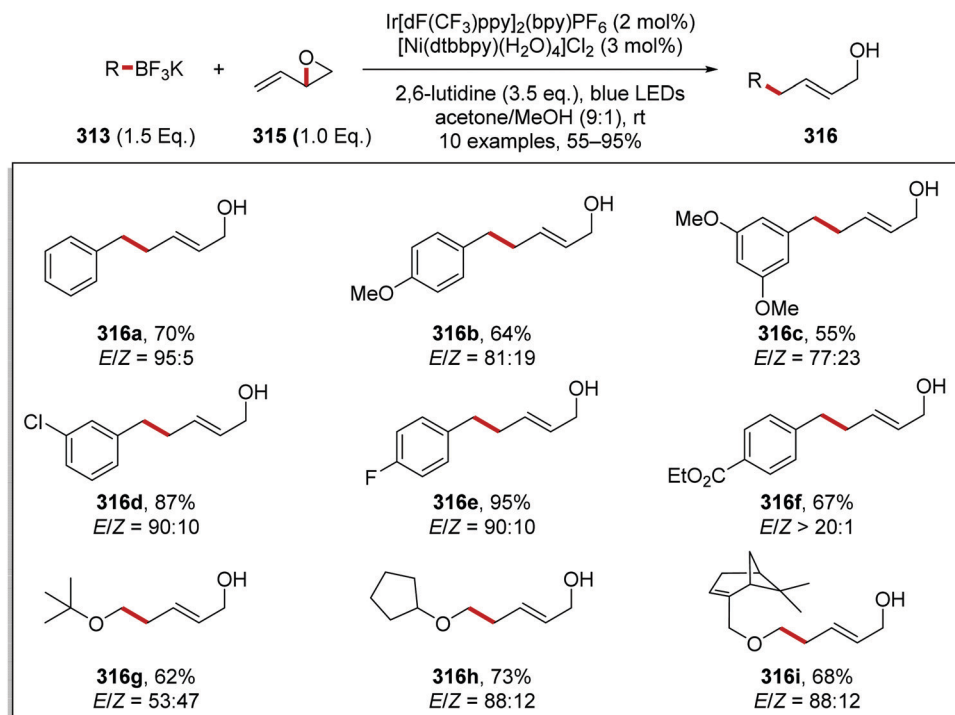
gave the dehalogenated compound (mechanism shown inset in Scheme 94). [This issue was solved by replacing TTMSS with tris(trimethylsilyl)silanol (**335**), as the chemistry of **335**, shown in Scheme 94, never features an Si–H bond.] Finally, the addition of tetrabutylammonium bromide increased the efficiency of converting methyl tosylate (**342**) to methyl bromide **340** *in situ* and this allowed for **341a** to be prepared in 72% isolated yield (Scheme 95). When the optimised reaction conditions were trialled on a range of 14 substrates, this resulted in good-to-high yields of methylated analogues **341**. The reaction tolerated functional groups and allowed for preparation of amide **341a** and trifluoromethyl analogues **341b** and **341f**. Protecting groups were also accommodated under the reaction conditions affording *N*-Boc **341c** (71%), and *N*-tosyl **341d** (70%) analogues.

More complicated alkyl bromides were also successful coupling partners when one was used in large excess (Scheme 96). This allowed for two alkyl bromides (**337** and **343**) to be coupled together. A wide-range of coupled products was accessed (from diverse examples of **343**) that included alkyl **344a**, ethers **344b**, *N*-Boc amine **344c**, ester **344d**, ketone **344e** and pyridine **344f** derivatives.

An iterative coupling synthesis was then demonstrated using this chemistry with dibromide **345** (Scheme 97). Utilising TTMSS **332**, the aryl bromide component of **345** was selectively functionalised over the alkyl bromide **346** and this gave **347** in 61% yield. With **347** in hand, reverting to tris(trimethylsilyl)-silanol **335**, the alkyl bromide was activated for a coupling reaction with 4-bromotetrahydro-2*H*-pyran and this gave pyran **348** in 50% yield.

Sulfonium salts as radical precursors. The conversion of aryl bromides **333** to aryl trifluoromethyl compounds **352** was achieved with an iridium and copper catalytic strategy.[154] The slow oxidative addition to Cu has limited its use in cross-coupling chemistry, even though it readily undergoes reductive

This journal is © The Royal Society of Chemistry 2021

Chem. Soc. Rev., 2021, **50**, 9540–9685 | **9585**

Ir[dF(CF$_3$)ppy]$_2$(bpy)PF$_6$ (2 mol%)
[Ni(dtbbpy)(H$_2$O)$_4$]Cl$_2$ (3 mol%)

R—BF$_3$K + [epoxide] ———————————————————→ R [OH chain]

2,6-lutidine (3.5 eq.), blue LEDs
acetone/MeOH (9:1), rt
10 examples, 55–95%

313 (1.5 Eq.)   **315** (1.0 Eq.)   **316**

316a, 70%
E/Z = 95:5

316b, 64%
E/Z = 81:19

316c, 55%
E/Z = 77:23

316d, 87%
E/Z = 90:10

316e, 95%
E/Z = 90:10

316f, 67%
E/Z > 20:1

316g, 62%
E/Z = 53:47

316h, 73%
E/Z = 88:12

316i, 68%
E/Z = 88:12

Scheme 86 Results of a Ni/Ir promoted Tsuji–Trost reaction.

317a

318a   **319a**

Ir(III)*   **320a**

light   Ir(II)

Ir(III)   Ni(0)

   Ni(I)

Ni(I)—Br

322a   Br—Ni(III)   **321a**
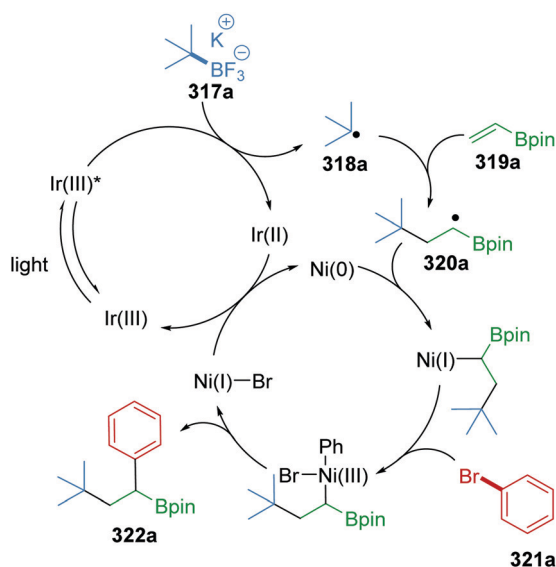
Scheme 87 Formation of boronic ester **322a** from boronate salt **317a**, alkene **319a** and aryl bromide **321a**.

elimination. Therefore, it was explored whether two successive radical additions to a Cu(ɪ) complex would result in an efficient coupling reaction. The preparation of trifluoromethyl arenes **352** from bromoarenes **333** with the Mes-Umemoto reagent (**350**) was chosen to investigate this proposal. Under irradiation by blue light, the Ir(ɪɪɪ) complex was excited to the Ir(ɪɪɪ)* complex (Scheme 98). Silanol **335** (E_{ox} = 1.54 V *vs.* SCE) was oxidised by Ir(ɪɪɪ)* [Ir(dFFppy)$_2$(4,4′-dCF$_3$bpy)PF$_6$ E_{red}* = +1.55 V *vs.* SCE] giving, after rearrangement and proton loss, the

silyl radical **336**. Bromine abstraction from **333a** led to aryl radical **349a**. At the same time, the reduced iridium catalyst (E_{ox} = −0.83 V *vs.* SCE) reduced sulfonium cation **350** (E = −0.52 V *vs.* SCE) and this gave trifluoromethyl radical **351** whilst reforming Ir(ɪɪɪ) photocatalyst, closing the iridium catalytic cycle. Successive radical additions of **351** and **349a** to Cu(ɪ) complex resulted in the formation of a Cu(ɪɪɪ) complex. Reductive elimination of Cu(ɪɪɪ) complex reformed Cu(ɪ) catalyst and gave trifluoromethyl arene **352a** as product.

Under an iridium and copper catalytic system, the desired trifluoromethyl compounds **352** were produced in yields ranging from 38% to 96% (Scheme 99). The optimal base and iridium catalyst varied, depending upon the substrate being used in the reaction. Nevertheless, a wide range of different functional groups was tolerated under the reaction conditions with **352a–e** being formed in 80–96% yields. Heterocyclic products **352f–h** were isolated in 38–64% yields. Furthermore, celecoxib (COX-2 inhibitor) derivative **352i** was also isolated in 77% yield.

Alkane C–H functionalisation. The functionalisation of adamantane **353a** with electron-poor alkenes **357** was achieved with the HAT catalyst quinuclidin-3-yl benzenesulfonate (**28e**) and an iridium complex.[55] In competition experiments, it was found that HAT catalyst **28e** was highly selective for adamantane compounds. In a reaction mixture with equal amounts of adamantane (**353a**) and *n*-octanal (**354**), preferred functionalisation of **353a** was observed affording alkylated adamantane derivative **355a** in 63% yield and aldehyde-derived alkylated compound **356a** in 7% yield (Table 4, entry 1). Using quinuclidine (**28b**) as HAT catalyst in conjunction with an Ir photoredox agent, also favoured the formation of **355a** over **356a** but the reaction
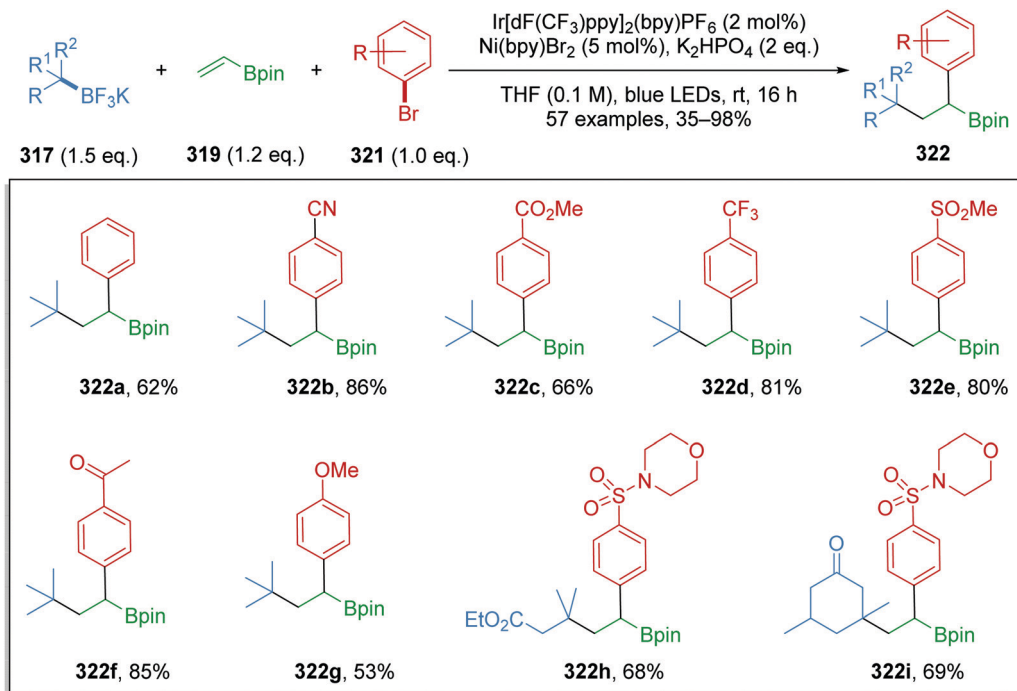
Scheme 88 Preparation of boronic esters **322** via a Ni/Ir mediated three-component reaction.
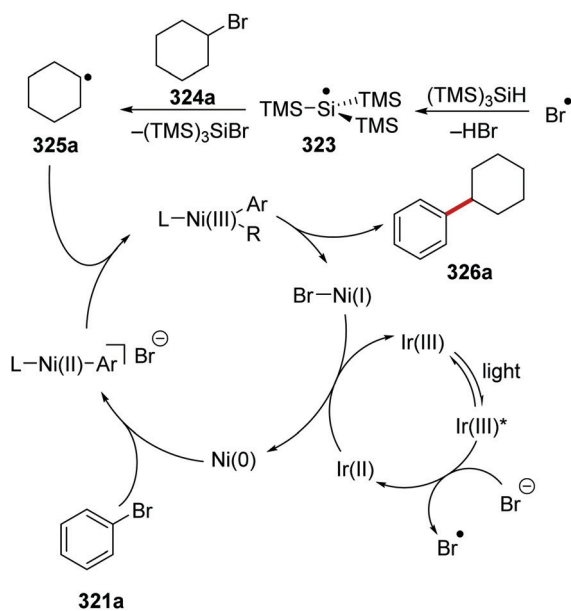
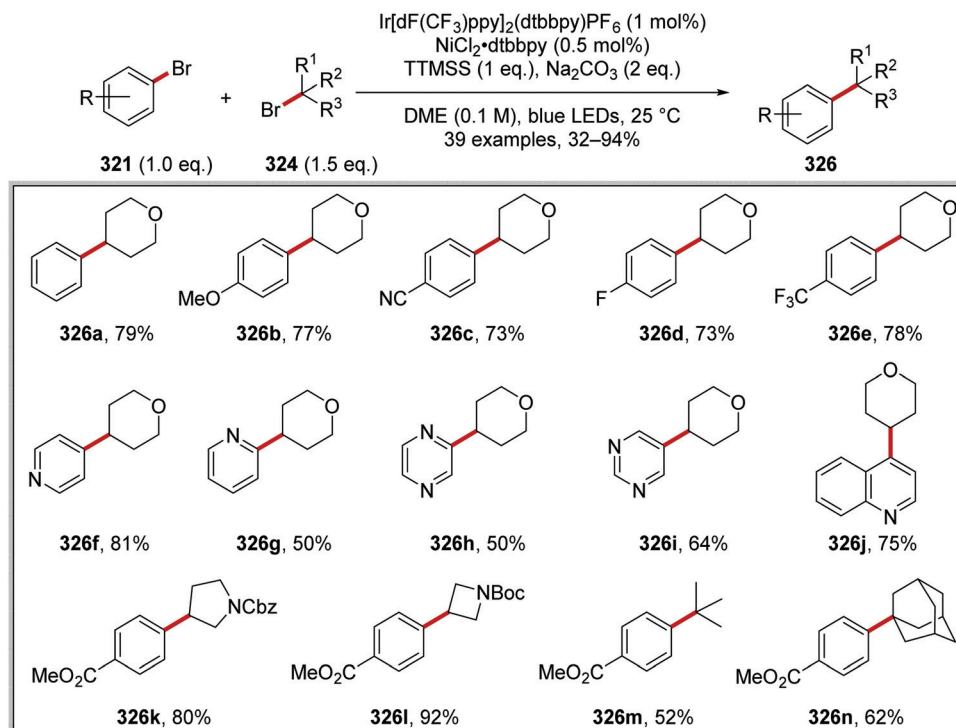**Scheme 89** Radical coupling of aryl bromides **321** with alkyl bromides **324**.

was less successful (entry 2). The use of an acridinium photocatalyst in conjunction with a phosphate base gave equal amounts of **355a** and **356a** (entry 3). The catalysts 5,7,12,14-pentacenetetrone **358** and 2-chloroanthraquinone **359** gave a slight preference for the aldehyde-derived product **356a** instead of the desired alkylated compound **355a**. Strong preference for aldehyde-derived analogue **356a** was observed

with the HAT catalysts tetrabutylammonium benzoate (oxidised by Ir(III)*) and tetrabutylammonium decatungstate (entries 6 and 7). These competition reactions demonstrated the exquisite selectivity of quinuclidin-3-yl benzenesulfonate (**28e**) as a HAT catalyst.

As it was established that the electron-poor quinuclidine HAT catalyst **28e** was optimal for activating the tertiary C–H bonds in adamantane, the reaction was optimised. When the reaction was performed with $Ir[dF(CF_3)ppy]_2[d(CF_3)bpy]PF_6$ (2 mol%) and quinuclidin-3-yl benzenesulfonate (20 mol%) an isolated yield of 72% was obtained for **355a**. When the more electron-rich 3-acetoxyquinuclidine was employed as a HAT catalyst, a yield of 74% was attained for **355a.** This trend was continued when quinuclidine was used as HAT catalyst with **355a** being given in a 33% GC yield. Replacement of $Ir[dF(CF_3)ppy]_2[d(CF_3)bpy]PF_6$ with $Ir[dF(CF_3)ppy]_2[d(tBu)bpy]PF_6$ also led to a diminished yield, affording **358a** in 16% GC yield. This can be explained with the oxidation potentials of the iridium catalyst and the HAT catalyst. The catalyst $Ir[dF(CF_3)ppy]_2[d(tBu)bpy]PF_6$ has an excited reduction potential of +1.21 V vs. SCE and $Ir[dF(CF_3)ppy]_2[d(CF_3)bpy]PF_6$ has an excited reduction potential of +1.68 V vs. SCE.[55,155,156] As quinuclidin-3-yl benzenesulfonate has an $E_{1/2}^{red}$ + 1.41 V vs. SCE only excited $Ir[dF(CF_3)ppy]_2[d(CF_3)-bpy]PF_6$ is a sufficiently strong oxidant to oxidise quinuclidin-3-yl benzenesulfonate. With optimal conditions being found, adamantane was coupled to various electron-poor alkenes and this led to a range of coupled products **355a–h** (Scheme 100).

From a high-throughput study, tetrabutylammonium benzoate was an effective quenching agent of $Ir[dF(CF_3)ppy](dtbbpy)_6$ complex, indicating electron transfer from benzoate **360** to Ir(III)*

This journal is © The Royal Society of Chemistry 2021

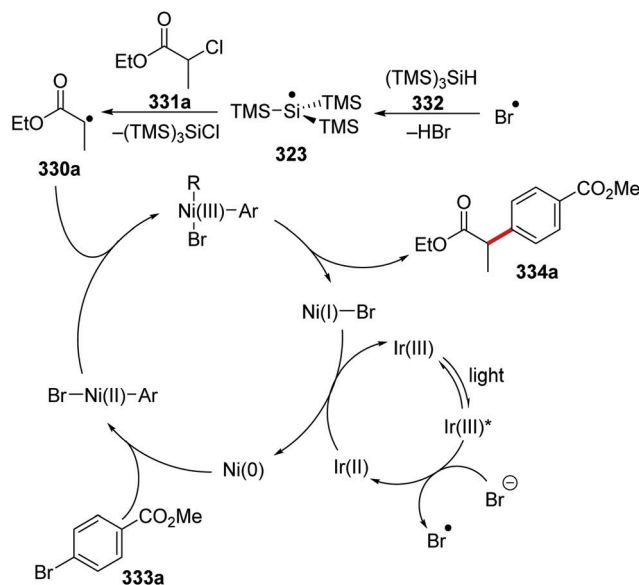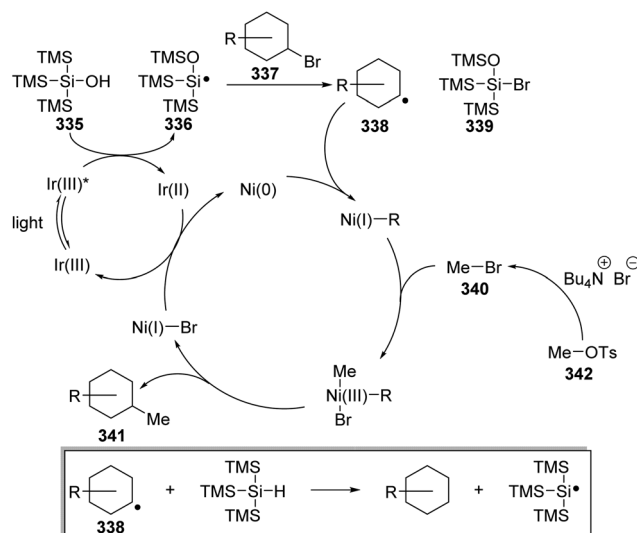*Chem. Soc. Rev.*, 2021, **50**, 9540–9685 | **9587**

Scheme 90 Results of radical coupling between aryl bromides **321** and alkyl bromides **324**.
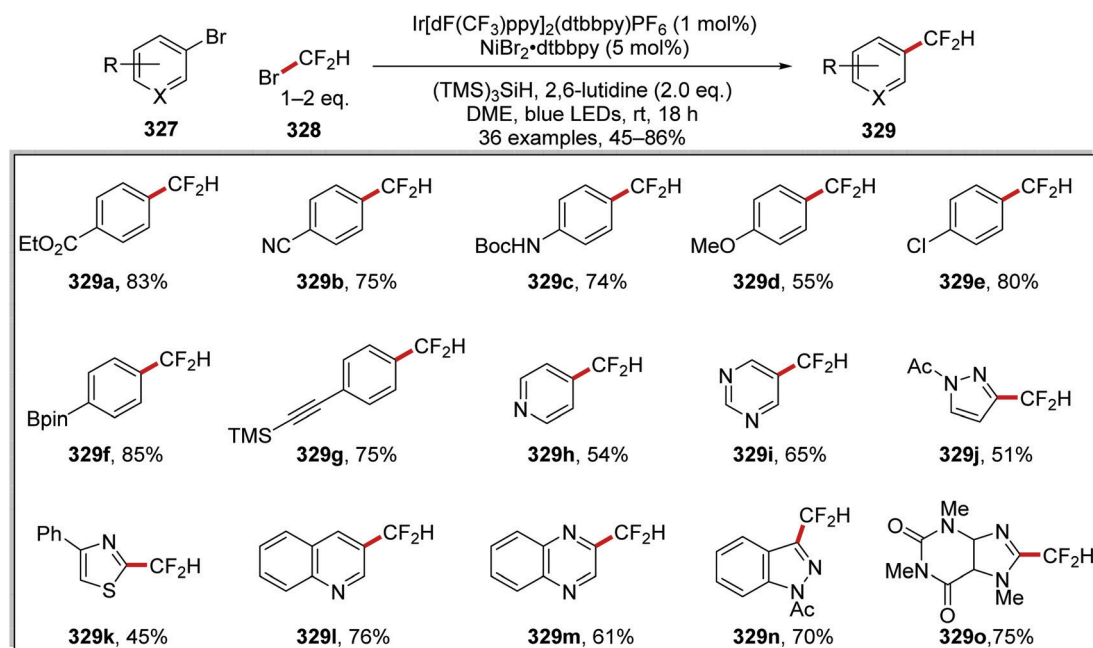
Scheme 91 Results of Ir/Ni catalysed difluoromethylation of aryl bromides **327**.

and this gave oxygen-centred radical **361** (Scheme 101).[157] These radicals are slow to undergo radical decarboxylation and they participate in HAT reactions.[158] Due to the great strength of O–H bonds (BDE of benzoic acid O–H bond = 111 kcal mol⁻¹) it was proposed that **361** could activate strong non-activated C–H bonds.[159] When benzoate ester **362a** was in the presence of **361**,

hydrogen atom abstraction was observed from the most electron-rich C(sp³)–H bond and this gave tertiary radical **364a**. The use of N-(trifluoromethylthio)phthalimide (**359**) resulted in formation of trifluoromethylsulfide **365a** and phthalimidyl radical **366** from alkyl radical **364a**. The iridium catalytic cycle was closed with SET to phthalimidyl radical **366** from Ir(II) complex with anion **367**

9588 | Chem. Soc. Rev., 2021, **50**, 9540–9685

This journal is © The Royal Society of Chemistry 2021

Scheme 92 Coupling of aryl bromide **333a** to α-chloroester **331a**.

Scheme 94 Coupling of alkyl bromide **337** with methyl tosylate **342** via methyl bromide **340**.

being given. Benzoate anion **360** was regained with proton exchange between phthalimidyl anion **367** (pK_a of phthalimide = 8.3, in water) and benzoic acid (**363**) (pK_a of benzoic acid = 4.2, in water). Calculation of average radical chain length (ϕ/Q) supported this mechanism over a radical-chain mechanism with a value of 2.0 being determined. The average radical chain length was calculated from the quantum yield of the reaction (ϕ = 1.76) and the quenching fraction (Q) (86% of the photons absorbed by the Ir catalyst participated in productive electron transfer). Further evidence for this mechanism was the high selectivity obtained.

The selectivity was found to be >20:1 for methine C–H bonds, which suggested abstraction by radical **361**, as it has been previously shown that the phthalimidyl radical **366** is much less selective.[160]

Initially, the reaction was performed with tetrabutylammonium benzoate (5 mol%) and Ir[dF(CF$_3$)ppy](dtbbpy)PF$_6$ (2 mol%) and this gave **365a** in 96% isolated yield and with high regioselectivity (>20:1). Further study showed that this transformation would also operate with 1 mol% of Ir catalyst and the use of the more accessible sodium benzoate also gave **365a** in 96% yield. With the
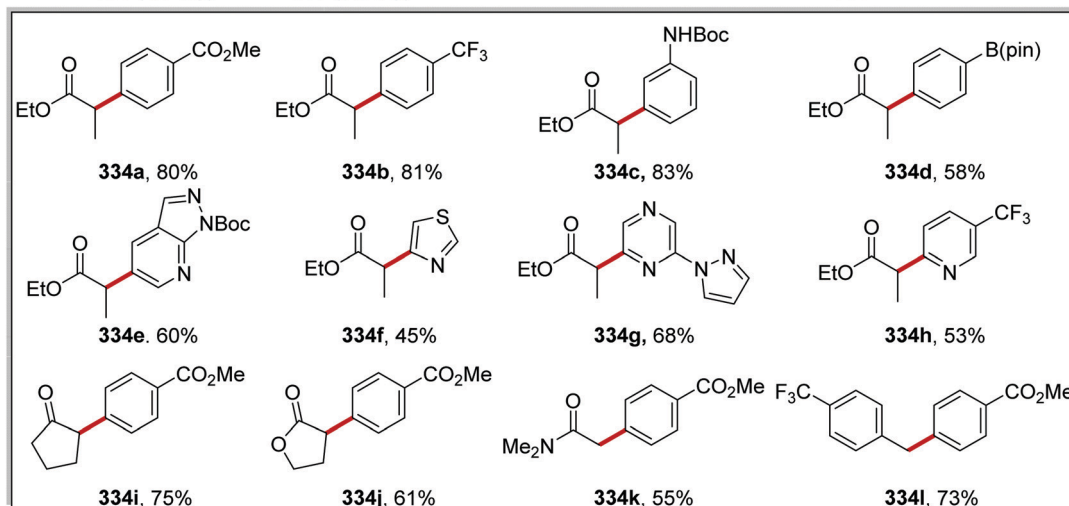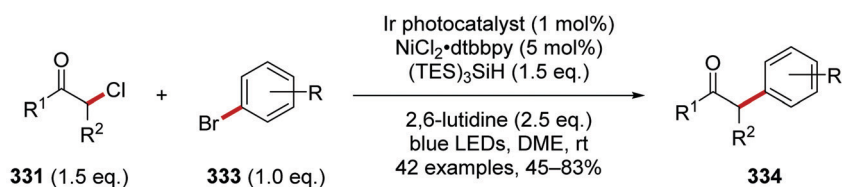
Scheme 93 Radical coupling between α-chlorocarbonyl **331** and aryl bromides **333**.
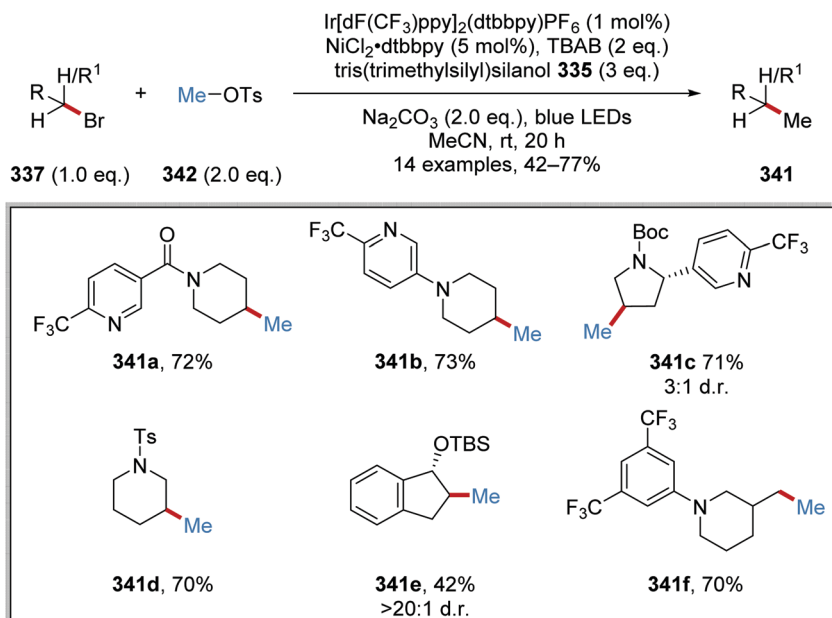
Scheme 95 C_{sp^3}–C_{sp^3} radical cross-coupling of alkyl bromides **337** and methyl tosylate **342**.
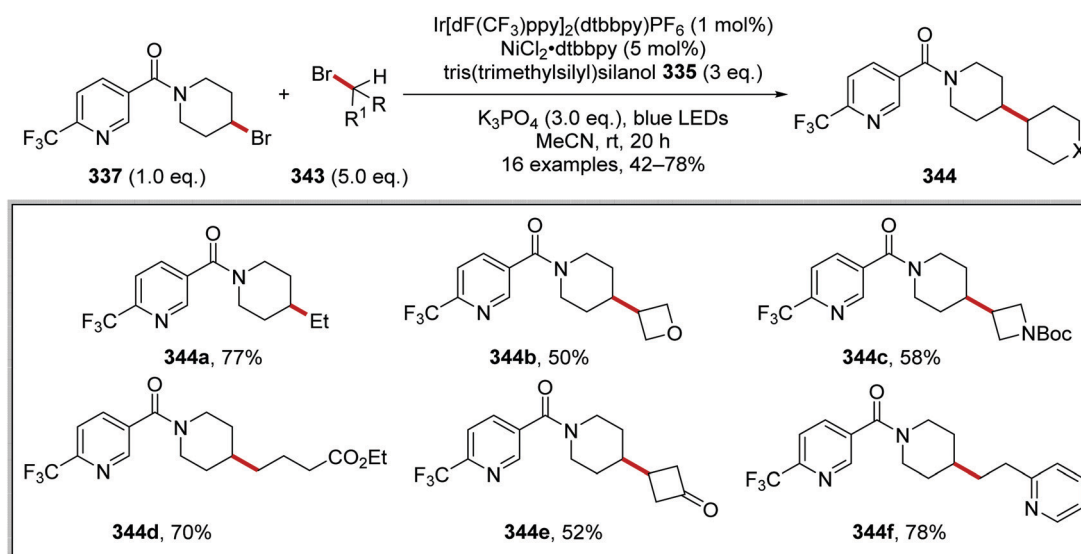
Scheme 96 C_{sp^3}–C_{sp^3} radical coupling between two alkyl bromides **337** and **343**.

optimised reaction conditions, a small library of 26 compounds **365** was prepared (Scheme 102). Benzoate **365b** was obtained in higher selectivity than acetate product **365c**. The reaction conditions were also tolerant of a strained cyclopropyl ring and this gave **365d** in 92% yield, with a >20:1 site-selectivity. Generally, methylene C–H bonds reacted slowly under these conditions. However, methylene C–H bonds neighbouring heteroatoms were excellent substrates, and this allowed for **365e** to be isolated in 95% yield. Heterocycle-bearing substrates were tolerated in this process; for example, **365f** was given in 80% yield. Bioactive molecules such as leucine and 5α-cholestan-3β-acetate were satisfactory substrates for this reaction and thus fluorinated

derivatives **365g** and **365h** were prepared in 68% yield and 35% yield, respectively.

Giese reaction between diesters **370** and organic compounds bearing C–H functionality, **369**, was achieved with hydrogen atom abstraction by chlorine atoms.[161] Originally, investigations began with Ir[dF(CF3)ppy]2(dtbbpy)PF6 (2 mol%) photocatalyst and tetrabutylammonium chloride (10 mol%) to generate the chlorine atoms from chloride ions. However, it was then found by using the chloride salt of the iridium photocatalyst, the TBACl co-catalyst could be omitted and this gave **371a** in a slightly improved yield. Therefore, investigations into the substrate scope were conducted with Ir[dF(CF3)ppy]2(dtbbpy)Cl catalyst (Scheme 103).
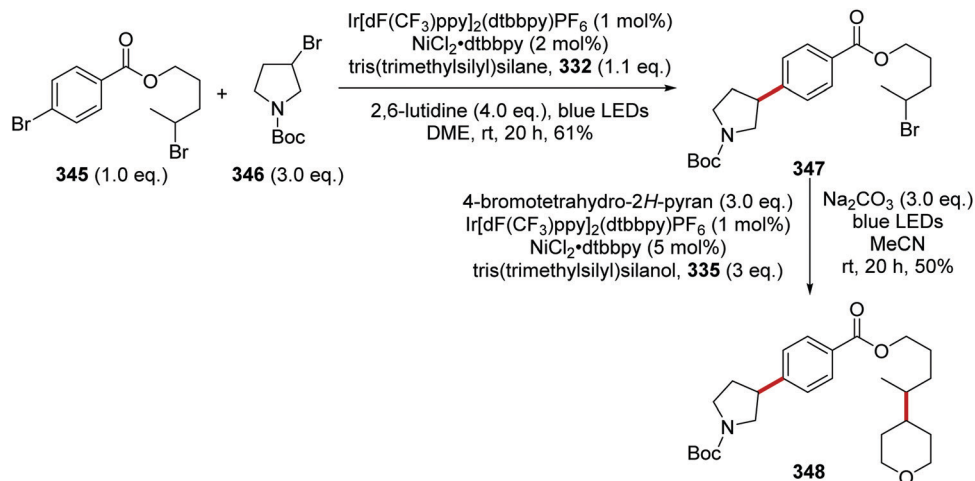
Scheme 97   Iterative coupling strategy.
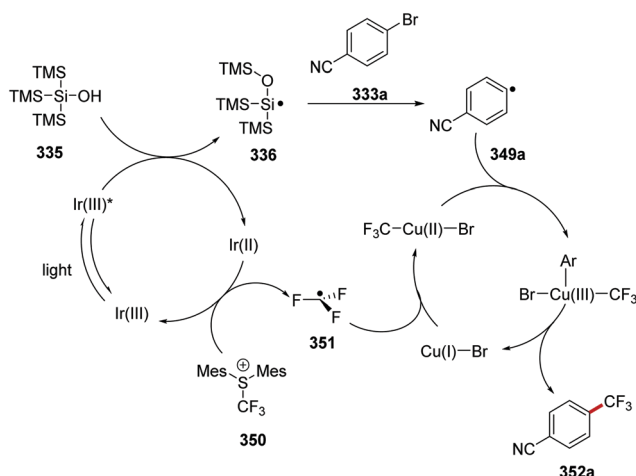
Scheme 98   Tandem catalytic process for the generation of aryl trifluoromethyl compound 352a from aryl bromide 333a.

These reaction conditions were applied to a wide range of substrates. Cyclohexane was converted to diester 371a in 69% yield. Tetrahydrofurans were suitable coupling partners; for example, THF was used in the preparation of 371b in 55% yield, as a single regioisomer. Both esters and amides were capable substrates, and this allowed for compounds 371c and 371d to be isolated. Aldehydes with weak C–H bonds were found to be suitable in this transformation – for example, n-pentanal gave ketone 371e in 95% yield after column chromatography. When cyclopentanol was used in the reaction, the cyclised lactone 371f was given as product in 33% yield. Silanes or phosphorus-containing compounds were successfully coupled to the electron-poor alkenes and this gave compounds such as 371g and 371h. During the determination of the substrate scope, it was found that benzylic C–H bonds were not suitable targets. Therefore, compounds such as toluene and mesitylene could not be coupled to alkenes 370.
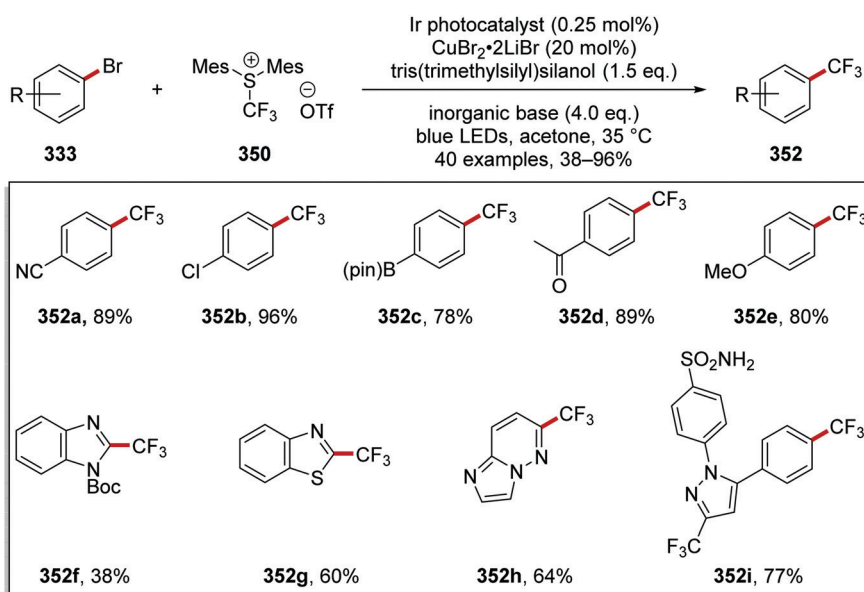
Scheme 99   Trifluoromethylation of aryl bromides.

This journal is © The Royal Society of Chemistry 2021

Chem. Soc. Rev., 2021, 50, 9540–9685 | 9591

Table 4 Selectivity of different catalytic systems

Entry	Catalyst	Yield of **355a** (%)	Yield of **356a** (%)	Selectivity
1	Ir[dF(CF$_3$)ppy]$_2$[d(CF$_3$)bpy]PF$_6$ quinuclidin-3-yl benzenesulfonate (**28e**)	63	7	4.5 : 1.0
2	Ir[dF(CF$_3$)ppy]$_2$[d(tBu)bpy]PF$_6$ quinuclidine	55	13	4.2 : 1.0
3	Acridinium photocatalyst HPO$_4^{2-}$	7	7	1.0 : 1.0
4	5,7,12,14-Pentacenetetrone **358**	13	26	1.0 : 2.0
5	2-Chloroanthraquinone **359**	11	24	1.0 : 2.2
6	Ir[dF(CF$_3$)ppy]$_2$[d(tBu)bpy]PF$_6$ NBu$_4$OBz	7	34	1.0 : 4.9
7	(Bu$_4$N)$_4$(W$_{10}$O$_{32}$)	8	41	1.0 : 5.1
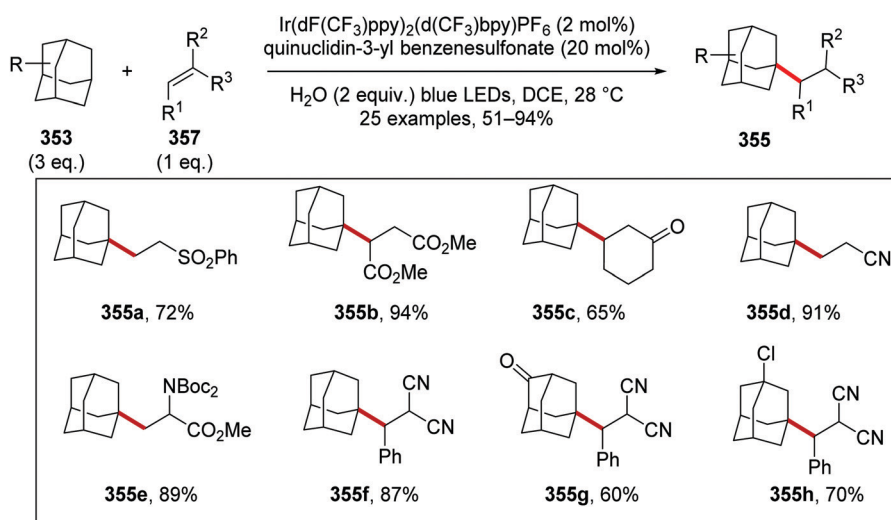
Scheme 100 Results of coupling to adamantanes.
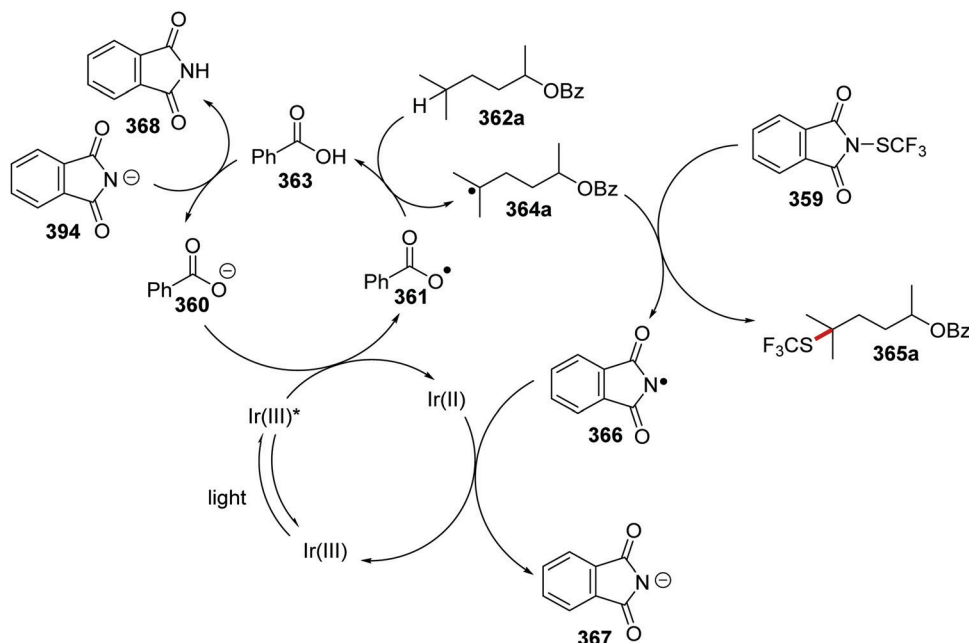
Scheme 101 Formation of trifluoromethylthio derivative **365a** from **362a** with **359**.

9592 | *Chem. Soc. Rev.*, 2021, **50**, 9540–9685

This journal is © The Royal Society of Chemistry 2021
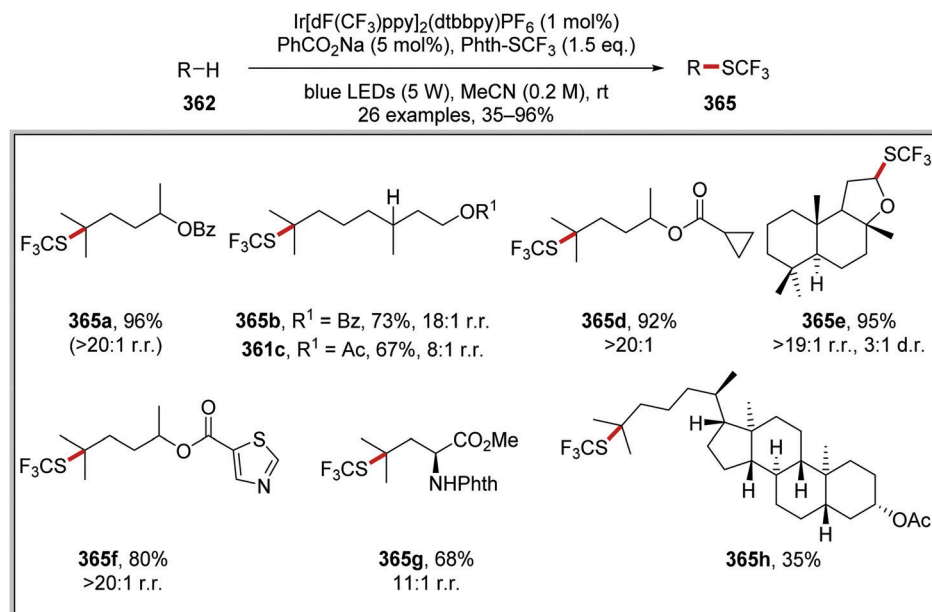
Scheme 102 Substrate scope of the trifluoromethylthiolation reaction.
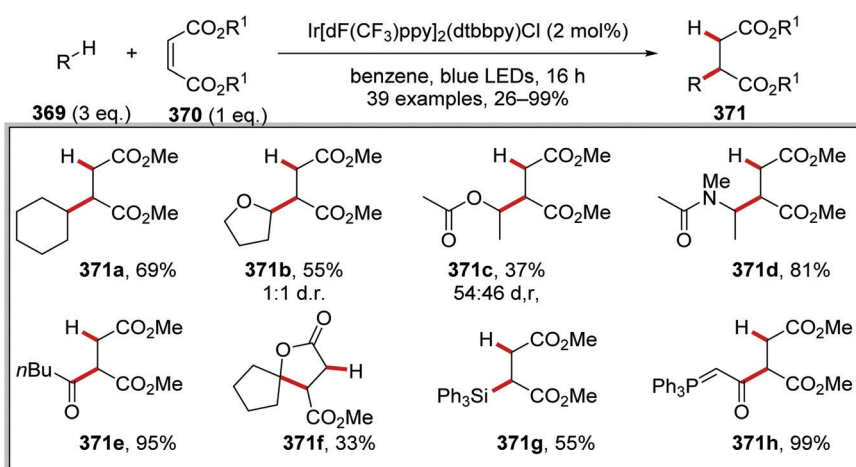
Scheme 103 Giese coupling with a Cl-atom HAT strategy.

The selectivity of the reaction was tempered by choice of the reaction solvent (Scheme 104).[161] With cyclopentyl methyl ether (369i) as substrate reacting with dimethyl maleate, a preference for the reaction of the methine C–H bond over the methyl C–H bond was found. In benzene, using the Ir chloride photocatalyst, a yield of 64% with a 4.4:1 mixture of regioisomers

was obtained for 371i. This was improved with the use of pyridine as the reaction solvent, with 371i being isolated in 64% yield with a 10:1 mixture of regioisomers.

Carbon α-heteroatom C–H functionalisation

Giese coupling. The Giese coupling of tertiary amines was achieved with the use of an iridium photoredox catalyst.[37]
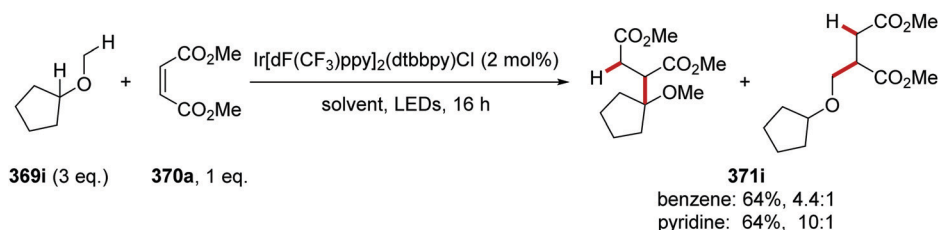
Scheme 104 Effect of solvent upon selectivity.

This journal is © The Royal Society of Chemistry 2021

Chem. Soc. Rev., 2021, **50**, 9540–9685 | 9593

Scheme 105 Formation of **378a** from **372a**. [The asterisk * denotes alternative connectivity in formation of alternative regioisomers.]

Irradiation with blue light gave excited Ir(III)* species from Ir(III) complex. Electron transfer from *N*-methylmorpholine (**372a**, E_{ox}^p = +1.10 V)[38] to Ir(III)* [Ir[(dFCF$_3$)ppy]$_2$dtbbpy(PF$_6$)], (E_{red}^* = +1.21 V *vs.* SCE)[8b] gave amine radical cation **373a** and Ir(II) species (Scheme 105). Deprotonation of **373a** led to the carbon-centred radical **374a**. For some substrates, such as **373a**, more than one deprotonation site exists (highlighted in blue) and this gave rise to products being isolated as mixtures of regioisomers. Nevertheless, radical **374a** added to alkene **375** and this gave captodative radical **376a**. The iridium catalytic cycle is closed with electron transfer from Ir(II) to **376a** giving the original Ir(III) complex along with anion **377a**. Protonation of **377a** led to the formation of **378a**, which was isolated from the reaction mixture.
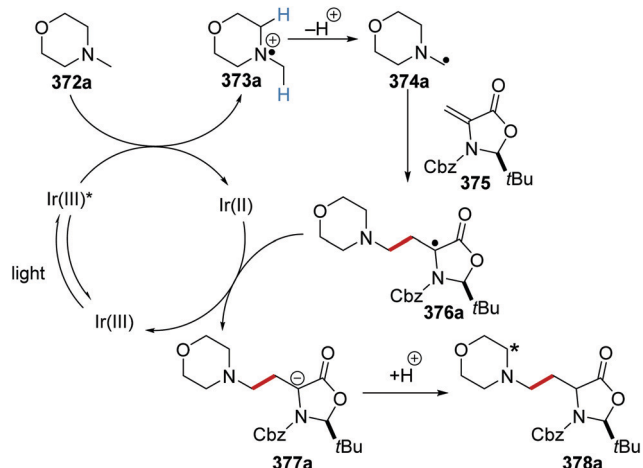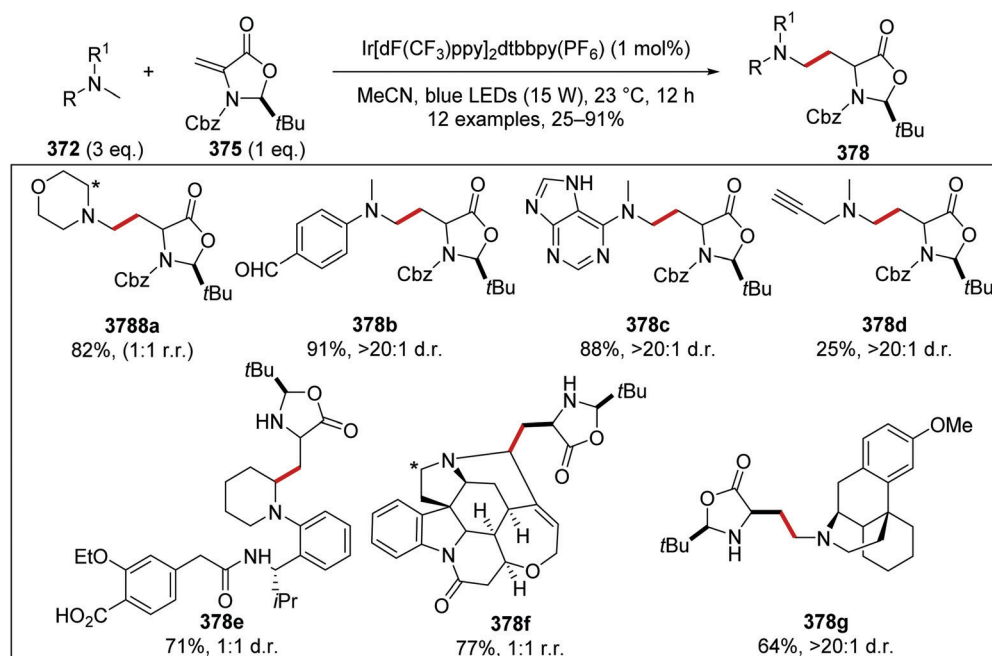
Under these conditions, 12 different amines **372** were alkylated with oxazolidinone **375** with Ir[df(CF$_3$)ppy]$_2$dtbbpy(PF$_6$) in MeCN, giving functionalised oxazolidinones **378** (Scheme 106). The yields of isolated 4-oxazolidinones **378** ranged from 25–91%, and alkyne **378d** was isolated in 25% yield. As mentioned earlier, when compounds such as *N*-methylmorpholine and strychnine were used as substrate, this gave **378a** and **378f** as mixtures of regioisomers as proton loss occurred competitively at two different sites for these substrates.

The synthetic utility of this methodology was then demonstrated with the functionalisation of peptides (Scheme 107). There was no control of stereochemistry of the new chiral centre and therefore this gave a 1:1 mixture of diastereoisomers. The high degree of chemoselectivity in this process was remarkable. For example, while peptide **379** has several reactive functional groups, including primary amines, aniline peptide **380** was selectively prepared in 67% yield.

Regioselective addition of benzylamines to electron-poor alkenes was investigated under photoredox conditions mediated by an iridium photocatalyst.[162] When *N*-benzyl-*N*-methylaniline (**381a**) was reacted with methyl vinyl ketone (3 eq.) using Ir(ppy)$_2$(dtbbpy)PF$_6$ in dichloromethane, functionalisation at the benzylic position was observed giving **382a** in 74% yield (Table 5, entry 1). When the reaction was conducted in MeCN, the site-selectivity of the reaction was completely reversed, there was no functionalisation at the benzylic position, and instead **383a** was the sole-product in 70% yield (entry 2). Addition of TFA (0.4 eq.) to the reaction mixture gave **382a** in 49% yield even when performed in MeCN (entry 3). From this optimisation study, it was observed that **383a** gave a maximum yield with 1.1 eq. of methyl vinyl ketone, 0.3 eq. of DBU as additive and with the reaction performed in MeCN (entry 4). The use of

Scheme 106 Products from radical Michael addition to electron-poor alkenes.

9594 | *Chem. Soc. Rev.*, 2021, **50**, 9540–9685

This journal is © The Royal Society of Chemistry 2021

Scheme 107 Selective functionalisation of peptide **379**.

Table 5 Site-selective functionalisation of aniline **381**
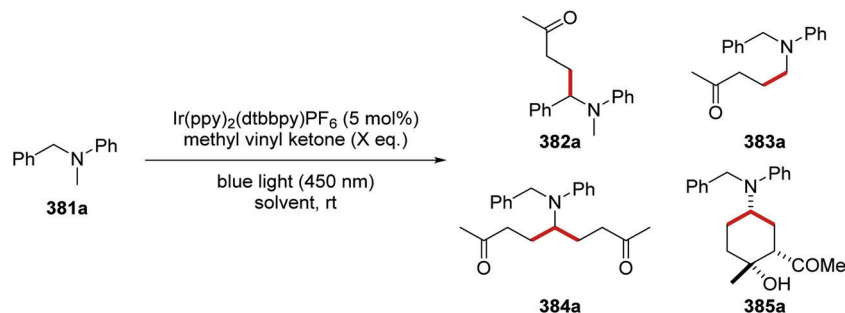
Entry	Methyl vinyl ketone, eq.	Solvent	Additive	Isolated yield (%)			
				382a	**383a**	**384a**	**385a**
1	3	CH$_2$Cl$_2$		74			
2	3	MeCN			70		
3	3	MeCN	TFA	49			
4	1.1	MeCN	DBU		84		
5	3	MeCN	DBU			76	<5
6	3	MeCN	K$_3$PO$_4$			<5	70

higher loadings of methyl vinyl ketone led to more than one Giese addition giving **384a** in 76% yield (entry 5). The inclusion of an inorganic base gave aldol product **385a** in 70% isolated yield as the major product (entry 6).
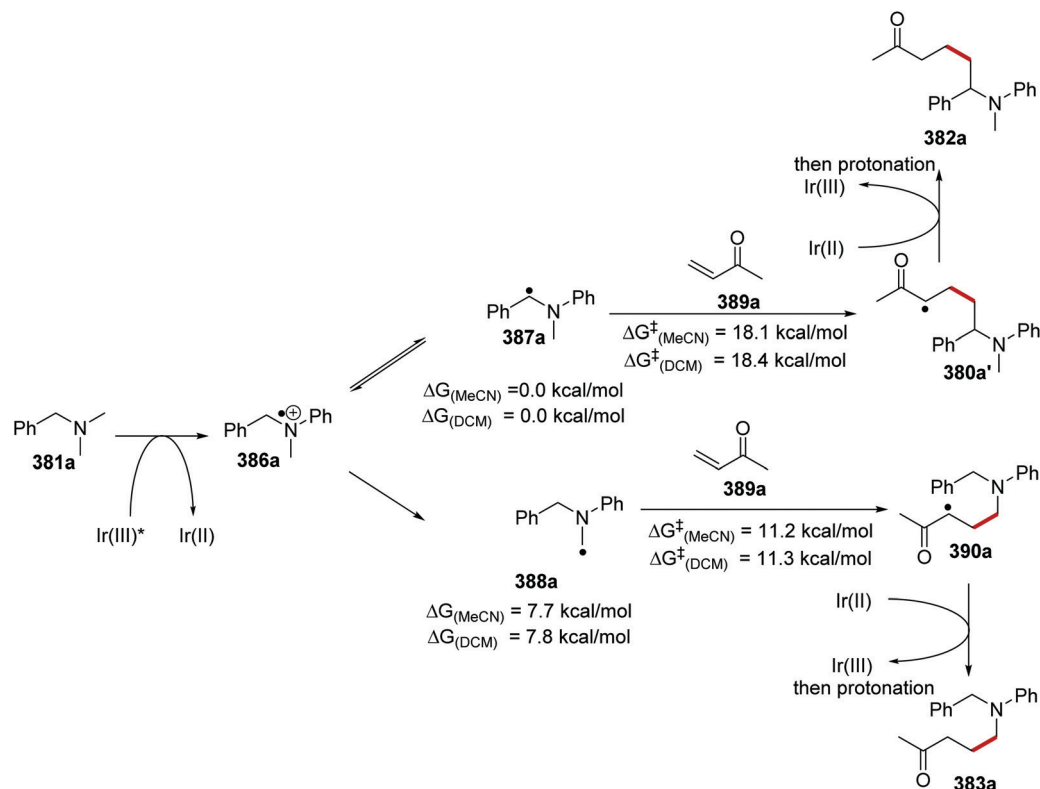
A mechanism was proposed for the observed regioselectivity in these reactions (Scheme 108). A PET to Ir(III)* from aniline **381a** resulted in radical cation **386a**. It was then suggested that reversible proton loss occurred at the more acidic benzylic position (pK_a 2.4, methyl position pK_a = 8.2) to give **387a** and this explained some of the experimental observations. When the reaction was conducted in dichloromethane, very fast addition to MVK (**389a**) occurred and this resulted in ketone **382a** being formed under the reaction conditions. However, when the reaction was conducted in MeCN, the reverse reaction from **387a** to **386a** was more significant, perhaps due to enhanced stabilisation of the charged species **386a** in the more polar MeCN, and from this the N-methyl radical **388a** formed. DFT calculations indicated that Giese addition of **388a** to give **390a** would have a lower transition state by 6.9 kcal mol^{-1} compared to addition of **387a**, when the reaction was conducted in MeCN. The lower transition state energy in the reaction of **388a** with **389a** would result in a rapid and irreversible formation of radical **390a**. Electron transfer from Ir(II) complex to

390a would result in formation of the corresponding enolate and, after proton transfer, the ketone **383a**.[163]

With four unique reaction conditions optimised, aniline **381** was converted into a wide range of different compounds **382–385**. When aniline **381a** was reacted with electron-poor alkenes **389** (2 eq.) in dichloromethane mediated by an iridium photocatalyst, the benzylic functionalised compounds **382a–c** were returned in 74%, 77% and 40% yield, respectively. When the reaction was performed with lowered equivalents of electron-poor alkene (1.1 eq.) and in MeCN, the N-methyl functionalised compounds were produced. For example, ketone **383a** and ester **383b** were isolated in 85% and 82% yield. Sequential N-methyl functionalisation was performed, and this gave compounds such as **384b** (71% yield) and **384c** (82% yield) from **383a**. This was accomplished from the reaction of **383a** with electron-poor alkene (2.0 eq.) in MeCN mediated with the iridium photocatalyst. Cyclic aldol compounds, such as **385a** and **385b** were produced when **381** was treated with methyl vinyl ketone (3 eq.), in the presence of K$_3$PO$_4$ and the Ir photocatalyst in MeCN (Scheme 109).

The radical coupling of protected amines **391** with electron-deficient alkenes **392** was investigated with iridium photocatalysis.[164] The use of N-propyl triflamide and benzyl acrylate as substrate with Ir[dF(CF$_3$)ppy]$_2$dtbbpy(PF$_6$) and caesium carbonate as base

This journal is © The Royal Society of Chemistry 2021

Chem. Soc. Rev., 2021, **50**, 9540–9685 | **9595**

Scheme 108 Selectivity of products determined by solvent.
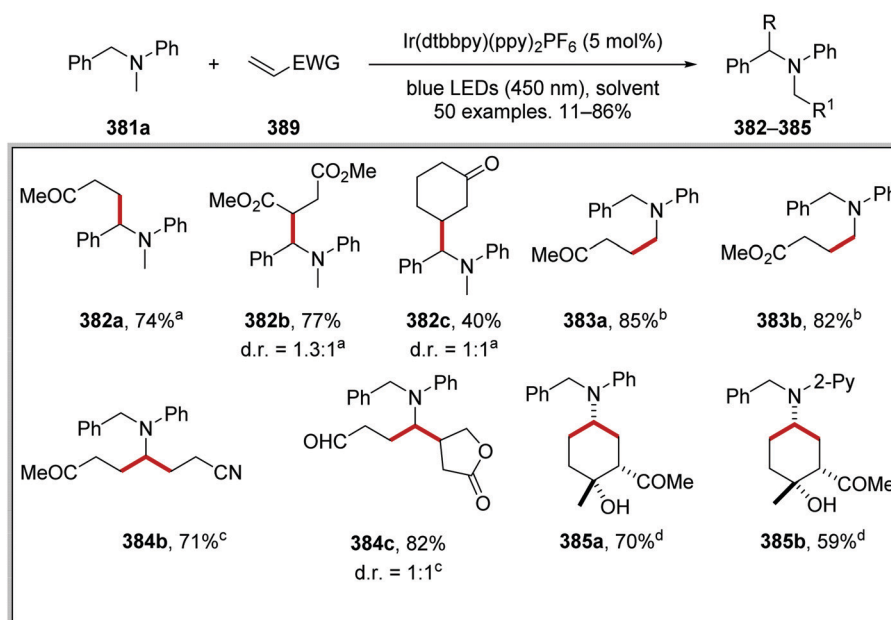
Scheme 109 Substrate-scope for site-elective coupling. [a] **389** (2 eq.), CH$_2$Cl$_2$, rt, 24 h. [b] **389** (1.1. eq.), DBU (0.3 eq.), MeCN, rt, 24 h. [c] **389** (1.1 eq.), DBU (0.3 eq.), MeCN, rt, 24 h then **389'** (2.0 eq.), DBU (0.3 eq.), MeCN, rt, 24 h. [d] **389** (3.0 eq.), K$_3$PO$_4$ (0.3 eq.), MeCN rt, 24 h.

gave ester **397** in 50% yield (Table 6, entry 1). Studies with other inorganic bases and other iridium catalysts determined that comparable yields of **397** were generated with Ir[dF(CH$_3$)ppy]$_2$dtbbpy(PF$_6$) (entries 2–4). However, increased efficiency was discovered when quinuclidine was employed as base and *tert*-butyl acrylate as electron-poor alkene giving **397** in 77% yield (entry 5). This reaction was only feasible when the triflamide protecting group was used (entries 5–8).

It was inferred that two feasible mechanisms could apply, depending upon the base employed in the reaction. When

9596 | *Chem. Soc. Rev.*, 2021, **50**, 9540–9685

This journal is © The Royal Society of Chemistry 2021

Table 6 Reaction optimisation. Catalyst A = Ir[dF(CF$_3$)ppy]$_2$dtbbpy(PF$_6$), catalyst B = Ir[dF(CH$_3$)ppy]$_2$dtbbpy(PF$_6$). Yields determined by ^{1}H NMR spectroscopy, asterisk denotes isolated yield

Entry	PG	Photocatalyst	R	Base	Yield (%)
1	Tf	A	Bn	Cs$_2$CO$_3$	50
2	Tf	A	Bn	K$_2$CO$_3$	54
3	Tf	A	Bn	K$_3$PO$_4$	58
4	Tf	B	Bn	K$_3$PO$_4$	65
5	Tf	B	tBu	Quinuclidine	77*
6	COCF$_3$	B	tBu	Quinuclidine	0
7	Ts	B	tBu	Quinuclidine	0
8	Ac	B	tBu	Quinuclidine	0

quinuclidine (**28b**) was used as base, it was thought, under the reaction conditions, triflamide **391a** was deprotonated with an equivalent of **28b** to give the anion **393a** (Scheme 110). Deprotonation of **391a** was supported by experimental pK_a values, N-methyltrifluoromethanesulfonamide and phenyl trifluoromethanesulfonamide have pK_a values of 7.56 and 4.45 respectively in water,[165] and the pK_a of quinuclidine conjugate acid is 11.3 in water.[166] It was thought that the excited iridium photocatalyst [Ir[(dFCF$_3$)ppy]$_2$dtbbpy(PF$_6$), (E_{red}* = +1.21 V vs. SCE) oxidised quinuclidine (E_{ox} = +1.1 V vs. SCE).[156] A selective HAT of the activated α-amino C–H bond of anion **393a** with quinuclidine radical **28b′** resulted in the formation of radical anion **394a**. Stern–Volmer experiments showed that effective quenching of Ir(III)* complex was seen with **28b**. Electron-rich radical **394a** was then

trapped with an electron-poor alkene **392a** and this gave coupled radical **395a**. SET and protonation of **395a** led to the formation of ester **397a** and closure of the iridium catalytic cycle. When K$_3$PO$_4$ was used as base, a different mechanism was thought to be in operation (Scheme 110, inset). The combination of **391a**, K$_3$PO$_4$ and excited Ir(III)* gave N-centred radical **393•** either through a concerted PCET process or a sequential deprotonation and SET event. The mechanism was supported by Stern–Volmer studies that showed quenching of Ir(III)* was achievable with **393a**. Radical **393•** was then able to react with another molecule of **393a** and this generated key intermediate **394a** for C–C bond formation with alkene **392a**.

When optimal reaction conditions were employed, the site-selectivity of this reaction was then demonstrated with the preparation of glucose **397g**, N-Boc **397h** and benzyl ether **397i** derivatives. Finally, it was shown that a range of different electron-poor alkenes could be used in this transformation, for example, compounds **397b–e** were prepared in yields of 32–73% (Scheme 111).

Quinuclidine (**28b**) was used as a HAT catalyst alongside photoredox catalyst Ir[dF(CF$_3$)ppy]$_2$(dtbbpy)PF$_6$ in the preparation of lactams **405** from primary amines **398** and methyl acrylate (**399a**) (Scheme 112).[167] Quinuclidine radical cation **28b′** was generated with SET to excited Ir(III)* complex (Ir[dF(CF$_3$)ppy]$_2$-dtbbpy(PF$_6$) E_{red}* = +1.21 V vs. SCE) from quinuclidine (E_{ox} = +1.1 V vs. SCE). As the reaction was performed under carbon dioxide, carbamate **400** was formed from amine **398** and carbon dioxide. The formation of carboxylate **400** assisted in the HAT event and formation of **401**, due to the electrostatic attraction between the negatively charged carboxylate ion and the positively
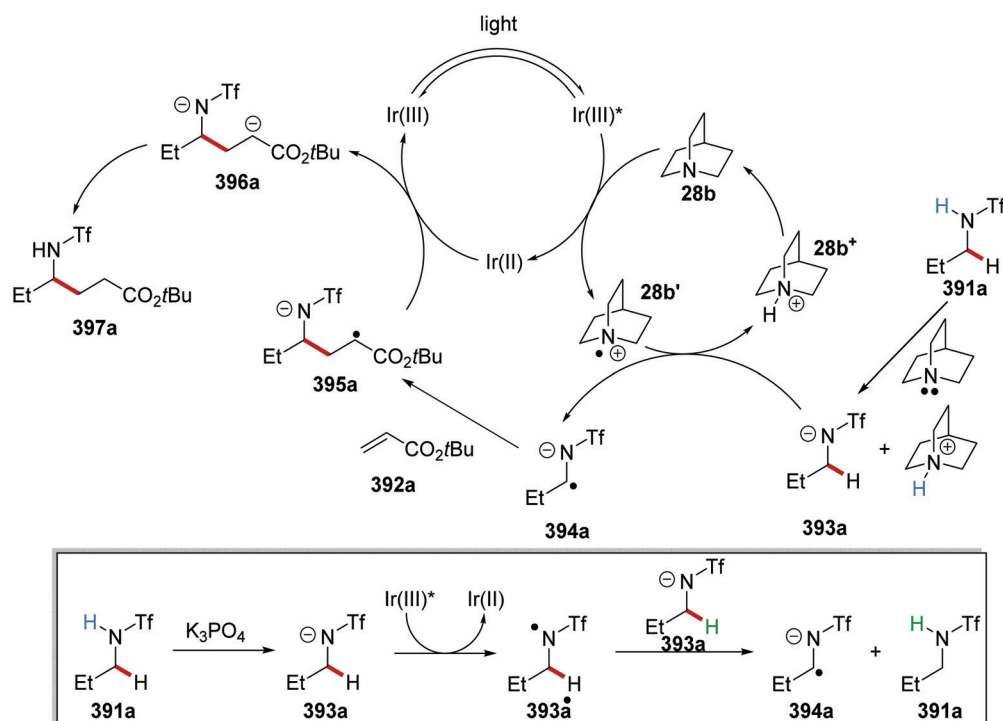
Scheme 110 α-C–H functionalisation of triflamides **391** with electron-poor alkenes **392**.

This journal is © The Royal Society of Chemistry 2021

Chem. Soc. Rev., 2021, 50, 9540–9685 | 9597
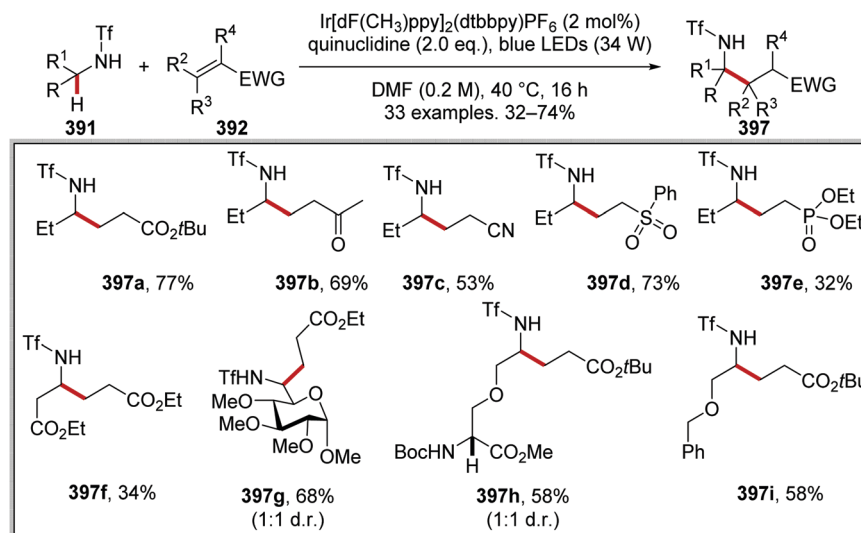
Scheme 111 α-C–H functionalisation of triflamides **387** with electron-poor alkenes **388**.
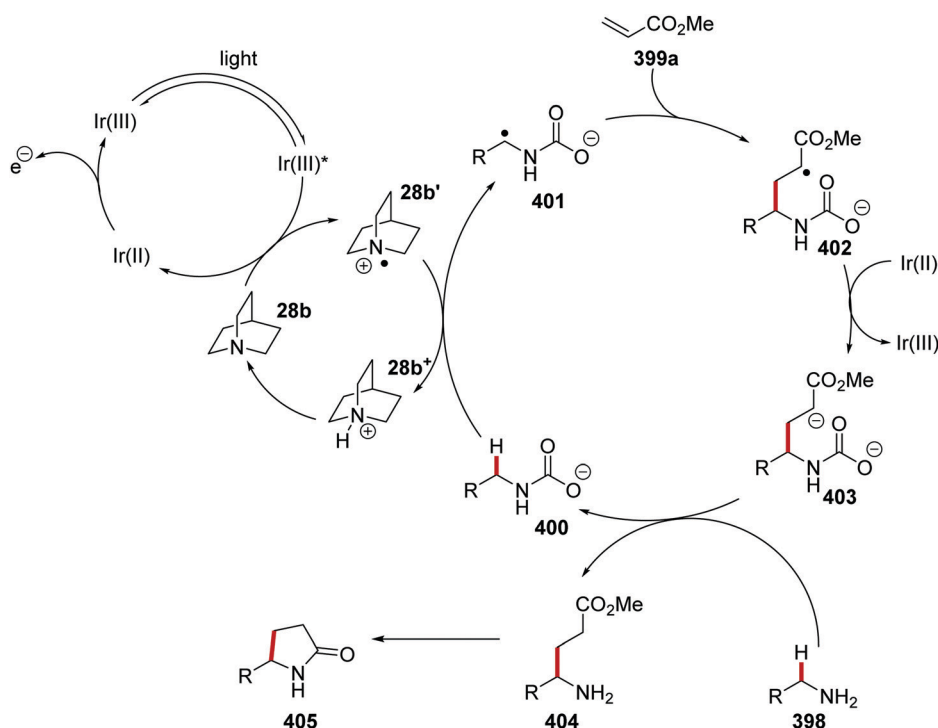
Scheme 112 Lactam formation from primary amines.

charged **28b′**; this enhanced the selectivity with abstraction at the most hydridic C–H bond. Once alkyl radical **401** was delivered, it reacted with the electron-poor alkene **399a** and this gave α-carbonyl radical **402**. Electron transfer from the reduced Ir(II) complex to radical **402** resulted in the generation of the original Ir(III) species and enolate anion **403**. Protonation of anion **403** and loss of carbon dioxide gave amine **404**. Lactam **405** was formed from **404** with the loss of methanol.

Optimisation of the reaction conditions found that quinuclidine was the best HAT catalyst. When 3-acetoxyquinuclidine

(**28d**) was used instead of quinuclidine (**28b**), a decreased ^{1}H-NMR yield of lactam **405a** was obtained. Use of DABCO instead of quinuclidine led to no observable product formation. When the reaction was performed with no carbon dioxide, the ^{1}H-NMR yield decreased from 85% to 25%. With optimal conditions being established, a library of 45 lactams **405** was prepared in 41–80% yields (Scheme 113 for selected examples). The reaction was tolerant of functional groups with trifluoromethyl **405b**, ester **405c**, silyl protected alcohols **405d**, alkynes **405f**, acetals **405g** and heterocyclic **405h** analogues all being

9598 | Chem. Soc. Rev., 2021, **50**, 9540–9685

This journal is © The Royal Society of Chemistry 2021
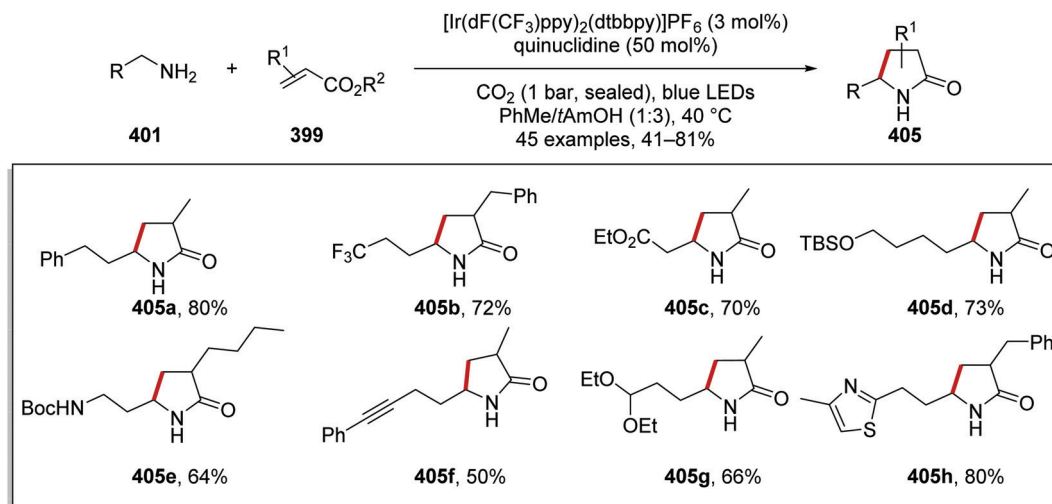
Scheme 113 Products from lactam formation from primary amines.

synthesised. The directing effect of carboxylate intermediate 400 with quinuclidine radical 28b′ was demonstrated with the preparation of N-Boc amine compound 405e as there was no alkylation adjacent to the N-Boc group.

It was shown that amidyl radicals could be used as effective HAT catalysts.[168] The combination of Ir[dF(CF$_3$)ppy]$_2$(5,5′-dCF$_3$-bpy)PF$_6$ and dibutyl phosphate (406) gave amidyl radical 407 from N-ethyl-4-methoxybenzamide (408) thro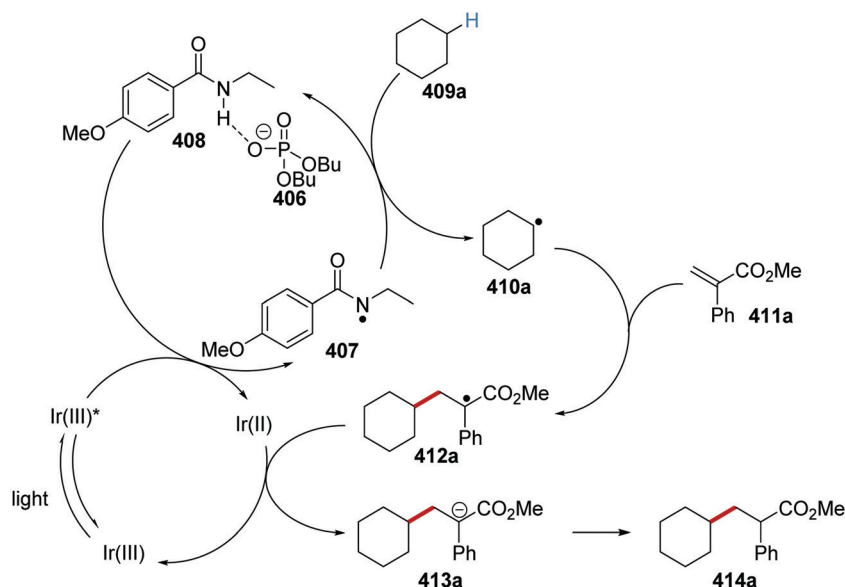ugh PCET when irradiated with blue LEDs (Scheme 114). Amide 408 (E_p = +1.48 V vs. Fc/Fc$^+$) was unable to directly quench the Ir catalyst (Ir[dF(CF$_3$)ppy]$_2$(5,5′-dCF$_3$bpy)PF$_6$ $E_{1/2}$* = +1.30 V vs. Fc/Fc$^+$) but the presence of tetrabutylammonium dibutyl phosphate resulted in large decrease in emission intensity. Radical 407 abstracted a hydrogen atom from cyclohexane (409a) and this gave alkyl radical 410a. A Giese coupling between 410a and electron-poor alkene 411a resulted in C–C bond formation

giving α-ester radical 412a. The iridium catalytic cycle was closed with an outer-sphere electron transfer from Ir(ii) to 412a and this gave anion 413a, which was converted to 414a with protonation.

The use of amidyl radicals as HAT reagents allowed for C–H activation of alkanes, ethers, and amines. Thus, with electron-poor alkenes, 414a, 414b and 414c were prepared (Scheme 115).

Alkenation. The preparation of alkenes 417 was achieved with amines 415 and vinyl sulfones 416 using an iridium photoredox catalyst (Schemes 116 and 117).[169] Under the reaction conditions, the excited Ir(iii)* complex (Ir[dF(CF$_3$)ppy]$_2$(dtbbpy)$^+$ E_{red}* = +1.21 V vs. SCE) underwent SET from amine 415a (N-phenylpiperidine E_{ox} = +0.72 V vs. SCE) and this gave Ir(ii) complex and amine radical cation 418a. Proton loss from 418a led to carbon centred-radical 419a, which added to 416a resulting in benzylic radical 420a.

Scheme 114 Preparation of 414a with amidyl HAT catalyst.

This journal is © The Royal Society of Chemistry 2021

Chem. Soc. Rev., 2021, 50, 9540–9685 | 9599
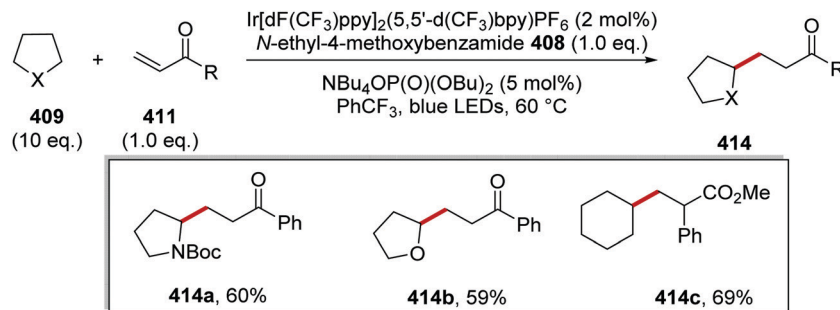
Scheme 115 Applications of amidyl HAT catalyst **408**.
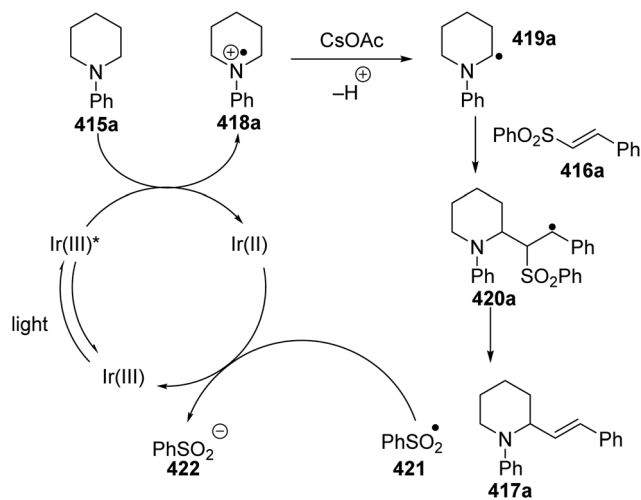
Scheme 116 C–H activation and radical coupling to electron-poor alkenes.

Elimination of sulfonyl radical **421** from **420a** afforded alkene **417a**, and the iridium catalytic cycle was closed with SET to **421** from Ir(II).

This transformation was then realised with the use of Ir(dF(CF₃)ppy)]₂(dtbbpy) photocatalyst and CsOAc as base (Scheme 117). This system allowed for the preparation of 28

alkenes **417** from the corresponding amines **415** and vinyl sulfones **416**. In most cases, the E isomer was predominantly formed.

The coupling of heteroaryl chlorides **423** to dialkylanilines **415** was investigated and this gave amines **424** (Scheme 118).[170] A wide range of coupled products **424a**–**424i**, was prepared in 72–94% yields although only 22% yield was obtained for compound **424j**.

Gandotnib (**428**) is a selective inhibitor of JAK2-V617F and is currently being studied in phase 2 clinical trials in patients with myeloproliferative neoplasms (ClinicalTrials.gov Identifier: NCT01594723).[171] Preparation of key intermediate **426** was carried out with C–H activation and radical coupling chemistry (Scheme 119). The coupling of unfunctionalised pyridazine **425** with N-methylmorpholine (20 eq.) was achieved with an Ir(ppy)₃ photocatalyst (0.5 mol%). From extensive investigation, it was found that a solvent system of 10:1 DMA/H₂O gave the highest selectivity for desired regioisomer **426**. The reaction, performed in DMA as the sole solvent, led to a substantial amount of unwanted endo compound **427**; however, the addition of water minimised this byproduct. Product **426** was isolated from the reaction mixture by the addition of 3:1 H₂O:EtOH and this afforded the product in 56% isolated yield and with 90% purity. Highly pure **426** was obtained with an acid/base recrystallisation procedure which gave **426** in 98% UPLC purity.
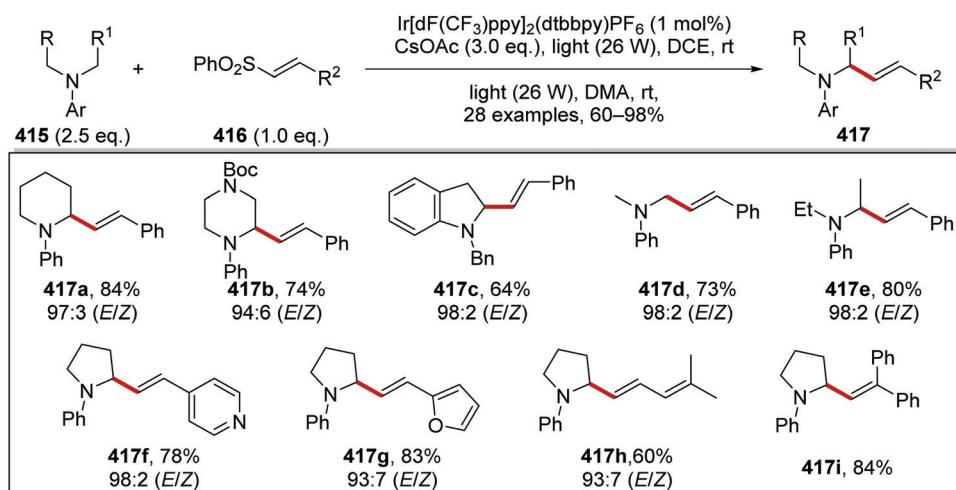
Scheme 117 Results of radical coupling between amines **415** and vinyl sulfones **416**.
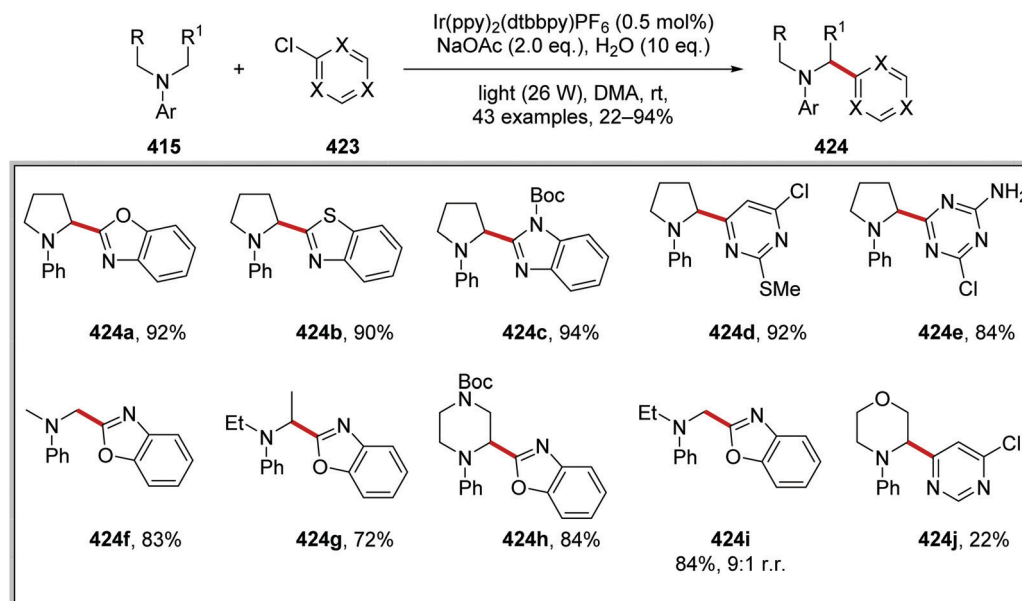
Scheme 118 Results of coupling between heteroaryl chlorides **423** and alkylanilines **415**.
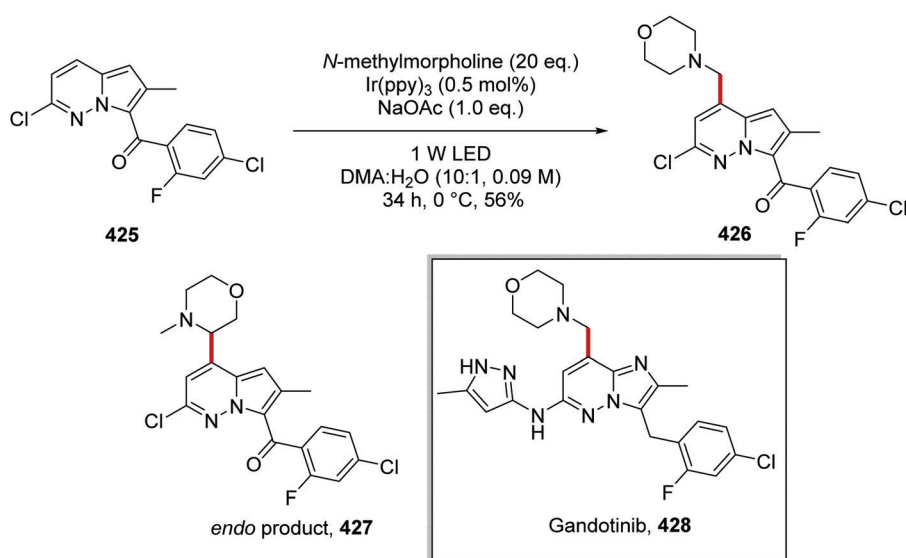
Scheme 119 Preparation of intermediate **426** for the synthesis of **428**, a selective inhibitor of JAK2-V617F.

Radical–radical coupling. The direct α-monofluoroalkenylation of α-heteroatom C–H bonds **429** with *gem*-difluoroalkenes **430** was achieved with an iridium HAT catalytic system (Scheme 120).[155a] A mechanism was proposed by the authors that was based upon previous work by Hashmi.[155b] Radical cation (**28b'**) was formed from a PET to Ir(III)* complex ($E_{red}^* = +1.21$ V *vs.* SCE) from quinuclidine ($E_{ox} = 1.1$ V *vs.* SCE). HAT from the *N*-Boc amine **429a** to **28b'** gave α-amido radical **431a**. The iridium catalytic cycle was closed with SET to alkene **430a** ($E_{red} = -1.04$ V *vs.* SCE) from reduced iridium catalyst ($E_{ox} = -1.37$ V *vs.* SCE) delivering radical **432a**. A radical–radical coupling reaction between the two radicals was proposed to lead to alkene **433a**. However, radical–radical couplings are rare, unless at least one of the radicals has

substantial lifetime in solution. This may be the case for **431a**. In the paper, a control experiment was carried out where the combination of alkene **430b** and *N*-Boc pyrrolidine **429a** resulted in formation of tetracycle **433b** under the reaction conditions (see box). This was taken to support the intermediacy of fluoroalkenyl radicals **432**. However, it can also support the formation of the precursor to **432**, namely a vinyl radical anion **434**. Thus, perhaps the formation of **433a** involves the coupling of **431a** with radical anion **434a** to give anion **435**. Expulsion of fluoride would then afford product **433a**.

The use of 1 mol% of Ir(dFCF$_3$ppy)$_2$(dtbbpy)(PF$_6$) as photocatalyst and 20 mol% quinuclidine under basic conditions gave coupling between **429** and **430** after 24 h at room temperature.

This journal is © The Royal Society of Chemistry 2021

Chem. Soc. Rev., 2021, **50**, 9540–9685 | **9601**
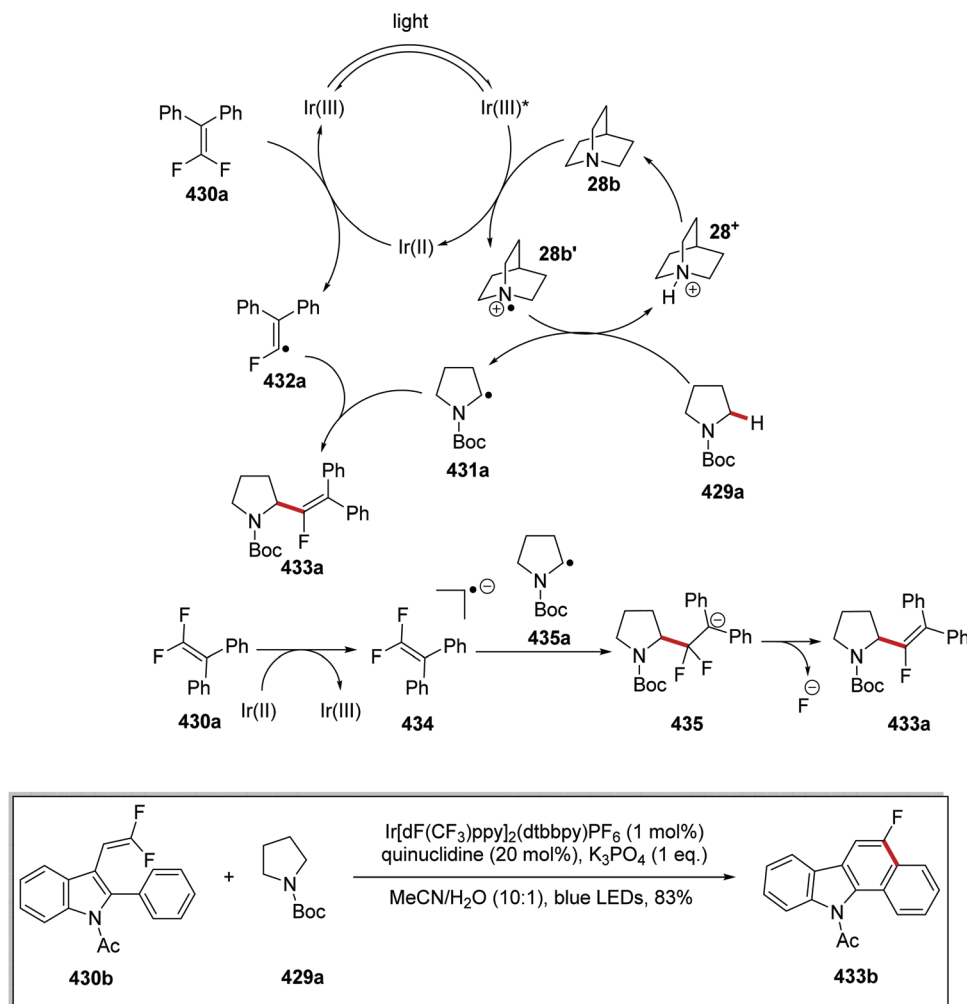
Scheme 120 HAT mediated coupling of *N*-Boc amine **429a** with *gem*-difluoroalkene **430a**.

From optimisation studies, it was found that the solvent system MeCN:H$_2$O (10:1 ratio) was optimal for the formation of **433a**. When MeCN was used as the sole reaction solvent, the yield decreased from 79% to 43% for **433a**. It was postulated that the inclusion of water in the reaction mixture increased the solubility of the base and this increased the efficiency of the reaction. The use of the HAT reagents aceclidine (3-acetoxyquinuclidine) or 3-quinuclidinol also led to a less successful reaction with **433a** being isolated in 40% or 0% yield, respectively. The use of potassium carbonate as base also led to an inferior reaction, forming **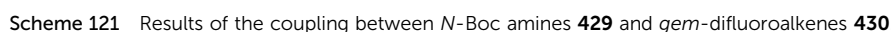433a** in 60% yield. No reaction proceeded when photocatalyst, HAT catalyst, light or base was absent from the reaction mixture. Furthermore, there was no reaction when Ru(bpy)$_3$(PF$_6$)$_2$ was used as the photocatalyst. This is understandable as the excited Ru complex is unable to oxidise quinuclidine. When optimised conditions were applied, a wide range of products was prepared **433a–k** (Scheme 121).

Nickel coupling. The C–H bonds adjacent to Boc-protected alkyl amines were utilised in carbon sp^3–sp^2 bond formation with aryl bromides.[48] The reaction was propagated with the

Ir[dF(CF$_3$)ppy]$_2$(dtbbpy)PF$_6$ photocatalyst, a quinuclidine-based HAT catalyst and a nickel-based cross-coupling catalyst. Under the reaction conditions, the iridium photocatalyst was excited to the Ir(III)* species (Scheme 122). The excited photocatalyst was quenched with 4-acetoxyquinuclidine (**28d**) and this gave amine radical cation **28d′** and an Ir(II) species. The SET transfer between Ir(III)* and **28d** was feasible with regards to redox potentials $[E_{1/2}^{red}(*Ir^{III}/Ir^{II}) = +1.21$ V *vs.* SCE, in MeCN and E_p of 3-acetoxyquinuclidine $= +1.22$ V *vs.* SCE, in MeCN]. Direct oxidation of *N*-Boc pyrrolidine (**434a**, $E_{ox} = +2.09$ V *vs.* SCE)[48b] with the iridium catalyst is unfeasible. However, **434a** has electron-rich α-amino C–H bonds, which were selectively abstracted by the electron-poor radical cation **28d′** and this gave radical **435a** and protonated amine **28d⁺**. The α-amido C–H bonds of **434** are weak (the α-amino C–H bonds of **434a** BDE = 92 kcal mol^{-1})[36] hence this HAT event is thermodynamically favourable with the formation of a strong quinuclidine N–H bond (N–H BDE of **28d⁺** = *ca.* 100 kcal mol^{-1}).[43,45] Carbon-centred radical **435a** was intercepted with a Ni(0) complex and this gave a Ni(I) complex. Oxidative addition between Ni(I) complex and aryl bromide **436a** gave a nickel(III) complex, which underwent

9602 | *Chem. Soc. Rev.*, 2021, **50**, 9540–9685

This journal is © The Royal Society of Chemistry 2021

Scheme 121 Results of the coupling between *N*-Boc amines **429** and *gem*-difluoroalkenes **430**.

Scheme 122 HAT-mediated radical cross-coupling.

reductive elimination, and coupled compound **437a** and Ni(I) complex were formed. The nickel and iridium catalytic cycles were closed between Ni(I) and Ir(II) complexes.

The combination of Ir[dF(CF$_3$)ppy]$_2$(dtbbpy)PF$_6$ (1 mol%), 3-acetoxyquinuclidine (1.1 eq.), NiBr$_2$ (1 mol%), the ligand 4,7-dimethoxy-1,10-phenanthroline (1 mol%) gave **437c** in 81% yield from *N*-Boc pyrrolidine and 4-bromobenzoate. The reaction was regioselective with only one regioisomer being detected. The compound **434a** was functionalised at the most hydridic C–H bond. The optimised reaction conditions were trialled on a range of substrates and this produced 40 coupled compounds (Scheme 123). Functionalisation of α-carbamate C–H bonds was achieved and coupled compounds **437a–437h** were achieved in yields of 62–81%. Benzylic C–H functionalisation was also achievable; for example, diaryl compound **437i** was

isolated in 54% yield. From the substrate scope, it was observed that this transformation preferred to functionalise the most sterically accessible site. For example, when *N*-Bac butylmethyl-amine was treated with these optimised conditions, a 4:1 mixture of regioisomers was obtained for **437f** in favour of functionalisation on the methyl group over the methylene group. Additionally, only one regioisomer was obtained for starting amines possessing α-methyl or methylene and α-methine groups, see compounds **437g** and **437h**. Therefore, no functionalisation at α-amino methine groups was achievable under these conditions.

Carbon sp^3–sp^3 bonds were formed with functionalisation of α-amido C–H bonds with the use of alkyl bromides **438** with a similar iridium/nickel/quinuclidine catalytic system (Scheme 124).[156] It was observed that C–H functionalisation occurred at the site of least steric hindrance. Therefore, the preparation of coupled

This journal is © The Royal Society of Chemistry 2021

Chem. Soc. Rev., 2021, **50**, 9540–9685 | **9603**
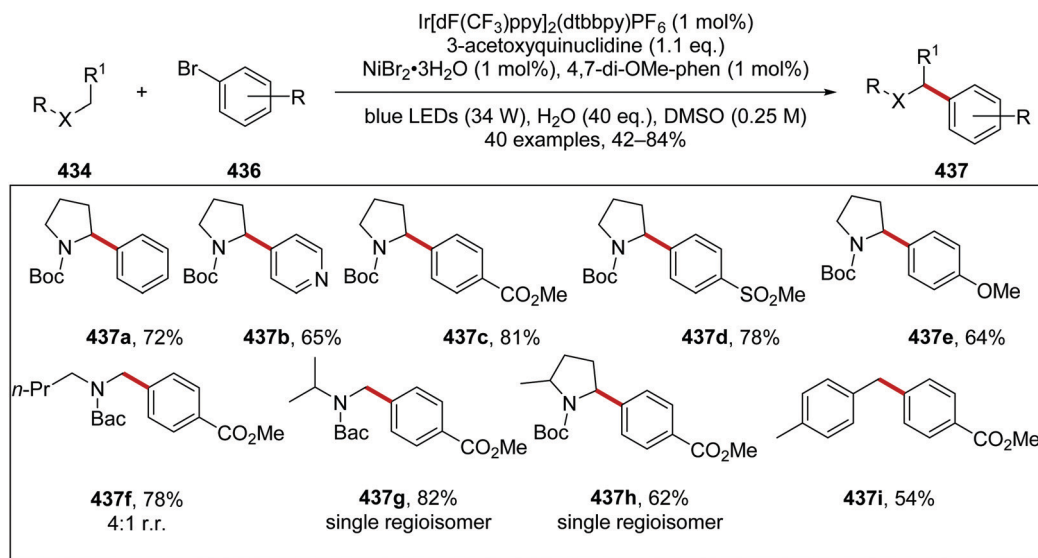
Scheme 123   Results of HAT mediated radical cross-coupling.
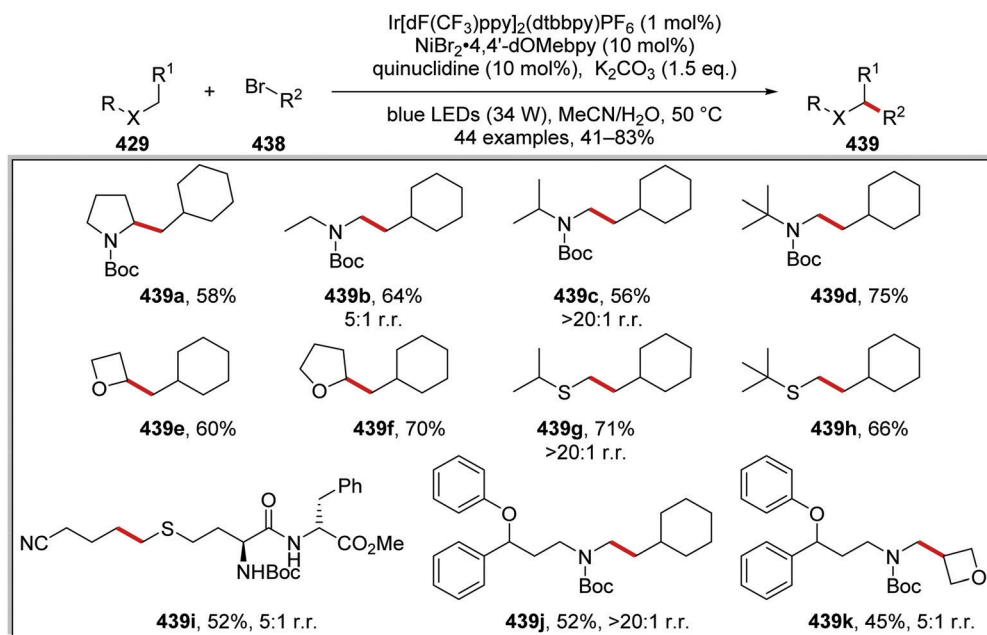
Scheme 124   HAT catalyst mediated sp^3–sp^3 coupling reaction.

compounds **439b, 439c, 439g, 439j** and **439k** was achieved with a high degree of regiocontrol. In addition, C–H bonds adjacent to oxygen atoms and sulfur atoms were susceptible to functionalisation and this gave coupled compounds **439e–439i**.

The coupling of aryl chlorides **440** with ethers **441** was achieved with iridium photoredox conditions, blue-light irradiation and the use of chlorine atoms as HAT catalysts.[49] The reaction occurred *via* oxidative addition of aryl chloride **440** to Ni(0) complex **A** and this gave Ni(II) c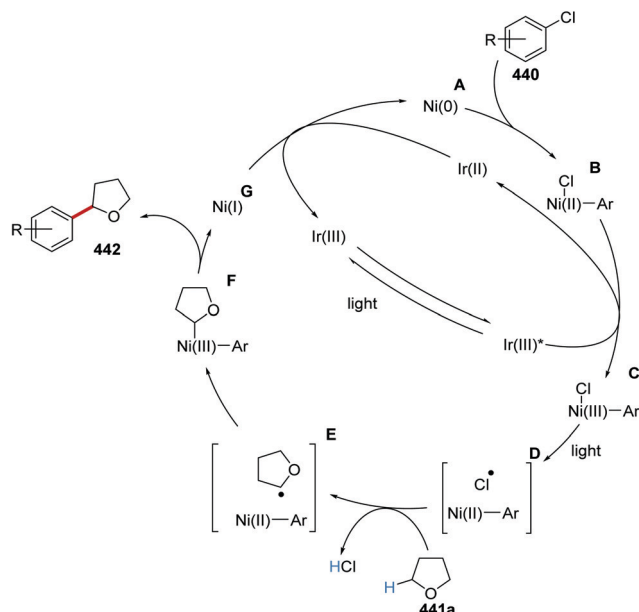omplex **B** (Scheme 125). This was followed with a SET between **B** and excited Ir(III)* complex and gave Ir(II) complex and Ni(III) complexes **C**. From cyclic voltammetry, it was found that oxidation of Ni(II) complex **B** (E_p = +0.85 V *vs.* SCE) was

achievable with Ir(III)* species ($E_{1/2}$* = +1.21 V *vs.* SCE). Furthermore, from a Stern–Volmer quenching study, it was found that Ni(II) complex **B** significantly quenched the excited Ir(III)* complex. It was reported that a chlorine atom dissociated under irradiation with light.[172] Therefore, it was thought that, under the reaction conditions, Ni(III) complex **C** liberates a chlorine atom. HAT from tetrahydrofuran substrate **441a** (THF C–H BDE = 92 kcal mol^{-1}) to a chlorine atom (H–Cl BDE = 102 kcal mol^{-1}) resulted in the alkyl radical and this culminated in Ni complex **F**. Desired product **442** was formed with the reductive elimination from **F**. SET between Ni(I) complex **G** and Ir(II) complex closed both catalytic cycles.
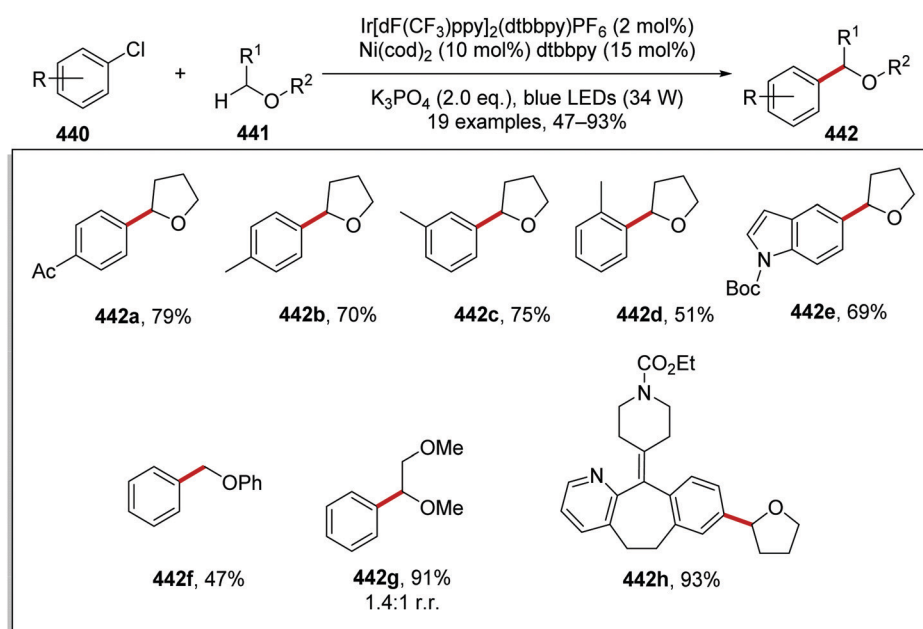
9604 | *Chem. Soc. Rev.,* 2021, **50**, 9540–9685

This journal is © The Royal Society of Chemistry 2021

Scheme 125 Formation of tetrahydrofuran **442** with chlorine atom HAT catalysis.

From optimisation studies, it was observed that the combination of Ni(cod)$_2$, dtbbpy, Ir[dF(CF$_3$)ppy(dtbbpy)PF$_6$ and K$_3$PO$_4$ allowed for the preparation of **442a** in 92% ^{1}H-NMR yield and 79% isolated yield (Scheme 126). The less oxidising photocatalyst, Ru(bpy)$_3$(PF$_6$), gave no product. When NiCl$_2$·glyme was used as a Ni source, a diminished NMR yield of 61% of **442a** was obtained. This transformation also operated without the use of base. However, this gave a less productive process affording **442a** in 13% ^{1}H-NMR yield. The source of light also had a crucial bearing upon the efficiency of this

reaction. When a blue LED array (25 W) was used as a light source for the preparation of **442a**, a 33% GC-FID yield was obtained, after 72 h. However, using a blue LED lamp (34 W) this yield was increased to 65%. When the optimised reaction conditions were established, the scope of this transformation was explored. It was found that a range of tolyl products could be prepared, **442b**–**442d**, while carbamate-protected heterocyclic compound **442e** was given in 69% yield. When methyl phenyl ether and dimethoxyethane were employed in the reaction, compounds **442f** and **442g** were given. For **442g** a mixture of regioisomers was obtained with a ratio of 1.4∶1 in favour of the branched isomer. Therefore, this indicated selectivity for the weaker C–H bond. Furthermore, this transformation could be carried out on bioactive molecules, for example, the medicinal compound loratadine and this gave compound **442h** in 93% yield.

Aldehyde C–H functionalisation. The formyl C–H bond of the aldehyde functional group is weak [the BDE for ethanal (CH$_3$C(O)–H) is 86.0 kcal mol^{-1} and the BDE for benzaldehyde (C$_6$H$_5$C(O)–H) is 86.9 kcal mol^{-1}].[51] Therefore, these bonds make appropriate targets for HAT catalysis and this was achieved with a tri-catalytic reaction system.[173] The combination of an iridium photoredox catalyst, quinuclidine **28b** and a nickel cross-coupling catalyst allowed for the functionalisation of aldehyde **443a** with aryl bromide **444a** and this produced ketone **445a** (Scheme 127). Irradiation of the reaction mixture with blue light gave the excited Ir(III)* catalyst. The excited iridium catalyst (E_{red}^* = +1.21 V *vs.* SCE) underwent SET from quinuclidine (**28b**) (E_{ox} = +1.1 V *vs.* SCE) and this resulted in radical cation **28b′**. Radical **28b′** abstracted a hydrogen atom from the weak RC(O)–H bond giving **446a** from **443a**. Acyl radical **446a** was intercepted by Ni(0) complex, this gave a Ni(I) complex, which underwent oxidative addition with **444a** and this yielded a

Scheme 126 Chlorine atom as HAT catalyst.

This journal is © The Royal Society of Chemistry 2021

Chem. Soc. Rev., 2021, **50**, 9540–9685 | 9605
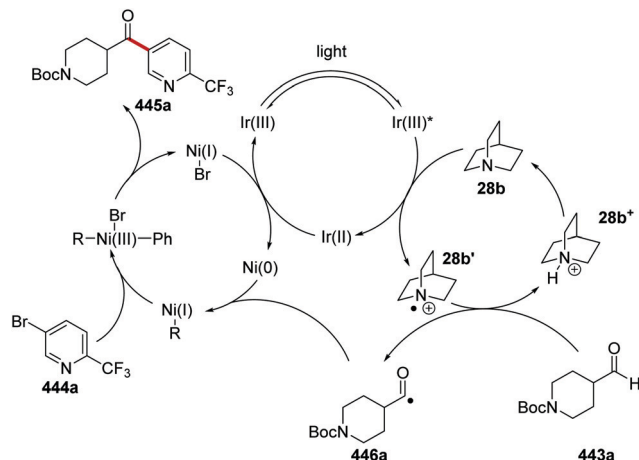
Scheme 127   Formation of **445a** with a tricatalytic system.

Ni(III) complex. Reductive elimination of the Ni(III) complex gave ketone **445** and Ni(I) complex. Both the iridium and nickel catalytic cycles were closed with an electron transfer from the Ir(II) complex to Ni(I).

Optimal reaction conditions were found in the preparation of ketone product **445a**. Initially, the reaction was attempted in DMSO and MeCN, and this gave **445a** in 2% and 8% yield, respectively. The low yields were due to a competing α-amido C–H abstraction mechanism. However, this was overcome when the reaction was performed in 1,4-dioxane, which gave ketone compound **445a** in 87% isolated yield (Scheme 128). It was thought that the solvent dielectric constant was crucial in stabilising the ionic quinuclidinium radical cation, which influenced the roles of BDEs and bond polarization upon the kinetics of this transformation. With these optimised reaction conditions, 44 coupled compounds were prepared in yields ranging from 50% to 92%. Electron-poor **445b** and electron-rich **445c** arenes were prepared, as well as alkyl ketones **445d**.

The aldehyde coupling partner was also varied and this gave ketones **445e–445h**.

Aldehydes **447** were functionalised with benziodoxole-derived alkynes **448** mediated with sodium 2-iodobenzoate as a HAT catalyst and an iridium photocatalyst, and this gave alkyne products **449** (Scheme 129).[174] From these conditions, 36 alkynes **449** were prepared in yields ranging from 46% to 90%. Silyl functional groups such as TIPS were accommodated under the reaction conditions and this gave **449d** in a 70% yield. Aromatic and non-aromatic heterocycles were also suitable substrates, giving **449e** and **449f** in a 65% and a 77% yield, respectively. The reaction conditions also tolerated ester functionality and ester **449g** was prepared in 56% yield.

The reaction mechanism for this reaction (Scheme 130) proposes that the photoactivated iridium catalyst was quenched by iodobenzoate **450** which was oxidised to the corresponding carboxyl radical **451**. This then abstracted the formyl hydrogen from the aldehyde substrate **447**. The resulting acyl radical **453** attacks the alkyne of the alkynyl benziodoxolone **448** displacing the benziodoxolonyl radical **454**. This can either isomerise to the carboxyl radical **451** or can oxidise the Ir(II) complex back to Ir(III).

Alcohol C–H functionalisation. The regioselective arylation of α-hydroxy C–H bonds was accomplished with a quinuclidine HAT catalyst, with stoichiometric amounts of zinc chloride under basic conditions.[175] The combination of base and ZnCl$_2$ allowed for the formation of zinc alkoxide, which accentuated the hydridic character of the α-hydroxy C–H bonds (Scheme 131). However, the dative coordination between ZnCl$_2$ and amines diminished the hydridic nature of α-amino C–H bonds and this increased the site-selectivity for α-hydroxy C–H bonds. As mentioned above, under the basic reaction conditions, alcohol **455a** was converted to zinc metal alkoxide **456a**. Concurrently, irradiation of the reaction mixture with blue light gave Ir(III)* complex ($E_{red}^* = +1.21$ V *vs.* SCE) which oxidised quinuclidine (**28b**, $E_{ox} = +1.1$ V *vs.* SCE) producing **28b'**. The nature of the key
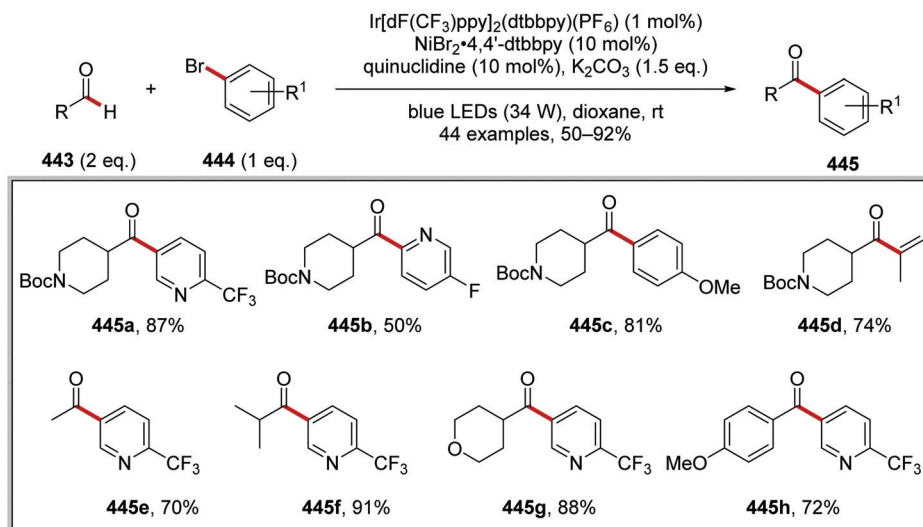
Scheme 128   Preparation of ketones **445** from aldehydes **443**.
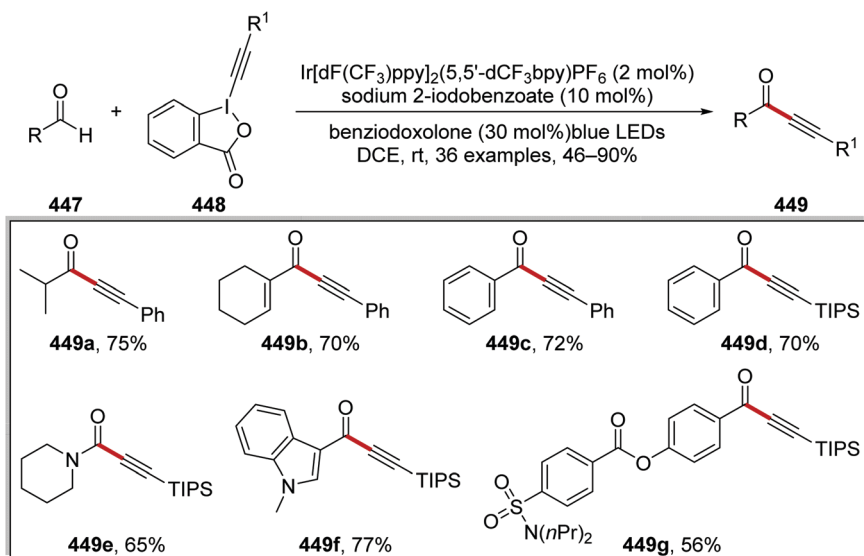
Scheme 129 Formation of alkyne compounds **449** from aldehydes **447**.
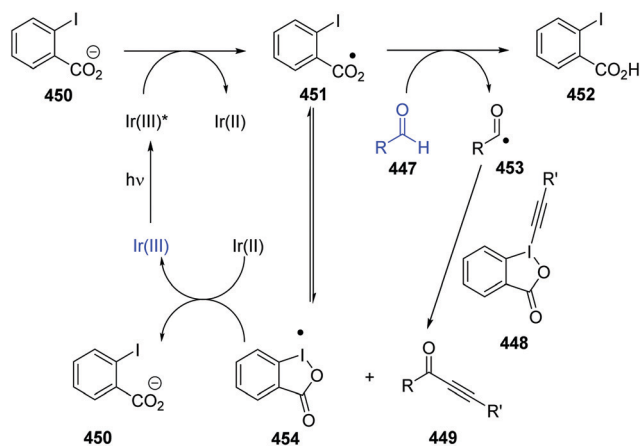
Scheme 130 Mechanism for coupling alkynes to aldehydes.

intermediate **456a** promoted HAT with electron-poor radical cation **28b′**. The HAT event between **28b′** and **456a** gave α-oxyalkyl radical **457a** and quinuclidinium (**28b⁺**). Radical **457a** was intercepted with Ni(0) complex to give a Ni(ɪ) complex. Oxidative addition of **458a** to Ni(ɪ) complex gave a Ni(ɪɪɪ) species, which underwent reductive elimination returning coupled alcohol **459a** and Ni(ɪ) complex. Both iridium and nickel catalytic cycles were closed with SET between Ni(ɪ) and Ir(ɪɪ) complexes.

The reaction was optimised with the preparation of alcohol **459a** (Schemes 131 and 132). Initially, when no Lewis acid was present, this resulted in exclusive Ar–O bond formation (yield of the ether product was 54%) and **459a** was isolated in a 3% yield. From a survey of Lewis acids, it was found that the Lewis acids $ZnCl_2/ZnBr_2$ gave maximal yields of **459a**. When $ZnCl_2$ was employed as Lewis acid, with quinuclidine (3 eq., as base and HAT catalyst),
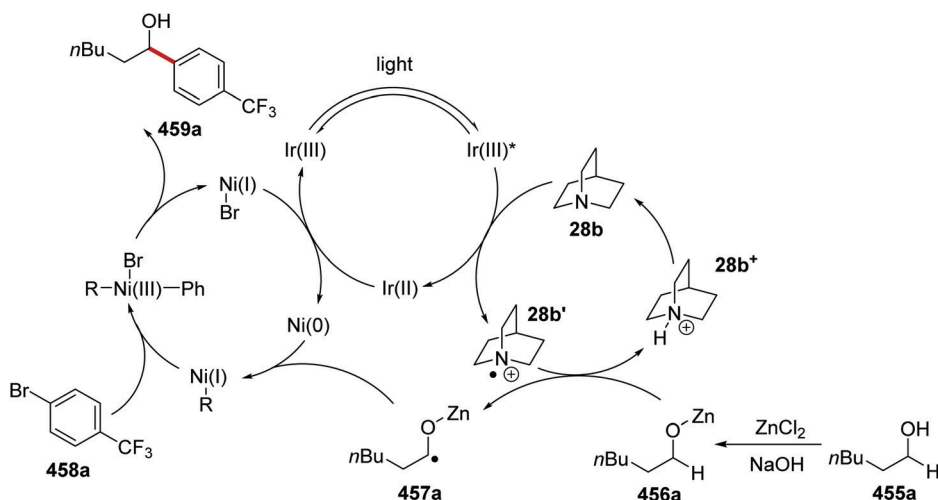
Scheme 131 Formation of benzylic alcohol **459a** from *n*-hexanol (**455a**).

This journal is © The Royal Society of Chemistry 2021

Chem. Soc. Rev., 2021, **50**, 9540–9685 | 9607
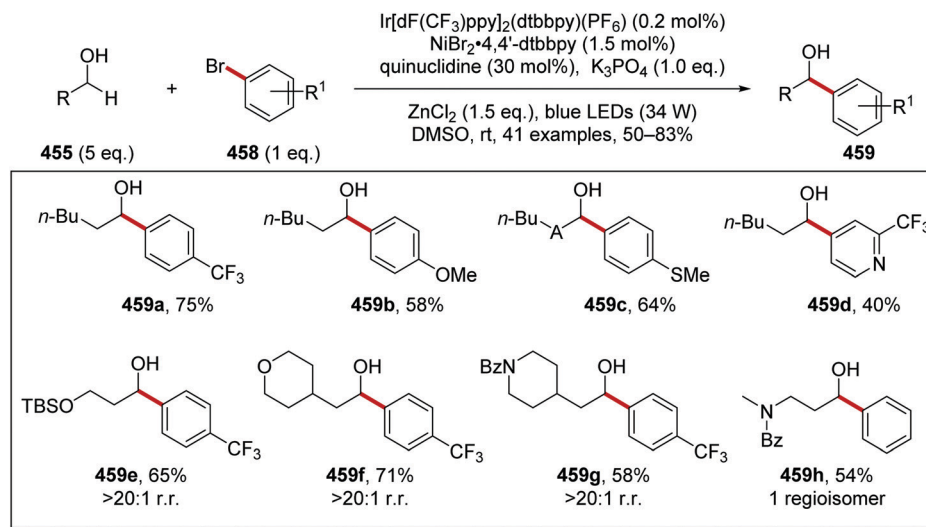
Scheme 132 Preparation of benzylic alcohols 459.

this delivered 459a in 44% yield. When the reaction was performed with sodium hydroxide and a lower loading of quinuclidine (30 mol%), this gave 459a in 66% yield. When the reaction was performed with the base, potassium phosphate, and ZnCl$_2$ (1.5 eq.), this afforded 459a in 75% yield and these were taken as optimal conditions (Scheme 132). With these conditions, the scope of the reaction was studied. From the substrate scope, it was observed that n-hexanol was coupled to both electron-rich and electron-poor aryl rings; this gave hydroxy compounds 459a–459d. Functionalisation was site-selective for α-hydroxy C–H bonds, despite when multiple "hydridic" C–H bonds were present. This was demonstrated with the preparation of silyl-protected alcohol 459e, ether 459f and N-benzoyl amide 459g analogues, all with pronounced site-selectivity. The synthetic utility of this process was demonstrated with the preparation of N-benzoyl amide compound 459h, an intermediate for the drug-molecule Prozac.

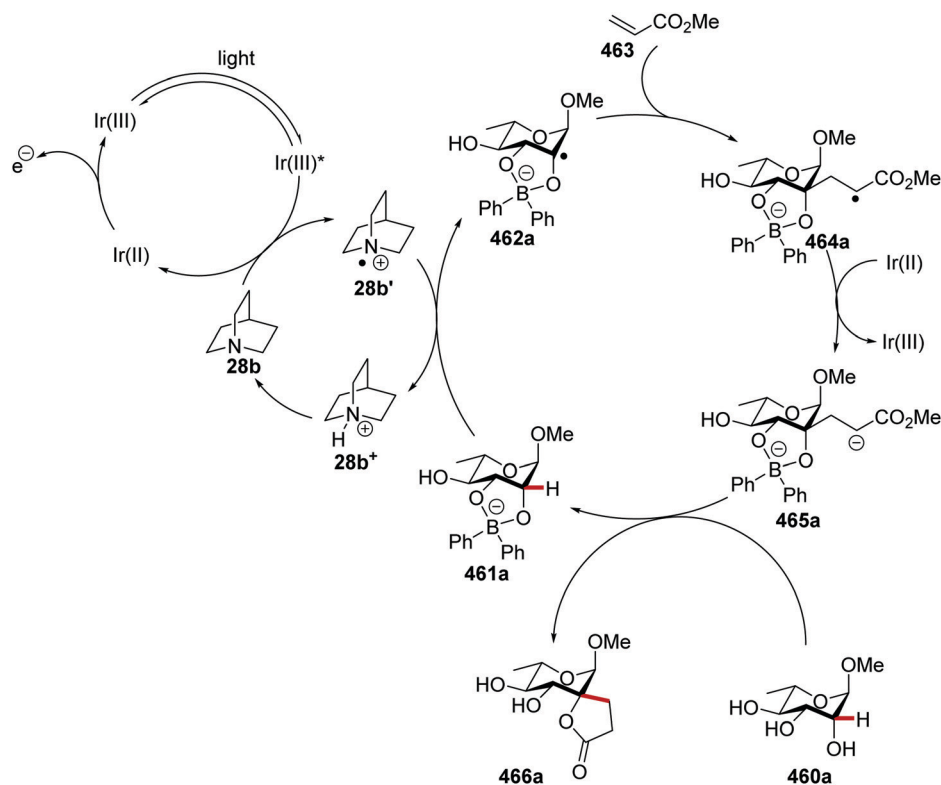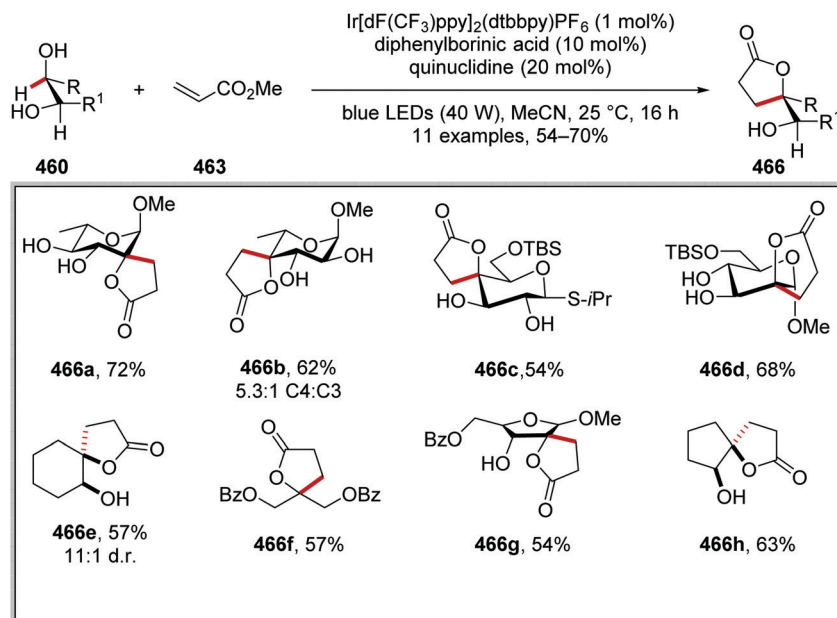The stereo- and site-selective C–H alkylation of carbohydrate-based compounds was achieved with the implementation of a tri-catalytic reaction system.[176] The functionalisation of sugar molecules was facilitated with Ir[dF(CF$_3$)ppy](dtbbpy)$_2$PF$_6$ as photocatalyst, quinuclidine (28b) as HAT catalyst and diphenylboronic acid as cocatalyst. The tricatalytic reaction system allowed selective radical alkylation of C–H bonds of cis-1,2-diol moieties at the equatorial position. Under the reaction conditions, the iridium photocatalyst was excited with blue light and this gave Ir(III)* species (Scheme 133). Ir(III)* converted 28b to radical cation 28b'. At the same time, diphenylboronic acid coordinated to rhamnopyranoside (460a) and this gave boronate adduct 461a. This activated the less hindered equatorial C–H bond for HAT. The selectivity of the HAT process was due to the greater hydridic nature of the C–H bond and the electrostatic attractions between boronate 461a and the positively charged radical species 28b'. The HAT event between 28b' and 461a resulted in radical 462a and protonated quinuclidinium (22$^+$). Giese addition between carbon-centred radical 462a and electron-poor alkene

463 resulted in α-carbonyl radical 464a. The iridium catalytic cycle was closed with SET between reduced Ir(II) complex and radical 464a, which resulted in anion 465a and Ir(III) complex. Anionic compound 465a underwent protonation, dissociation of boronic acid and transesterification and this gave lactone compound 466a. From control reactions, it was found that the absence of diphenylboronic acid from the reaction mixture resulted in compound 466a being given in 5% yield and the C-2 epimer of 466a was isolated in 22% yield. When diphenylboronic acid was present in the reaction mixture (10 mol%) this gave 466a in 72% yield with no other regioisomers being formed. Therefore, this demonstrated the importance of diphenylboronic acid in the reaction mixture. To further understand this reaction, a computational study was performed, the BDEs and transition state energies of compounds on the methyl α-L-rhamnopyranoside (460a) route were calculated. It was determined that monosaccharide 460a had a weak C–H bond at the C4 position (BDE 87.4 kcal mol^{-1}), which was weaker than the C–H bond at the C2 position (BDE = 89.6 kcal mol^{-1}). Therefore, this explained the poor conversion and selectivity when diphenylboronic acid was omitted from the reaction mixture. For the boronate compound 461a, the C–H bond at the C2 position was much weaker (85.1 kcal mol^{-1}). This made it the weakest C–H bond present in the compound and this increased the efficiency and selectivity of the reaction when diphenylboronic acid was in the reaction mixture.

From optimisation studies, it was found that diphenylboronic acid was the optimal boronic acid for this process as it gave 466a in the highest yield (72%) (Scheme 134). A series of 11 lactones 457 was prepared in yields of 54–70%, with notable regio- and stereoselectivity. Silyl protected alcohols were tolerated under the reaction conditions giving lactones 466c and 466d in 54% and 68% yield respectively.

γ-Ketone C–H functionalisation. Site-specific γ-ketone C–H functionalisation was accomplished via imine adducts 468

9608 | Chem. Soc. Rev., 2021, 50, 9540–9685

This journal is © The Royal Society of Chemistry 2021

Scheme 133 Formation of lactone **466a** from methyl α-ʟ-rhamnopyranoside **460a**.

Scheme 134 Products from lactone formation.

using an iridium photocatalyst (Scheme 135).[177] These imine adducts were coupled to electron-poor alkenes. Under the basic reaction conditions, the carboxylate salt of **468a** was oxidised with Ir(ɪɪɪ)* complex and yielded radical **469a** and Ir(ɪɪ) complex. As previously mentioned, the iridium catalyst Ir[dF(CF₃)ppy]₂-dtbbpy(PF₆) would be able to oxidise **468a**, see Scheme 73.

Expulsion of carbon dioxide and ethanal from unstable intermediate **469a** produced iminyl radical **470a**. An intramolecular HAT resulted in carbon-centred radical **471a**. Key C–C bond formation between radical **471a** and electron-poor alkene **466a** resulted in stable α-ester radical **472a**. The iridium catalytic cycle was closed with SET to **472a** from Ir(ɪɪ) complex, this also
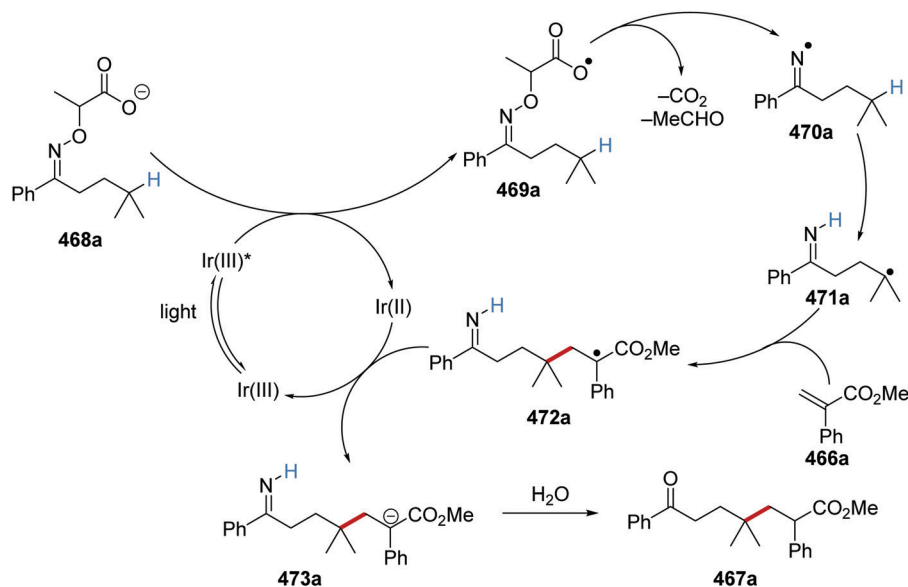
Scheme 135 Tandem reactions of iminyl radicals.

formed anion **473a**. At the end of the reaction, water was added to hydrolyse the imine, and thus ketone **467a** was isolated as the product from the reaction mixture.

The conversion of **468a** to ketone **467a** was trialled with three different iridium photocatalysts. From a short optimisation study it was found that Ir(dF(CF$_3$)ppy)]$_2$(dtbbpy)PF$_6$ gave optimal yields of **467a** (75% isolated yield, Scheme 136). The optimal conditions were used for a substrate scope and this gave a library of 32 ketones **467** in yields of 31–81%. The reaction was applied to a wide range of substrates and aryl bromides, heterocycle, benzyl esters and ketone groups were all tolerated (**467b–e**). However, a low yield was obtained for **467f** when methyl vinyl ketone was used. It was suggested that competitive polymerisation reactions resulted in this low yield.

The similar reaction conditions were also used with unsaturated α-iminoxyacetic acid compounds **468** with electron-poor alkenes **466** and this led to dihydropyrroles **474** (Scheme 137).[178]

These reaction conditions were highly successful as 32 dihydropyrrole compounds were prepared in yields 42–91%. Various electron-withdrawing groups were suitable for this transformation as highlighted with compounds **474a–f**. The reaction was amenable to heterocyclic substrates, and this allowed thiophene **474g** to be accessed in 68% yield. Substrates where R = alkyl also performed well under the reaction conditions and thus compounds **474h** and **474i** were given in the yields shown.

PCET processes. A radical cascade coupling reaction was reported where unsaturated amides **475** were converted to coupled lactams **476** (Scheme 138).[179] A proton-coupled electron transfer (PCET) was the key step in this transformation, in which a hydrogen-bond interaction between amide **475** and weak phosphate base gave adduct **477**. Support for a PCET mechanism was provided by Stern–Volmer studies and electrochemical redox potentials. The organometallic catalyst, Ir[dF(CF$_3$)ppy]$_2$bpy(PF$_6$)
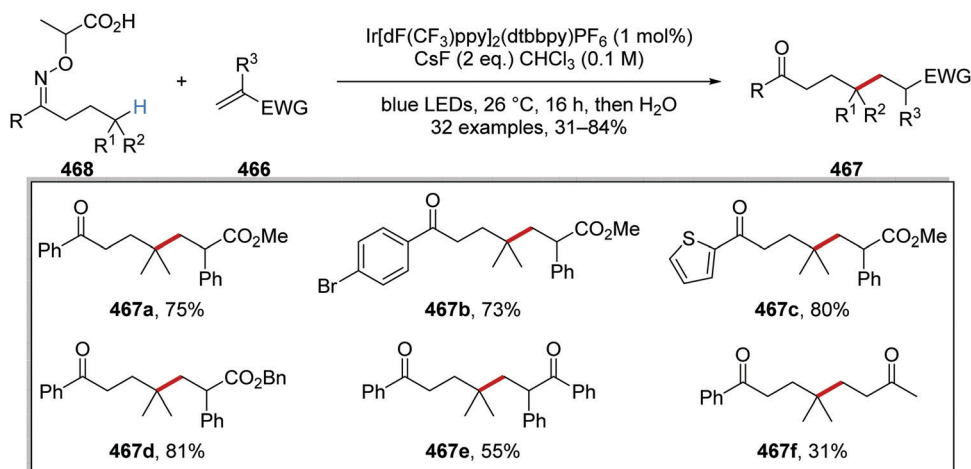
Scheme 136 Products arising from tandem reactions arising from iminyl radicals.

9610 | *Chem. Soc. Rev.*, 2021, **50**, 9540–9685

This journal is © The Royal Society of Chemistry 2021
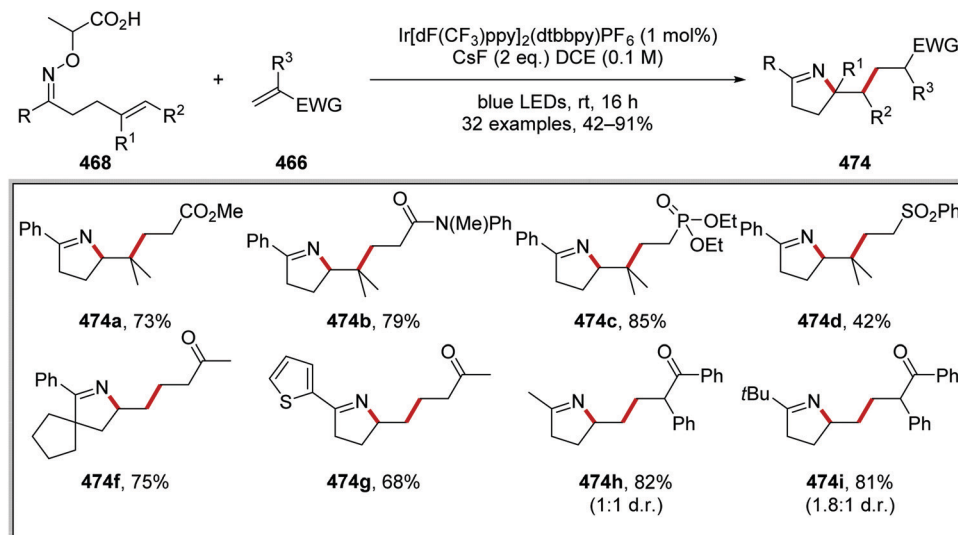
Scheme 137 Scope of products.
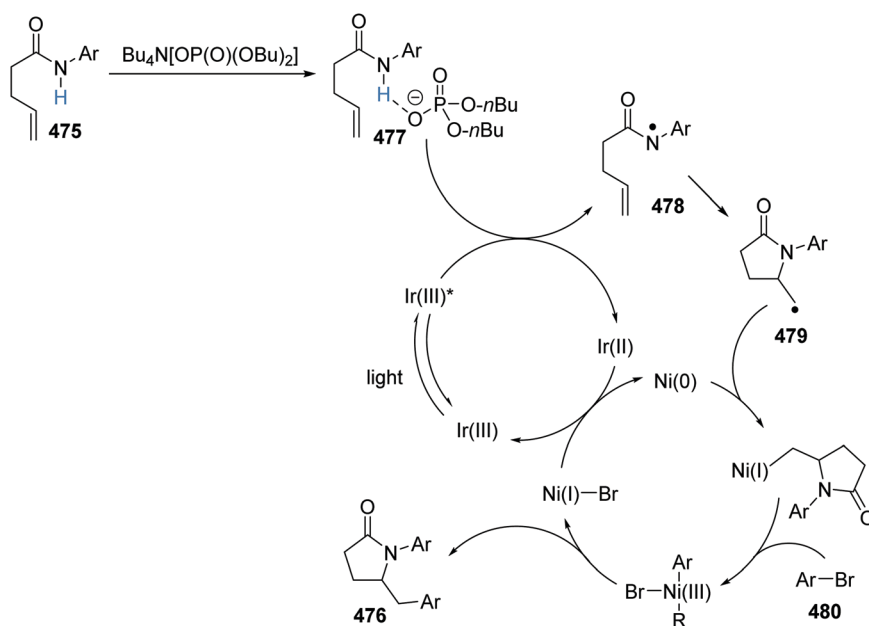
Scheme 138 PCET and radical cascade and coupling of **466**.

(E_{red}* = +1.32 V *vs.* SCE) was unable to oxidise **475a** (E_{ox} = +1.78 V *vs.* SCE) but upon addition of 2.5 eq. of base the redox potential of the amide was significantly decreased (E_{ox} = +1.27 V *vs.* SCE). This allowed for concerted proton and electron transfer, which broke the strong N–H bond[180] and gave amidyl radical **478**. A radical 5-*exo*-trig cyclisation delivered lactam radical **479**, which was intercepted by Ni(0) complex and this gave Ni(I) complex. Oxidative addition to this Ni(I) complex with an aryl bromide **480** gave a Ni(III) complex, which underwent reductive elimination giving functionalised lactam **476**. The iridium and nickel catalytic cycles were closed with a SET between Ni(I) and Ir(II) complexes.

This process was utilised in the preparation of 50 lactams, **476** (Scheme 139). This methodology allowed for the preparation of

nitrile analogue **476a** in 78% yield. Spirocyclic **476b**, bicyclic **476c**, dinitrile **476d**, *N*-Boc amine **476f**, and thiophene **476g** derivatives were all prepared with this transformation.

A site-selective remote C–H activation, inspired by the Hofmann–Löffler–Freytag reaction, and involving a photocatalytic reaction with a PCET was reported.[168] Under the reaction conditions, the combination of amide **481a** and phosphate base resulted in hydrogen-bond interactions as in adduct **482a** (Scheme 140). A concerted PCET with adduct **482a** and Ir(III)* complex allowed for cleavage of the strong N–H bond (*N*-methylacetamide has an N–H BDE = 106.5 kcal mol⁻¹, in DMSO)[42] and formation of amidyl radical **483a** and Ir(II) species. This PCET process was confirmed with Stern–Volmer experiments,

This journal is © The Royal Society of Chemistry 2021

Chem. Soc. Rev., 2021, **50**, 9540–9685 | **9611**
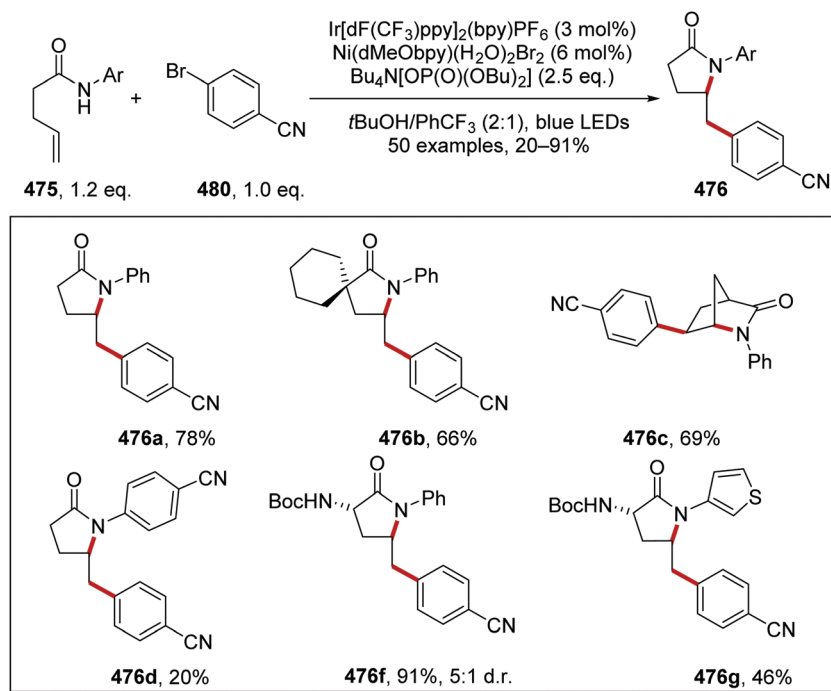
Scheme 139 Results of PCET and radical cascade and cross-coupling of **475**.
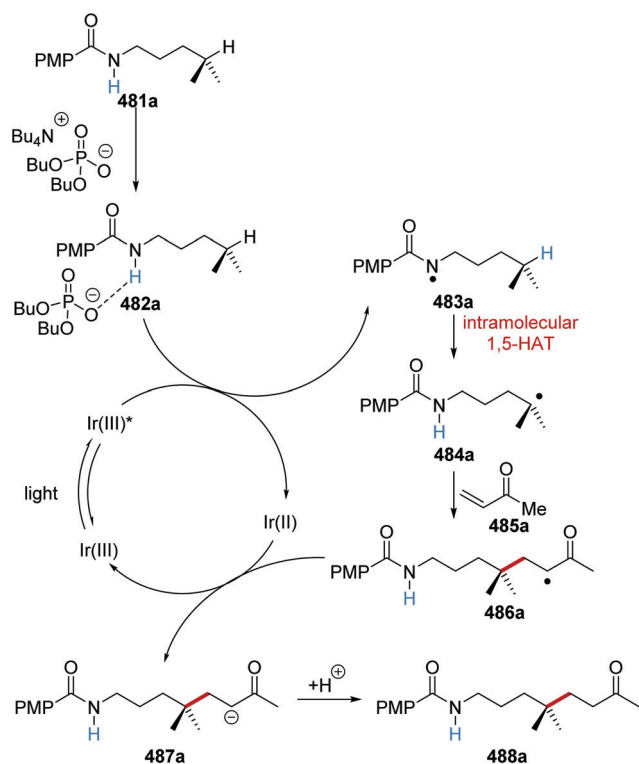
Scheme 140 Iridium-promoted HLF type reaction.

where it was shown that efficient quenching of Ir(III)* only occurred when both amide and base were present. Additionally, as shown above (Scheme 138), the addition of base to an amide drastically facilitates the oxidation of amides. Amidyl radical **483a** effected

1,5-HAT giving radical **484a**. Giese addition between radical **484a** and electron-poor alkene **485a** gave α-keto radical **486a**. The iridium catalytic cycle was closed with electron transfer from the Ir(II) complex to radical **486a**. Protonation of anion **487a** led to coupled compound **488a**.

Ir[dF(CF$_3$)ppy]$_2$(5,5'-dCF$_3$bpy)PF$_6$ was the optimal catalyst for this process, as it gave **488a** in the highest yield (78%, Scheme 141). Optimised reaction conditions allowed for the preparation of 27 alkylated compounds **488** in 29–87% yield. Silyl-protected hydroxy groups were tolerated and thus compound **488b** was isolated in 66% yield. Furthermore, the site-selectivity of this process was maintained even with N-Boc groups being present giving product **488c** in 45% yield. The high degree of selectivity of this process is due to the cyclic HAT transition state, and this ensured only one site of hydrogen atom abstraction was feasible. Both acrylate and acrylamide were poor coupling partners, providing only trace amounts of alkylated products. It was concluded that this was due to mismatching of the reduction potentials of the α-carbonyl radicals and Ir(II) complex, which led to sluggish electron transfer and thus diminished yields. However, when the more reactive dicarbonyl coupling partners were used, this resulted in formation of diester **488d** in 87% yield. This PCET transformation was also applicable to sulfonamides and N-Boc carbamates, providing **488e** and **488f** in 74% and 29% yield, respectively.

Aryl iodides as radical precursors. A visible light-promoted Meerwein reaction of styrenes **489** with aryl halides **490** and potassium formate (**491**) gave ester products **497** under photo-redox conditions in a radical-polar crossover reaction.[181] The reaction required the use of Ir(ppy)$_2$(dtbbpy)PF$_6$ as photocatalyst
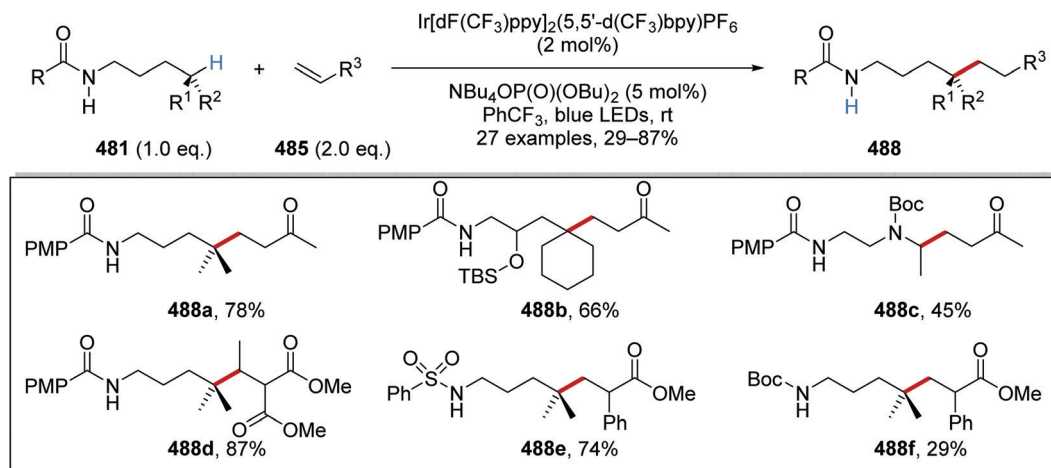
Scheme 141 HLF-inspired reaction with PCET.

for PET and DABCO as a HAT catalyst. Irradiation with blue light produced Ir(III)* ($E_{red}*$ = +0.66 V vs. SCE)[8b] which oxidised DABCO (**28a**, E_{ox} = 0.69 V vs. SCE)[38] forming the amine radical cation **28a'** (Scheme 142). PET between DABCO and Ir(III)* was confirmed with Stern–Volmer quenching studies, where Ir(III)* was effectively quenched in the presence of DABCO. Hydrogen atom transfer from anion **491** gave formate radical anion **492** and cation **28a⁺**. The C–H bond in formic acid is weak (87 kcal mol⁻¹) and sodium formate had an even weaker C–H bond as, with gentle heating, sodium formate decomposes to sodium oxalate and hydrogen gas.[182] Therefore, the DABCO radical cation should

certainly be able to undergo HAT with **491**. Formate radical anion **492** is a strong electron-donor (E^0 = −2.21 V vs. SCE) and it reduced iodobenzene **490a** (E^0 = −2.24 V vs. SCE),[183] which produced aryl radical **493a**, carbon dioxide, and iodide. Addition of radical **493a** to styrene **489a** gave stabilised benzylic radical **494a** which was reduced to the corresponding anion by Ir(II). Nucleophilic attack on carbon dioxide resulted in the formation of carboxylate **496a** which was methylated by iodomethane to give methyl ester **497**. The generation of anion **495a** was confirmed with anion trapping experiments where 4-fluorobenzaldehyde and deuterium oxide were used as electrophiles.
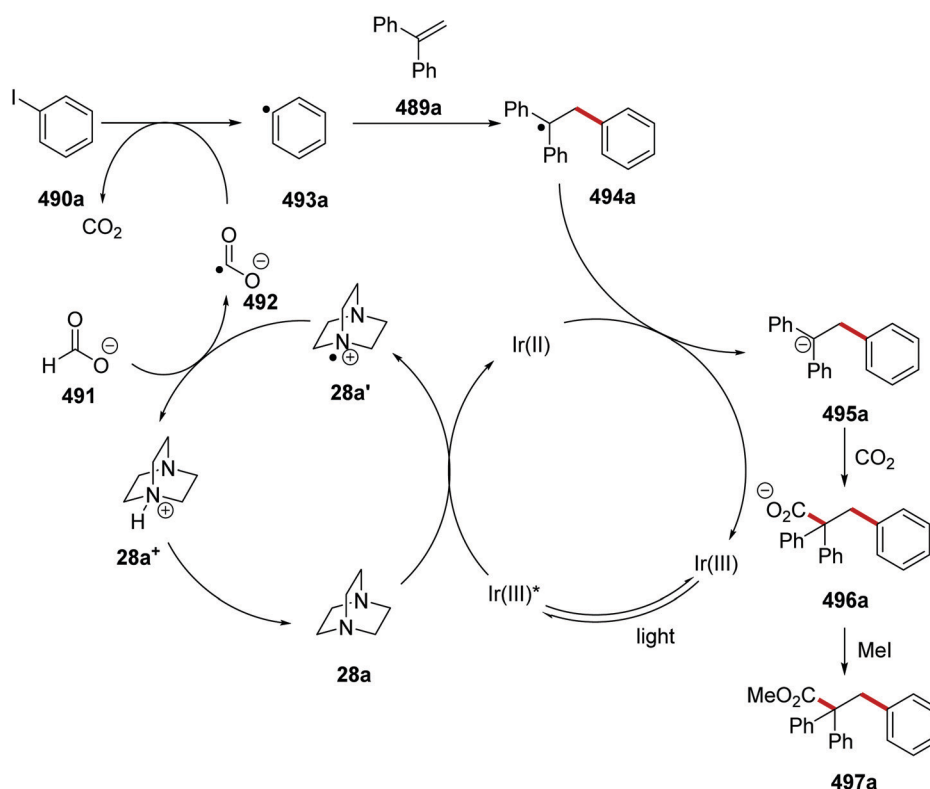
Scheme 142 DABCO-facilitated Meerwein reaction.

This journal is © The Royal Society of Chemistry 2021

Chem. Soc. Rev., 2021, **50**, 9540–9685 | **9613**
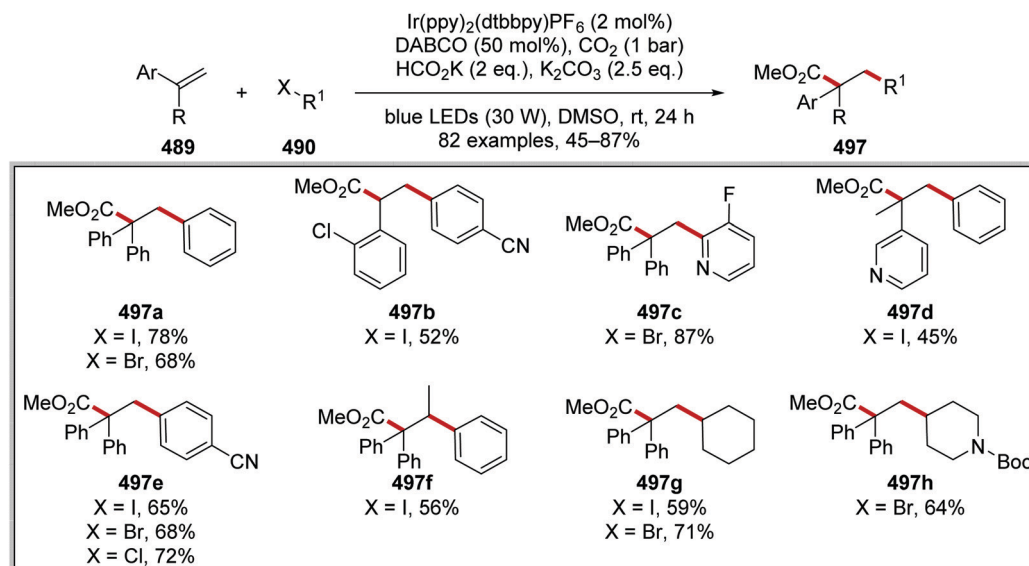
Scheme 143 Selected products from a DABCO 'photo-Meerwein' reaction.

Optimal conditions for this reaction used $Ir(ppy)_2(dtbbpy)PF_6$ as photocatalyst, DABCO as HAT catalyst, potassium carbonate as base, DMSO as the solvent, and this gave **497a** in 78% yield (Scheme 143). A library of 82 compounds was prepared with the use of these optimal conditions. Functional groups and heterocycles were accommodated under the reaction conditions and thus compounds **497b–f** were prepared. It was found, alongside aryl iodides or bromides, that aryl chlorides could also be used in this transformation and **497e** was prepared in 72% yield from the aryl chloride. The use of an α,β-substituted styrene allowed for the formation of compound **497f** in 56% yield. Alkyl bromides and alkyl iodides under the reaction conditions gave **497g** and **497h**, in 59–71% yields.

Asymmetric Minisci reactions. Enantioselective Minisci reactions were achieved by the team of Phipps with an iridium complex by using a chiral Brønsted acid such as TRIP in their reactions (Scheme 144).[184–186] This was followed by an investigation to uncover the mechanism of the reaction and in particular, the steps that controlled the stereoselectivity. Reductive cleavage of the phthalimidoylcarboxylates **499**, resulted in a carboxyl radical. Loss of CO_2 then afforded the stabilised radicals (see **501**) that were active in coupling. Association of the chiral phosphoric acid with the N–H protons of the radical and also of the protonated heteroaryl substrate **501** led to reversible addition to the heteroarene. Surprisingly, C–H deprotonation of the adduct **502** was achieved by the N-acyl group prior to final oxidation of the resulting radical **503** to afford the final product **500**. This approach was effectively used to afford products including **500a–e** a wide range of substrates and was also applied to late-stage modification of pharmaceuticals, as instanced in the conversion of metyrapone to **500f**.

It might be imagined that the initial reduction of the substrates **499** occurred by the photoactivated Ir(III)* complex. However, investigations by the authors concluded that this is

unlikely as Ir(III)* has insufficient reducing power. Instead, they propose that Ir(II) is produced off the main catalytic cycle, and perhaps by reduction of Ir(III)* by a TRIP anion. The resulting Ir(II) complex would then reduce substrates **499** as above. This proposal is supported by electrochemical potential values reported elsewhere. The compound N-hydroxyphthalimide benzoate (E_{red} = −1.4 V *vs.* SCE)[184b] can undergo irreversible SET with the reduced iridium catalyst (Ir(II) E_{ox} = −1.37 V *vs.* SCE).[8b] The transformation of radical **503** to product **500** provides the electron that closes the redox catalytic cycle.

2.4 Catalytic cycles featuring Ir(III)/Ir(IV)

Carboxylates as radical precursors. The radical coupling between benzonitriles **504** and carboxylic acid radical precursors **505** was reported.[187] Irradiation of the reaction mixture with blue light gave Ir(III)* species from Ir(III) complex (Scheme 145). SET reduction of terephthalonitrile (**504a**, E_{red} = −1.61 V *vs.* SCE) with Ir(III)* [For the related (Ir(ppy)$_3$ [E_{ox}* = −1.73 V *vs.* SCE]] resulted in the formation of radical anion **506a** and an Ir(IV) complex. The iridium catalytic cycle was closed with a SET transfer from carboxylate **507a** to Ir(IV) complex. After decarboxylation, α-amino radical **508a** added to **506a**, and subsequent cyanide loss afforded coupled product **509a**.

The coupling of carboxylic acids **505** to electron-poor benzonitriles **504** succeeded and this gave a range of arylated compounds **509** in yields of 52–89% (Scheme 146).[187] Many α-amino-acids provided acceptable substrates for this transformation and afforded arylated products **509a–d** in high yields. A range of different electron-withdrawing groups was employed in this transformation as seen in electron-poor aromatic products **509e–h**.

An Ir and Cu catalytic system was used to prepare disubstituted BCPs in one step from hypervalent-iodine species **510** and [1.1.1]propellane (**512**)[104] (Scheme 147). SET from excited Ir(III)* complex to radical precursor **510a** (E_{red} = −0.82 V *vs.* SCE) resulted in alkyl radical **502a** and electron-deficient Ir(IV) complex.
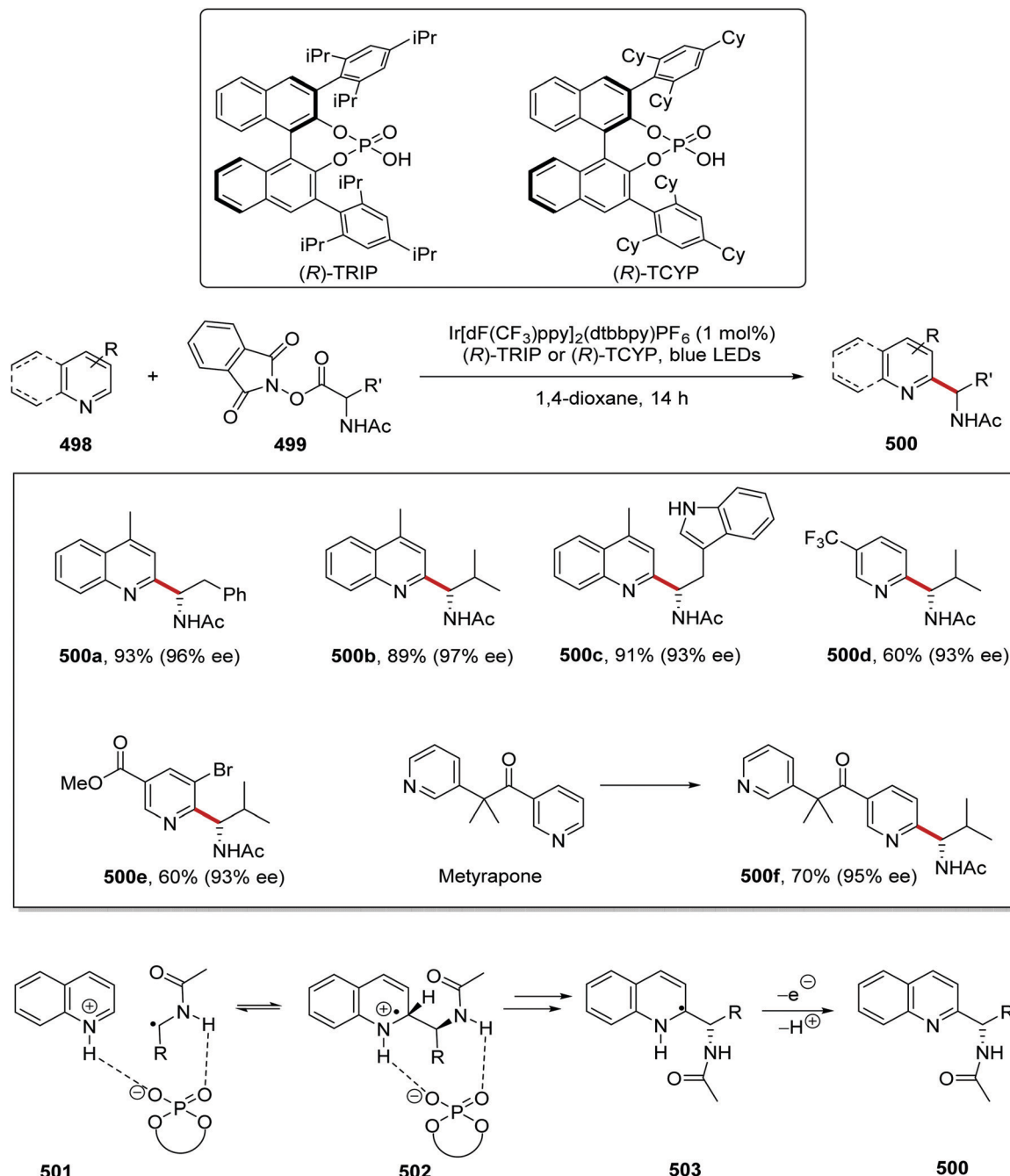
Scheme 144 Stereoselective Minisci reaction.

Radical addition of **511a** to [1.1.1]propellane (**512**) broke the weak central C–C bond and formed BCP radical **513a**. Coincidentally, Cu(I) complex underwent ligation with nucleophile **514a** and this resulted in Cu(I) complex **B**. Oxidation of Cu(I) complex **B** with the aforementioned Ir(IV) complex, resulted in the closure of the iridium catalytic cycle and Cu(II) complex **C**. Addition of alkyl radical **513a** to **C** gave Cu complex **D**. Reductive elimination of complex **D** resulted in the closure of the copper catalytic cycle and formation of BCP **515a**.

This three-component reaction was successful as it allowed carboxylic acid precursors **516** to be converted to bioisostere **515** *via* iodine intermediate **517** (Scheme 148). Variation of carboxylic acid precursors allowed for a range of different bioisosteres to be formed. For example, the formation of ether **515a**, *N*-Boc amine **515b** and *gem*-difluoroalkane **515c** analogues were achieved. It was also observed that different nucleophiles made successful coupling partners and derivatives **515d–f** were prepared in yields of 53–80%.

Activated alkyl bromides **518** were also substrates for this transformation (Scheme 149). Therefore, a range of BCP compounds **515g–l** was prepared from the corresponding α-bromocarbonyl compounds.

This journal is © The Royal Society of Chemistry 2021

Chem. Soc. Rev., 2021, **50**, 9540–9685 | **9615**
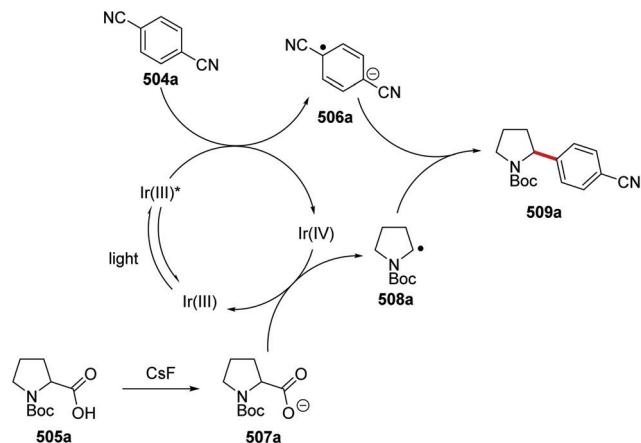
Scheme 145 Radical coupling between benzonitrile **504a** and carboxylic acid radical precursor **505a**.

Carbon α-heteroatom C–H functionalisation. The coupling of amines **514** with dicyanobenzene **519** was achieved with the Ir(ppy)$_3$ photocatalyst, and sodium acetate (Scheme 150).[188] Ir(III)* (E_{ox}* = −1.73 V vs. SCE)[8b] reduced **519a** (E_{red} = −0.82 V vs. SCE) to its radical anion **520a**. The iridium catalytic cycle was closed with SET from N-phenylpyrrolidine (**514a**, E_{ox} = 0.82 V vs. SCE)[188b] to the Ir(IV) complex (E_{red} = +0.77 V vs. SCE). This gave amine radical cation **521** and after proton loss, carbon-centred radical **522a**. Coupling between **520a** and **522a** formed anion **523a**. Loss of the cyanide ion from **523a** gave the coupled product **524a**.

The photocatalyst tris[2-phenylpyridinato-C^2,N]iridium(III) resulted in high yields of coupled compounds **524** from anilines **514** and electron-poor benzonitrile compounds **519** (Scheme 151). Further investigation showed that the reaction worked well when
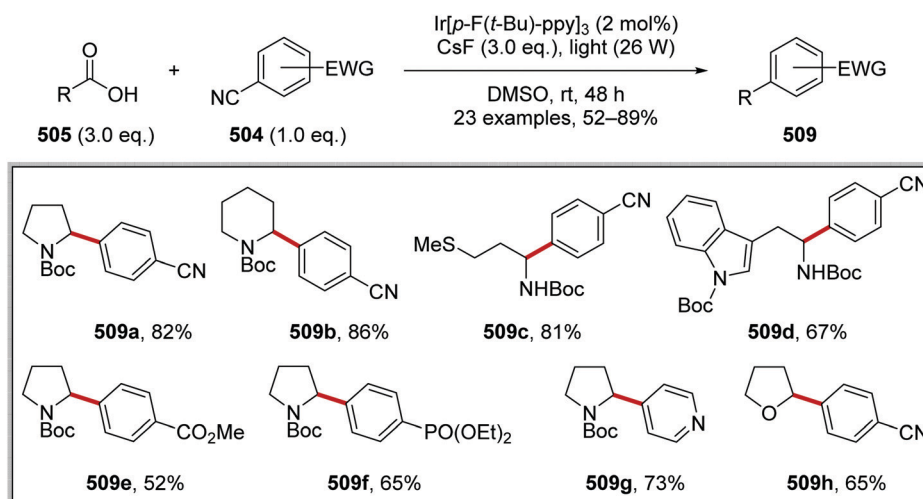
Scheme 146 Products of radical coupling between benzonitriles **504** and carboxylic acid radical precursors **505**.
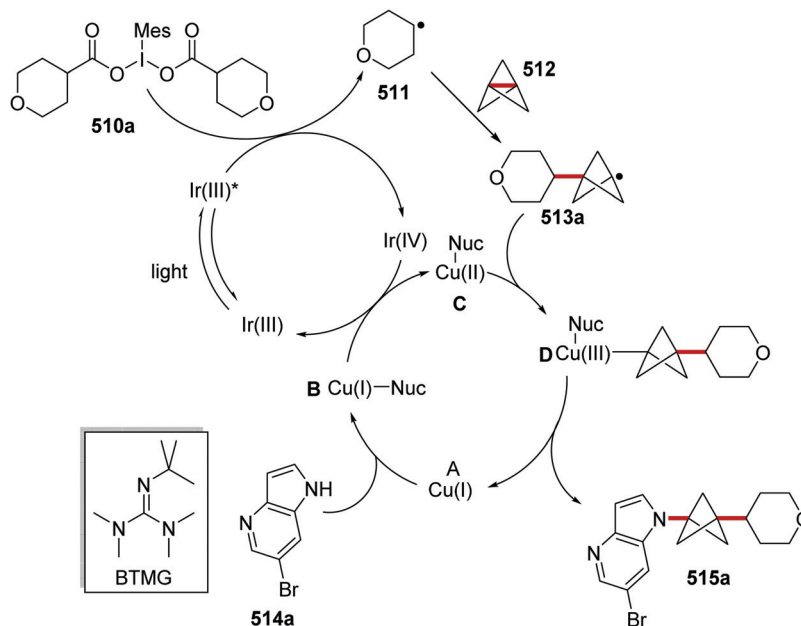
Scheme 147 Formation of disubstituted BCP analogue **515a**.

9616 | *Chem. Soc. Rev.*, 2021, **50**, 9540–9685

This journal is © The Royal Society of Chemistry 2021
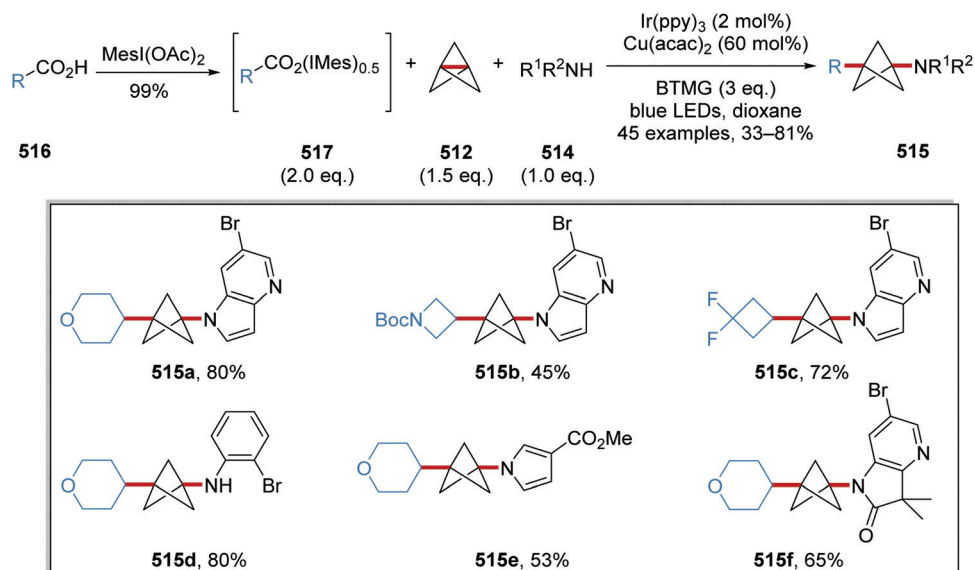
Scheme 148 Results of radical coupling to form disubstituted BCPs **515**.
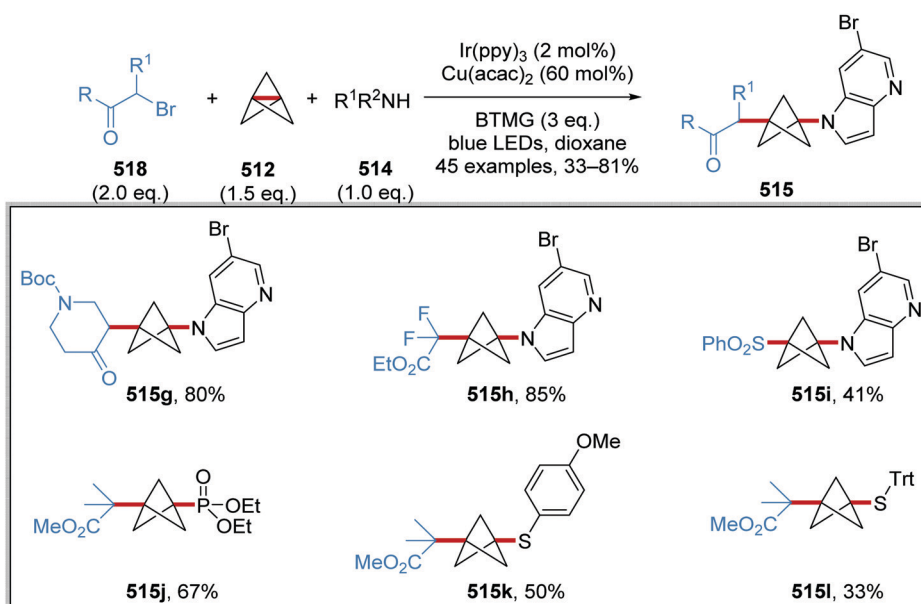
Scheme 149 Formation of disubstituted BCPs **515** from α-bromocarbonyl compounds **518**.
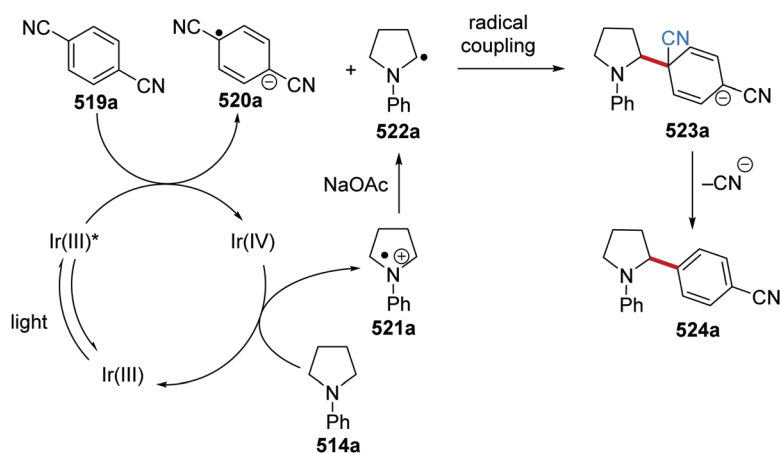
Scheme 150 α-Aminoalkyl radical **522a** coupling to benzonitrile analogue **519a**.

This journal is © The Royal Society of Chemistry 2021

Chem. Soc. Rev., 2021, **50**, 9540–9685 | **9617**
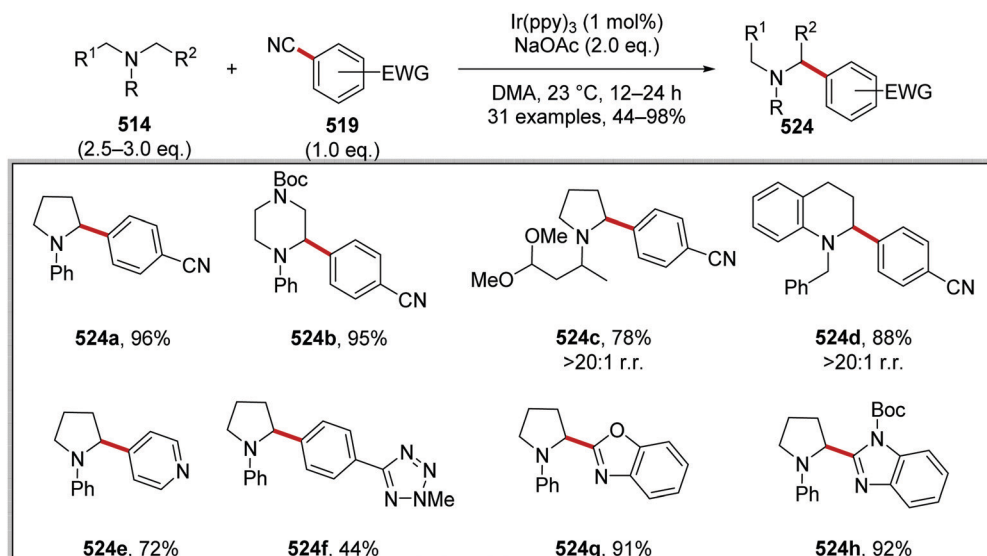
Scheme 151 Results of amines **514** coupling to benzonitriles **519**.

carried out in DMA with sodium acetate as base. Application of the optimised reaction conditions to the corresponding substrates gave acetal **524c**, N-Boc amines **524b** and **524h** derivatives in yields of 78–95%. Heterocycles were compatible with the reaction conditions, and thus coupled compounds **524e**–**524h** were prepared and isolated in yields of 44–92%. This reaction was regioselective; for example, coupled product **524d** formed as a mixture of regioisomers (20 : 1 ratio), with arylation taking place upon the less sterically hindered α-amino C–H bond. The regioselectivity was observed for substrates with α-amino methylene and methine positions, with the methylene functionalised compound **524c** being isolated as the only isomer.

The synthetic utility of this methodology was demonstrated with the preparation of derivative **526** from the antibiotic, linezolid (**525**, Scheme 152). With the use of Ir(ppy)₂(dtbbpy) photocatalyst, linezolid was coupled to 2-chlorobenzoxazole and this gave linezolid derivative **520** in 58% yield.

Minisci coupling. Minisci reactions between ethers **527** and nitrogen-based heterocycles **528** were achieved with an iridium photocatalyst, TFA and sodium persulfate.[189] Ethers have high oxidation potentials and this makes them difficult to oxidise. Therefore, a HAT strategy targeting the weak α-oxy C–H bond (C–H BDE for THF = 92 kcal mol⁻¹) is a preferable strategy for C–H functionalisation.[32,190] Under the reaction conditions, an excited Ir(III)* species is formed from the Ir(III) photocatalyst

(Scheme 153). The excited Ir(III)* catalyst [Ir{dF(CF₃)ppy}₂-(dtbbpy)PF₆, ($E_{ox}^* = -0.88$ V vs. SCE) reduced persulfate salt **66** ($E_{red} = ca. \leq 0.35$ V vs. SCE, see ref. 189) and this resulted in sulfate radical anion radical **531**, sulfate ion and Ir(IV) species. Radical anion **531** abstracted a hydrogen atom from tetrahydropyran **527a** with the formation of a strong O–H bond, giving α-alkoxyalkyl radical **529a**. Concurrently, the nitrogen-based heterocycle, isoquinoline **528a** was protonated by TFA and this gave **530a**. Carbon–carbon bond formation between electron-rich radical **529a** and electron-poor heterocycle **530a** resulted in amine radical cation **532a**. Loss of the acidic proton from **532a** gave carbon-centred radical **533a** which was oxidised by the Ir(IV) complex to form cation **534a**.

When the reaction was being optimised, it was found that the addition of water to the reaction mixture gave increased yields of **536a** (Scheme 154). When water was added to the reaction mixture, this resulted in a biphasic mixture and it was inferred that this allowed for greater photon penetration leading to a more successful reaction. Higher yields of **536a** were obtained when sodium persulfate was used in the reaction, over potassium persulfate and ammonium persulfate. Therefore, it was concluded that the optimal conditions for this transformation were: Ir[dF(CF₃)ppy](dtbbpy)PF₆ as photocatalyst (2 mol%), sodium persulfate (2 eq.), TFA (1 eq.), ether substrate (50 eq.) and N-based heterocycle (1 eq.) (Scheme 154). These optimised conditions gave an 88% yield of **536a**. 1,3-Dioxolane gave **536b**
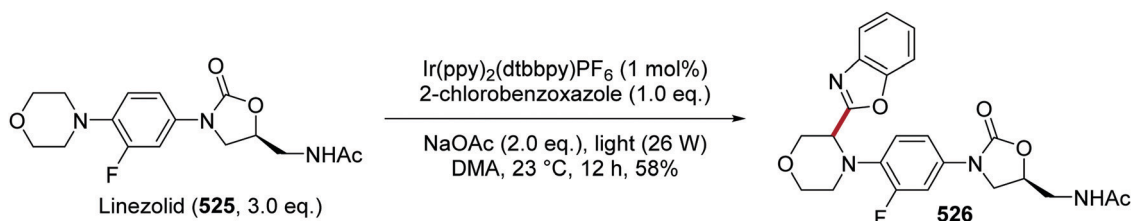
Scheme 152 C–H functionalisation of linezolid **525**.

9618 | Chem. Soc. Rev., 2021, 50, 9540–9685

This journal is © The Royal Society of Chemistry 2021
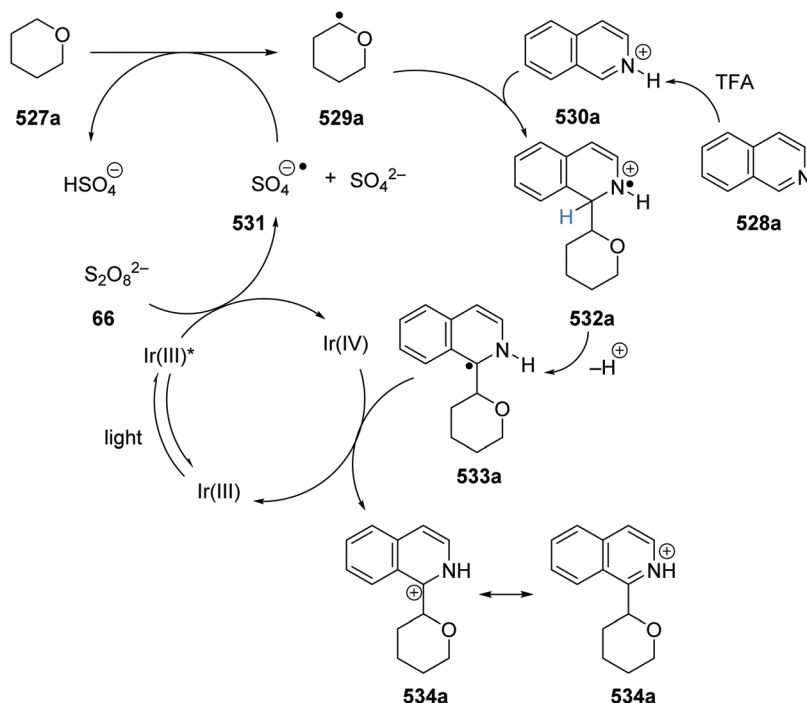
Scheme 153 Ether-derived radicals undergo Minisci reaction.
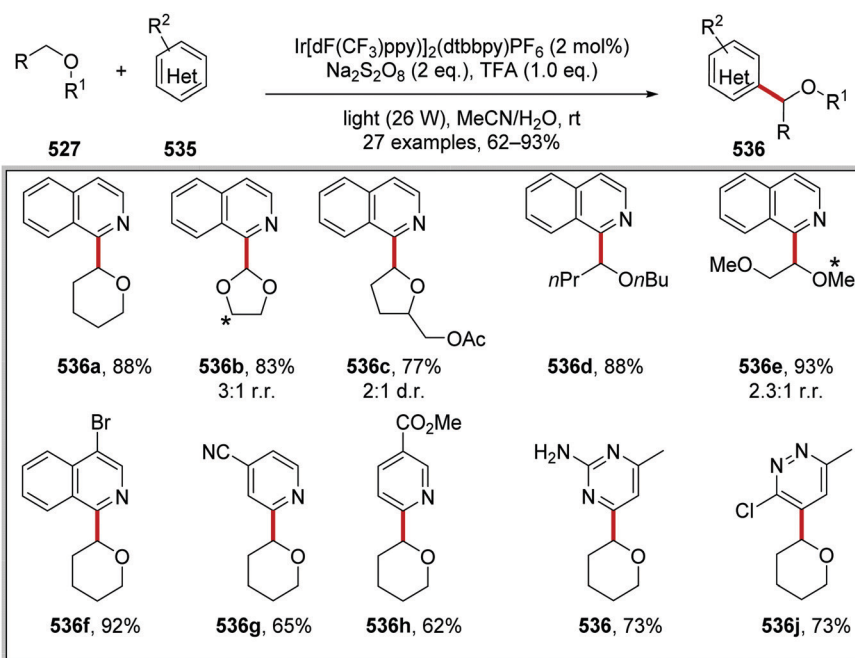
Scheme 154 Scope of products from Minisci reaction. (Asterisk * indicates an alternative site of attachment.)

as the product in 83% yield with 3:1 ratio of regioisomers. Tetrahydrofurfuryl acetate as substrate gave tetrahydrofuran product **536c** in 77% yield with a 2:1 ratio of diastereoisomers and only one regioisomer was isolated, highlighting the site-selectivity of this process. Ether **536d** was isolated in 88% yield when dibutyl ether was employed as the substrate. A 2.3:1 mixture of regioisomers (with preferred functionalisation at the

methylene position) was obtained, in 93% yield for coupled compound **536e** when dimethoxyethane was used as substrate. It was shown that coupling to various N-based heterocycles was feasible with the preparation of coupled heterocycles **536f–j**.

The Minisci coupling of N-based heterocycles **538** with amine derivatives **537** was investigated, with particular attention paid to protecting group influences (Scheme 155).[191] The photocatalyst

This journal is © The Royal Society of Chemistry 2021

Chem. Soc. Rev., 2021, **50**, 9540–9685 | **9619**
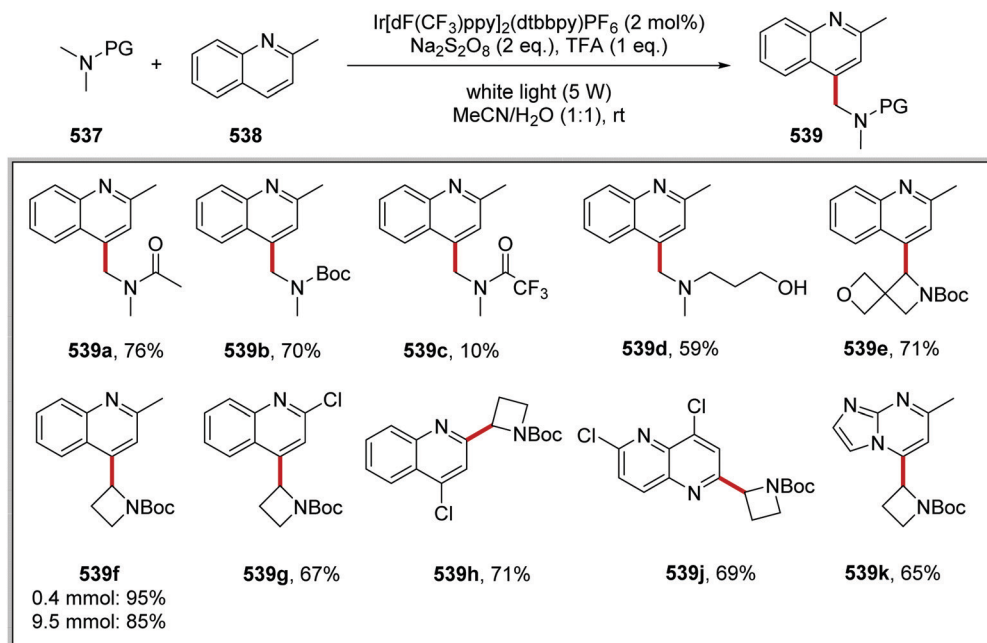
Scheme 155 Range of products from the sodium persulfate-initiated Minisci reaction.

Ir[dF(CF$_3$)ppy]$_2$(dtbbpy)PF$_6$, TFA and sodium persulfate were used to facilitate the Minisci reaction; under these conditions acetamide, trifluoroacetamide and Boc-protected amines were investigated. The use of DMA and *tert*-butyl *N,N*-dimethyl-carbamate (BDC) afforded coupled amine compounds **539a** and **539b** in 76% and 70% yields respectively. However, *N,N*-dimethyltrifluoroacetamide (DTA) gave coupled amine compound **539c** in 10% yield after 13 days of reaction. To understand this phenomenon, the BDE of DMA, BDC and DTA were calculated, and it was found that all three compounds had similar α-amino C–H bond energies. The calculated α-amino C–H BDE for these compounds were: DMA = 97.7 kcal mol^{-1}, BDC = 99.0 kcal mol^{-1} and DTA = 99.9 kcal mol^{-1}. Therefore, this indicated that the HAT event had limited influence upon the success of this transformation. The SOMO orbitals energy levels of these substrates were then calculated and from this, it was found that the SOMO energy levels of the radicals derived from *N*-BocNMe$_2$ and DMA (−134.2 and −138.4 kcal mol^{-1}, respectively) were much higher than for DTA (−151.3 kcal mol^{-1}). This implied that the corresponding carbon-centred radical of DTA is much less nucleophilic and more stable than the DMA and BDC radicals and this inhibited reactivity with the heterocycle. With the understanding gained from these control experiments and calculations, 34 Minisci coupled products **539** were prepared. Previous work reported that high loadings of ether coupling partner (50 eq.) were required for successful coupling.[189] However, it was shown that a much lower number of equivalents was required for this process and, for some transformations, two equivalents of **537** were sufficient. These optimised conditions were mild, and thus sensitive functional groups were tolerated, and compounds like hydroxy-functionalised quinoline **539d** and spiroether product **539e** were prepared in 59% and 71% yield, respectively. In preparing analogue **539e**, no reactivity was

observed at the α-alkoxy position and only one regioisomer was given. 2- and 4-Chloroquinoline led to the formation of **539g** and **539h** in 67% and 71% yield, respectively. Furthermore, the use of 1,5-naphthyridine and imidazo[1,2-*a*]pyrimidine analogues as substrates gave **539j** and **539k** in 69% and 65% yield, highlighting the range of heterocycles that can be used in this transformation. The reaction was insensitive to scale and compound **539f** was prepared on a 0.4 mmol scale in a yield of 95%. The preparation of **539f** on a 9.5 mmol scale led to isolation of the material in 85% yield. The reaction was still operative without the use of light or Ir photocatalyst, as it was demonstrated that carbamate **539f** was prepared in 47% yield simply by heating the reaction mixture at 50 °C.

The origin of the high site-selectivity observed for derivative **539e** was investigated with competition reactions (Scheme 156). When a mixture of oxetane **537l** (15 eq.) and *N*-Boc azetidine **537f** (15 eq.) wi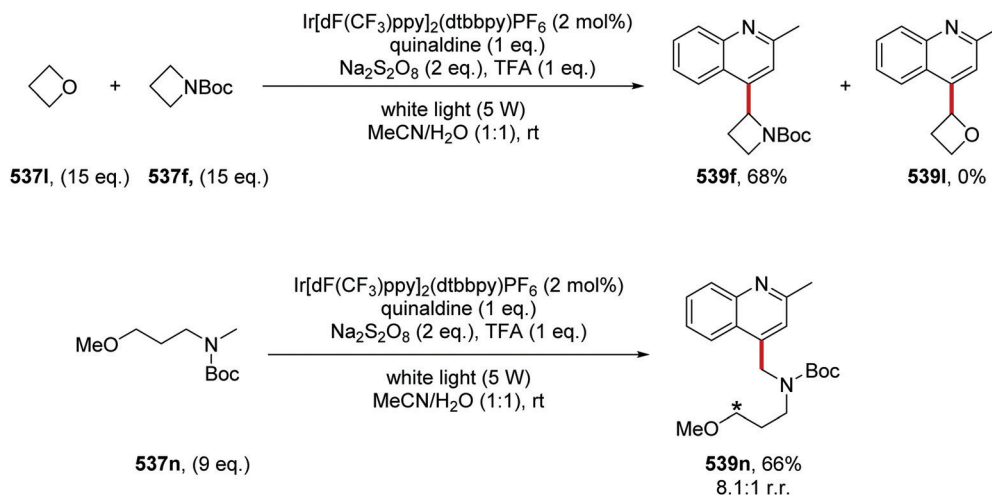th quinaldine (**538**, 1 eq.) was reacted under standard reaction conditions, this gave carbamate **539f** in 68% yield as sole-product, and no ether coupled compound **539l** was detected (Scheme 156). However, when THF was the substrate, the reaction did yield some α-alkoxy functionalised compound, but the selectivity was biased for azetidine **539f**. An intra-molecular competition experiment was also carried out with bifunctional compound **537n**, which featured both ether and *N*-Boc amine functionalities. This gave **539n** in 66% yield as an 8.1 : 1 mixture of regioisomers with the α-carbamate function-alised compound as the major regioisomer. The results of these competition experiments were not explained with the BDE or calculated SOMO energies from *ab initio* calculations. There-fore, it was postulated that the observed selectivity was due to polar effects with the HAT event taking place at the most hydridic C–H bond being attacked by the electrophilic sulfate radical anion.

9620 | *Chem. Soc. Rev.*, 2021, **50**, 9540–9685

This journal is © The Royal Society of Chemistry 2021

Scheme 156 α-Carbamate and α-alkoxy C–H competition experiments.

Alcohol C–H functionalisation. The alkylation of N-hetero-cycles **543** with alkyl alcohols **540** was achieved with an iridium photocatalyst and a thiol HAT catalyst **541** *via* a Minisci reaction.[192] Under the reaction conditions, the Ir(III) catalyst was excited by blue light and this gave excited Ir(III)* species (Schemes 157 and 158). The catalytic process for the formation of alkylated heterocycle **542a** was initiated with a sacrificial quantity of protonated heterocycle **543a** (see box). This allowed

for the formation of the strongly oxidising Ir(IV) complex [Ir(ppy)₂(dtbbpy)]²⁺, E_{red} = +1.21 V *vs.* SCE]. Evidence of protonated heterocycle oxidatively quenching the excited iridium catalysts was obtained with Stern–Volmer studies. The iridium catalytic cycle was closed with SET with thiol **541** (E_{red} = +0.85 V *vs.* SCE for cysteine) and this gave thiyl radical **544** which abstracted an H-atom from methanol (**540a**) resulting in α-hydroxyalkyl radical **545a** and recovery of thiol **541**. This HAT is likely to be
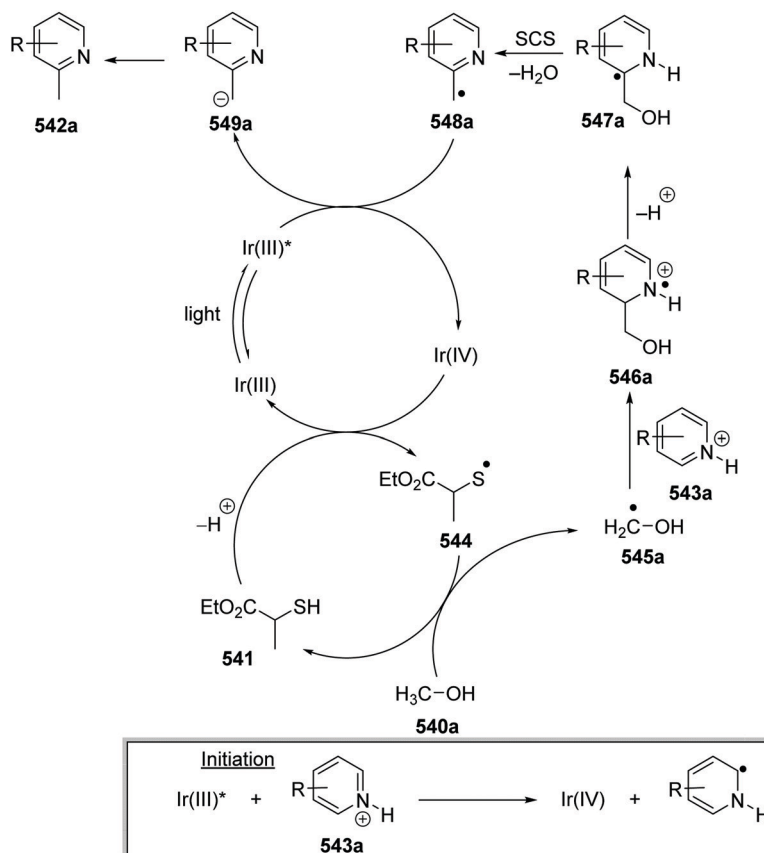
Scheme 157 Preparation of alkylated heterocycles *via* spin-centred-shift (SCS).

This journal is © The Royal Society of Chemistry 2021

Chem. Soc. Rev., 2021, **50**, 9540–9685 | 9621
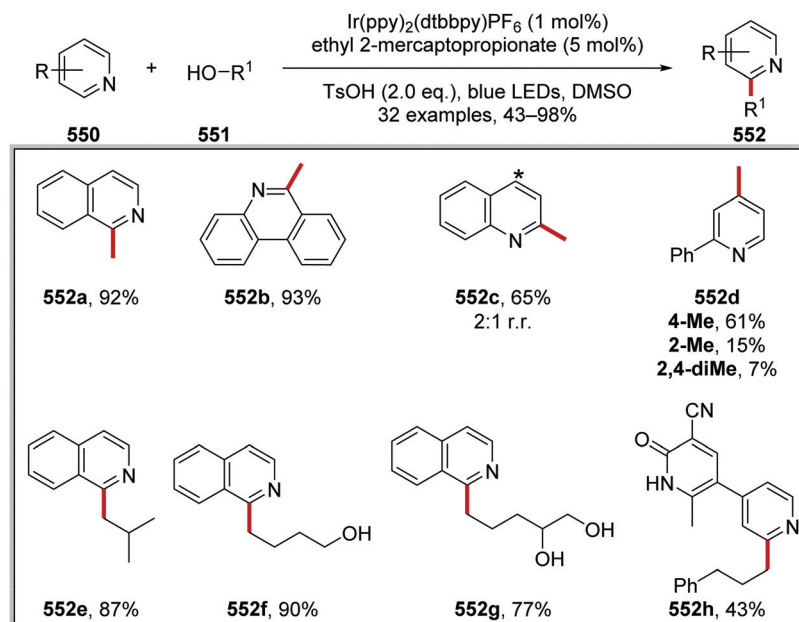
Scheme 158   Products from the dehydrative Minisci variant.

thermodynamically disfavoured as the S–H BDE of methyl thioglycolate is 87.2 kcal mol^{-1} and methanol has a C–H BDE of 94.6 kcal mol^{-1},[41,45,193] so the next steps of the reaction need to be thermodynamically favourable to move material through this bottleneck. Radical 545a added to protonated heterocycle 543a and this generated amine radical cation 546a. Proton loss from radical 546a gave α-aminoalkyl radical 547a. A spin-centred-shift (SCS)[194] transformed 547a to benzylic radical 548a with the loss of water. Benzylic radical 548a was reduced by Ir(III)* species and this gave benzylic anion 549a and protonation resulted in the observed product 542a.

The combination of photoredox catalyst Ir(ppy)$_2$(dtbbpy)PF$_6$ (1 mol%), ethyl 2-mercaptopropionate (5 mol%) and p-toluenesulfonic acid (1 eq.) in DMSO with methanol (co-solvent) gave methylated heterocycles 552a–d. Isoquinoline and phenanthridine as substrates gave methylated products 552a and 552b, in a regioselective manner, in 92% and 93% yield, respectively. When quinoline was treated to the reaction conditions, this gave 552c as a 2 : 1 mixture of regioisomers (the site of the other regioisomer is denoted with an asterisk) in 65% combined yield. 2-Phenylpyridine as substrate led to the formation of three compounds 552d in 84% combined yield. Other alcohols were also used as alkylating agents. The coupling of isoquinoline and isobutanol (10 eq.) gave alkylated analogue 552e in 87% yield. Coupling of tetrahydrofuran (10 eq.) with isoquinoline resulted in the formation of alcohol 552f in 90% yield. Similar reactivity was observed when tetrahydrofurfuryl alcohol (10 eq.) was used as coupling partner and this gave diol 552g in 77% yield. Bioactive compounds were functionalised with this reaction protocol. For example, milrinone, a phosphodiesterase 3 inhibitor was selectively alkylated with 3-phenylpropan-1-ol (10 eq.) and this gave 552h in 43% yield.

The use of methyl 2-mercaptoacetate (553) alongside an iridium photoredox catalyst allowed for C–C coupling between benzylic ethers 554 and electron-poor benzonitriles 555, and this gave benzhydryl products 556.[50] Under the reaction conditions, the Ir(ppy)$_3$ complex was excited with blue light and this afforded excited Ir(III)* complex (Scheme 159). SET to 555a (E_{red} = −1.61 V vs. SCE in MeCN) and Ir(III)* (E_{ox}* = −1.73 V vs. SCE in MeCN) resulted in the formation of Ir(IV) species and arene radical anion 557a. The iridium catalytic cycle was closed with SET from thiol 553 to Ir(IV) (E_{red} = +0.77 V vs. SCE) and this gave thiyl radical 558a and it was inferred that 558a was formed via a PCET process. The reaction was performed under weakly basic conditions with the base K$_2$HPO$_4$ being used and as mentioned above in the text accompanying Scheme 157, Ir(IV) might be unable to directly oxidise the thiol by HAT. Therefore, the pre-association of the S–H proton with the phosphate base allowed for a PCET and this avoided high-energy intermediates.[57] Radical 558a abstracted an H atom from benzylic ether 554a, to give radical 559a. This reaction was thermodynamically favourable as the BDE for the S–H of 553 (BDE of S–H bond of the analogous methyl 2-mercaptoacetate = 86.8–87.2 kcal mol^{-1}) is likely greater than the BDE for the C–H present in 554a (benzyl methyl ether has an αC–H BDE = 85.8 kcal mol^{-1}). Coupling between arene radical anion 557a and benzylic radical 559a gave anion 560a and, after cyanide ion loss, this gave coupled product 556a.

As the reaction was optimised it was found that the use of Ir(ppy)$_3$ (1 mol%), cysteine (20 mol%) as HAT catalyst in MeCN with K$_2$HPO$_4$ gave a 14% yield of 556a. Investigations then revealed that the addition of an aldehyde (octanal) was critical in forming 556a in a higher (32%) yield. It was postulated that the presence of the aldehyde was beneficial as it sequestered the cyanide anion. When DMA was used as reaction solvent instead of MeCN and methyl 2-mercaptoacetate (553) was used as HAT catalyst instead of cysteine, this gave 556a in 77% yield.

9622 | Chem. Soc. Rev., 2021, 50, 9540–9685

This journal is © The Royal Society of Chemistry 2021
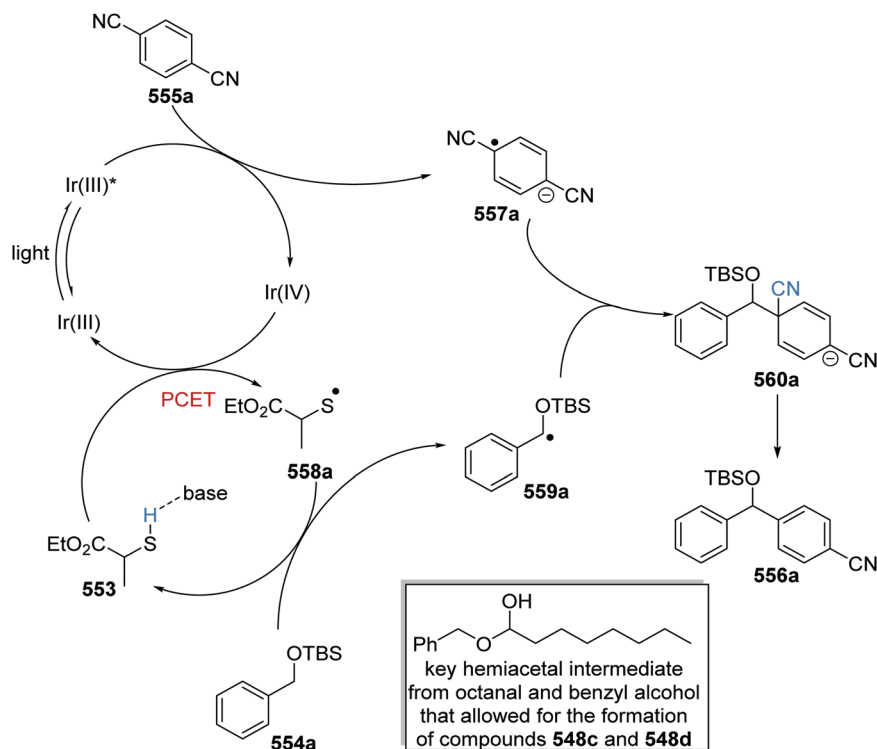
Scheme 159 Benzyl silyl ethers couple to 1,4-dicyanobenzene.

These optimised reaction conditions were then applied to various substrates resulting in the preparation of 28 coupled compounds **556** in yields of 41–86% (Scheme 160). Various benzylic ethers were suitable substrates and methoxy **556a** and cyclic ether **556b** derivatives were isolated. Benzylic ethers were substrates for this transformation and alcohols **556c** and **556d** were isolated in 77% and 72% yield, respectively. The use of silyl-protected benzylic alcohol allowed for the preparation of ester **556e**, *o*-cyano **556f**, pyridine **556g** and azaindole **556h** coupled analogues in yields ranging from 41–76%. During optimisation and substrate scope studies, there was no evidence of oxidation of the alcohol substrates to the corresponding aldehyde or ketone products

nor of any *O*-functionalised products. Control reactions were performed to elucidate the importance of octanal with these alcohol compounds. When this reaction was conducted without octanal, this resulted in exclusive aldehyde formation and with no aryl coupling. Analysis by ^{1}H-NMR spectroscopy of the reaction mixture revealed a transient hemiacetal intermediate (Scheme 159, inset), which was responsible for C–C bond formation and the prevention of benzylic oxidation.

Allylic C–H functionalisation. Iridium catalysis facilitated *ipso*-coupling between electron-poor benzonitriles **557** and alkenes **558** (Scheme 161).[53] The reaction propagated with
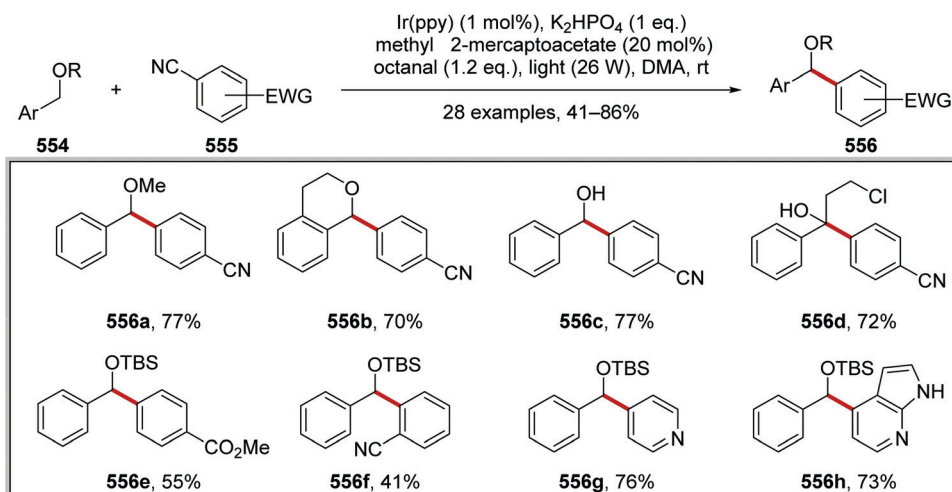
Scheme 160 Benzylic C–H activation and coupling of the resulting radicals.

This journal is © The Royal Society of Chemistry 2021

Chem. Soc. Rev., 2021, **50**, 9540–9685 | 9623
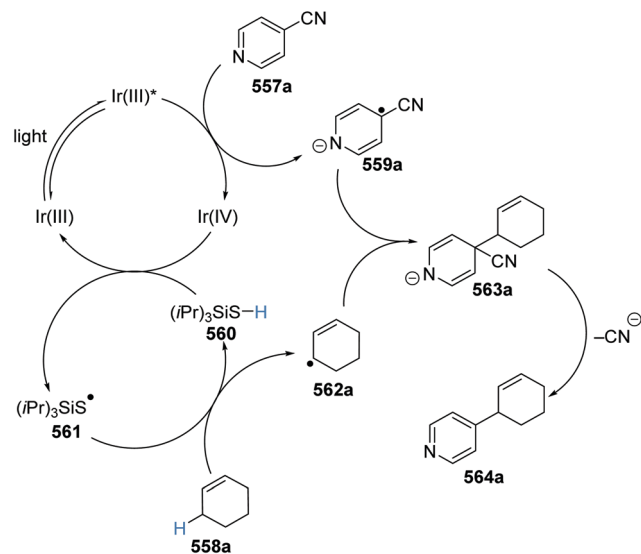
Scheme 161 HAT of allylic hydrogen atoms on sp^3 carbon and coupling to electron-poor aryl systems.

SET from Ir(III)* [Ir(ppy)$_3$, ($E_{ox}^* = -1.73$ V *vs.* SCE) to **557a** ($E_{red} = -1.84$ V *vs.* SCE).[53b] This resulted in an Ir(IV) complex and arene radical anion **559a**. Ir(IV) is a strong oxidant ($E_{red} = +0.77$ V *vs.* SCE) and although it was inferred that it might not be able to directly oxidise a thiol (butanethiol, $E_{ox} = +1.12$ V) it would be able to oxidise a thiolate (butanethiolate, $E_{ox} = -0.85$ V *vs.* SCE). Therefore, under the basic reaction conditions it oxidised thiol **560** and this gave thiyl radical **561**, which acted as a HAT reagent. Removal of a hydrogen atom from **558a** with **561** resulted in the formation of allylic radical **562a**. The HAT event was thermodynamically favourable as the allylic C–H bond (BDE = 83.2 kcal mol^{-1}) is weaker than the strong S–H bond present in compound **560** (BDE = 87.0 kcal mol^{-1}). Radical anion **559a** and allylic radical **562a** combined, and after cyanide loss, yielded **564a**.

The applicability of this methodology was then demonstrated with the preparation of 27 coupled products (Scheme 162). With regards to the cyanoarene, it was demonstrated that the EWG could either be in the *para* or *ortho* position with **564b** being prepared in a 50% yield from 1,2-dicyanobenzene. When 1-(tri-methylsiloxy)cyclohexene was used in this transformation, this resulted in ketone **564d** in 83% yield. It was also found that the reaction was tolerant of ester functional groups and heterocycles with the preparation of compounds **564e** and **564f**.

2.5 Ir(III) energy transfer reactions

Progress in radical aromatic decarboxylation reactions of aromatic carboxylic acids has been slow due to the inherent stability of these substrates.[158,195] This problem was overcome with an energy-transfer-mediated concerted fragmentation/decarboxylation process from a redox active ester. The iridium catalyst Ir[dF(CF$_3$)ppy]$_2$dtbbpy(PF$_6$) was promoted to its excited state Ir(III)*, which has a triplet energy of 60.8 kcal mol^{-1} and an excited state lifetime of 2.3 μs. Ir(III)* participated in an energy transfer with ester **565a** due to its lower triplet energy ($E_T = 46.4$ kcal mol^{-1}) and excited species **566a*** was produced (Scheme 163). Concerted N–O homolytic bond cleavage and decarboxylation of **566a*** resulted in carbon dioxide, iminyl radical **567a** and aryl radical **568a**. Aryl radical **568a** was trapped with a radical trapping reagent; chloroiodomethane gave aryl iodide **569a**, but alternative trapping agents were also used as seen in products **573a–d**. Concurrently, iminyl radical decomposed to byproducts **570–572**, which were always detected in optimisation and substrate scope reactions.

An iridium-catalysed approach has been reported for the construction of azetidine compounds **574** *via* an intramolecular aza Paternò–Büchi reaction.[196] Under the reaction conditions, the iridium catalyst became excited with irradiation with blue light and this gave Ir(III)* species (Scheme 164). From Stern–Volmer studies it was shown that styrene moieties **575** quenched the excited catalyst, which returned the Ir(III) complex and triplet styrene **576a**. Reversible C–C bond formation resulted in cyclic
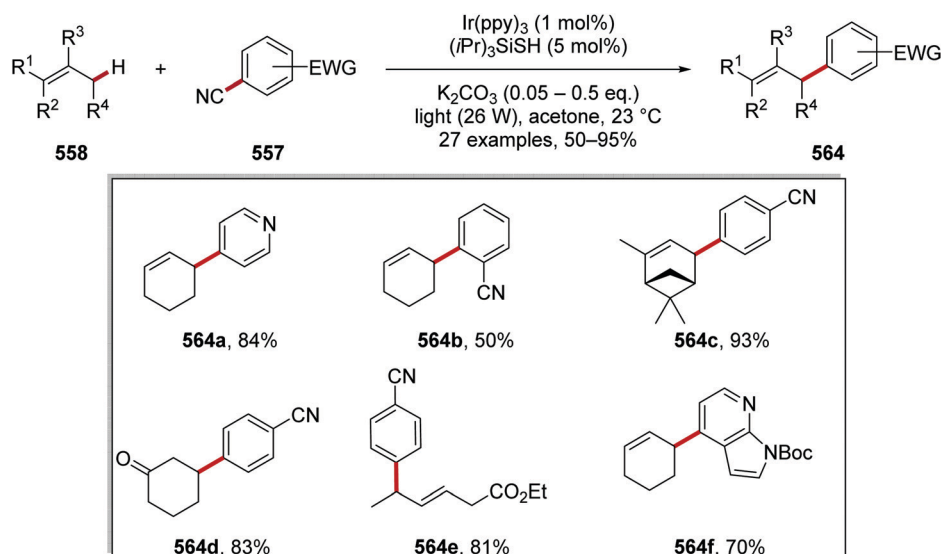
Scheme 162 Results of HAT of allylic hydrogen atoms on sp^3 carbon and coupling to electron-poor aryl systems.

9624 | *Chem. Soc. Rev.*, 2021, **50**, 9540–9685

This journal is © The Royal Society of Chemistry 2021
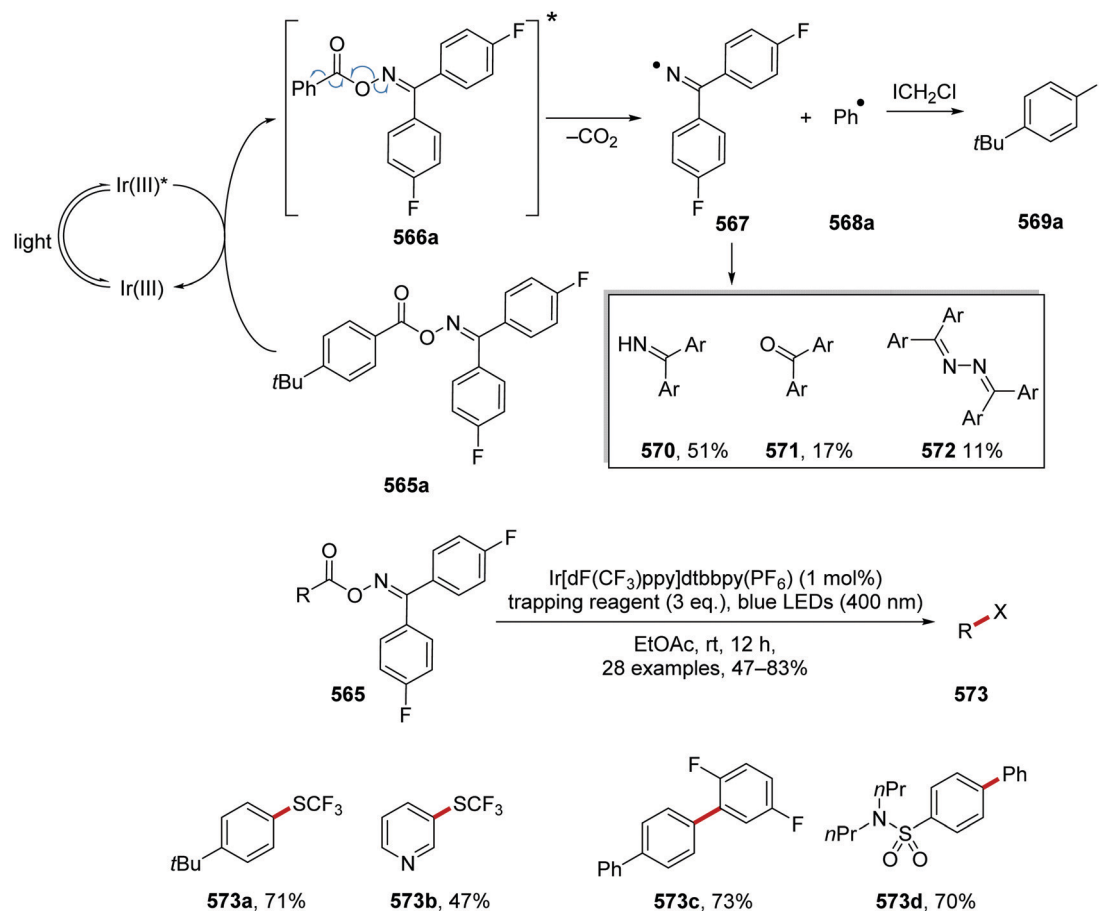
Scheme 163 Coupling of aryl radicals arising from decarboxylation.
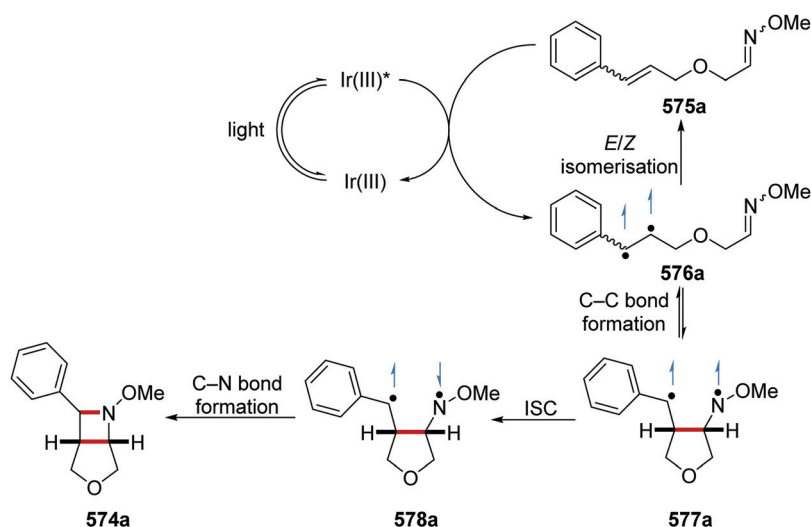
Scheme 164 Aza-Paternò–Büchi reactions.
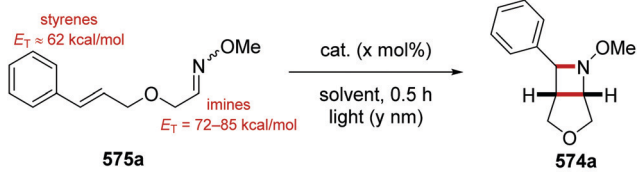
intermediate **577a.** Free rotation around the C–N bond present in **577a** led to the observed oxime *E/Z* scrambling as styrene **575a** was returned from **577a** after ring-opening and deexcitation pathways. Cyclic intermediate **577a** was also able to partake in

an ISC process and this delivered singlet biradical **578a,** which allowed for C–N bond formation and giving azetidine **574a.**

A challenge for this transformation was the selective excitation of the alkene over the imine motif. It has been found that

This journal is © The Royal Society of Chemistry 2021

Chem. Soc. Rev., 2021, **50**, 9540–9685 | **9625**

Table 7   Optimisation of reaction conditions for Aza-Paternò–Büchi reactions

Entry	Catalyst (mol%)	E_T (kcal mol^{-1})	Wavelength (nm)	Solvent	Yield of 574a[a] (%)
1	None	—	365	CH$_2$Cl$_2$	6
2	Xanthone (30)	74	365	MeCN	43
3	Ru(bpy)$_3$(PF$_6$)$_2$ (2.5)	49	427	THF	0
4	Ir(ppy)$_3$ (2.5)	58	427	THF	39
5	Ir[dF(CF$_3$)ppy]$_2$dtbbpy(PF$_6$) (0.5)	62	427	THF	98

[a] Yield determined by quantitative ^{1}H NMR spectroscopy with an internal standard.

aza-Paternò–Büchi reactions work less well than Paternò–Büchi reactions, as imine excitation leads to non-productive radiationless decay processes. The addition of a sensitiser to the reaction mixture overcomes the problem of non-productive imine excitation.[61] Oxime 575a was chosen as substrate to find optimal reaction conditions. Initially, it was found that direct excitation of 575a with UV-light led to the formation of 574a in 6% yield (Table 7, entry 1). The use of catalytic amounts of xanthone (E_T = 74.1 kcal mol^{-1}) gave 574a in 43% yield (entry 2).[197] With complete consumption of starting material, it was postulated that the strong photoredox properties of xanthone led to decomposition of the substrate. When Ru(bpy)$_3$(PF$_6$) was used as catalyst, no conversion to product was observed (entry 3), and this was due to the triplet energy of this catalyst being too small to effectively transfer energy to 575a. Styrenes have a triplet energy of *ca.* 62 kcal mol^{-1}; therefore an

effective energy transfer catalyst has to have a triplet energy greater than this.[198] Imines have greater triplet energy, and arylimines have triplet energy levels between 72–85 kcal mol^{-1}.[199] The Ir(ppy)$_3$ photocatalyst has a triplet energy of 58 kcal mol^{-1} and thus this gave 574a in 39% yield. The use of Ir[dF(CF$_3$)ppy]$_2$-dtbbpy(PF$_6$) that has a triplet energy level of 62 kcal mol^{-1} efficiently generated 574a in 98% yield with only 0.5 mol% of catalyst.

Optimised reaction conditions led to the generation of 21 azetidine compounds 574 from the corresponding alkene-imine substrates 575 (Scheme 165). This methodology allowed for the preparation of bicyclic fused tetrahydrofuran analogues 574a and 574b in 96% and 85% yield, respectively. The reaction proceeded smoothly even with the presence of ester, silyl-protected alcohol and alkene groups and thus compounds 574d–f were all prepared. The generation of heterocycle-containing products and preparation
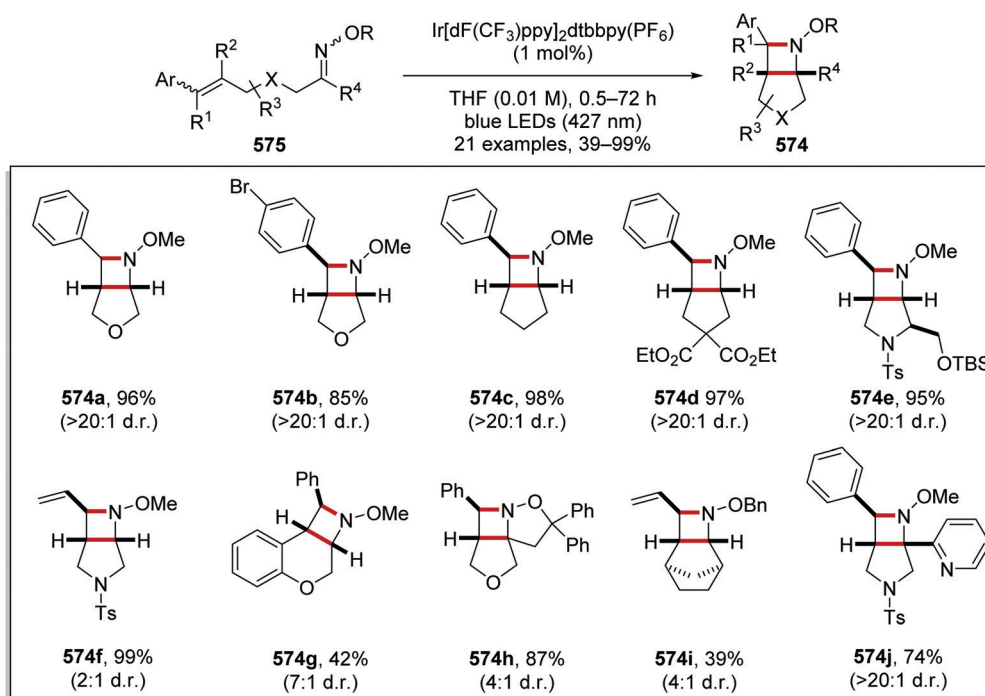
Scheme 165   Product scope for Ir-promoted 4-membered ring formation.

of polycyclic compounds was also achieved and **574g–j** were all produced.

3 Radical coupling reactions triggered by organic photoredox agents

3.1 Xanthene and related dyes

Xanthene dyes undergo photoexcitation. The excited species can act as electron donors or electron acceptors or as energy transfer agents. Fluorescein **4**, Eosin Y **5**, Rose Bengal **6** and erythrosine **73** are all members of this family (Fig. 16). The molecules can have various protonation states but are represented above in their electron-rich 'basic' forms. Nitrogen-substituted analogues of this family are the rhodamines, represented here by rhodamine-6G **578** and rhodamine B **579**, while another closely related structure is methylene blue **580**.[8,200] As mentioned previously, Eosin Y does have an efficient ISC (ϕ_{ISC} = 0.33) and the strength of its oxidising/reducing abilities does vary between the excited singlet (E_{red}^* = +1.23 V $vs.$ SCE, E_{ox}^* = −1.58 V $vs.$ SCE) and triplet state (E_{red}^* = +0.83 V $vs.$ SCE, E_{ox}^* = −1.15 V $vs.$ SCE), with the excited singlet state being a stronger oxidant and reductant.

Eosin Y **5** is widely reported for a range of reaction types. The photoexcited forms of Eosin and related molecules are generally mild electron donors but they react well with good electron acceptors such as arenediazonium salts (Scheme 166). Single electron transfer from **5** (E_{ox}^* = −1.58 V $vs.$ SCE)[8a] reduces the diazonium cation **581** (E_{red} = +0.33 V $vs.$ Ag/AgCl and 4-methyl-benzenediazonium tetrafluoroborate E_{red} = −0.18 V $vs.$ SCE) to the corresponding radical, from which a molecule of N_2 is lost to afford an aryl radical. This couples regioselectively to the 2-position of electron-rich heteroarenes like furans, thiophenes and N-Boc pyrroles as reported by König et al.[202] The reaction works well for a wide range of substituted diazonium salts.

Zhou's team has used diazonium salts in benzannulation reactions (Scheme 167).[203] Diazonium salt **584**, derived from a biaryl, illustrates the point. The salt was activated as above, and the aryl radical so created reacted with methyl propiolate **585**. The resulting vinyl radical then cyclised onto the remaining aryl ring to give an intermediate cyclohexadienyl radical. The final product formed following electron transfer [likely to another molecule of diazonium salt or to the oxidised dye], followed by deprotonation. A range of phenanthrenes was prepared in similar manner as exemplified by **586a–g**.
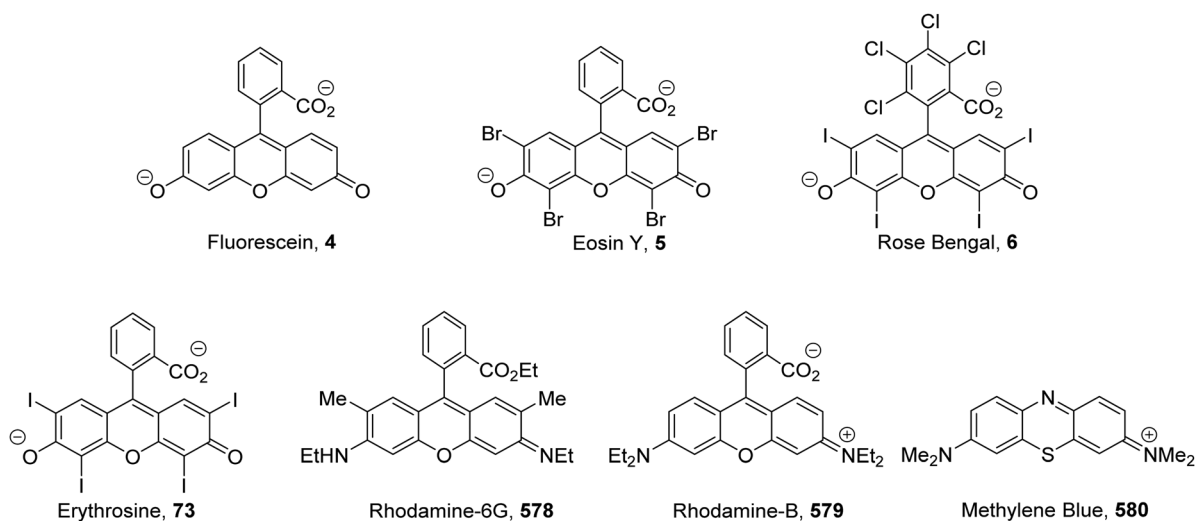
Fig. 16   Eosin Y (**5**) and structurally related dyes.
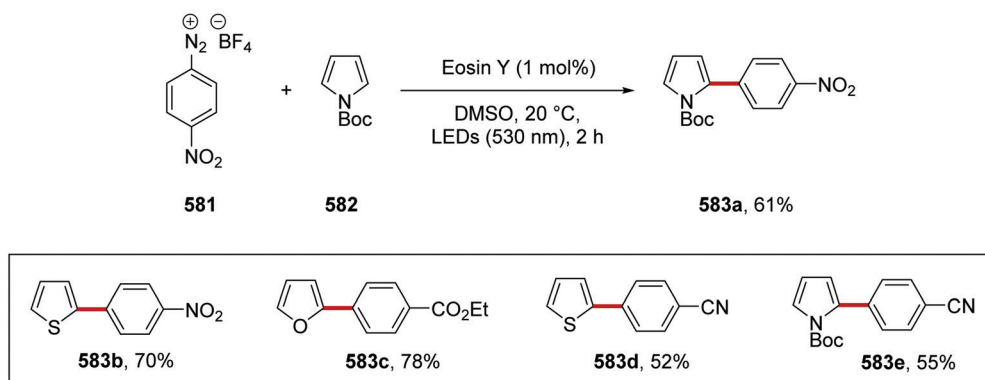
Scheme 166   Photoactivated Eosin Y reduced arenediazonium salts to aryl radicals.

This journal is © The Royal Society of Chemistry 2021

Chem. Soc. Rev., 2021, **50**, 9540–9685 | **9627**
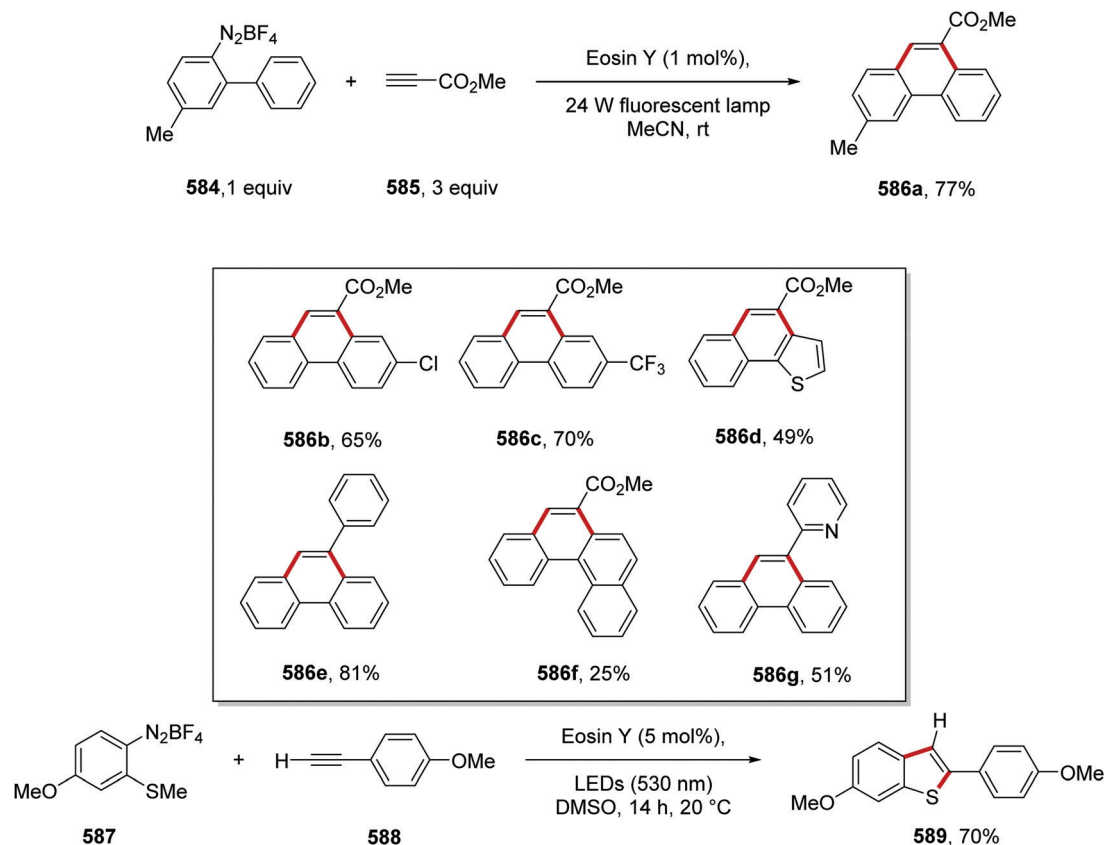
Scheme 167 Reductive annulation with photoexcited Eosin Y as electron donor.

Similarly, König prepared fused heterocycles such as the dibenzothiophene **589**. In these cases, an aryl radical, formed from **587** as described above, reacted with an alkyne **588** to form a vinyl radical.[204] Cyclisation of the vinyl radical onto sulfur afforded a hypervalent sulfur radical. Oxidation transformed this to a sulfonium salt, which was demethylated to give the benzothiophene product.

Diazonium salts have also been deployed in acylation chemistry (Scheme 168). Following SET to **590** (E_{red} = −0.22 V vs. Ag/AgCl)[205b] and loss of N_2, the resulting aryl radical reacted with CO to form an aroyl radical (Scheme 169). In turn, this underwent electron transfer to the oxidised form of the redox dye to afford the corresponding acyl cation. This was then trapped by alcohols to form esters **591** by Jacobi von Wangelin[205] and, separately, Xiao.[206] Likewise, aroyl cations, generated from diazonium salts, have been subjected by Gu *et al.* to Friedel–Crafts chemistry by arene nucleophiles thereby forming diaryl ketones **596**.[207]

Here the diazonium salt quenches (E_{red} = −0.22 V vs. Ag/AgCl)[205b] the excited state Eosin Y* by electron transfer giving the oxidised form of Eosin Y. Loss of dinitrogen from **597** leads to an aryl radical **598**. This reacts with CO to form the acyl radical **599**, and this radical then reduces the oxidised form of Eosin Y while being converted into an acyl cation **600**, that is trapped by isopropanol. In principle, the cycle could be more direct if the acyl radical can act as electron donor to a fresh molecule of diazonium salt.

Eosin Y (**5**) (E_{ox}^* = −1.15 V vs. SCE)[8a] has been used to reduce other types of functional groups also. The excited state can lead to cleavage of labile C–halogen bonds. Thus, the electron-poor ethyl bromofluoroacetate **602** is a good electron acceptor leading to a fluoroacetate radical and a bromide anion (Scheme 170).[208] The intermediate indole α-fluoroester **603** loses fluoride anion and the resulting conjugated iminium electrophile is attacked by nucleophilic arene, to yield the observed product. Symmetrical or unsymmetrical products (*e.g.* **605d**) can be targeted.

Electron-poor arenes such as bromopentafluorobenzene **606** (E_{red} = −1.39 V vs. SCE) can also be reduced by photoactivated Eosin[209] (E_{ox}^* = −1.58 V vs. SCE) as shown by the team of König. Electron transfer forms the radical anion of the substrate that expels bromide ion, leaving a perfluoroaryl radical, which couples to arene partners such as benzene **607**, to afford products **608** (Scheme 171).

Zeitler *et al.* used[210] excited state Eosin Y **5** as an electron donor to enones and related systems that were activated through hydrogen bonding to appropriate thioureas *e.g.* **610** (Scheme 172). Monocyclisation occurred to give products **611** in the presence of a Hantzsch ester **612** as an H-atom donor. Similar cyclisations can also be achieved,[211] using alternative redox active reagents *e.g.* the radical anion of DCA or the chrysene radical anion and Ru redox reagents, in the presence or absence of acids.[212] It was proposed that the excited catalyst underwent SET from the Hantzsch ester and it was the reduced catalyst that was responsible for

9628 | *Chem. Soc. Rev.*, 2021, **50**, 9540–9685

This journal is © The Royal Society of Chemistry 2021
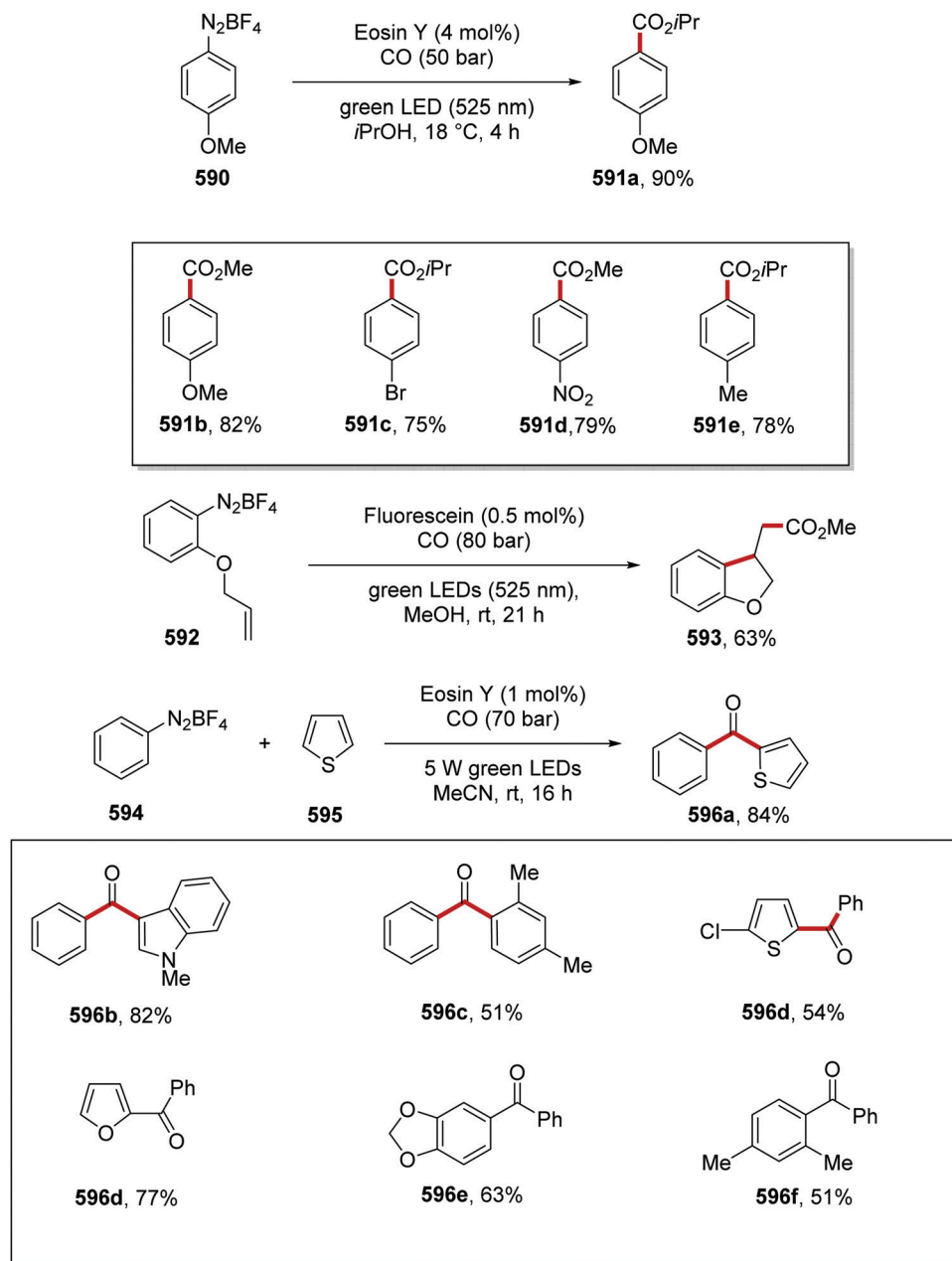
Scheme 168   Acylation of diazonium salts.

electron-donation to the enone system that was activated by the thiourea. Both electron-rich and electron-poor aromatic enones underwent successful cyclisation with Eosin Y due to their low reduction potential (enone **609** E_{red} = −1.20 V *vs.* SCE).[210b] However, it was observed that aliphatic enones could not be reduced by Eosin Y, due to their more negative reduction potential;[210c] in these cases an iridium catalyst [Ir(dtbbpy)(ppy)$_2$PF$_6$, ($E_{(M/M^-)}$ = −1.51 V *vs.* SCE) was found to be very successful.

Leonori *et al.* reported photoactivated Eosin Y **5** as an electron donor to dinitroaryl oxime ethers such as **613**.[213] The resulting radical anions fragmented to dinitrophenolate anions and iminyl radicals; the radicals cyclised and the resulting carbon-centred radicals abstracted H from 1,4-cyclohexadiene

to form products **614** and analogues (Scheme 173). When the cyclohexadiene was omitted, then the final radical instead attacked a nitro group, ultimately resulting in formation of alcohols **615**. During the study, the reduction potential of the oxime was of critical importance in ensuring a successful reaction as it must match the oxidation potential of the Eosin Y catalyst. The model substrate **613-m** (see inset, Scheme 173) was studied by cyclic voltammetry (E_{red} = −0.55 V *vs.* SCE) it was found it could be reduced by Eosin Y (E_{ox}^* = −1.15 V *vs.* SCE) and thus this provided an efficient reaction. However, when the aromatic ring only contained a single *para*-nitro group this gave a more negative reduction potential (E_{red} = −0.93 V *vs.* SCE) and this translated into a more challenging substrate for Eosin Y to

This journal is © The Royal Society of Chemistry 2021

Chem. Soc. Rev., 2021, 50, 9540–9685 | 9629

Scheme 169   Reaction pathway for acylation of arenediazonium salts.

Scheme 171   Photoactivated Eosin Y reductively activates a reactive bromoarene.

reduce with SET. When an analogue containing just a single aromatic *para*-nitro group Eosin Y delivered the corresponding cyclised product in 7% isolated yield, the more strongly reducing Ir(ppy)$_3$ (E_{ox}* = −1.77 V *vs.* SCE) in 91% yield.

Although Eosin Y **5** is the most commonly used of these dyes, other members of the family have also found applications. Rhodamine B (**579**) was found to be the best of a number of related dyes that were tested for the activation of perfluoroalkyl iodides *e.g.* **617** and other electron-deficient alkyl iodides (Scheme 174).[214,215] Electron transfer from **579** (E_{ox}* = −1.3 V *vs.* SCE) to **617** (E_{red} = −1.00 V *vs.* SCE)[214b] leads to the perfluoroalkyl radical. This adds to the less hindered end of an alkene to form an alkyl radical that, in the simplest case, reacts by iodine atom transfer to afford the product, (*e.g.* **618**) and also to form another perfluoroalkyl radical, thereby sustaining a chain reaction. Many of the substrates *e.g.* **619**, **621** are 1,6-dienes which allow cyclisation of an intermediate carbon radical before iodine atom transfer.

However, in a separate study, perfluoroalkyl halides **623** were coupled to terminal alkenes **624**, which gave fluorinated alkene **625** *via* an atom transfer radical addition elimination (ATRE) process, promoted by Eosin Y photocatalyst (Scheme 175).[216]

Alkene **625a** was formed when the reaction mixture was irradiated with white light (16 W household fluorescent lamp) and this resulted in excited Eosin Y* (**5***) from **5**. SET from **5*** (E_{ox}* = −1.1 V *vs.* SCE)[215] to halide **623a** (E_{red} = −1.10 V *vs.* SCE)[216b] gave perfluoroalkyl radical **626a** and oxidised catalyst **5•+**. Radical addition of **626a** to alkene **624a** gave the carbon-centred radical **627a**. The exact reaction pathway to reach alkene **625a** from **627a** was not fully elucidated and three different reaction pathways were feasible. A radical-chain mechanism may have been operative with an abstraction of an iodine atom from **623a** with radical **627a** and this would have given **628a**. The combination of **628a** with base would have resulted in an E2 elimination and this would have produced alkene **625a**. Alternatively, SET between radical **627a** and oxidised catalyst **5•+** would have resulted in the formation of cation **629a** and closure of the Eosin Y catalytic cycle. Proton loss from **629a** would have resulted in the formation of the alkene product. However, a charge combination between cation **629a** and iodide was also possible this would have delivered alkyl iodide **628a**, from which alkene **625a** is accessed through an E2 elimination. During the optimisation of this reaction, alkyl iodide **628a** was sometimes the sole product; therefore, it may be a key intermediate for this transformation.

From optimisation studies, it was found that Eosin Y performed better than the other organic dyes, Rose Bengal, Rhodamine B and dibenzylamine. Highest yields of **625a** were obtained when caesium carbonate was used as the base. DBU, triazabicyclodecene, DIPEA and K$_2$HPO$_4$ were also tested. Product **625a** was formed in the highest yields when DMA was used as the solvent. The use of THF or water as solvent gave alkyl iodide **628a** as the sole product in 66% and 63% ^{1}H-NMR yield, respectively. With these optimised
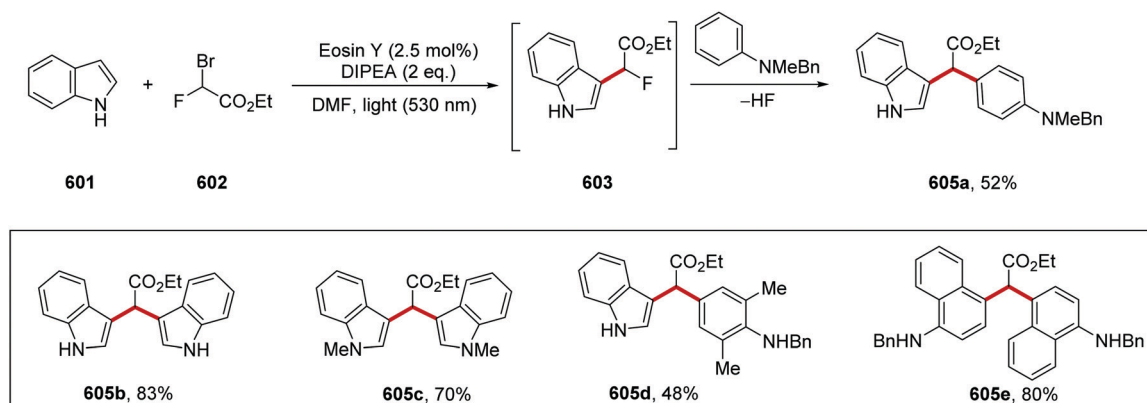
Scheme 170   Double arylation of ethyl bromofluoroacetate.

9630 | *Chem. Soc. Rev.*, 2021, **50**, 9540–9685

This journal is © The Royal Society of Chemistry 2021
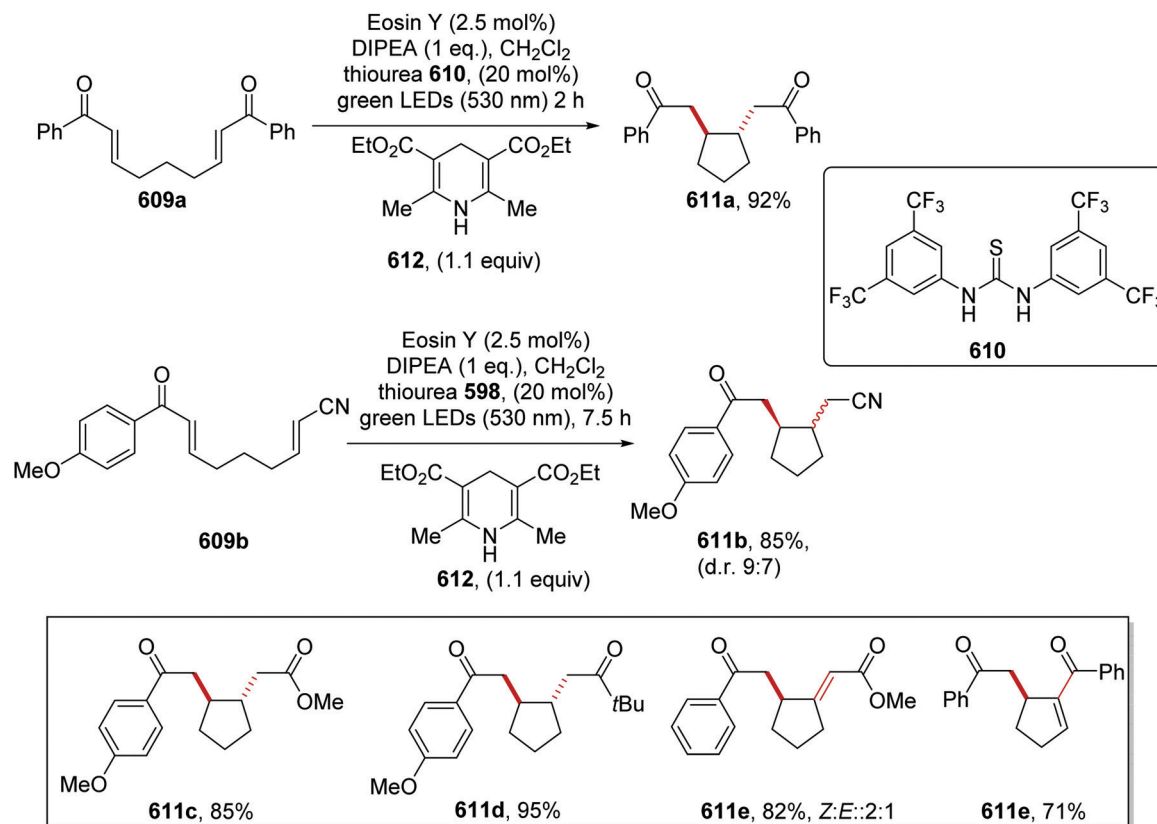
Scheme 172 Reductive cyclisation of activated bis-enones and related compounds mediated by Eosin Y and Hantzsch esters.

reaction conditions, a range of 30 perfluoroalkylated alkene products **625** was prepared in 51–95% yields (Scheme 176). Synthetically useful functional groups were tolerated under the reaction conditions and N-alkylphthalimide analogue **625c** was isolated in 86% yield, allowing for later conversion to an amine. Difluoroalkyl bromides were accessible under the reaction conditions when difluorodibromomethane was used in the reaction and this gave difluorobromomethyl compounds **625d–e** in yields of 74–80%. When ethyl 2,2-difluoro-2-iodoacetate was used in the reaction, this gave ester derivatives **625f–g**. The reaction was also amenable to complex substrates, for example, steroid compound **625g** was prepared in 95% yield in a 5 : 1 mixture of stereoisomers.

Meanwhile, Scaiano *et al.* used photoactivated methylene blue **580** to activate Togni's reagent **631** towards the release of trifluoromethyl radicals that substituted onto pyrroles, indoles and thiazoles giving trifluoromethylated products (Scheme 177).[217] Specific examples include **632a-d**. In addition, products derived from addition to alkenes and alkynes were isolated. A probable mechanism would be SET from 3-methylindole (E_{ox} = +1.12 V *vs.* SCE) to an excited (T$_1$) molecule of methylene blue (E_{red}^* = +1.60 V *vs.* SCE).[8a] The resulting reduced catalytic species should be able to provide an electron to reagent **631** (E_{red} = −1.34 V *vs.* SCE).

A clever application is reported by König *et al.* for Rhodamine 6G, **578**, where the effective reduction potential is dependent on the wavelength of radiation.[218] 2,4,6-Tribromopyrimidine, **633**, nicely illustrates the point (Scheme 178). Excitation of rhodamine-6G, **578**, with green light afforded the excited state

(E_{ox}^* = *ca.* −0.8 V *vs.* SCE) and this was reduced by electron transfer from DIPEA to afford the radical anion ($E_{ox}^{-•}$ = *ca.* −1.0 V *vs.* SCE), which is a stronger reducing reagent. This species has sufficient driving force to reduce the tribromopyrimidine **633** to its radical anion, which expels bromide ion to form the aryl radical. This was now used to couple to heteroaromatics; an example shows N-methylpyrrole reacting to yield the dibromoproduct **634**. However, if the reaction was performed under blue light a different reaction pathway was feasible. When the reaction mixture was irradiated with blue light it was speculated that the radical anion became excited, and this created the strongly reducing reagent Rh-6G*$^{-•}$ (E_{ox}^* = −2.4 V *vs.* SCE), the exact electronic transition was not identified. It was proposed that it was this strongly reducing species that could reduce pyrimidine **634** and thus under blue light pyrimidine **633** was converted through **634** to pyrrole derivative **635**. The reaction was also performed stepwise through the two activations, and this allowed for selective substitutions as in the conversion of **633** to **637**. Alongside pyrimidine **633**, 1,3,5-tribromobenzene (E_{red} = −1.61 V *vs.* SCE)[218b] was used extensively as substrate in this paper.

Boronates as radical precursors. The preparation of alkenes **640** from trifluoroborates **638** and sulfones **639** with the photoredox catalyst Eosin Y was recently reported in the literature.[219] The reaction was performed in DMF and 49–77% yields were obtained and high levels of stereocontrol were observed for the *E*-isomer (Scheme 179). Eosin Y (E_{red}^* = +0.83 V) could oxidise trifluoroborates (**638**, E_{ox} = +0.78 V *vs.* SCE).

613a

Eosin Y **5** (2 mol%)
1,4-cyclohexadiene (2 eq.)
K$_2$CO$_3$ (2 eq.), acetone
green LEDs

614a, 94%

613-m

614b, 68%, 1:1, d.r.   **614c,** 65%   **614d,** 70%, 3:1, d.r.   **614e,** 37%, 1:1, d.r.

613

Eosin Y **5** (2 mol%)
Et$_3$N (2 eq.), MeCN
green LED

615a, 61%

615b, 81%, 1:1, d.r.   **615c,** 67%   **615d,** 66%, 3:1, d.r.   **615e,** 29%, 1:1, d.r.
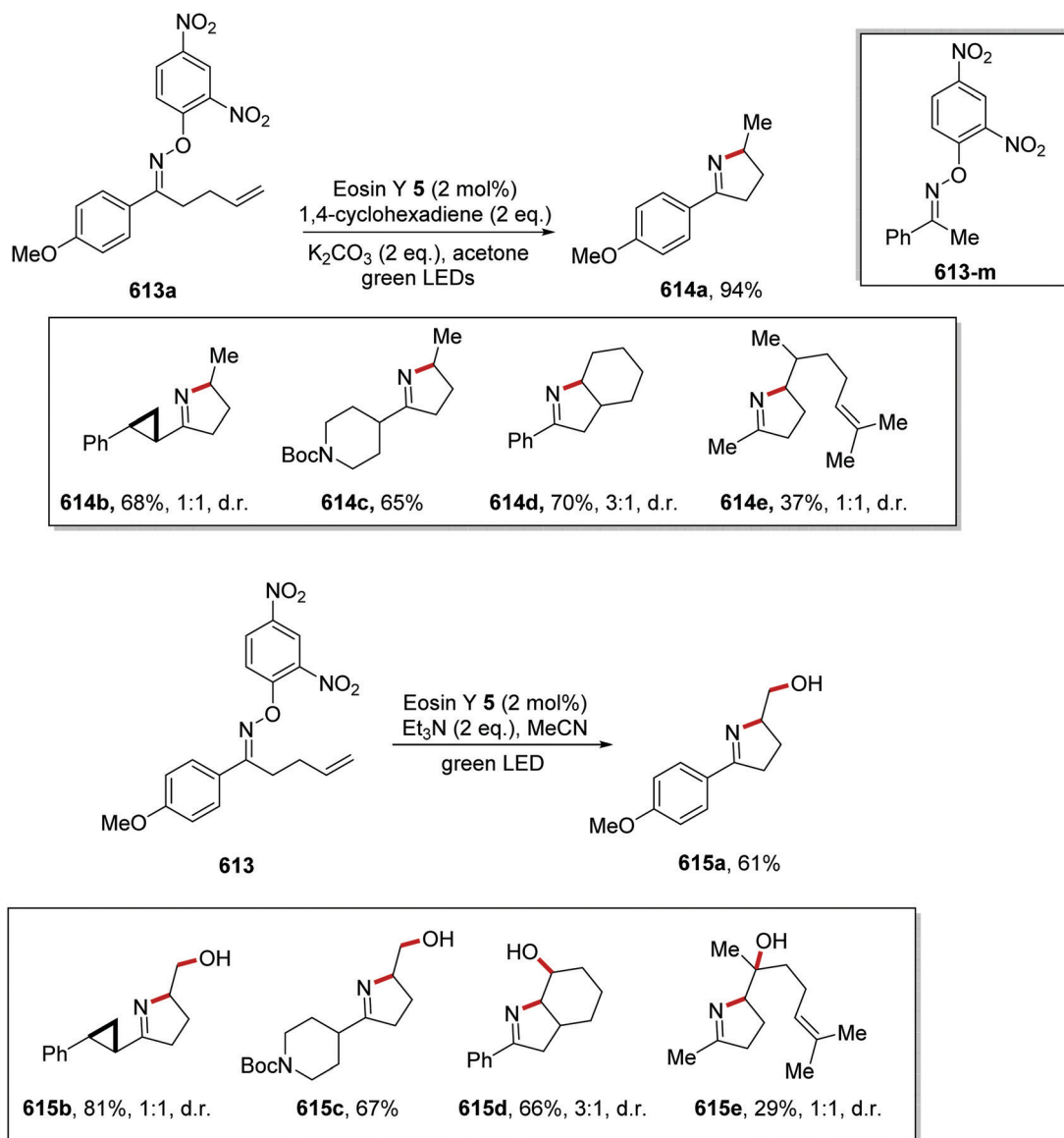
Scheme 173   Iminyl radicals are formed through reduction of oxime ethers.

616   + i-C$_3$F$_7$—I   **617**

Rhodamine B **579** (5 mol%)
DIPEA (1.1 eq.)
H$_2$O, rt, 1h, LED

618 90%

619 i-C$_3$F$_7$—I
(5 equiv)   **617**

Rhodamine B **579** (5 mol%)
DIPEA (1.1 eq.)
H$_2$O, rt, LED, 0.5 h

620, 93% (69 *cis* : 31 *trans*)

621 i-C$_3$F$_7$—I
(5 equiv)   **617**

Rhodamine B **579** (5 mol%)
DIPEA (1.1 eq.)
H$_2$O, rt, LED, 5 h

622, 74% ('79 *cis* : 21 *trans*')
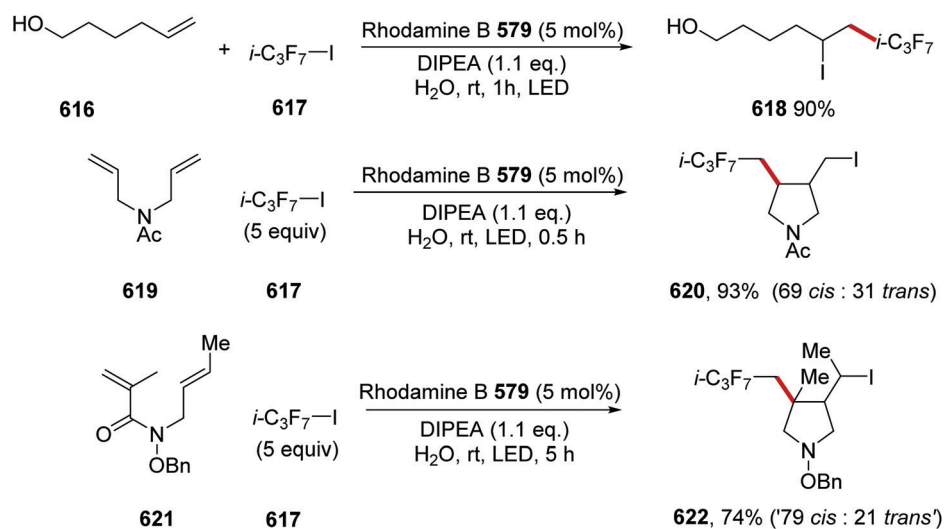
Scheme 174   Trifluoromethylations are readily achieved through photoactivated dyes acting as electron donors.

9632 | *Chem. Soc. Rev.*, 2021, **50**, 9540–9685

This journal is © The Royal Society of Chemistry 2021
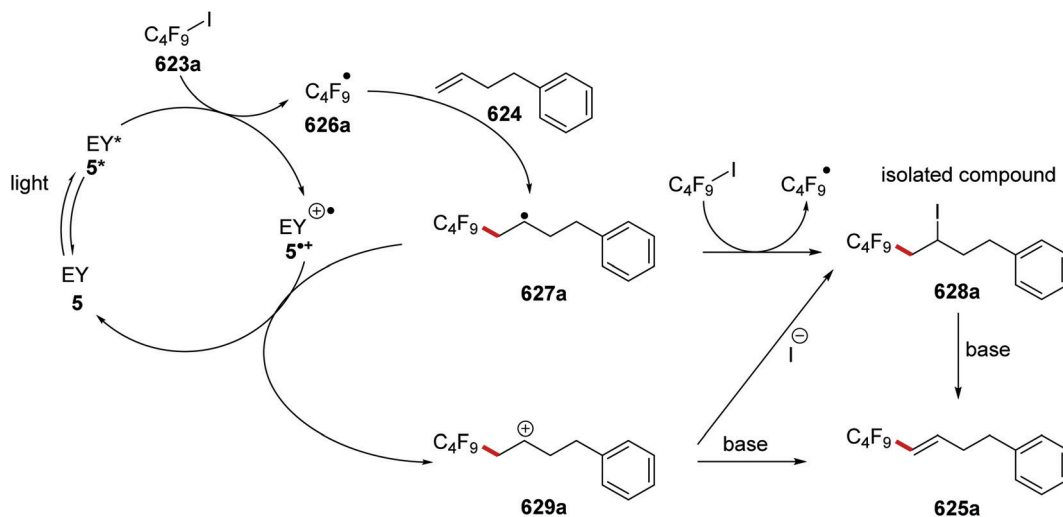
Scheme 175   Perfluoroalkyl radical addition to alkene **624**.
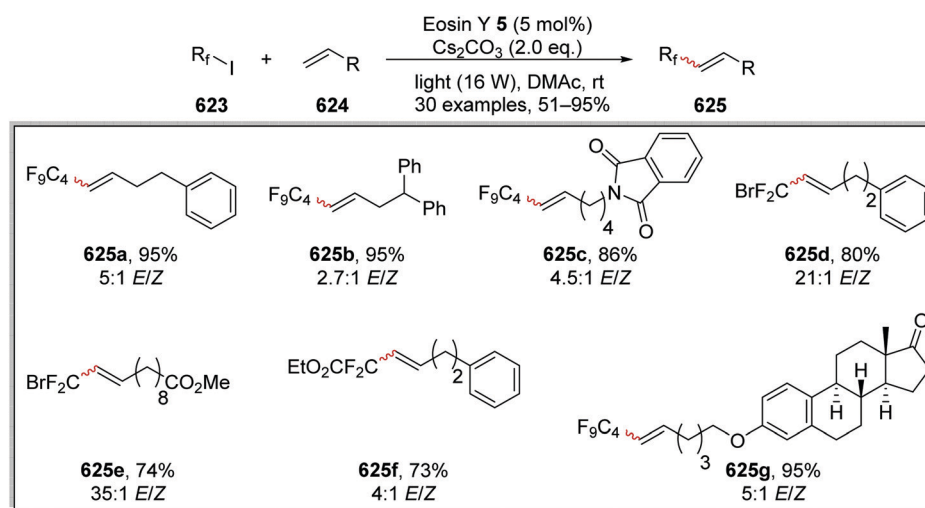
Scheme 176   Scope of alkene products.
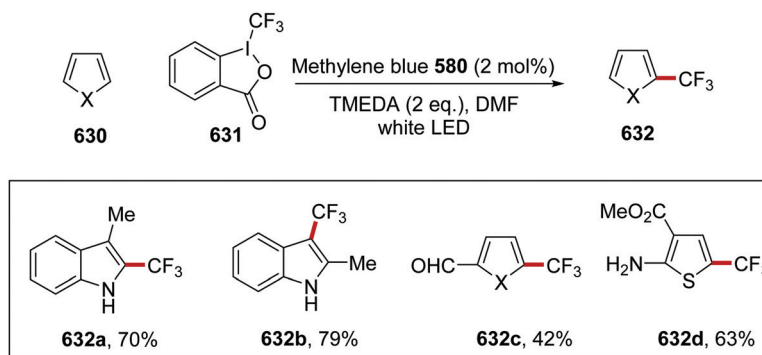
Scheme 177   Togni's reagent as a source of trifluoromethyl radicals.

α-Heteroatom functionalisation. The asymmetric alkylation of lactams **641** with ketones **642** was achieved with catalytic amounts of proline **645** and Eosin Y, **5**.[220] From Stern–Volmer analysis, it was established that lactam **641a** was able to reductively quench the excited state of Eosin Y dye **5**. Therefore, it was proposed that under the reaction conditions **641a** (in terms of published anilines, N,N-dimethylaniline has E_{ox} = +0.74 V vs. SCE) quenched **5*** (E_{red}^{*} = 0.83 V vs. SCE) and this gave amine

This journal is © The Royal Society of Chemistry 2021

Chem. Soc. Rev., 2021, **50**, 9540–9685 | 9633

$$\text{Rh-6G} \xrightarrow{\text{green light}} \text{Rh-6G*} \longrightarrow \text{Rh-6G}^{\ominus \bullet} \xrightarrow{\text{blue light}} \text{Rh-6G*}^{\ominus \bullet}$$

$E^*_{ox} = -0.8$ V vs SCE $E^*_{ox} = -1.0$ V vs SCE $E^*_{ox} = -2.4$ V vs SCE

633 → Rh-6G **578**, LEDs (530 nm), DIPEA, DMSO, 25 °C, *N*-methylpyrrole (18 eq.) → **634**, 67%

633 → Rh-6G **578**, LEDs (455 nm), DIPEA, DMSO, 25 °C, *N*-methylpyrrole (26 eq.) → **635**, 42%

633 → MeO/OMe/OMe, Rh-6G, **578**, 530 nm, DIPEA, DMSO, 25 °C → **636**, 46% → Rh-6G, **578**, 455 nm, DIPEA, DMSO, 25 °C → **637**, 21% over 2 steps

Scheme 178 Wavelength-dependent control of substitution of polyhaloarenes.

638 + **639** → Na₂-Eosin Y (10 mol%), DMF (0.05 M), 50 °C, light (CFL (26 W)), 15 examples, 49–77% → **640**

640a, 73%, 98:2 *E:Z*   **640b**, 61%, 98:2 *E:Z*   **640c**, 62%   **640d**, 49%
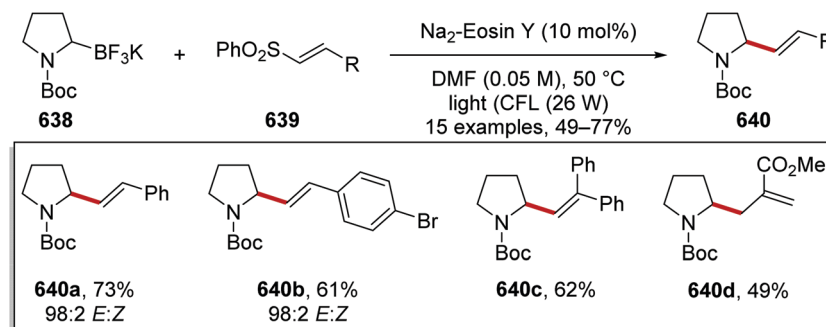
Scheme 179 Eosin-mediated coupling with α-aminoalkylboronates.

radical cation **643a** (Scheme 180) and the reduced form of the Eosin dye. This, in turn, passed an electron to dioxygen in air to form superoxide radical anion, and superoxide was proposed to convert **643a** to **644a** oxidised the amine radical cation to imine **644a**. [The reaction was inhibited when it was conducted in the absence of oxygen.] Meanwhile, acetone **642a** and L-proline **645** reacted to form enamine **646a**, which reacted with the imine to give **648a** in a Mannich reaction with stereochemistry being set by transition state **647a**.

The transformation was successful when Ir(ppy)₃, Ru(bpy)₃Cl₂, acridinium dye and Eosin Y were used as photoredox catalysts.

However, to give a more sustainable and cost-effective transformation, further investigations were carried out with Eosin Y. MeCN, PhMe, CHCl₃ and DMF were all screened as solvents for this reaction, and it was found that, when DMF was used as solvent, this gave the greatest yield for **648a**.

From these optimised reaction conditions, a library of 22 coupled compounds was prepared. The use of various lactams gave coupled compounds **648a–d** in high yields with high enantiomeric excess (Scheme 181). However, the use of assorted ketones resulted in greater variation in the optical purity of the coupled compounds **648f–h**. The reaction was regioselective

9634 | *Chem. Soc. Rev.*, 2021, **50**, 9540–9685

This journal is © The Royal Society of Chemistry 2021
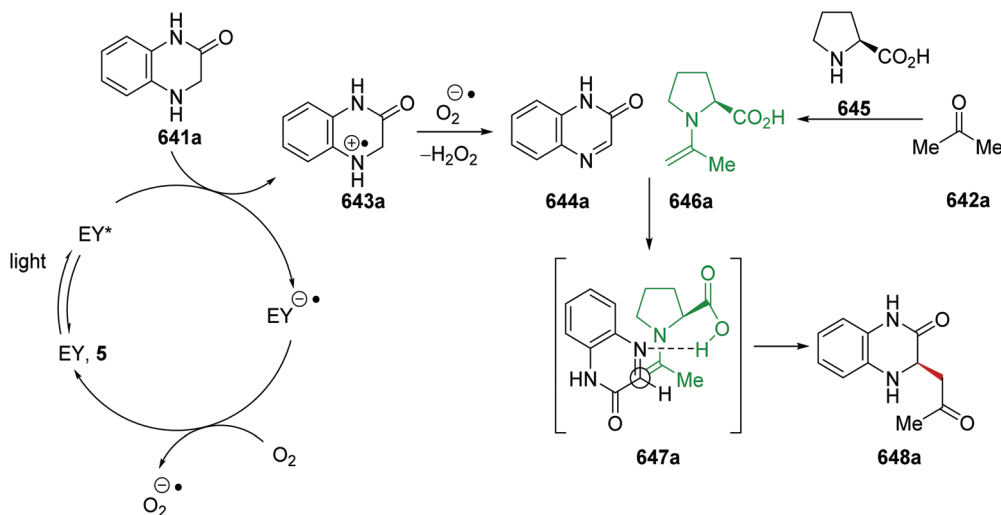
Scheme 180 Eosin Y and proline-dependent asymmetric Mannich reaction.
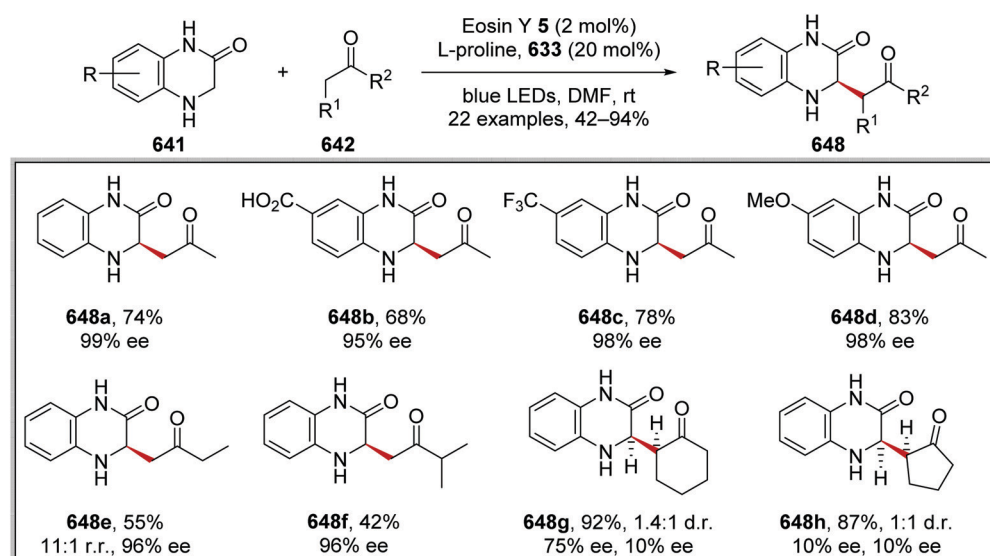
Scheme 181 Stereoselective coupling of ketones **642**.

when unsymmetrical ketones were used. For example, when 2-butanone was used as the substrate, this was functionalised at the less sterically encumbered position (methyl *vs.* methylene) giving coupled compound **648e** in 55% yield in a 11 : 1 ratio of regioisomers. Greater regioselectivity was observed between α-methyl and α-methine groups as demonstrated with the formation of **648f** with only one regioisomer being detected. When prochiral ketones were employed as the substrates, no control of diastereoselectivity was observed with a 1 : 1 mixture of diastereoisomers being given, as seen for example, with coupled compounds **648g** and **648h**.

Aldehyde C–H functionalisation. Additions of acyl radicals, derived from aldehydes **649**, to electron-poor alkenes **650** were facilitated with an excited state HAT with Eosin Y photocatalyst.[221] Under the reaction conditions, irradiation with blue light led to excited Eosin Y species **5*** (Scheme 182). HAT to **5***

from aldehyde **649a** gave acyl radical **651a** and protonated Eosin Y complex **5′**. Concurrently, electron-poor alkene **650** added to Rh catalyst **213** and this gave Rh complex **A**. Acyl radical **651a** was intercepted by Rh complex **A** and this gave Rh complex **B**, which formed the key C–C bond. A reverse hydrogen atom transfer (RHAT) between complex **B** and **5′** closed the Eosin Y catalytic cycle with formation of Rh complex **C**. The catalytic cycle was closed with the dissociation of dicarbonyl product **652** as product and association of another molecule **650**.

A maximum ^{1}H-NMR yield (52%) of compound **652a** was obtained when water (20 eq.) was added to the reaction mixture. When water was absent from the reaction mixture this was diminished to 6% ^{1}H-NMR yield. The reaction did not propagate when Ru(bpy)$_3$Cl$_2$ or Ru(phen)$_3$Cl$_2$ was used instead of Eosin Y, highlighting the HAT activity required to activate aldehyde **649a**. A decreased yield of product was obtained when

This journal is © The Royal Society of Chemistry 2021

Chem. Soc. Rev., 2021, **50**, 9540–9685 | 9635
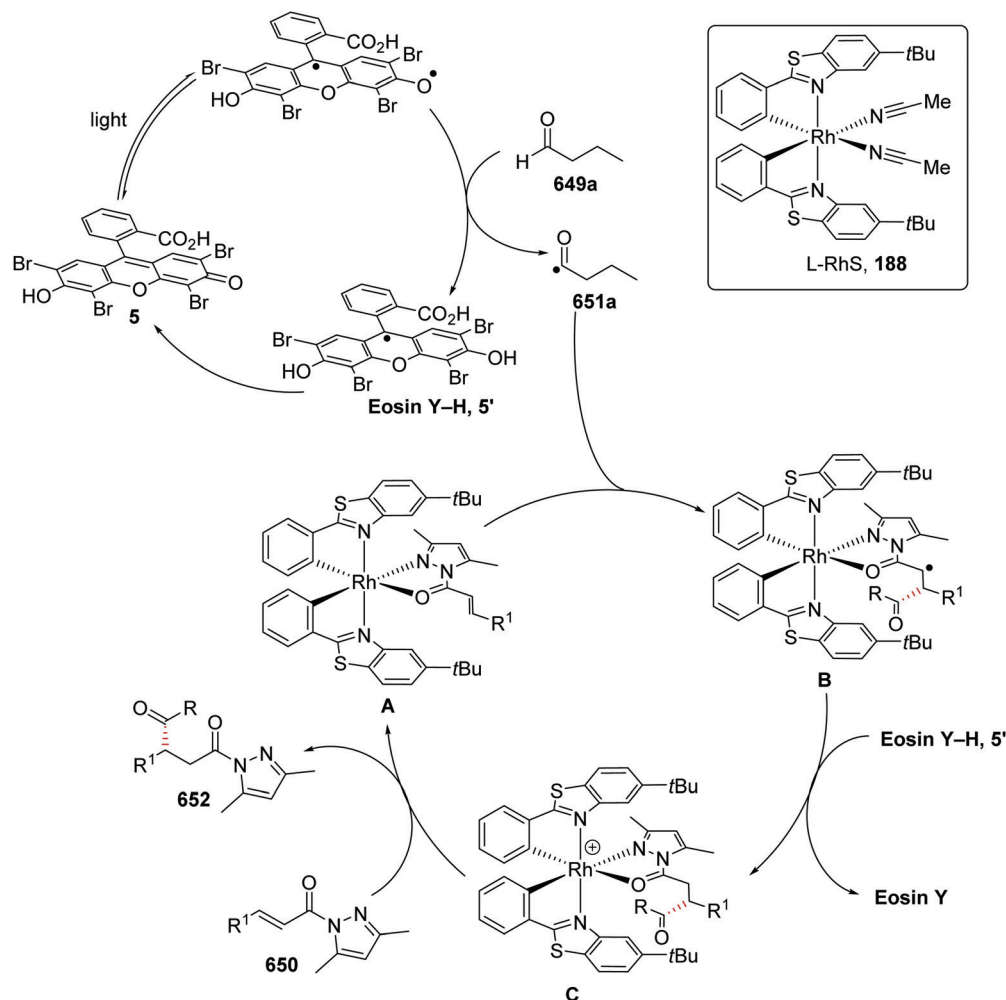
Scheme 182 Tandem Eosin Y and Rh-dependent Giese reaction.

fluorescein was used instead of Eosin Y, with **652a** being given in 11% ^{1}H-NMR yield. When the reaction was performed at 30 °C instead of 10 °C, the enantiomeric excess decreased from 94% to 76%. It was also established that TBME was the optimal reaction solvent, with **652a** being given in lower yields when acetone or benzene was used instead (Scheme 183). A range of dicarbonyl compounds **652** was produced with these optimised reaction conditions in 23–99% yields. The use of cyclopropane-carboxaldehyde as substrate under these conditions gave cyclopropane analogue **652b** in 60% yield and with 81% ee. Aromatic aldehydes were also compatible with the reaction conditions and giving compound **652c** in 44% yield and with 99% ee. Sensitive functional groups were tolerated under the reaction conditions and this allowed for acetals **652d** and **652e** to be prepared in 73% yield (99% ee) and in 99% yield (59% ee), respectively. The ethers, tetrahydrofuran and 2-methyltetrahydrofuran were successful coupling partners for this transformation and products **652f** and **652g** were isolated in high yields (81% and 78%) and high ee (96% and 70%). The reaction with 2-methyltetrahydrofuran led to the formation of the more sterically hindered compound **652g**, *via* the more stable radical intermediate. The use of dimethylaniline as a coupling

partner resulted in amine compound **652h** in 48% yield and with 96% ee.

3.2 N-Phenylphenothiazine and related heterocycles

N-Phenylphenothiazine **653** (PTH) was deployed by the teams of Hawker and Read de Aerániz[222] for radical dehalogenations of aryl and alkyl halides (the reactions are not shown here). The work was eminently successful, leading to this and related photoactivated redox agents being adopted by a number of authors. Alemán *et al.* irradiated PTH at 385 nm ($E_{ox}^* = -2.1$ V *vs.* SCE) in the presence of iPrEt$_2$N in methanol on aryl halides including **654** ($E_{red} = -2.21$ V *vs.* SCE for the related 4-iodoanisole) (Scheme 184).[223] This resulted in formation of aryl radicals that then cyclised onto appropriate functional groups within the substrate to form C–S, C–P or C–Si bonds. Examples of C–S bond formation are shown below, featuring cyclisations onto sulfinate esters. The authors confirmed that the iPrEt$_2$N did not quench the PTH* and hence that the initial SET occurs to the aryl halide.

The aryl iodide **654** quenches the excited state PTH*. In so doing it forms an aryl radical **656** and iodide anion as well as the radical cation of PTH. The radical then cyclises onto sulfur.
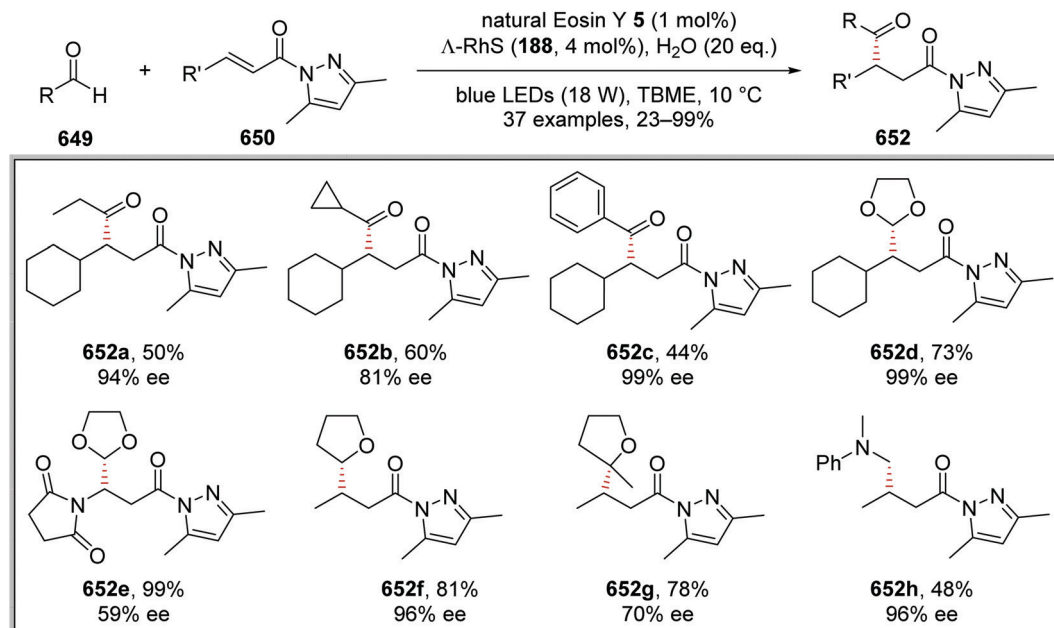
Scheme 183 Eosin Y and Rh Giese reaction.
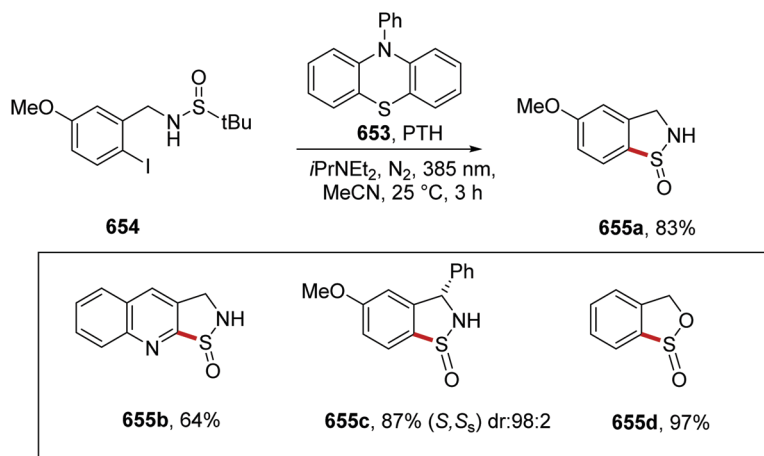
Scheme 184 Photoexcited N-phenyl phenothiazine as electron donor.
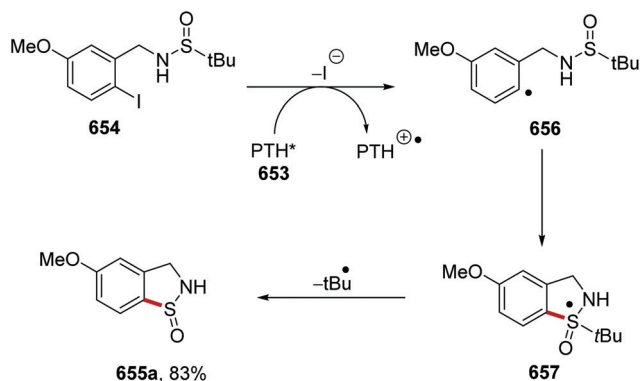
Scheme 185

A hypervalent intermediate **657** may be present before loss of the *tert*-butyl radical (Scheme 185).

Jui *et al.* have exploited blue LEDs to activate PTH (**653**, $E_{ox}^* = -2.10$ V *vs.* SCE) for electron transfer to aryl iodides **658** (as an estimate, iodobenzene $E_{red} = -2.30$ V *vs.* SCE),[224b] allowing the aryl radical to add to enamides **659**.[224] The photoactivated PTH initiates the cycle. The nucleophilic radical resulting from the addition abstracts an H atom from a thiol, and the formed thiyl radical then abstracts H from formate ion to give the radical anion of carbon dioxide which propagates the chain by electron transfer (Scheme 186).

Procter *et al.* used excited state PTH as an electron donor to activate dibenzothiophenylium salt derivatives of arenes, *e.g.* **663**, prepared *in situ* by interrupted Pummerer reactions of arene **661** (Scheme 187).[225] This afforded aryl radicals that were then used to couple to arenes and heteroarenes. SET between

This journal is © The Royal Society of Chemistry 2021

Chem. Soc. Rev., 2021, **50**, 9540–9685 | **9637**
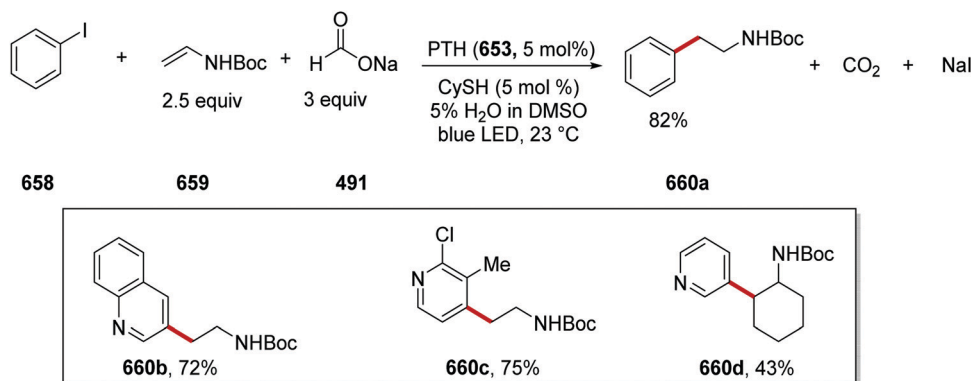
Scheme 186 Additions of aryl radical to enamides initiated by electron transfer from photoactivated PTH.
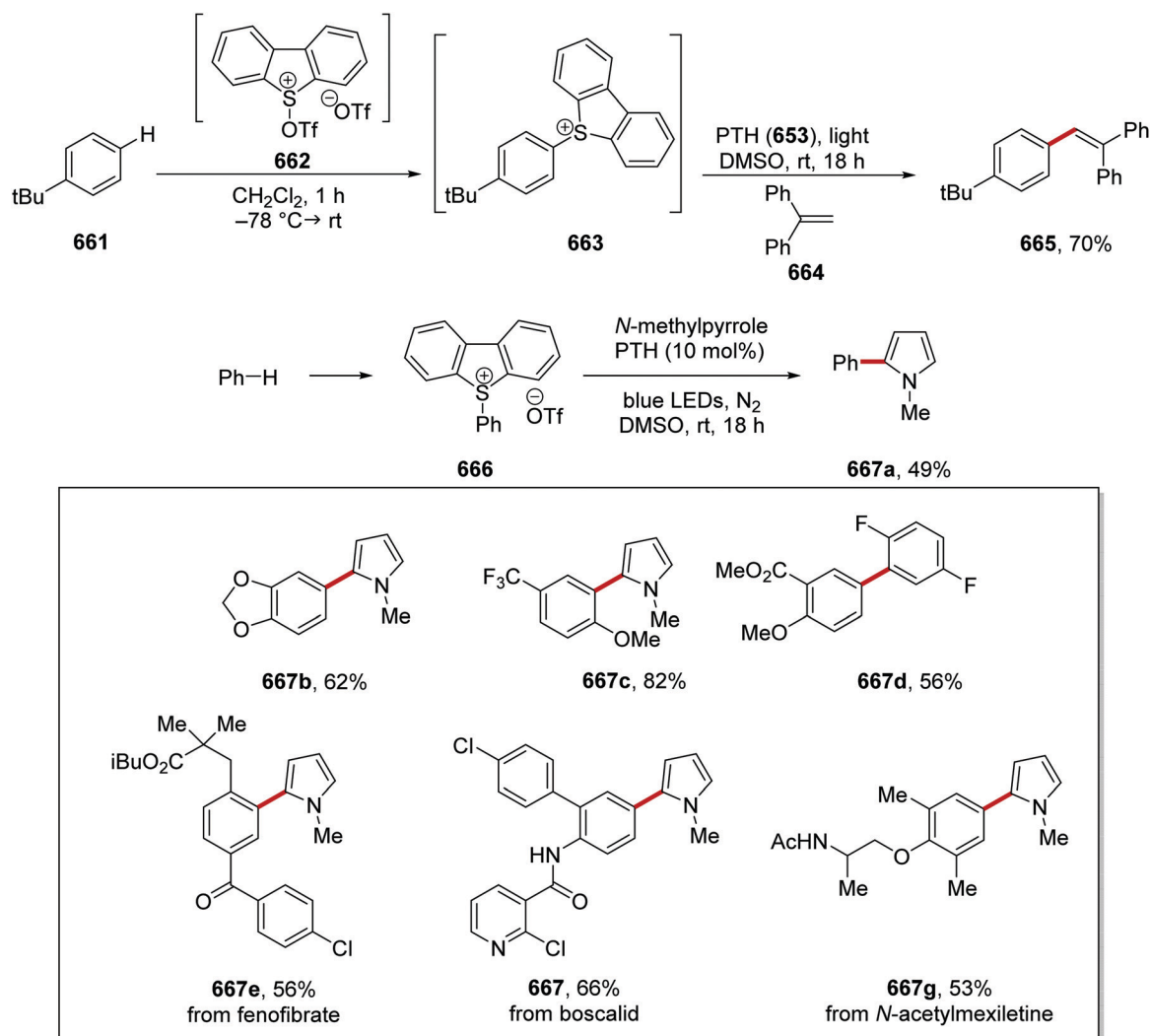
Scheme 187 Interrupted Pummerer reactions provide substrates for reductive cleavage by PTH*.

PTH* (E_{ox}* = −2.1 V $vs.$ SCE) and **663** (E_{red} = −1.10 V $vs.$ SCE) was thermodynamically feasible. Excitation was performed with a blue Kessil lamp. The method was applied to the formation of simpler biaryls $e.g.$ **667a–d**, but also to products arising from late-stage functionalisation of pharmaceutically relevant molecules **667e–g**.

Aleman et $al.$[226] developed wavelength-dependent transformations access to (E)- or (Z)-products in allylic substitution (Scheme 188). The allylic acetate **668** (E_{red} = −2.35 V $vs.$ SCE) was substituted by indoles in their 3-position or by pyrroles in their 2-position when appropriate photocatalysts were used. The (Z)-isomers were the predominant products when PTH
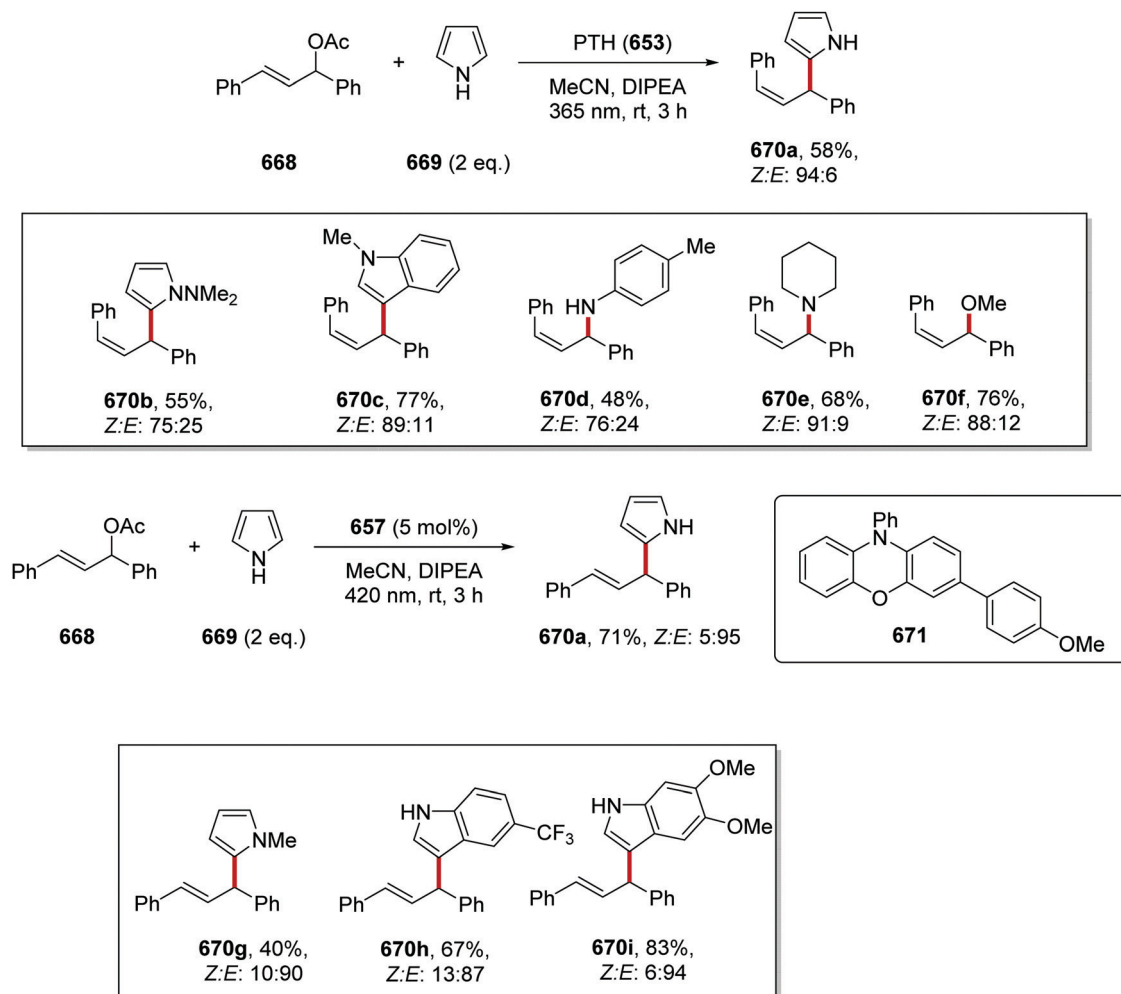
Scheme 188 Allylic acetate **668** undergoes photoredox allylic arylation, where the stereochemistry of the product is dependent on the wavelength used.

(**653**, $E_{ox}^* = -2.1$ V *vs.* SCE) was irradiated at 365 nm, while the (*E*)-isomers were selectively formed when heterocycle **671** was irradiated at 420 nm. A study of the mechanism of the substitution reaction showed electron transfer to the allylic acetate, with loss of acetate ion as a leaving group. The resulting allylic radical then transferred an electron back to the oxidised form of the electron donor to give an allylic cation, and this was intercepted by nucleophiles. Electron-rich arenes including pyrroles, indoles and anilines, as well as aliphatic amines and alcohols acted as suitable nucleophiles. Stern–Volmer studies again showed that DIPEA or pyrrole **669** did not quench the excited state of **653**. However, acetate **668** was a strong quencher of **653*** indicating that **668** was the acceptor in the initial electron transfer. To rationalise the stereoselectivity, studies indicated that the starting acetate **668** was selectively photoisomerised to its *Z*-isomer through irradiation at 365 nm, but not at 420 nm. On the other hand, catalyst **671** facilitated the preparation of *E* alkenes as it could be excited at 420 nm due to its extended conjugation.

Xu *et al.* used a family of photoexcited heterocycles including **675** (PMP = *p*-methoxyphenyl) as electron donors to afford aroyl

radicals from aroyl chlorides as shown for benzoyl chloride, **673** ($E_{red} = -1.56$ V *vs.* SCE). It was calculated from ground-state redox potentials and excited-state energy levels that **675** was capable of reducing **672** both in its S_1 state ($E_{ox}^* = -1.91$ V *vs.* SCE) and its T_1 state ($E_{ox}^* = -1.65$ V *vs.* SCE). Catalyst **675** was also used to accomplish conversion of activated aryl iodides, bromides and chlorides to aryl radicals for a range of reactions (Scheme 189).[227]

Wagenknecht *et al.* harnessed forceful photoredox agents for the Markovnikov photoaddition of alcohols to styrenes.[228] Here, the authors propose that electron transfer from photoexcited donor **678*** ($E_{ox}^* = -2.5$ to -2.6 V *vs.* SCE) to the styrene **676** ($E_{red} = -2.5$ to -2.7 V *vs.* SCE) produced the corresponding radical anion **679** (Scheme 190). Protonation then left a benzylic radical **680** that was oxidised to the benzylic cation before product **677** formed as a result of interception by the alcohol.

Ohmiya *et al.* took activated *N*-oxyphthalimide esters of tertiary alkylcarboxylic acids **681** (Scheme 191).[229] Electron transfer from PTH analogue **684** ($E_{ox}^* = -1.97$ V *vs.* SCE, for the S_1 state) gave the phthalimide anion and the carboxyl radical, which rapidly lost carbon dioxide to give a tertiary alkyl radical.

This journal is © The Royal Society of Chemistry 2021

Chem. Soc. Rev., 2021, **50**, 9540–9685 | 9639
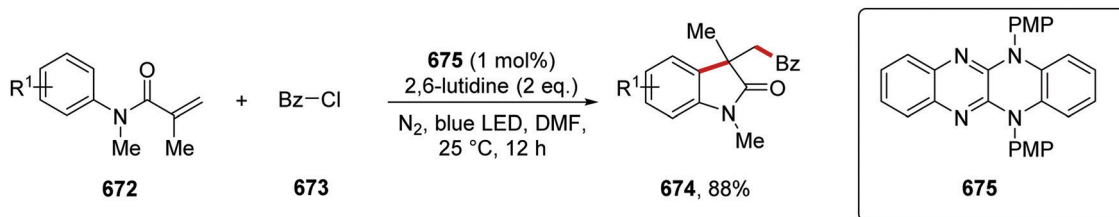
Scheme 189 Aroyl radicals are produced by aroyl chlorides.
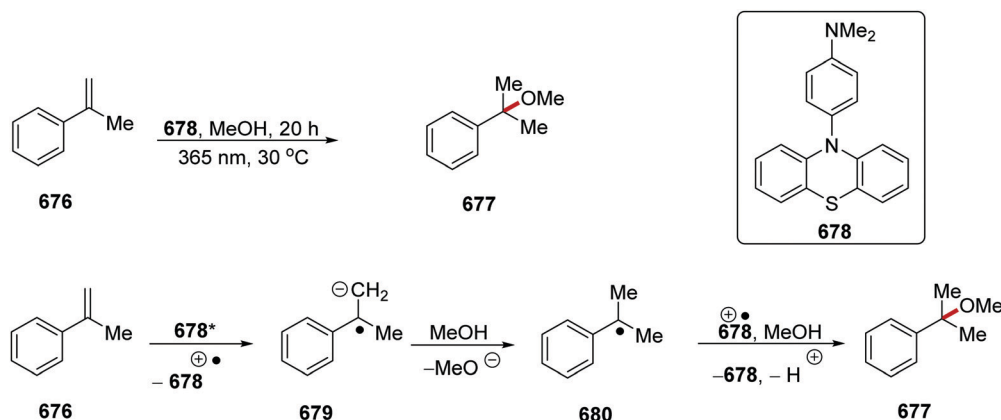
Scheme 190 Styrene activation through its radical anion and a benzylic cation leads to Markovnikov addition of alcohols.

or back-electron transfer to form t-butyl cation, then interception by the alcohol
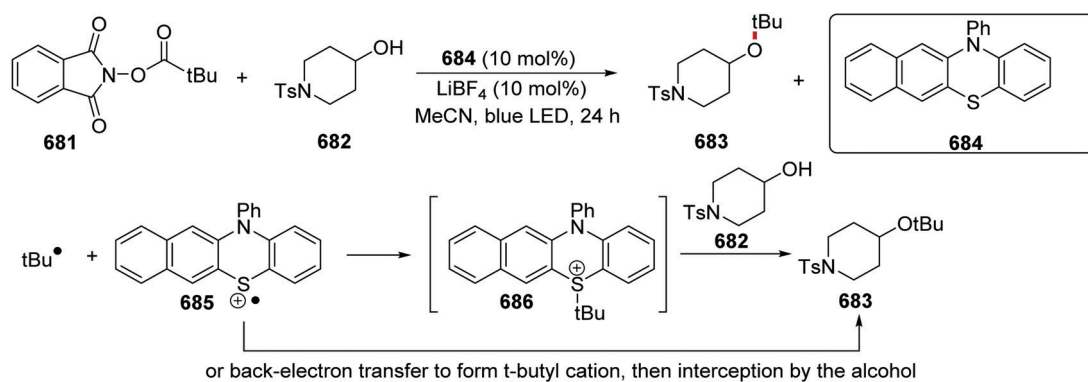
Scheme 191 Reduction of N-hydroxyphthalimide esters leading to ether formations.

This radical was then converted to the corresponding tertiary allyl cation by back electron transfer to the oxidised form of the photocatalyst, before the ether product was formed as a result of attack by alcohol nucleophiles such as **682**. When **684** was used as catalyst an isolated yield of 81% was recorded for **683** whereas PTH (E_{ox}^{*} = −2.1 V $vs.$ SCE) gave 26% yield.

3.3 Flavin photocatalysts

Carboxylic acids as radical precursors. The site-selective alkylation of peptides and proteins was studied with a photoredox decarboxylative strategy with a flavin photocatalyst.[95] Initial investigations probed Giese coupling between tetrapeptide **687** (E_{ox} = +1.3 V $vs.$ SCE) and diethyl ethylidene malonate with a range of photocatalysts (Scheme 192). From the initial screen of catalysts, it was found that the photocatalysts

Ir[dF(CF$_3$)ppy]$_2$(dtbbpy)PF$_6$ (E_{red}^{*} = +1.21 V $vs.$ SCE) and Ru(bpz)$_3$Cl$_2$ (E_{red}^{*} = +1.45 V $vs.$ SCE)[95b] resulted in no formation of coupled product **688**. Due to their high aqueous solubility, a range of flavin photocatalysts was investigated for this reaction and riboflavin analogues **689–691** gave low yields for Giese reaction product **688**. However, the use of riboflavin tetrabutyrate **688** (E_{red}^{*} = +1.5 V $vs.$ SCE) afforded peptide **688a** in 75% yield.

Optimised reaction conditions were applied to a range of tetramer peptides with the Giese-coupled peptides **688** being given as products. For the majority of peptides tested with these conditions, the reactions worked very well (Table 8, entries 1–11). However, in some cases, decreased yields were obtained (entries 12–14); this was due to deleterious oxidations of the sidechain (R) of these residues. The oxidation of Tyr, His and Lys was overcome with the reaction being performed at a lower pH (pH = 3.5) and
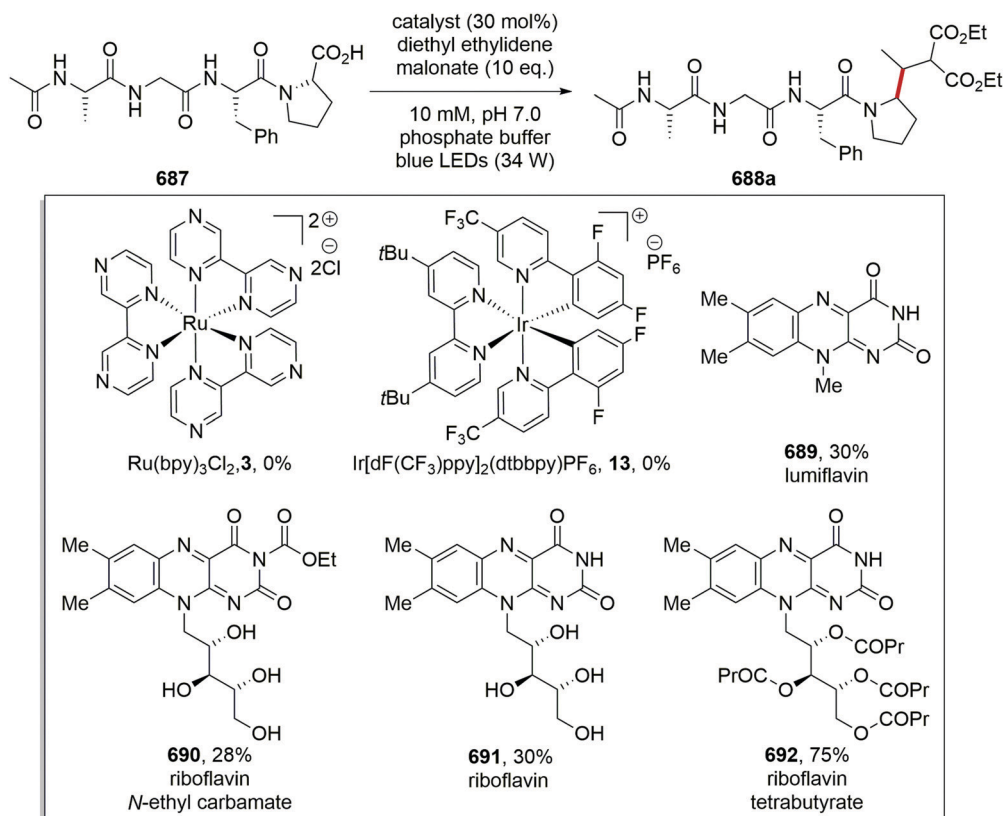
Scheme 192

Table 8 Results of decarboxylative alkylation with **692**

Entry	R =	Yield at pH 7.0, 8 h (%)	Yield at pH 3.5, 8 h (%)
1	Ala	79	92
2	Arg	71	87
3	Asn	76	91
4	Asp	77	93
5	Gln	71	94
6	Glu	75	91
7	Ile	77	90
8	Leu	74	95
9	Ser	75	87
10	Thr	73	90
11	Val	76	95
12	Tyr[a]	8	23
13	His	11	70
14	Lys	52	65

[a] Indicates that flavin **689** was used as photocatalyst.

this significantly increased the yields. The preparation of the tyrosine-derived peptide (entry 12) worked best when flavin **689** was used as photocatalyst and this gave the coupled peptide in 23% yield.

This methodology was demonstrated upon human insulin, and this was alkylated with electron-poor enone **693** on a
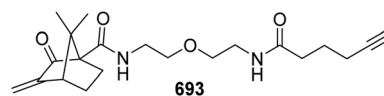
Fig. 17 Electron-poor enone.

500 nmol scale (Fig. 17). This reaction gave the ligated protein in 41% conversion as a single monoalkylated product (functionalising the C-terminal amino acid on the A chain of insulin) after 8 h with irradiation by blue light (34 W), based upon reverse-phase HPLC.

3.4 Cyanobenzene-derived photocatalysts

The tetracarbazolylisophthalonitrile 4CzIPN **15** is an organoredox reagent that has principally been used for oxidative interactions with substrates. However, in a one-pot procedure, Sherwood et al.[230] converted aliphatic carboxylic acids into their N-hydroxyphthalimide esters, and then, using 4CzIPN as reducing agent, transformed these into alkyl radicals which performed Minisci reactions on protonated derivatives of pyridines, quinolines e.g. **694** and related heterocycles (Scheme 193). N-Hydroxyphthalimide esters (E_{red} = −1.26 to −1.39 V vs. SCE) have reduction potentials that can be targeted by photocatalysts (E_{ox}^* = −1.73 V vs. SCE) for Ir(ppy)$_3$. It was speculated that the use of 4CzIPN that the reduced species (4CzIPN$^-$, E_{ox} = −1.21 V vs. SCE) might be the active species as it is a stronger reductant that the excited species (4CzIPN*, E_{ox}^* = −1.04 V vs. SCE).

This journal is © The Royal Society of Chemistry 2021

Chem. Soc. Rev., 2021, 50, 9540–9685 | 9641
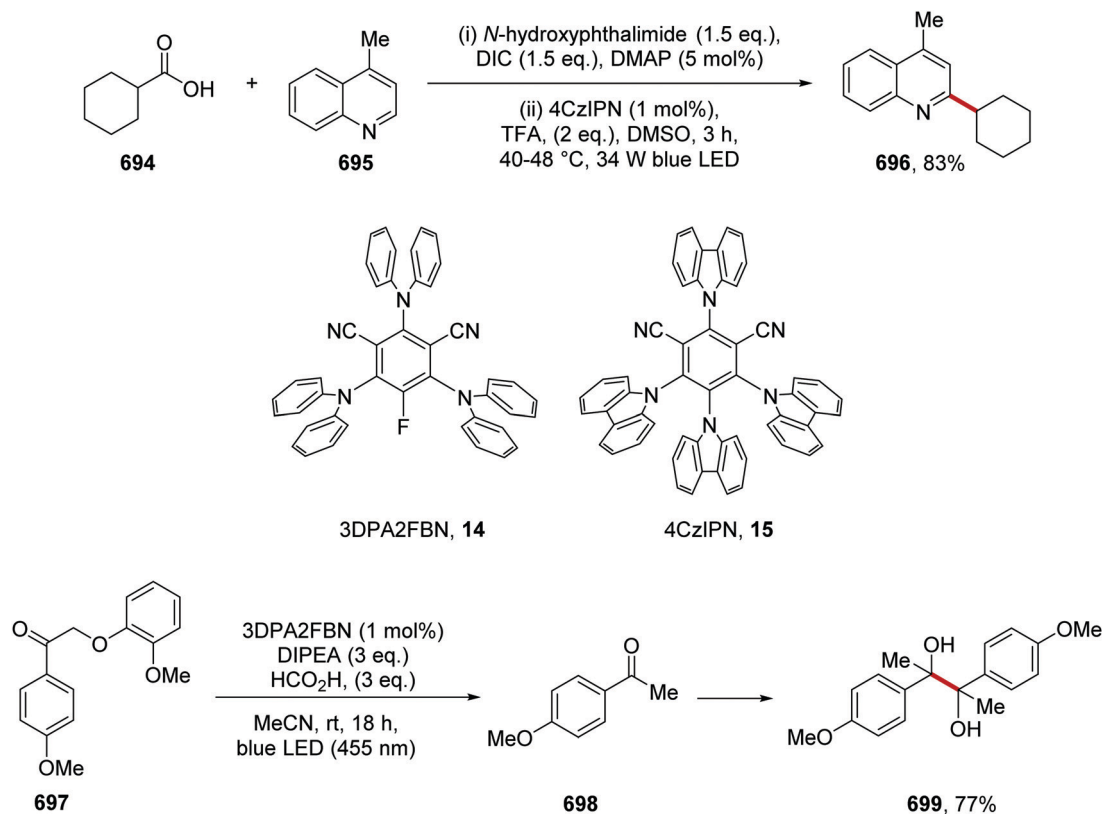
Scheme 193 Excited state 3DPA2FBN as a potent electron donor.

4CzIPN is an attractive redox reagent and is becoming more widely used; as new analogues become available, the potentials can be modulated. This was the thrust of the report by Zeitler *et al.*[33a] who made a wide investigation of the redox activity of derivatives of 4CzIPN, **15**, notably the analogue 3DPA2FBN, **14**.[33b] This compound in its photoexcited state performed a series of challenging reactions. With ketone **697**, reduction led to expulsion of *o*-methoxyphenolate anion and formation of *p*-methoxyacetophenone **698**. This compound was then reduced further to its ketyl, resulting in coupling to form pinacol **699**. Consideration of the redox values for this reaction illustrates why the catalyst 3DPA2FBN is successful in this reaction. 2-Phenoxy-1-phenylethan-1-one, which can be used as a model compound for ketone **697** has a very reduction potential (E_{red} = −1.72 V *vs.* SCE).[33c] While the excited-state species of **14** (E_{ox}^{*} = −1.60 V *vs.* SCE) cannot reduce **697**, the radical anion of **14** ($E_{ox}^{\bullet-}$ = −1.92 V *vs.* SCE) can, and this can be formed with reductive quenching with DIPEA (E_{ox} = +0.64 V *vs.* SCE).[33d] The reduction of acetophenone **698** (E_{red} = −2.17 V *vs.* SCE)[33e] is more challenging, it was suggested that a LUMO-lowering activation of the carbonyl group with the radical cation of DIPEA could be promoting SET, by analogy with a similar coupling observed by Rueping *et al.* using iridium photoredox catalysts.[33f]

Carboxylic acids as radical precursors. The formation of diester **701** *via* the coupling of proline **700** (Boc-Pro-OCs, *E* = +0.95 V *vs.* SCE)[134] with diethyl maleate **370b** was investigated with

a range of different organic photoredox catalysts (Scheme 194).[77] When the photocatalyst 4CzIPN (**15**) was used for this transformation, it gave **701** in 80% yield. A comparable yield was obtained when 3CzClIPN (**702**) was used as photocatalyst with **701** being given in 77% yield. Diminished yields of **701** were obtained when less oxidising photocatalysts were used. For example, the penta-carbazole catalyst **703** gave **701** in 37% yield. Benzonitrile catalyst **703** had a lower excited reduction potential (E_{red}^{*} = +1.31 V *vs.* SCE) than **15** (E_{red}^{*} = +1.35 V *vs.* SCE) and **702** (E_{red}^{*} = +1.56 V *vs.* SCE) and this correlated with the decreased efficiency of this transformation. This trend was continued with the dyes **14** (E_{red}^{*} = +0.92 V *vs.* SCE) and **704** (E_{red}^{*} = +1.24 V *vs.* SCE), and these catalysts gave diester **701** in 20% and 12% yield, respectively. The acridinium dye **705** was also a good catalyst for this process and afforded diester **701** in 73% yield.

The bioconjugation of peptide chains was achieved under metal-free conditions.[231] The C-terminus of the peptide chain underwent radical decarboxylation and this gave the corresponding carbon-centred radical. The use of ethynylbenziodoxolone (EBX, **707**) in the reaction mixture resulted in the formation of alkyne product **708** (Scheme 195). One challenge for this transformation was the site-selectivity when aspartic and glutamic acid residues were present within the peptide substrate. However, this was overcome by taking into account the different oxidation potentials of the carboxylic acids.[95] To avoid the use of expensive transition metals this study focused on the use of organic dyes. Initially, the reaction of dipeptide Cbz-Gly-Pro-OH

9642 | *Chem. Soc. Rev.*, 2021, **50**, 9540–9685

This journal is © The Royal Society of Chemistry 2021
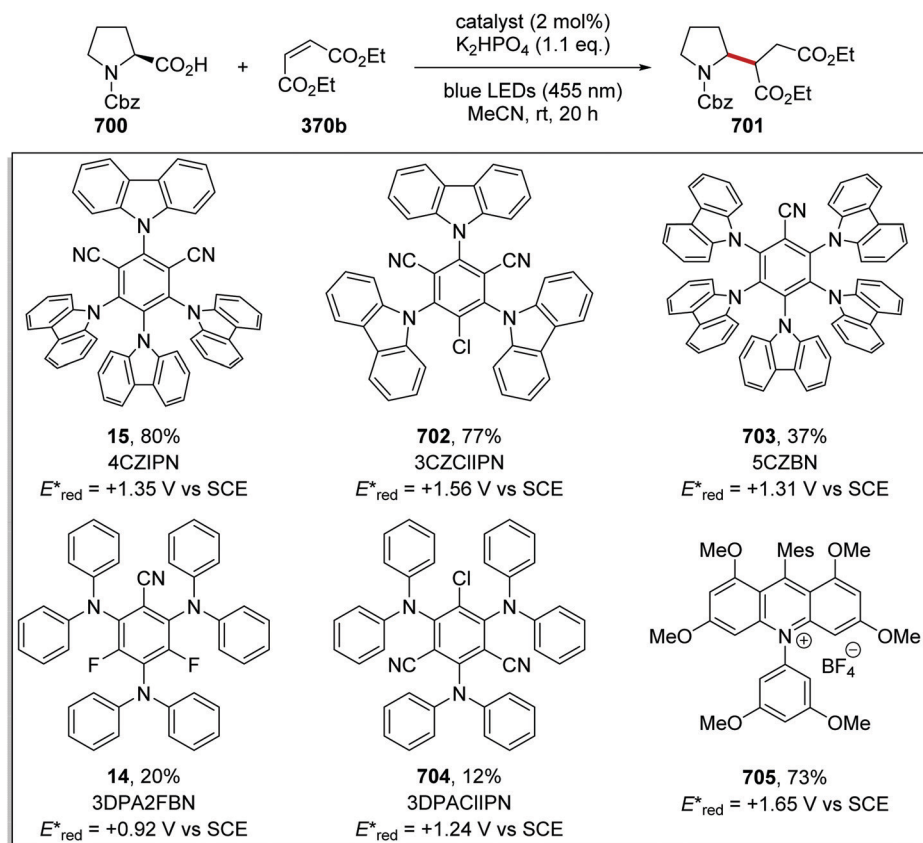
Scheme 194   Organic-photocatalyst mediated Giese-coupling.
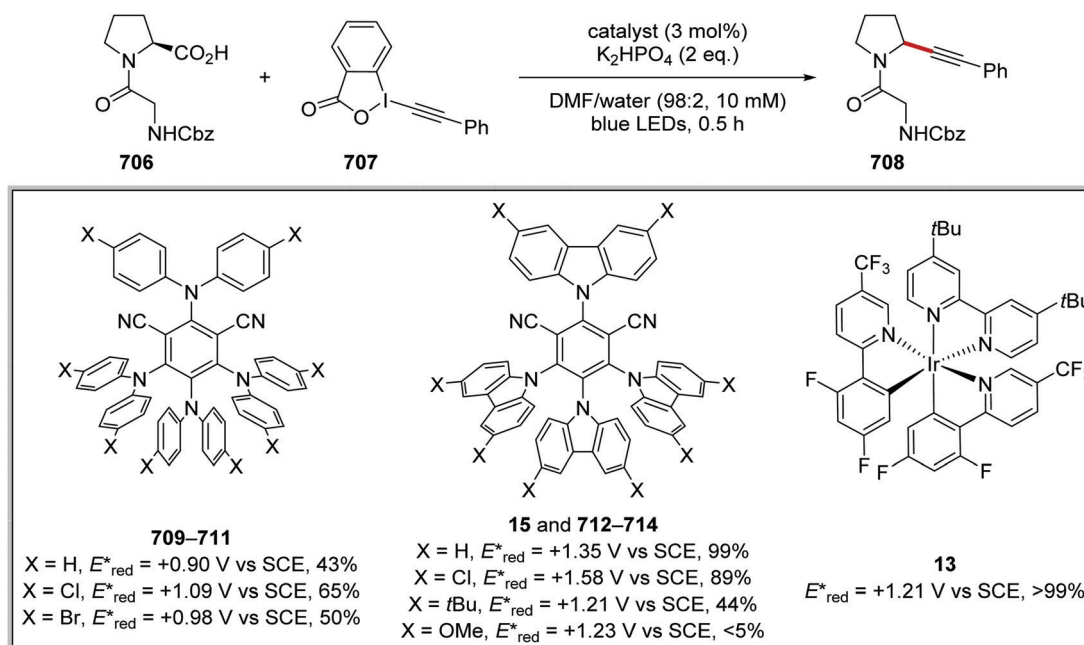
Scheme 195   Yields of **708** using a range of organic photoredox catalysts.

(**706**, E_{ox} = +0.95 V *vs.* SCE) for proline carboxylate with Ph-EBX (**707**, 1.5 eq.) was examined. Commercially available iridium photocatalyst **13** gave alkyne derivative **708** in 99% isolated

yield. A range of different organic dyes with various oxidation potentials (from +0.90 V to +1.58 V *vs.* SCE) was then tested. In general, the more oxidising organic dyes gave superior yields of

This journal is © The Royal Society of Chemistry 2021

Chem. Soc. Rev., 2021, **50**, 9540–9685 | 9643

the target compound. For example, when 4CzIPN (**15**) was used as catalyst, this gave **708** in 99% yield. From this finding, 4CzIPN was then used in the alkylation of di- and tetrapeptides. For the majority of amino acid combinations, smooth conversion to the alkylated product was achieved. Only substrates containing tryptophan and tyrosine residues were found to be problematic, due to their low oxidation potentials (tyrosine E_{ox} = +1.1 to 1.27 V *vs.* SCE and tryptophan E_{ox} = +0.77 to 1.66 V *vs.* SCE).

As stated, the selective oxidation of C-terminus carboxylic acids was achieved due to the differences in oxidation potentials. Therefore, the use of the right catalyst gave selective alkylation of the terminal acid over any internal carboxylate moieties. This was shown with 4CzIPN (**15**), as this resulted in the site-selective alkylated peptides **716a–h** (Scheme 196). This transformation was achieved on biologically relevant hexapeptides such as GRGDNP, a potent inhibitor of cell attachment to fibronectin. Azide **716e** and aldehyde **716f** derivatives were prepared in near-quantitative yield from protected a protected analogue of GRGDNP. The use of unprotected hexamer peptide as substrate allowed for preparation of azide **716g** in 57% yield and aryl bromide **716h** in 52% yield.

An organic photoredox-mediated radical decarboxylation followed by anion formation and addition to aldehyde was reported.[232] 4CzIPN (**15**) allowed for coupling between arylacetic acid **717** and carbonyl compounds **722** and this led to the formation

of alcohol **723** under blue light (Scheme 197). Mechanistic studies were carried out on this transformation to elucidate the reaction mechanism. From UV-vis spectroscopy, it was detected that photodecomposition of the photocatalyst was occurring under the reaction conditions. Isolation and X-ray crystallography determined the structure of this photodegraded product was 4CzBnBN (**726**). It was found that benzonitrile derivative **726** was formed from 4CzIPN (**15**) with phenylacetic acid **717a** under basic conditions with irradiation with blue light in 64% isolated yield. Benzonitrile **726** was less reactive to substitution than **15** as further benzyl substitution could only be detected in trace quantities. It was demonstrated that **726** was capable of catalysing the reaction between **717a** and **722a**. Therefore, it was concluded that **726** was the active catalyst in this process. Therefore, a reaction mechanism for this process was proposed with **725** as the active catalytic species. Photocatalyst **726** was excited with blue light and this gave excited compound **725***. SET between carboxylate **718a** (E_{ox} = +1.27 V *vs.* SCE for the tetrabutylammonium salt of phenylacetate) with **725*** (E_{red}* = +1.21 V *vs.* SCE) resulted in the formation of carboxyl radical **719a** and reduced catalyst **724**•⁻. Decarboxylation of **719a** resulted in benzylic radical **720a**, which underwent a SET reduction by **724**•⁻ and this gave benzyl anion **721a**. Cyclic voltammetry indicated that **724**•⁻ (E_{ox} = −1.72 V *vs.* SCE) could only reaction with radical **720a** (E_{red} = −1.43 V *vs.* SCE)
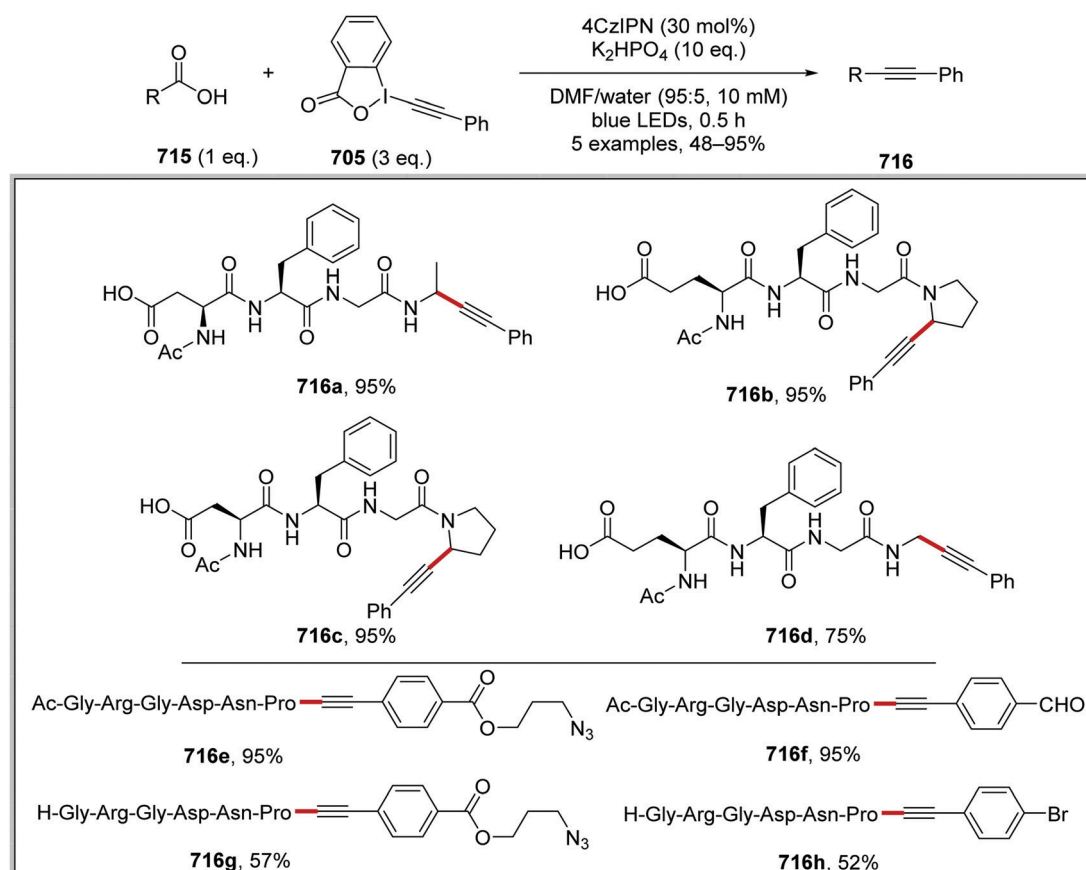
Scheme 196 Preparation of alkyne peptides **716**.

9644 | *Chem. Soc. Rev.*, 2021, **50**, 9540–9685

This journal is © The Royal Society of Chemistry 2021
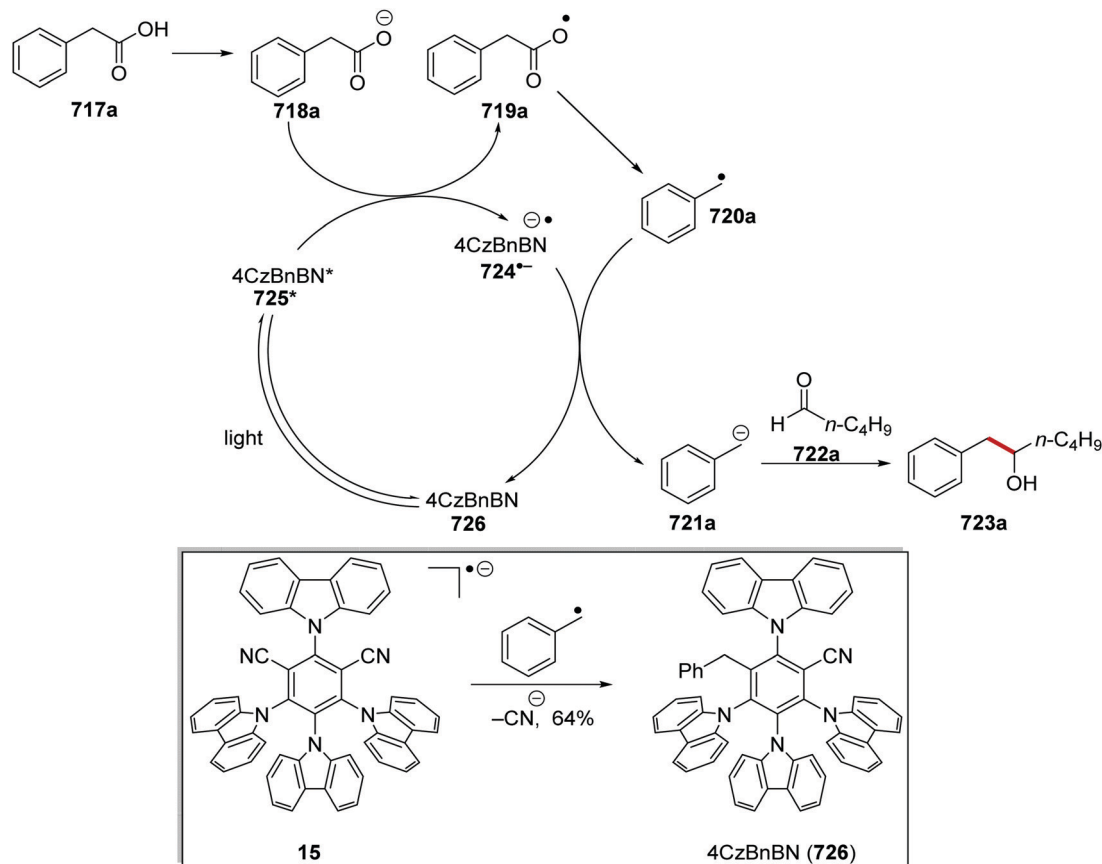
Scheme 197 Conversion of acid **717a** to alcohol **723a** with organic photocatalyst **726**.

and not with the alkyl aldehyde (E_{red} = −2.24 V *vs.* SCE for 3-methylbutanal). C–C bond formation is achieved with the reaction between the benzyl anion and aldehyde **722a** and this gave alcohol **723a**.

The reaction operated best when degassed DMA was used as solvent (Scheme 198). The yield of **723a** did not vary between anhydrous DMA and undried DMA although the addition of water (3 eq.) did result in a lower yield of **723a**. With the optimised reaction conditions, **723a** was prepared in 63% yield. Aryl fluoride **723b** and

aryl *meta*-methoxy compound **723c** analogues were prepared in 62% and 63% yield, respectively. When 4-methoxyphenylacetic acid was used as substrate, a poor yield of **723d** was obtained, whilst 75% of starting material was returned after 16 h of reaction time, indicating poor conversion. Both heterocyclic **723e** and *N*-Boc protected compounds **723f** were prepared using this methodology. Acetone was also used as a coupling partner, although only moderate yields for **723h** (32%) were obtained when the reaction was performed in a solvent mixture of acetone/DMA (1:1).
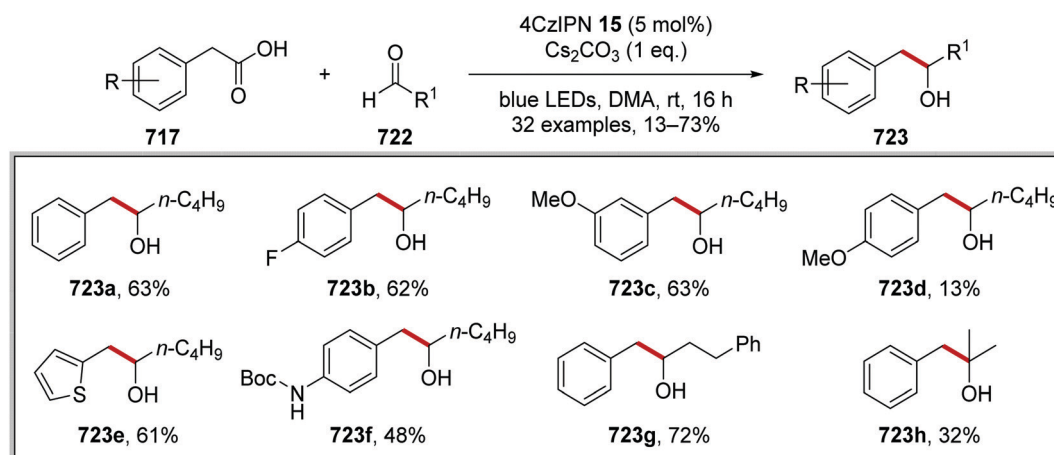
Scheme 198 Formation of alcohols **709**.

This journal is © The Royal Society of Chemistry 2021

Chem. Soc. Rev., 2021, **50**, 9540–9685 | **9645**
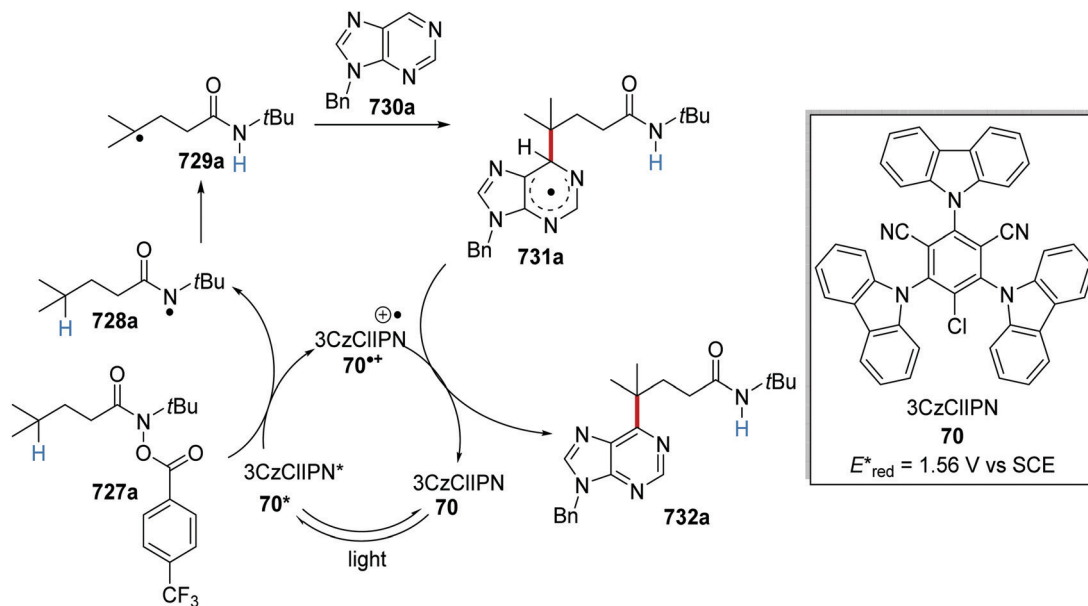
Scheme 199 Formation of alkyl radical **715a** and its coupling to heteroarene **718a**.

An HLF-inspired reaction mediated by the organic photocatalyst 3CzClIPN **70** was reported and this allowed for the site-selective remote heteroarylation of amides, such as **727a** (Scheme 199).[233] It was proposed in the paper and supported by DFT calculations that the following mechanism took place. Excited catalyst **70*** gave an electron to substrate **727a** with simultaneous N–O heterolytic bond cleavage. This resulted in formation of amidyl radical **728a** and oxidised catalyst **70•+**. An intra-molecular 1,5-HAT in **728a** resulted in carbon-centred radical **729a**. Under the basic reaction conditions (K$_2$CO$_3$), alkyl radical **729a** attacked heterocycle **730a** which afforded radical **731a**. SET from **731a** to oxidised catalyst **70•+** closed the catalytic cycle and, after proton transfer, afforded the observed product **732a**.

Under the optimised conditions of 3CzClIPN (2 mol%), K$_2$CO$_3$ (1.0 eq.), DMSO (0.2 M) and 90 W blue LEDs, compound **732a** was produced in 89% isolated yield (Scheme 200). Other photocatalysts gave inferior yields, for example, Ir(ppy)$_3$ gave 46% yield for **732a**, Ru(bpy)$_3$Cl$_2$ gave a 27%, Eosin Y gave 54% yield and 4CzIPN gave 67% yield. [A control experiment was carried out where no photocatalyst was added and this gave **732a** in 65% yield after 46 h. It was thought that an electron-donor–acceptor complex formed between **727a** and **730a**, and this facilitated the reaction.] With these optimal conditions using 3CzClIPN, the scope of the reaction was investigated. A range of different heterocycles was used in the reaction mixture, and this gave a range of products **732b–c**. The use of an adamantane-derived amide allowed gave benzothiazole **732d** in 67% yield. Ether functionalised compounds were suitable substrates for this transformation with **732e** and **732f** being isolated in 60% and 87% yield, respectively. This methodology was applied to late-stage functionalisation of bio-active compounds with the formation of **732g** and **732h**.

Boronates and silicates as radical precursors. Here, we only mention cases where the oxidation is achieved by an organic

oxidant, but readers can refer to references for reactions with transition metal-based oxidants and coupling agents.[234] The silicon-based reagents arise from studies by the team of Fensterbank, Ollivier et al.[235] who oxidised alkyl silylcatecholates **733** (E_{ox} = +0.3 to +0.9 V vs. SCE) in DMF with a range of organic oxidants, the most successful of which was photoexcited 4CzIPN, (**15**, $E_{red}*$ = +1.35 V vs. SCE) (Scheme 201). The liberated alkyl radicals **734** were trapped by a number of species, including allylic sulfones, e.g. **736**, forming product **737**. In this case, addition of the alkyl radical led to an intermediate, which expelled a sulfonyl radical **738**. This was reduced by the reduced radical anion form of 4CzIPN **15** to a sulfinate anion **739**, thereby regenerating 4CzIPN and rendering the process catalytic. Examples of products are **737a–c**. Besides allylic sulfones, a range of other acceptors, including **740–742**, proved successful.

Molander et al., using ammonium silane catecholates **743** and the photoactivated 4CzIPN as oxidant,[236] showed that the liberated radicals add to imines **742** to afford benzylic amine products **744** (Scheme 202). On the other hand, Mancheño et al. used benzyltrialkylsilanes as sources of benzyl radicals, but a strong oxidant, a mesitylacridinium salt was needed to liberate the radical in this case and the chemistry was limited to benzyl radicals,[237] while Bode et al. liberated alkoxyakyl radicals from trimethylsilyloxy groups using triphenylpyrylium salts as photoredox reagents for cyclisation reactions in flow-based chemistry (not shown here).[238]

Liberated alkyl radicals were also used[239] as precursors to acyl radicals **745** for addition to Michael acceptors yielding products **746**. Specific examples are shown as **746a–d** (Scheme 203).

4CzIPN (**15**, $E_{red}*$ = +1.35 V vs. SCE) allowed for α-amino functionalisation of 2,1-borazaronaphthyltrifluoroborates **747** (E_{ox} = +1.07 V vs. SCE for when R = H).[240] The inclusion of a nickel catalyst resulted in a cross-coupling reaction between the intermediate α-aminoalkyl radical and aryl bromides **748** and

9646 | Chem. Soc. Rev., 2021, **50**, 9540–9685

This journal is © The Royal Society of Chemistry 2021
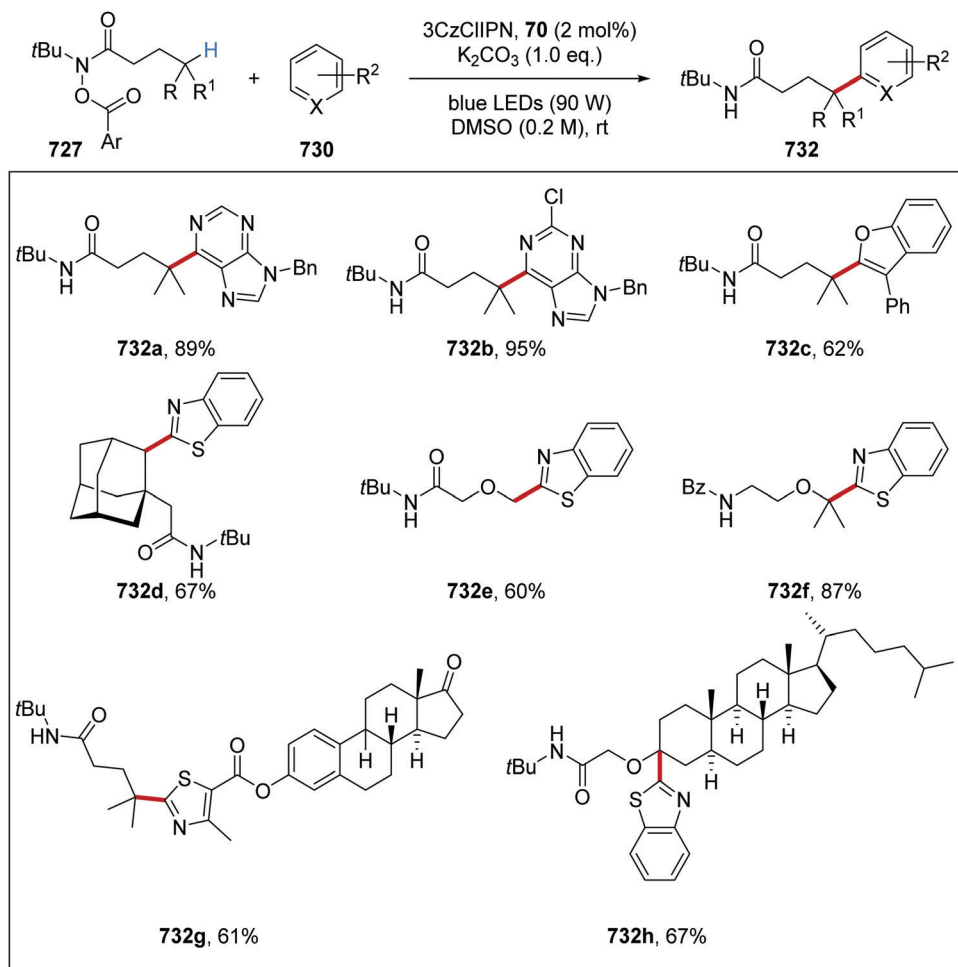
Scheme 200 Examples of coupling reactions arising from radical precursor **727**.

this gave coupled azaborine compounds **749** as products (Scheme 204). Initially, the reaction was optimised with the preparation of nitrile derivative **749a**. The reaction was first trialled with Ir[dF(CF$_3$)ppy]$_2$(bpy)PF$_6$ photocatalyst, caesium carbonate as base and this gave a 3.21 product : internal standard (P : IS) ratio. Minimal formation of **749a** (0.18 P/IS) was observed when Ru(bpy)$_3$PF$_6$ was used as photocatalyst. However, it was found that using 2,6-lutidine as base increased formation of **749a** with a 5.46 P/IS ratio being achieved. The more affordable 4CzIPN photocatalyst gave **749a** in a 4.98 P/IS ratio. Although 4CzIPN gave a lower yield for **749a** than the iridium catalyst, it was taken forward due to its lower cost. The preparation of **749a** with 4CzIPN was scaled up from a 0.100 mmol scale to a 0.500 mmol scale and this gave the azaborine compound in 80% yield. These optimised conditions were tried for a range of different coupling partners and this gave 1,3-benzodioxole **749b**, 2-fluoropyridyl **735c**, anethole **749d** and ketyl **749e** derivatives all in 50–88% yields. Analogously functionalised 2,1-borazaronaphthyl-trifluoroborates were used in this transformation as substrates and this gave benzothiophene **749f**, trifluoromethyl **749g**, benzofuran **749h** and intramolecular coupled product **749i**.

The synthetic utility of these 2,1-borazaronaphthyltrifluoroborates was investigated further with compound **750a** (Scheme 205). From this, it was found that a Minisci reaction with quinoline **751a** afforded derivative **753** in 48% yield. A radical-polar crossover reaction of **750a** in a defluorinative alkylation reaction gave *gem*-difluoroalkene **754**, a carbonyl bioisostere in 62%. Radical addition to the electron-poor alkene present in acrylonitrile gave nitrile **755** in 47% yield. The use of phenyl styryl sulfone gave alkene **756** in 48% yield and arenesulfonyl cyanide afforded **757** in 69% yield.

α-Heteroatom functionalisation. The functionalisation of α-secondary amines **758** to α-tertiary amines **759** with electron-poor alkenes **761** *via* a Giese reaction was achieved with the 4CzIPN photocatalyst and tetra-*n*-butylamine azide.[241] (Schemes 206 and 207). Photoexcited dye **15*** ($E_{red}^* = +1.35$ V *vs.* SCE) received an electron from azide anion ($E_{ox} = +0.87$ V *vs.* SCE for the tetrabutylammonium salt), giving reduced catalyst **15⁻** and radical **760**. Hydrogen atom abstraction from amine **758a** by **760** gave α-aminoalkyl radical **762a** and hydrazoic acid (**25**). The α-amino C–H bonds are quite weak (BDE = 89–91 ± 2 kcal mol^{-1}). Due to its thermal instability, hydrazoic acid has not been extensively studied, although in 1981 the N–H BDE was experimentally

This journal is © The Royal Society of Chemistry 2021

Chem. Soc. Rev., 2021, **50**, 9540–9685 | **9647**
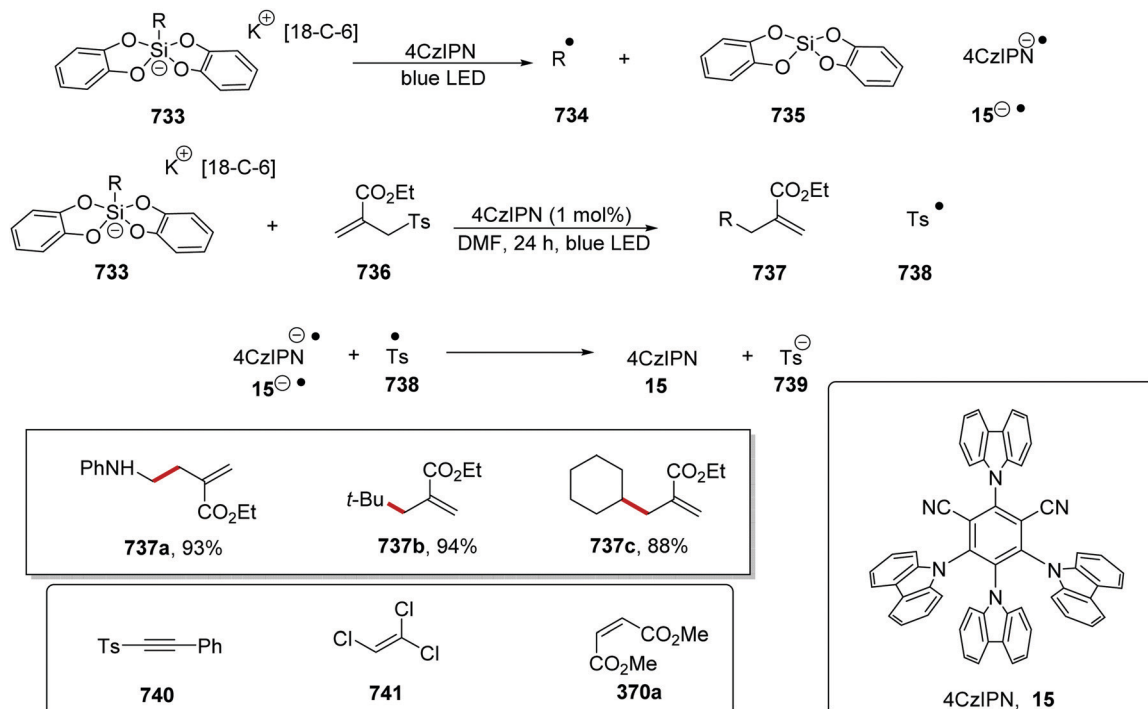
Scheme 201 Silanates act as electron donors to 4CzIPN **15**.
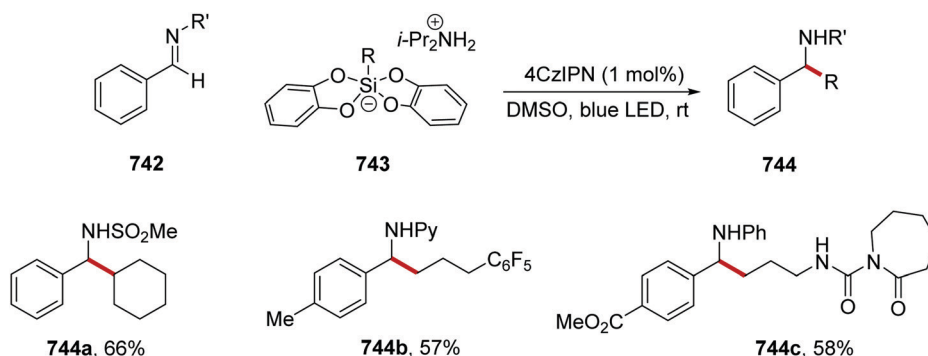
Scheme 202 Radicals are liberated from silanates and add to imines.
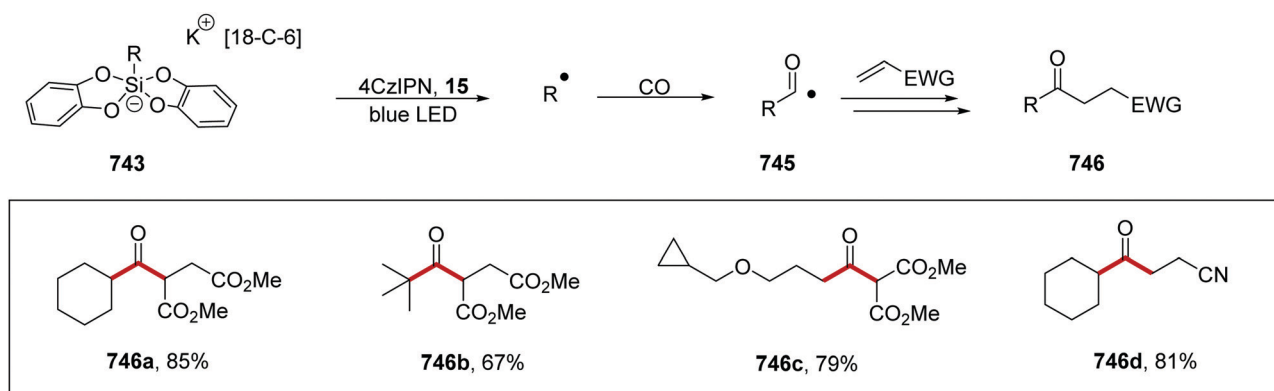
Scheme 203 Giese reactions, by acyl radicals, generated from carbonylation of radicals liberated from silanates.

9648 | *Chem. Soc. Rev.*, 2021, **50**, 9540–9685

This journal is © The Royal Society of Chemistry 2021
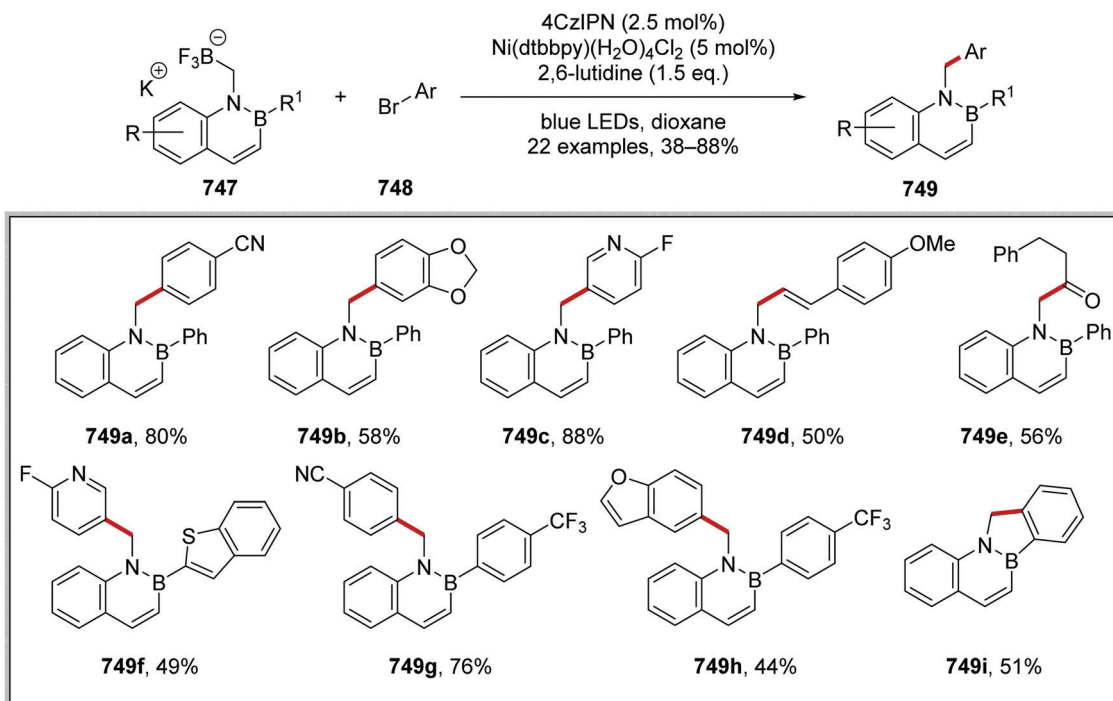
Scheme 204 Formation of azaborines **749**.
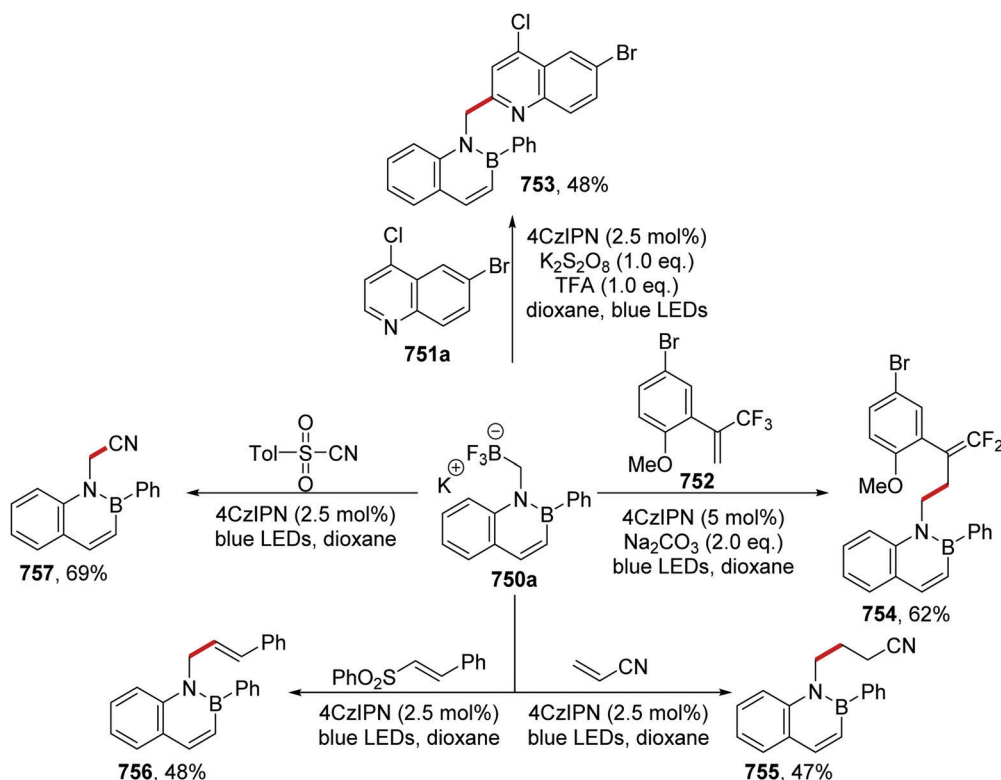
Scheme 205 Transformations of 2,1-borazaronaphthyltrifluoroborates **750a**.

found to be 92 ± 5 kcal mol⁻¹.²⁴² Therefore, the hydrogen abstraction from **758a** was feasible with radical **760**. Addition of radical **762a** to alkene **761a** resulted in α-carbonyl radical **763a**. Electron transfer to **763a** from **15⁻** closed the 4CzIPN catalytic cycle

and delivered enolate **764a**, which was protonated to afford the product **759a**. Due to relative BDE (α-amino C–H = *ca.* 90 kcal mol⁻¹ and α-ester C–H = *ca.* 96 kcal mol⁻¹) it was thought that a radical chain mechanism could be operative. However, the

This journal is © The Royal Society of Chemistry 2021

Chem. Soc. Rev., 2021, **50**, 9540–9685 | **9649**
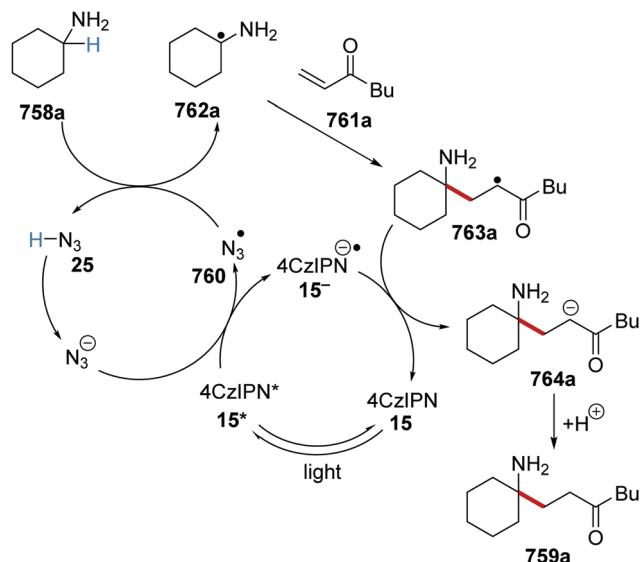
Scheme 206 Formation and reaction of α-aminoalkyl radicals.

calculation of a quantum yield value of 0.04 makes this mechanism improbable.

From the result of optimisation studies, it was found that the formation of α-tertiary amines **759** proceeded best when 4CzIPN and Bu₄N⁺N₃⁻ were used respectively as photocatalyst and precursor to the HAT catalyst and this gave **759a** in 85% isolated yield (Scheme 207). Similar yields were obtained with Ir[dF(CF₃)ppy]₂(dtbbpy)PF₆ as photocatalyst with **759a** being given in 83% yield. The use of quinuclidine or (TMS)₃SiH as HAT catalyst led to diminished yields of **759a**, 42% and 70% respectively. The concentration of the reaction was also crucial for this transformation. When the reaction was performed at a

0.075 M concentration, this gave **759a** in 85% yield. When the reaction was carried out at a 0.02 M concentration, **759a** was given in 84% yield and with a 0.4 M concentration, it was isolated in 44% yield. With a good process for the formation of α-tertiary amines **759** established, it was then demonstrated that pharmacologically valuable γ-lactams **765** could be prepared from **759**. For example, lactam **765b** was prepared from cyclohexylamine and methyl acrylate in 68% yield, over the two steps. It was also demonstrated that ketal **765c**, alcohol **765d**, thioether **765e**, *N*-Boc amine **765f** and ester **765g** analogues were prepared from cyclohexylamine. The use of other electron-poor alkenes led to the formation of lactams **765h–j** and amines **759k–l**.

N-Boc pyrrolidine **429a** was coupled to alkene **766** using an 3-acetoxyquinuclidine (**22d**)/4CzIPN (**15**) catalytic system and this gave cyclopropane **767** in 50% yield *via* a radical/polar crossover reaction. From an optimisation study, it was found that the inclusion of the inorganic base potassium bicarbonate led to the highest yield of **767** over potassium carbonate and caesium carbonate. Furthermore, it was established that a 1 : 1 solvent mixture of MeCN and DMSO gave the highest yield of **767** (Scheme 208).

The reaction propagated with irradiation by blue light and this gave excited compound **15*** from **15** (Scheme 209). SET to **15***(E_{red}^* = +1.35 V *vs.* SCE) from 3-acetoxyquinuclidine (**22d**, E_{ox} = +1.22 V *vs.* SCE)[48] resulted in the formation of **22d′**. HAT from *N*-Boc pyrrolidine **429a** to **22d′** gave α-amido radical **768**. Addition of radical **768** to alkene **766** gave benzylic radical **769** which was reduced by **15⁻** and this resulted in anion **770**. An intra-molecular polar substitution reaction of **770** gave cyclopropane product **767**.

Energy transfer. Dearomative rearrangements of naphthols and indoles were achieved with an organic photocatalyst, 2CzIPN (**72**) (Scheme 210).[79] Under irradiation with blue light (455 nm),
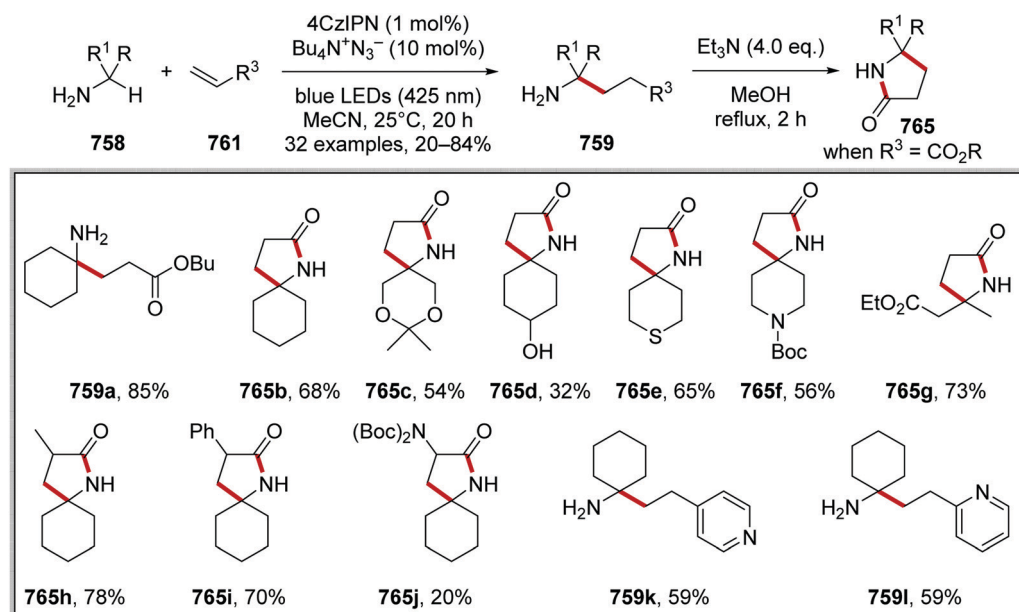
Scheme 207 Products from Giese reactions of α-aminoalkyl radicals.
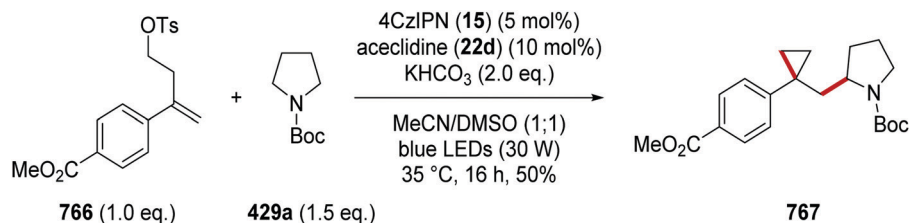
Scheme 208 Radical-polar crossover with *N*-Boc amine **429a**.
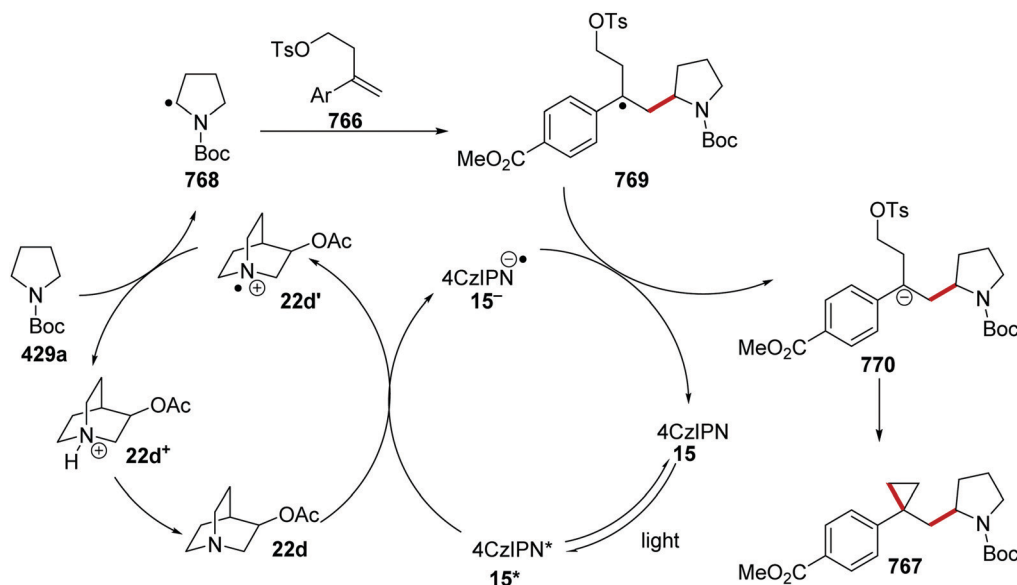
Scheme 209 4CzIPN mediated RPC with substrate **766**.
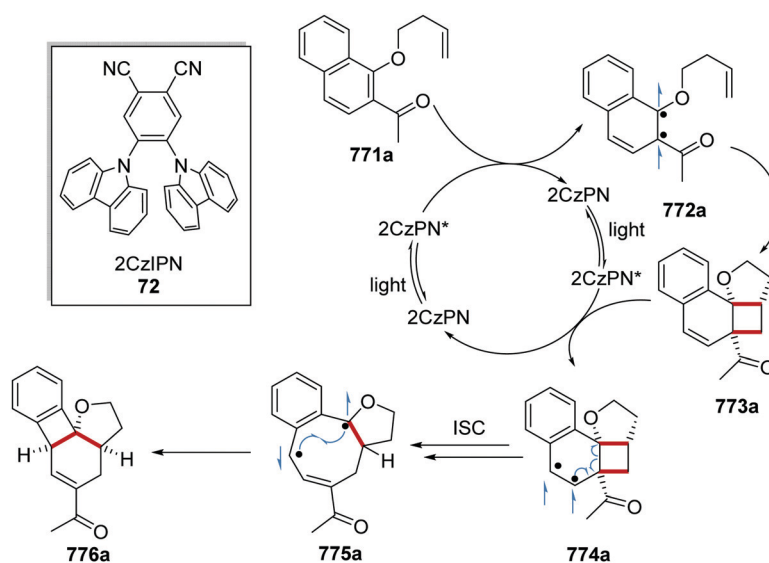
Scheme 210 Dearomatising rearrangements of naphthol derivative **771a**.

the organic photocatalyst was excited and this gave 2CzIPN*, which has a triplet energy of 60.6 kcal mol^{-1}. The triplet energy of biaryl compound **771a** was calculated to be 59.8 kcal mol^{-1}.[243] Therefore, 2CzIPN* was able to transfer its energy to naphthol

compound **771a** and this gave triplet diradical **772a** and the original photocatalyst. Diradical **772a** underwent a dearomatizing [2+2] giving the 6/6/4/5-tetracycle **773a**. From computational calculations, it was determined that this tetracycle **773a** had a

This journal is © The Royal Society of Chemistry 2021

Chem. Soc. Rev., 2021, **50**, 9540–9685 | 9651

Table 9 Optimisation of rearrangement of **771a**

Entry	2CzIPN (x mol%)	Solvent	Time (h)	Additive	Ratio of 773a : 7776a
1	5	1,4-Dioxane	17		1.2 : 1
2	5	PhMe	17		1.8 : 1
3	5	CHCl₃	17		16 : 1
4	1	CHCl₃	14		16 (94%) : 1
5	1	CHCl₃	17	Sc(OTf)₃ (0.1 eq.)	1 : 20

triplet energy of 55.9 kcal mol⁻¹ and thus it was able to receive energy from the photocatalyst. Therefore, a second Dexter-energy transfer event between **773a** and 2CzIPN* resulted in excited triplet species **774a**. This diradical underwent excited homolytic ring opening of the strained four-membered ring and, after ISC, this gave the singlet diradical **775a**. Carbon–carbon bond formation between the two radicals resulted in a 6/4/6/5-tetracycle **776a**, which was isolated as product.

In optimising the reaction, it was found that, dependent upon reaction conditions, the intermediate **773a** or tetracyclic compound **776a** was isolated, or a mixture of both. When the reaction was performed in 1,4-dioxane, full conversion of starting alkene **771a** was achieved but poor selectivity was achieved, with **773a** and **776a** being formed in equal amounts (Table 9, entry 1). A modest increase in the selectivity was achieved when the reaction was performed in toluene (entry 2). When the reaction was performed in chloroform, high levels of selectivity for the desired compound **776a** was obtained (16 : 1, entry 3). Fully optimised conditions employed low levels of catalyst (1 mol%) in chloroform and this returned **776a** in 94% isolated yield (entry 4). The selectivity of the reaction was reversed with the addition of catalytic amounts of scandium triflate (entry 5).

The optimised reaction conditions were applied to naphthol derivatives **771** (Scheme 211) and this resulted in the 6/4/6/ 5-tetracyclic compounds **776** as products. This allowed for the preparation of ketone **776a**, **776d–e** and ester **776b–c** analogues all within 14 h. The reaction was scaled up to gram quantities as 2.04 g of **776c** were isolated in 92% yield. Recycling of the
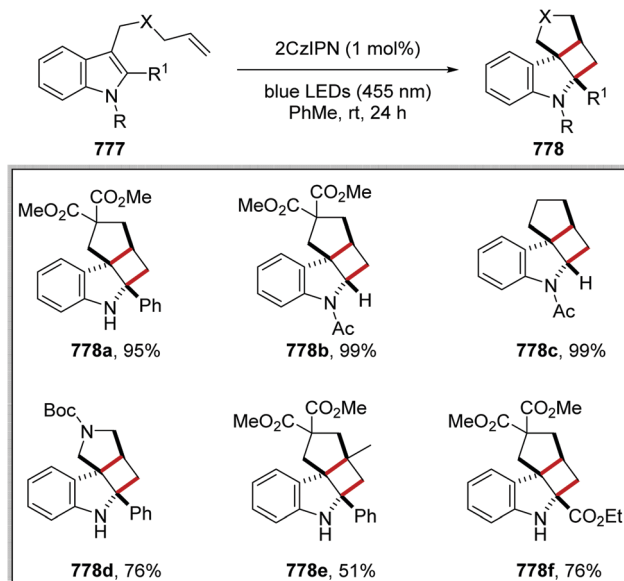
Scheme 212 Dearomatising rearrangements of indoles.

photocatalyst was also feasible, as recycled 2CzIPN gave **776d** in 88% isolated yield.

The reaction conditions developed for the synthesis of tetracyclic compounds **776** were also applied to indoles **777** and this gave compounds **778**, which had a 6/5/4/5-ring system (Scheme 212). Conversion of indoles **778** to tetracyclic compounds **778** worked better in toluene than CHCl₃. It was postulated that the use of a less polar solvent inhibited electron transfer and thus energy transfer processes were more dominant. The use of toluene as reaction solvent allowed for the preparation of six tetracyclic compounds **778** in 51–99% yields.

3.5 Dicyanoanthracene

Carboxylic acids as radical precursors. The coupling of amino acids **779** to electron-poor alkenes **780**[66] (and also to alkynes[244]) was investigated with DCA (**2**) as photocatalyst. The reaction

Scheme 211 Products arising from dearomatising rearrangements of naphthol **771**.

9652 | Chem. Soc. Rev., 2021, **50**, 9540–9685

This journal is © The Royal Society of Chemistry 2021

Table 10 Optimisation table

Entry	DCA (mol%)	Biphenyl	Time (h)	Yield of alkene
1	20	Yes	24	67
2	10	Yes	24	70
3	5	Yes	24	70
4	1	Yes	24	70
5	1	No	24	37
6	1	No	70	59

between phenylalanine (**779a**) and *E*-1,2-bis(phenylsulfonyl)-ethylene (**780a**) was promoted with the DCA (20 mol%) and biphenyl (BP) catalytic system and this led to alkene product **781a** in 67% yield, within 24 h (entry 1, Table 10). The loading of the DCA catalyst could be decreased down to 1 mol% (entries 2–4). The removal of biphenyl from the reaction mixture led to a diminished yield of **781a** (entry 5). Consumption of the starting material was not achieved when BP was absent from the reaction even with a reaction time of 70 h (entry 6).

The coupling of **779a** to **780a** under DCA/BP mediated conditions was achieved through the following mechanism (Scheme 213). Upon excitation, with blue light, DCA was promoted to its excited singlet state (S_1*, **2***). The S_1* state of DCA is a very strong oxidant (E_{red}* = +1.99 V *vs*. SCE) and it can oxidise both biphenyl [$E_{1/2}$(BP$^{•+}$/BP) = +1.95 V *vs*. SCE] and carboxylate ($E_{1/2}$(RCO$_2$$^{•}$/RCO$_2$$^{-}$) = +0.95 V *vs*. SCE). The S_1* state of DCA has a lifetime of *ca*. 15 ns in nitrogen-saturated acetonitrile and it has an inefficient intersystem crossing (ISC) to its triplet state (ϕ_{ISC} = 0.01 in MeCN). It has been communicated that a lifetime of 1 ns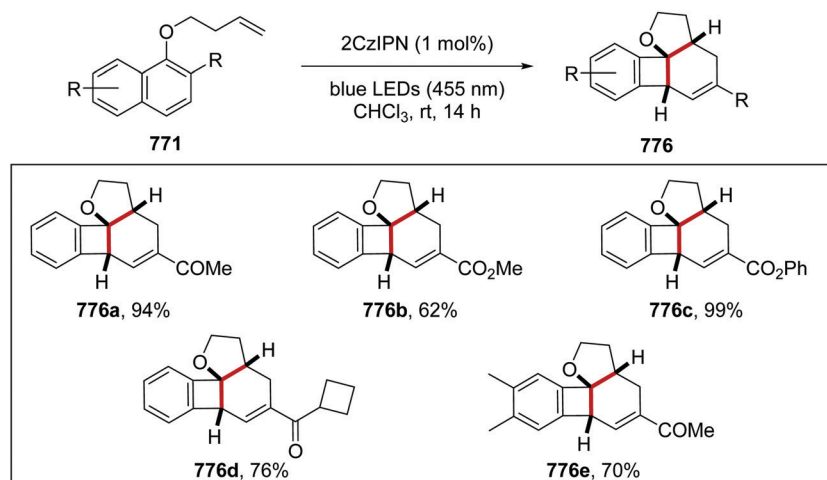 is sufficient for an effective SET process to occur.[8a] However, when the reaction is performed without BP, the reaction is slower and with compromised yields, even though **2*** is sufficiently long-lived for a SET from **782a**. Therefore, the role of BP could be

suppression of back-electron transfer (BET) and thus higher rates of reaction, although more investigation is required. SET between BP radical cation **70**′ and carboxylate **782a** gave **783a** and biphenyl (**74**). Carboxyl radical **783a** underwent decarboxylation and this gave α-amido radical **784a**, which was stabilised by the adjacent nitrogen atom. Radical coupling between this radical and alkene **780a** resulted in α-sulfone radical **785a**. The phenylsulfonyl radical **786** is a good radical leaving group and radical elimination of **786** resulted in alkene **781a**. The DCA catalytic cycle was closed with SET from **2**$^{•-}$ to **786**, giving anion **787** and DCA **2**.

The use of the DCA/BP catalytic system allowed for coupling of a range of carboxylic acids **779** with electron-poor alkenes **780** and this resulted in the preparation of 26 alkenes **781** in yields of 10–87% (Scheme 214). It was found that α-amino acids as substrates worked well in forming alkene products **781a–e**, due to radical stabilisation. However, the absence of an α-amino group led to diminished yields as shown in the preparation of **781f** (10%). A low yield of 30% was also obtained for **781g**, due to the lack of a stabilising α-amino group.

DCA* **2***, generated by irradiating the ground state parent with visible light had earlier been used as an oxidant by Pandey in the amidation of benzylic C–H bonds.[245] On the other hand, the radical anion of DCA, generated by photoinduced electron transfer from PPh$_3$, is a much more powerful reducing agent, and was used to generate the radical anion of conjugated enones (not shown here).[246]

However, in a different approach, the radical anion of DCA, produced electrochemically, was excited to its relatively stable excited state (lifetime of 13.5 ns), which then underwent SET, converting aryl chlorides **788**, **790** to aryl radicals for coupling to arenes and pyrroles (Schemes 215 and 216).[247] DCA ($E_{1/2}$ = −0.82 V *vs*. SCE) was reduced and this radical anion was excited by blue light and this gave the excited radical anion species. From DFT calculations suggested that this involved an electronic transition from the HOMO to the SOMO resulting in a SOMO–HOMO level inversion. This radical species was calculated to be strongly reducing (E_{ox} = −3.2 V *vs*. SCE, for comparison E_{ox} = −3.3 V *vs*. SCE for lithium metal). A highlight of this methodology was the reduction of 4-chloroanisole (E_{red} = −2.90 V *vs*. SCE) in the formation of **789a**.

In 2018 von Wangelin, Peres-Ruiz *et al.* used 9,10-dicyano-anthracene (9,10-DCA) **2** for coupling similarly activated aryl
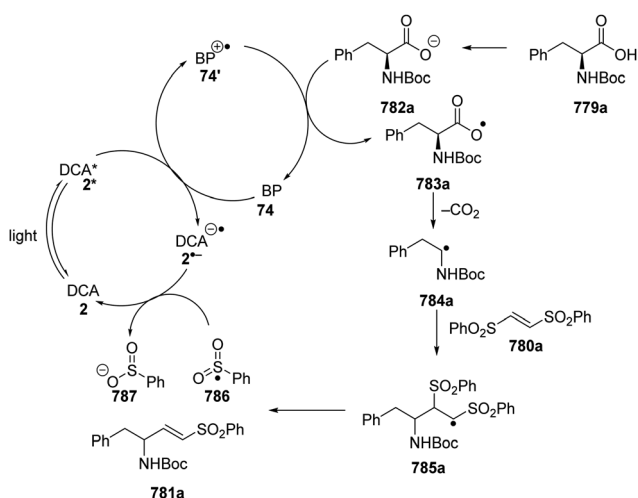
Scheme 213 DCA and BP-mediated Giese reaction.

This journal is © The Royal Society of Chemistry 2021

Chem. Soc. Rev., 2021, **50**, 9540–9685 | **9653**
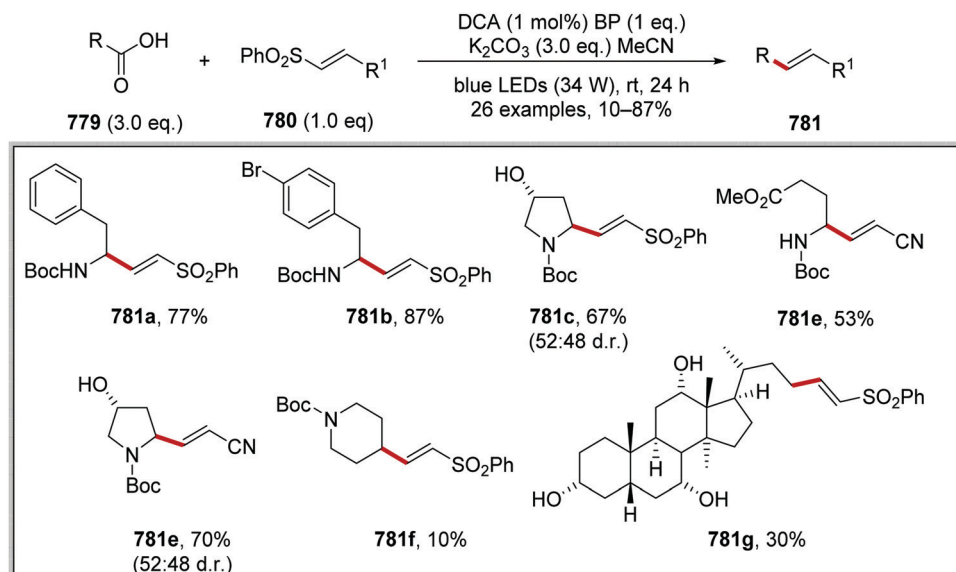
Scheme 214 DCA mediated coupling reaction with biphenyl (BP).
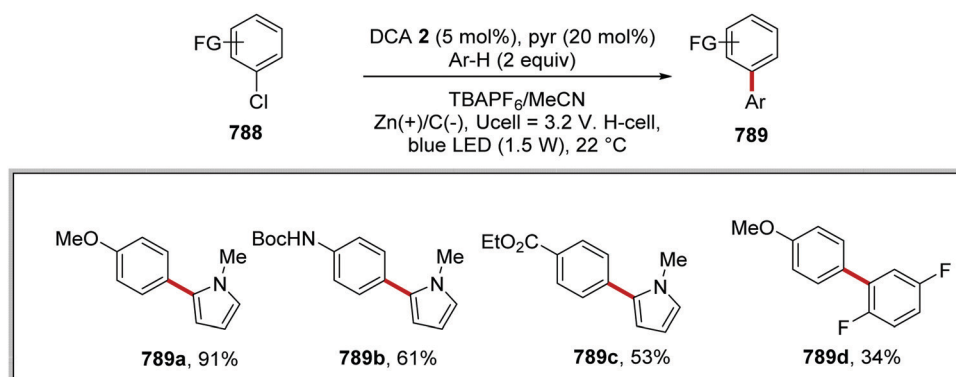
Scheme 215 Photoactivation of the radical anion of DCA, **2**, produced by electrochemical reduction.
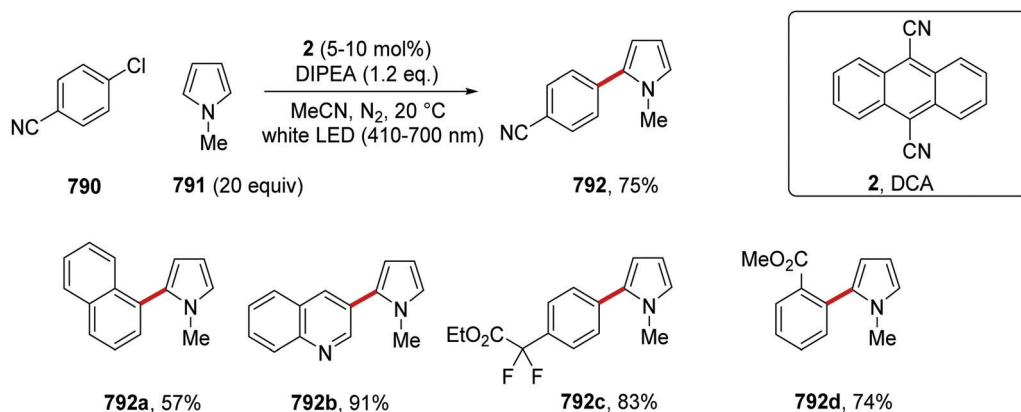
Scheme 216 Consecutive photoactivations of dicyanoanthracene (DCA, **2**) and its radical anion afford a strong electron donor.

halides **790** to heteroarenes **791** to form C–B, C–S and C–P bonds (Scheme 216).[248] In this case, however, the DCA **2** was photoexcited, and received an electron from DIPEA. The resulting radical anion then received a second quantum to form a donor

that activated aryl bromides and chlorides [usually bearing an additional electron-withdrawing substituent] for coupling to pyrroles to form products **792** or for formation of C–P, C–S or C–B bonds. This double quantum approach followed an earlier

9654 | *Chem. Soc. Rev.*, 2021, **50**, 9540–9685

This journal is © The Royal Society of Chemistry 2021
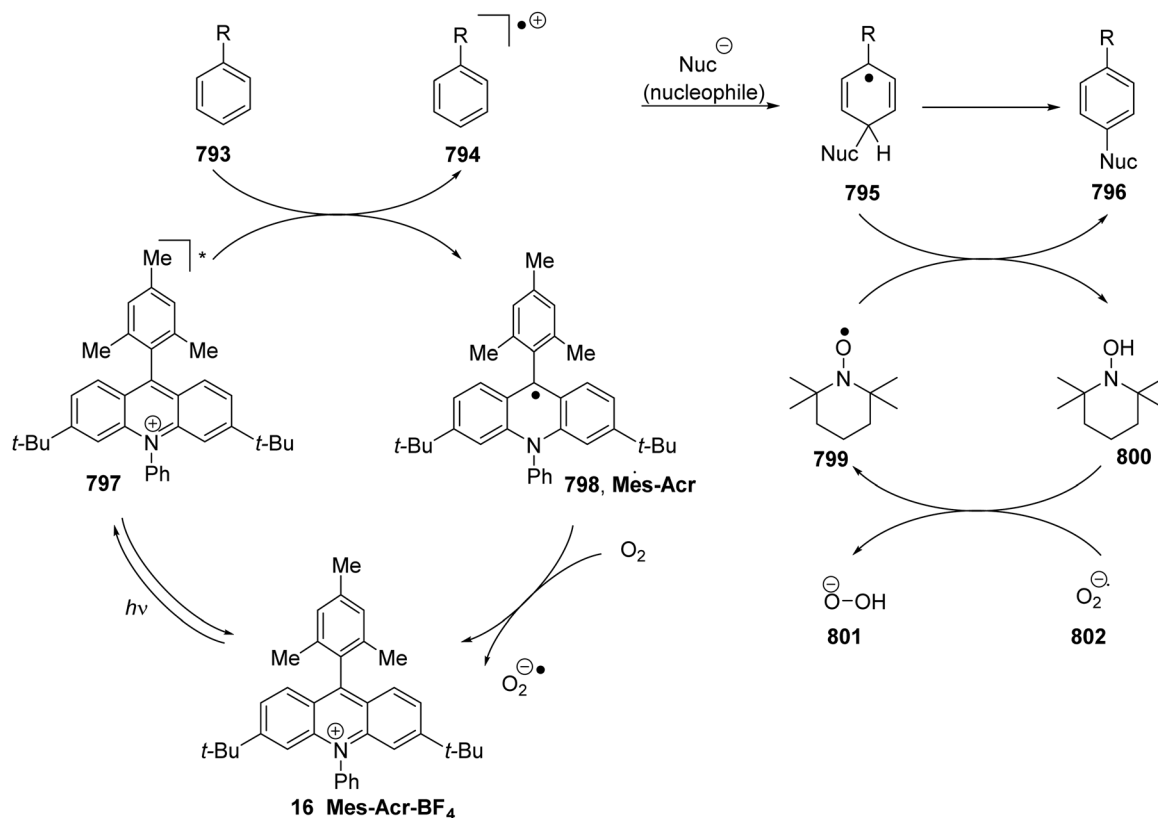
Scheme 217 General mechanism for C–H substitution of arene radical cations.

report of this conPET concept by König *et al.* in 2014 that will be discussed later in relation to Scheme 239.

3.6 Acridinium dyes

Among the most impressive organic redox agents are the acridinium salts. Initially championed by Fukuzumi *et al.*, their application to synthetic organic redox chemistry has principally been led by the team of Nicewicz.[8a] They have principally been recognised for the oxidative prowess of their excited states, but a recent example shows that, in the presence of a sacrificial electron donor such as diisopropylethylamine, a metastable mesitylacridyl radical is produced. Excitation of this radical to its excited state is accomplished at about 350 nm, and that excited state converts aryl chlorides and bromides to aryl radicals for hydrodehalogenation reactions and undertakes removal of arenesulfonyl groups from arenesulfonamides.[201] Until now, this has not been exploited for formation of the types of bonds discussed in this review. However, the more developed side of the chemistry of photoexcited acridinium salts is as strong oxidants. In particular, they oxidise many arene substrates to their radical cations. The radical cations are then subject to attack by nucleophiles, followed by the rearomatisation of the original arene. In these reactions, Ar–H or Ar–OMe (Ar–OR) or Ar–F are the usual candidates for substitution.

Examples of functionalisation reactions with Ar–H shown below and include C–H amination,[249] C–H cyanation,[250] and

C–H alkylation,[251] in addition to C–H fluorination.[252] Scheme 217 shows the likely general mechanism. The arene substrate **793** is converted into the corresponding radical cation **794** by electron transfer to the excited state redox agent, (**797**, $E_{red}^* = +2.15$ V *vs.* SCE) which itself is transformed to the acridinyl radical **798**. The radical cation derived from the substrate, **794**, can then be attacked by a nucleophile, normally *para* to the substituent. The resulting radical **795** undergoes loss of an H atom to air or TEMPO to afford the product **796**. Meanwhile the acridinyl radical can be reoxidised to **16** *e.g.* by air, to complete its catalytic cycle.

Examples of C–H amination are shown in Scheme 218.[249] Azoles including pyrroles (*e.g.* **804e**), pyrazoles (*e.g.* **804a, b**) imidazoles, triazoles (**804c**) and tetrazoles and a number of ring-fused analogues (**804d, 804f**) formed the majority of the reported examples. Direct amination, Ar–H → Ar–NH₂, was also achieved when ammonium carbamate (NH₄⁺ H₂N–CO₂–) was used as the source of the nitrogen nucleophile.

The cyanation protocol is shown in Scheme 219.[250] TMSCN was the most successful source of cyanide for these reactions, which were carried out open to air and in the presence of the pH 9 phosphate buffer. The process worked well also for more complex substrates. Thus N-Boc-melatonin was selectively cyanated to afford **805f** (26%), and naproxen methyl ester afforded a single regioisomer of cyanated product, *i.e.* **805g** (57%).

Alkylation was achieved using diazoesters as the alkylating agents (Scheme 220).[251] The mechanism for alkylation is a little different. Here, (Scheme 221) the arene is again proposed to be

This journal is © The Royal Society of Chemistry 2021

Chem. Soc. Rev., 2021, **50**, 9540–9685 | 9655
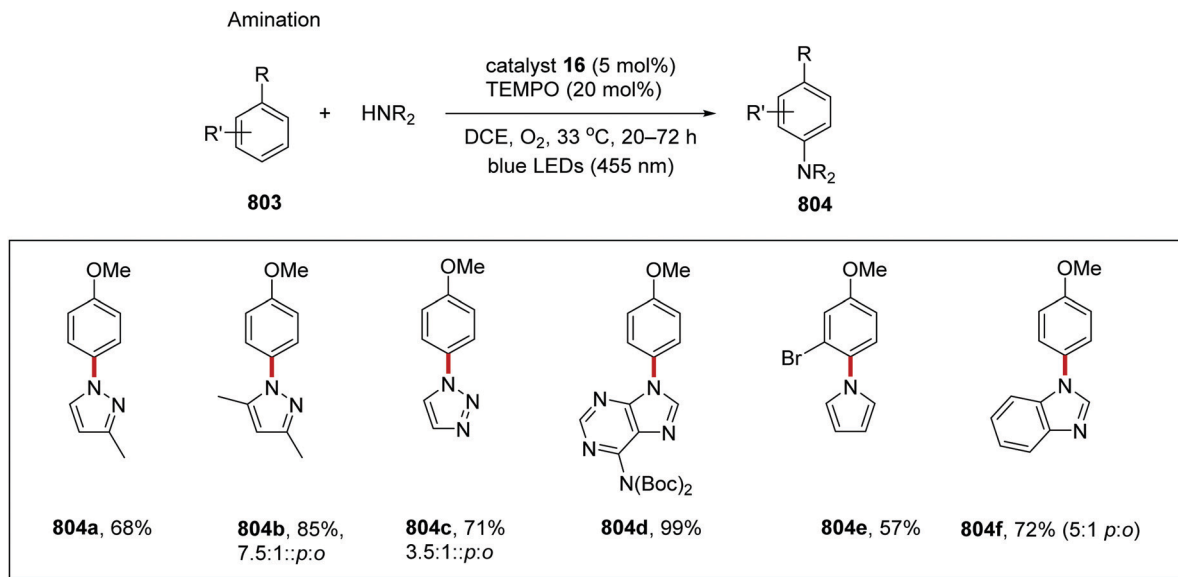
Amination

Scheme 218 C–H amination of arenes with azoles.
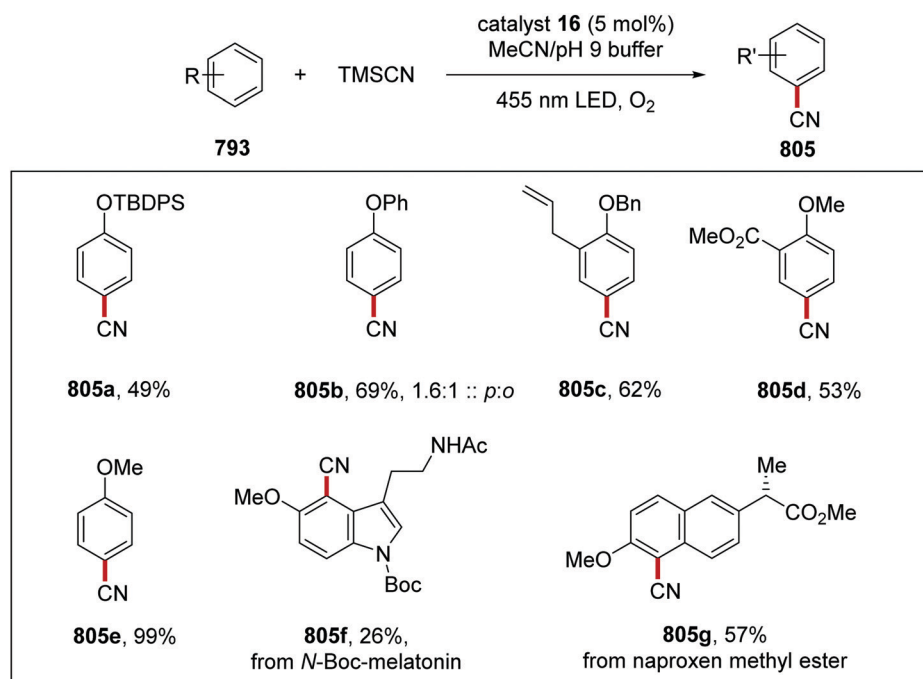
Scheme 219 C–H cyanation of arene radical cations.

oxidised to its radical cation, **794,** which is then attacked by the diazoester **806** as a nucleophile. This gives the diazonium intermediate **808** which then receives an electron from the reduced form of the MesAcrBF$_4$ photocatalyst to give **809.** Oxidation of this species opens the cyclopropane affording the distal radical cation **810.** Reductive electron transfer and deprotonation then yields the final product.

In addition to the reaction types just mentioned, direct Ar–H fluorination reactions have been extensively developed by the Nicewicz team.[252] One of the most useful applications of this work is in the direct incorporation of radioactive ^{18}F into organic molecules for positron emission tomography (PET) applications in medicine. An extensive range of substrates has been fluorinated in this way, and radiochemical yields (RCY) for some are presented in Scheme 222. Initially, the chemistry required 450 nm laser activation, but recent developments have allowed LED activation at 425 nm as well as the use of structurally optimised acridinium catalysts in a user-friendly manner and in flow. For these reactions, *tert*-butyl peracetate was used as the sacrificial oxidant. Labelling of xanthones had not been possible

9656 | *Chem. Soc. Rev.,* 2021, **50,** 9540–9685

This journal is © The Royal Society of Chemistry 2021
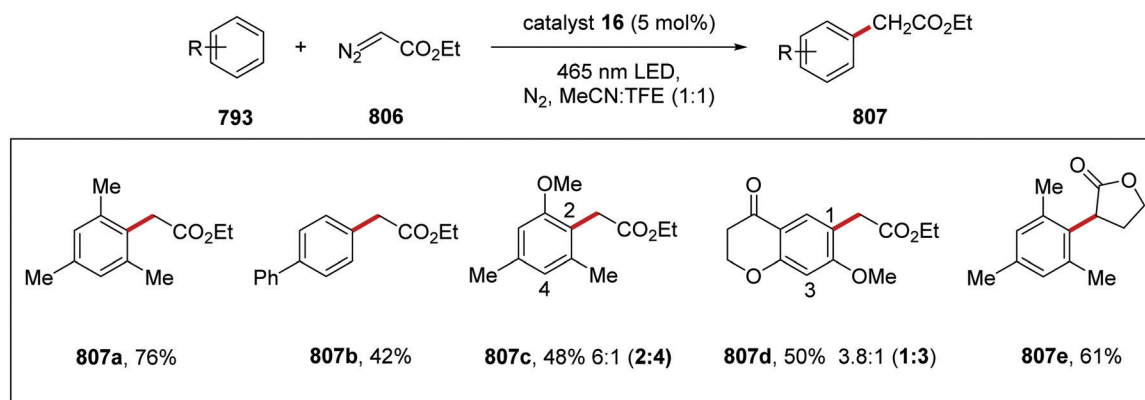
Scheme 220 C–H alkylation of arene radical cations.
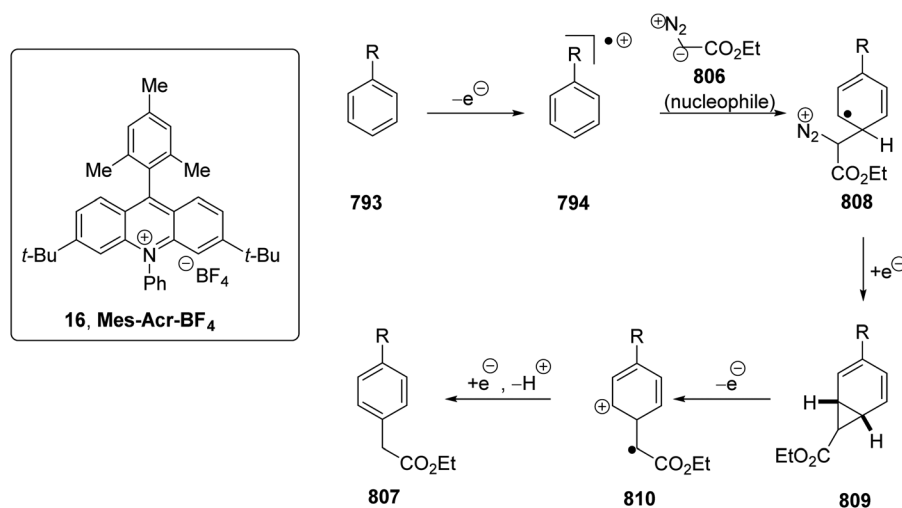
Scheme 221 Mechanism of alkylation of arene radical cations.

with the earlier technology but afforded a 22.9% RCY of product **812d** with the new methodology with catalyst **16-Cl**.[252b]

These reactions have all involved substitution of the incoming nucleophile onto an Ar–H position, with loss of the hydrogen atom as a proton. The alternative class of reactions involves displacement of an anionic leaving group, rather than a proton, from the arene. Initial reports featured deoxyaminations and deoxyfluorinations with loss of an alkoxide group from alkoxybenzenes. Deoxyfluorinations[253] are useful for the same reasons as the fluorinations just described, i.e. in PET medical applications using [18]F. A wide range of radiolabelled products have been produced in that way, but ^{19}F products can also be prepared, and Scheme 223 shows a range of these.

Deoxycyanation reactions[254] and deoxyamination reactions[255] have been developed. Scheme 224 below shows examples of the latter. For the deoxyamination reaction, questions of whether the arene or the amine was oxidised with the photoactivated acridinium salt were addressed through measurements of the rates of quenching of the catalyst fluorescence. Both amines and the arene substrates were effective quenching agents but, for the cases studied, the electron-rich arenes were more rapidly quenched than

the amines. When (R)-phenethylamine was used to prepare **813d**, the product was completely racemic. This likely arises due to oxidation of the product (but possibly also the amine starting material) to its radical cation, followed by reversible loss of the ArN–CH proton to afford an α-aminoalkyl radical at the original chiral centre.

Intramolecular displacements of leaving groups in the radical cations of arenes have also been reported for a number of cases, e.g. Smiles rearrangements **814 → 815**[256] and amination reactions, **816a → 817a**[256] have also been observed to work well. In this case, the cyclising amines can also be azoles as exemplified in formation of product **817b** (Scheme 225). The reactions are not limited to displacements by nitrogen nucleophiles, as seen in the Newman–Kwart reactions, using a pyrylium salt photoredox agent, exemplified by conversion **818 → 819**.[257]

The reactions of arene radical cations discussed here so far, featuring anionic leaving groups, have focussed on alkoxide leaving groups. However, recently, reports of displacement of fluoride anions from aryl fluorides have emerged from the laboratories of Nicewicz[258] and Lambert (see later, Scheme 244). Given that fluoroarenes **821** (E_{ox} = +2.24 V vs. SCE for 4-fluorotoluene) are

This journal is © The Royal Society of Chemistry 2021

Chem. Soc. Rev., 2021, **50**, 9540–9685 | **9657**
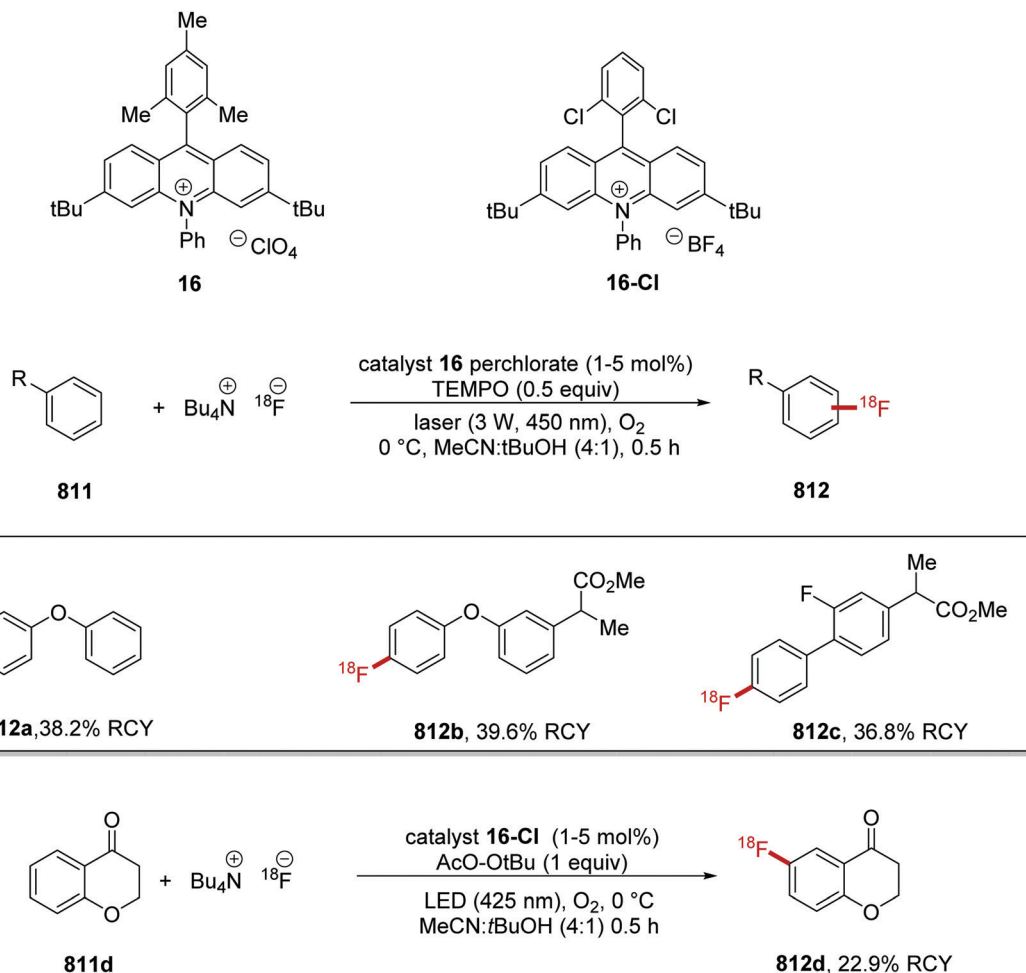
Scheme 222 C–H radiofluorination of arenes.
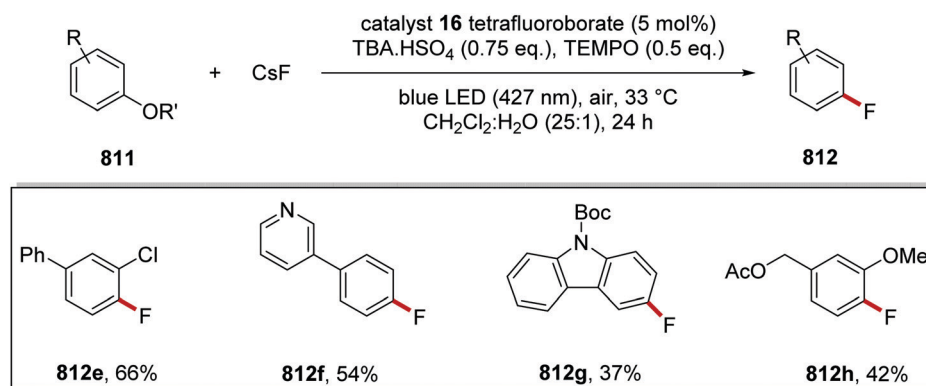
Scheme 223 Fluorodealkoxylation reactions of arene radical cations.

not generally easily oxidised, the conditions of the reactions are important. The acridinium salt **16** can mediate the desired oxidations to the arene radical cation provided that the oxidation potential of the arenes is less than +2.14 V *vs.* SCE (Scheme 226). Azoles, primary amines and carboxylates can then act as intermolecular nucleophiles affording products **822**. With less easily oxidised arenes, a more reactive xanthylium photocatalyst **820**

(E_{red}* = +2.57 V *vs.* SCE) is required. Here, pyrazoles and triazoles can act as intermolecular nucleophiles, in addition to carboxylates as successful [usually intramolecular] nucleophiles. With the acridinium salt reactions, different optimal conditions were devised for the three classes of nucleophile.

Although the majority of recent developments have been associated with the oxidation of arenes to their radical cations,

9658 | *Chem. Soc. Rev.*, 2021, **50**, 9540–9685

This journal is © The Royal Society of Chemistry 2021

Scheme 224 Deoxyamination of anisole radical cations.

Scheme 225 Substitutions involving cleavage of Ar–O bonds by sulfur and nitrogen nucleophiles.

Scheme 226 Defluorinative amination of fluorobenzenes.

This journal is © The Royal Society of Chemistry 2021

Chem. Soc. Rev., 2021, **50**, 9540–9685 | **9659**

Scheme 227 Tetrahydrofuran formation *via* alkene radical cations.

it has also been possible to oxidise certain alkenes to their radical cations which are subsequently attacked by nucleophiles, either intermolecular or intramolecular (Scheme 227).[259,260] This was achieved with acridinium catalyst **68** (E_{red}^* = + 2.18 V *vs.* SCE)[8a] and alkenes such as **821** (E_{ox} = +1.86 V *vs.* SCE, when R = H), **829** (E_{ox} = + 1.69 V *vs.* SCE) and **831** (E_{ox} = +1.61 V *vs.* SCE).

Photoactivated acridinium salts have also been used agents to liberate radicals from boron-based precursors.[261] Ley's team used acridinium salts as photoredox reagents. BPin esters **839** and boronic acids **843** in the presence of Lewis bases were studied under photoactivation of a mesitylacridinium salt **841** or 4CzIPN **15** and gave the desired products from reactions of radicals with Michael acceptors (Scheme 228).[262] They demonstrated success with both alkyl and aryl radicals. The Lewis bases were required to make the boronic esters more susceptible to SET oxidation. In a previous report it was shown that 4-methoxybenzylboronic acid (E_{ox} = +1.43 V *vs.* SCE) had a high oxidation potential but this was significantly decreased when it was complexed to DMAP (E_{ox} = +0.81 V *vs.* SCE, for boronic acid/ DMAP adduct).[262b] However, all these species listed should easily be oxidised by catalyst **841** (E_{red}^* = +1.65 V *vs.* SCE).

The Molander group used alkyltrifluoroborate salts for cyanation and allylation reactions.[263] Oxidation of the salts led to radicals which then reacted with tosyl cyanide displacing tosyl radicals,

which are reduced to toluenesulfinate anions to complete the catalytic cycle of the photoredox agent (see Scheme 229).

Minisci reactions were also carried out by Molander's team using photoactivated acridinium chemistry. For example, reaction between 2-trifluoroborato-4-chromanones **847** and N-heterocycles **848** mediated with acridinium dye **16** and potassium persulfate **66** was reported, affording products **849** (Scheme 230).[264] Irradiation with white light (26 W CFLs) gave excited dye **797*** from **16**. Electron transfer to **797*** (E_{red}^* = +2.20 V *vs.* SCE) from trifluoroborate **847a** (E_{ox} ≈ 1.11 V *vs.* SCE) gave α-alkoxyalkyl radical **850a**, which added to protonated heterocycle **851a** and this gave amine radical cation **852a**. Coincidentally, electron transfer from reduced catalyst **798•** (E_{ox} = −0.57 V *vs.* SCE)[266] to potassium persulfate **66** (E_{red} = *ca.* ≤0.35 V *vs.* SCE, see ref. 189) resulted in oxygen-centred radical **79** and sulfate ion. Hydrogen atom transfer to **79** from radical cation **852a** gave the coupled product **853a**, which was neutralised on workup to give **849a**.

Various photocatalysts were trialled for this transformation. Initially, Ir[dFCF$_3$ppy]$_2$(bpy)]PF$_6$ (2 mol%) was tested with K$_2$S$_2$O$_8$ (2 eq.) and this gave **849a** in 43% yield. The use of the organic dye Eosin Y gave **849a** in 40% yield. The yield of **849a** was increased to 57% when MesAcr **16** (1 mol%) was used as photocatalyst. Fully optimised conditions were established when the reaction was performed with one equivalent of TFA and this gave **849a** in 60%

9660 | *Chem. Soc. Rev.*, 2021, **50**, 9540–9685

This journal is © The Royal Society of Chemistry 2021
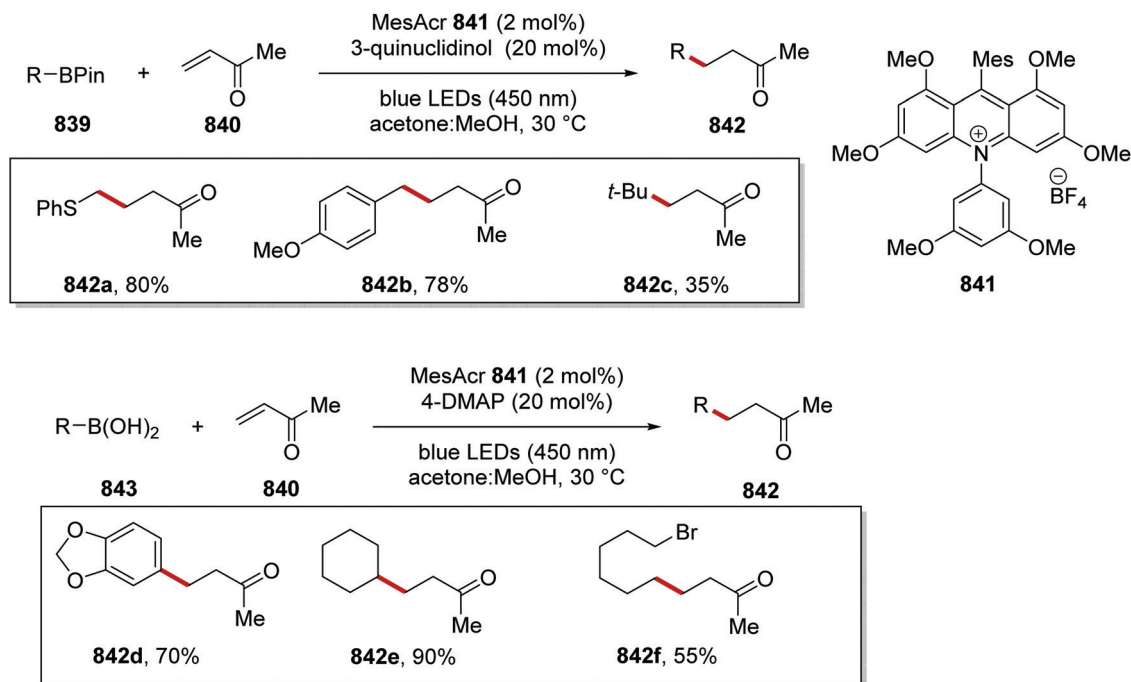
Scheme 228 Comparison of BPin esters and boronic acids as sources of radicals for Giese reactions.
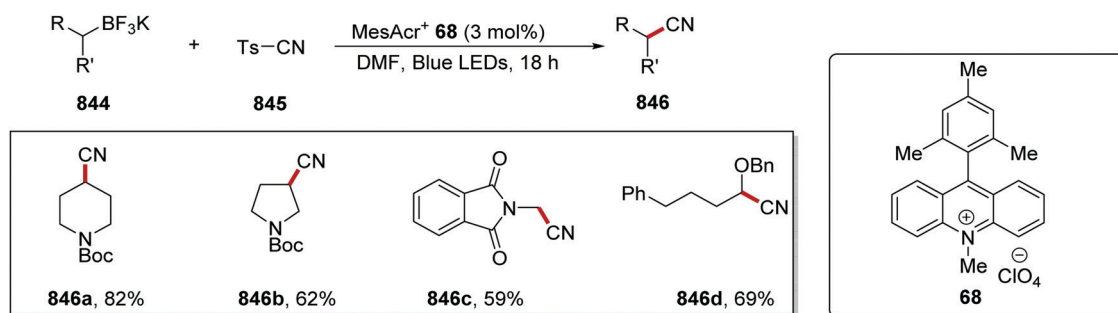
Scheme 229 Formation of nitriles using radicals liberated from oxidation of alkyl trifluoroborates.

yield (Scheme 231). These optimised conditions allowed for the preparation of 20 alkylated heterocycles **849b–e**, including a caffeine analogue **849f** which was given in 44% yield.

α-Heteroatom functionalisation. Coupling of *N*-Boc protected amines **854a** with electron-poor alkenes **855** was achieved with acridinium dye **16** and this resulted in γ-amidoketone compounds **856** (Scheme 232).[35] When the reaction mixture was irradiated with blue light (455 nm), this resulted in the formation of **856a** from *N*-Boc piperidine **854a** and methyl vinyl ketone **855a**. Acridinium dye **16** was excited by the blue light and this gave the excited species **797**, which is a strong oxidant ($E_{red}^{*} = +2.15$ V *vs.* SCE). *N*-Boc amine **854a** ($E_{p/2} = 1.96$ V *vs.* SCE) underwent SET with **797** and this resulted in amine radical cation **857a** and reduced catalyst **798**. Proton loss from **857a** resulted in carbon-centred radical **858a**, which added to alkene **855a** and this gave α-keto radical **859a**. The acridinium catalytic cycle was closed with SET to **859a** from **798**; this also gave anion **860a**, which was protonated and this resulted in γ-aminoketone **856a**.

Product **856a** was formed in the highest yields when the reaction was conducted in dichloromethane, with a reaction time of 6 h and a concentration of 0.1 M. These optimised reaction conditions were then applied to the preparation of products **856** in yields of 20–100%. With the optimised reaction conditions, *N*-Boc amines were coupled to methyl vinyl ketone, and this gave compounds **856a** and **856b** in 83% and 39% yield, respectively (Scheme 233). When *N*-Boc morpholine was used as the substrate, functionalisation occurred exclusively at the α-amino position and this formed **856c** in 62% yield. Furthermore, *N*-Boc protected tetrahydroisoquinoline resulted in exclusive reactivity at the more reactive benzylic position and this gave **856d** in 99% yield. When (2*S*)-2-methyl *N*-Boc piperidine was treated with methyl vinyl ketone under these reaction conditions, **856e** was given as a single regioisomer, in a 10 : 1 diastereomeric ratio (95 : 5, er). Various other enones were suitable coupling partners in this reaction and **856f** and **856g** were formed in 82% and 53% yield, respectively. The preparation of dinitrile **856h** was

This journal is © The Royal Society of Chemistry 2021

Chem. Soc. Rev., 2021, **50**, 9540–9685 | **9661**
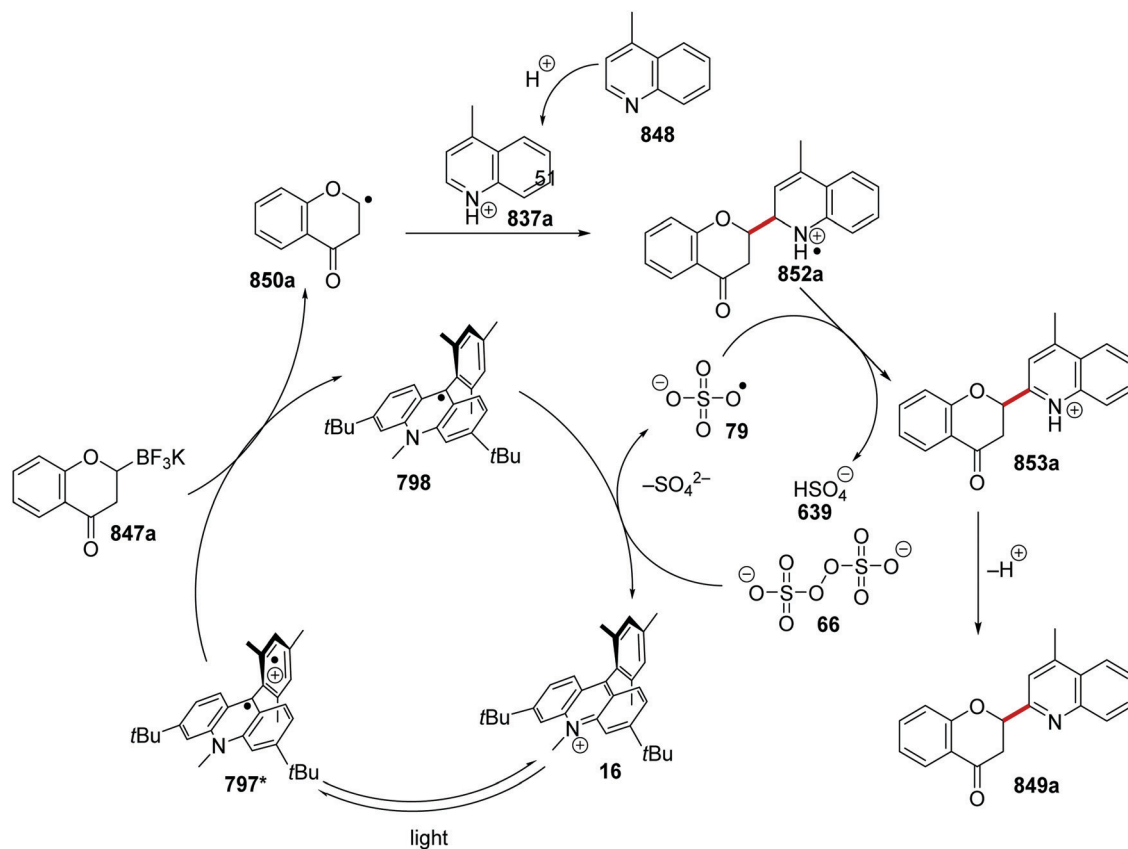
Scheme 230 Minisci reactions with trifluoroboronates mediated by acridinium salt **16** and persulfate.
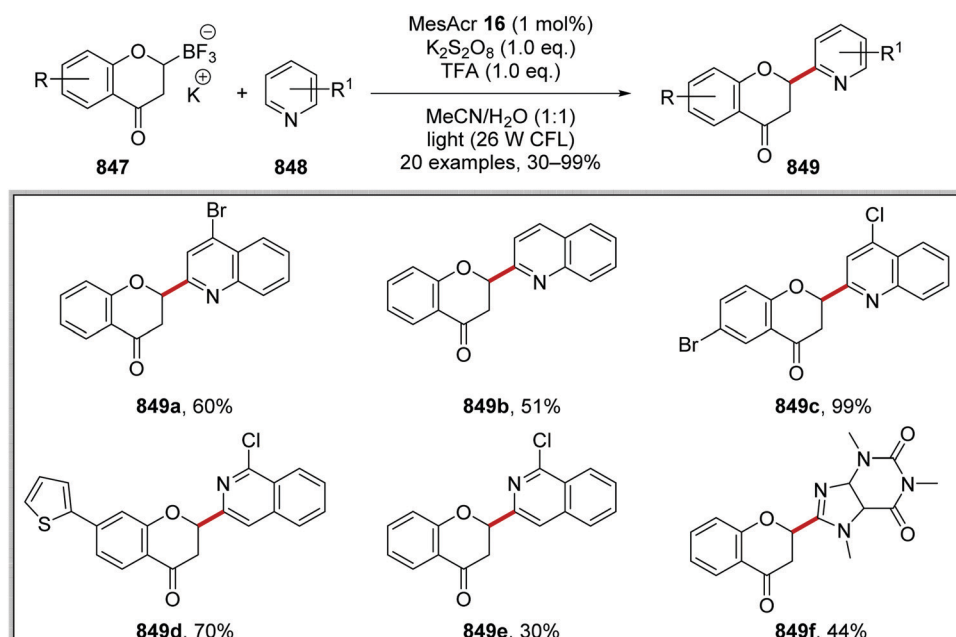
Scheme 231 Acridinium and persulfate-mediated Minisci reaction.

achieved in 94% yield on a 0.3 mmol scale. The preparation of **856h** was conducted on 15.0 mmol scale with a photochemical flow reactor and this gave the dinitrile compound in 94% yield (1.71 g).

The site-selective C–H functionalisation of piperazines **861** with electron-poor alkenes **855** was achieved through use of the acridinium catalyst **16** and this gave products of conjugate addition **862** (Scheme 234).[265] Initially, derivative **862a** was

9662 | *Chem. Soc. Rev.*, 2021, **50**, 9540–9685

This journal is © The Royal Society of Chemistry 2021
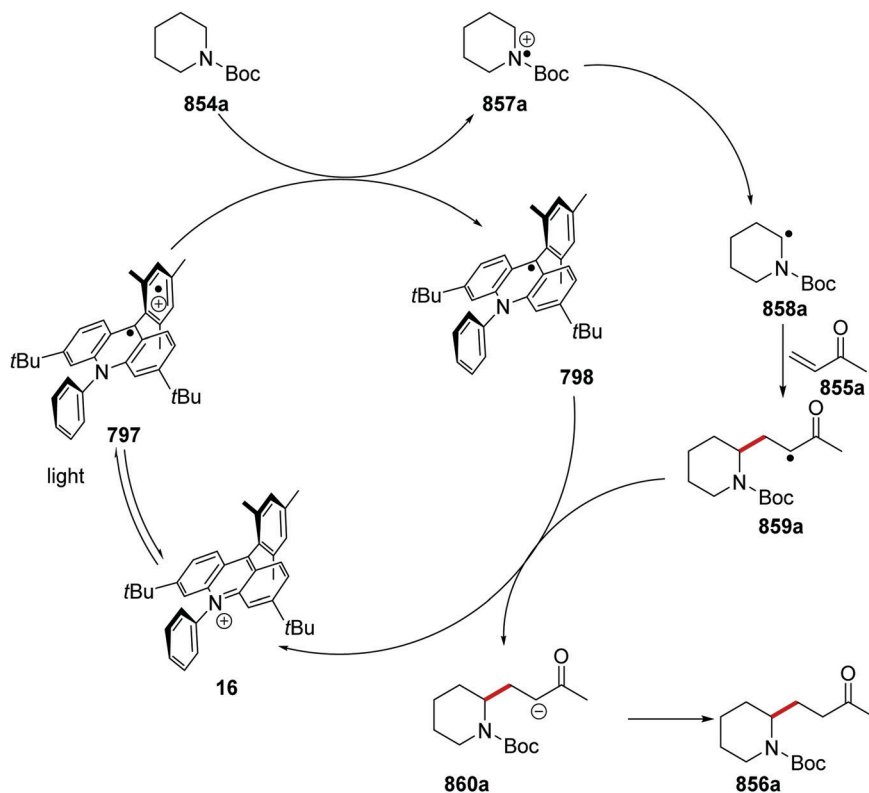
Scheme 232 Giese coupling of radicals derived from *N*-Boc piperidine **854**.
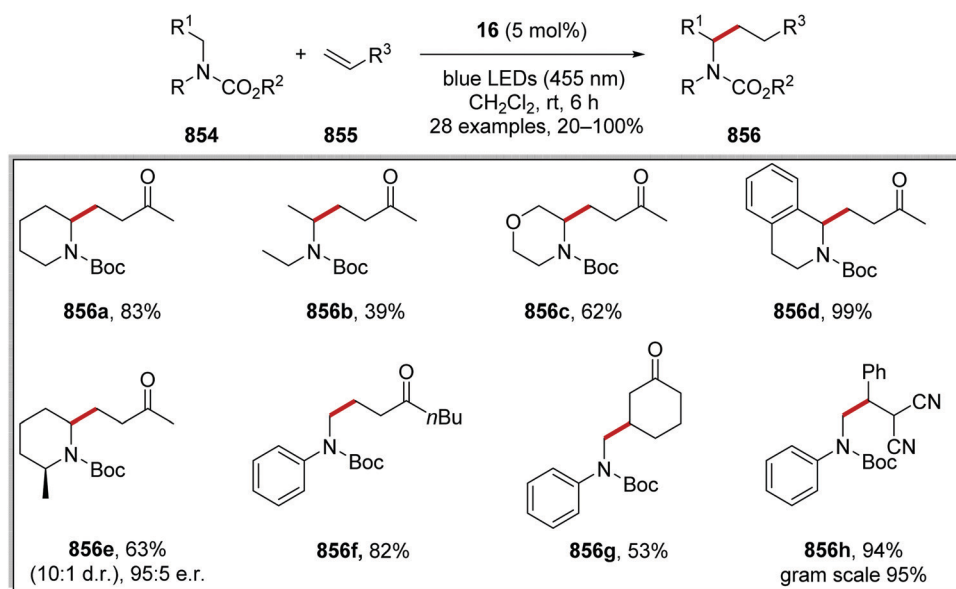
Scheme 233 Giese coupling with acridinium catalyst **16**.

prepared in 90% yield from 1,4-di-Boc-piperazine and methyl vinyl ketone. Replacement of a Boc group with the Fmoc protecting group resulted in preferential C–H functionalisation adjacent to the Boc protected amine and this gave **862b** as a 2.2 : 1 mixture of regioisomers in 71% yield. Greater site-selectivity was attained when *N*-Boc-*N*′-benzoylpiperazine was used as substrate, with **862c** being given in 81% yield with a 10 : 1 ratio of regioisomers at 29 °C. In the preparation of **862c**, the site-selectivity obtained was enhanced when the transformation was performed at 0 °C with the compound being given as a 21 : 1 mixture of regioisomers. Strongly deactivating groups such as *N*-sulfonamide resulted in the exclusive formation of

This journal is © The Royal Society of Chemistry 2021

Chem. Soc. Rev., 2021, **50**, 9540–9685 | 9663
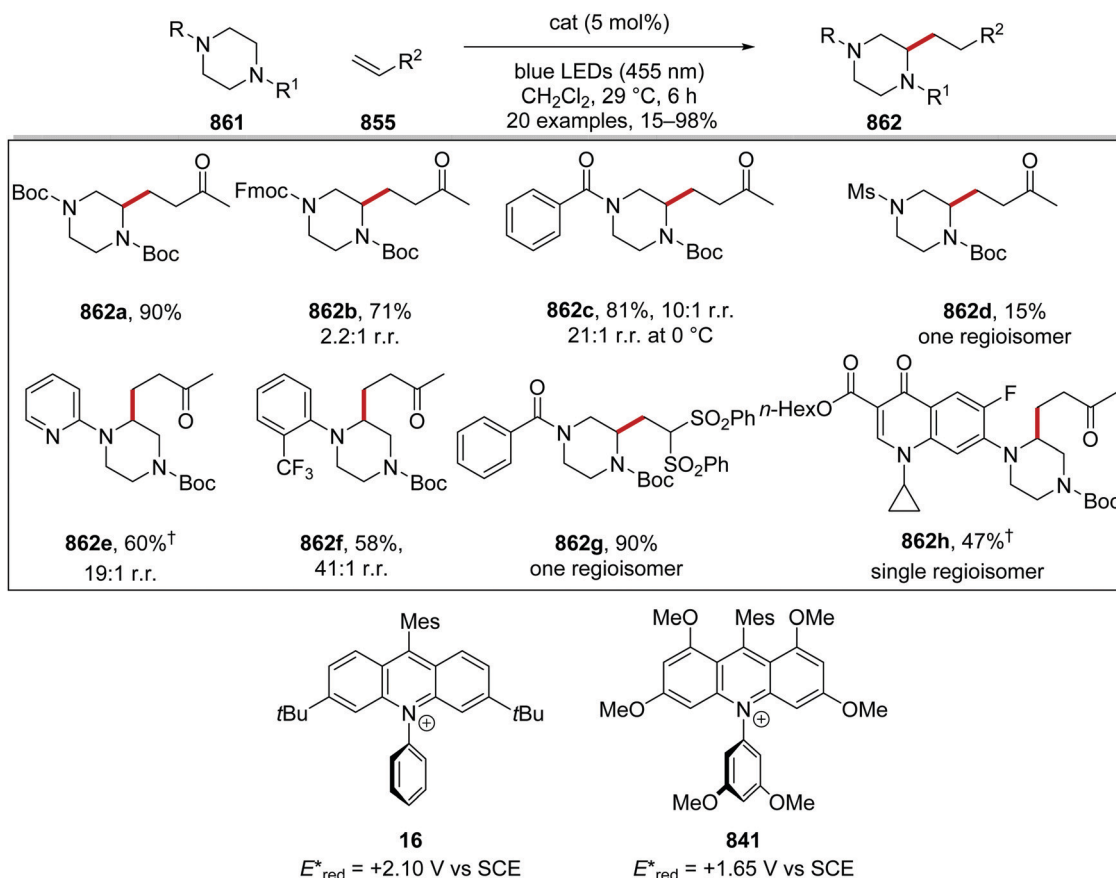
Scheme 234 Site-selective alkylation of piperazine, † denotes the use of **841**.

one regioisomer, for example, **862d** albeit a low yield was obtained. A reversal of selectivity was obtained when arylamines were used as substrates with a preference for the α-aminoaryl position over the α-amido position. For example, when 4-Boc-1-(2-pyridyl)piperazine was used as substrate this gave **862e** as a 19 : 1 mixture of regioisomers and the use of 4-Boc-1-(2-trifluoromethylphenyl)-piperazine gave **862f** as a 41 : 1 mixture of regioisomers in 58% yield. Enhancement in the regioselectivity was achieved for different electron-poor alkene coupling partners. For example, 1,1-bis(phenylsulfonyl)ethylene as coupling partner gave **862g** as a single regioisomer in 90% yield. The functionalisation of bioactive molecules was achieved; the use of the commercial antibiotic, ciprofloxacin as substrate gave **862h** in 47% yield and as a single regioisomer. From the course of the investigation, it was found that some substrates gave superior results when the less oxidising acridinium dye **841** ($E_{red}^* = +1.65$ V $vs.$ SCE) was used as catalyst, denoted with †.

Alkane functionalisation. A dual catalytic system of acridinium dye **16** and hydrogen chloride worked well for the coupling of a range of functional groups, such as alkanes, to electron-poor alkenes under blue light (Scheme 235).[266] Irradiation of the reaction mixture gave excited compound **797** from **16**. SET from chloride ion ($E_{ox} = +2.03$ V $vs.$ SCE) to **797*** ($E_{red}^* = +2.18$ V $vs.$ SCE) formed a chlorine radical and acridinyl radical **798**. The abstraction of a hydrogen atom from cyclohexane **863a** by the

chlorine atom resulted in alkyl radical **864a** and hydrogen chloride. C–C bond formation between electron-poor alkene **865a** and **864a** gave alkyl radical **866a**, which received an electron from reduced catalyst **798** ($E^{•-} = -0.57$ V $vs.$ SCE) forming anion **867a** and this step closed the acridinium catalytic cycle. Protonation of **867a** gave **868a**.

This transformation performed best when performed in a "stop-flow microtubing reactor" (SFMT) instead of a traditional batch reactor (Scheme 236). This allowed for the preparation of 34 dinitrile compounds **868**. From the course of this investigation, it was found that alkanes gave coupled compounds **868a–e** as products. Benzylic C–H bonds were activated, and this gave **868f** in 69% yield. The use of ethers and alcohols led to compounds such as **868g** and **868h** in 75% and 90% yield, respectively. This reaction was also performed in a continuous-flow reactor, and this gave **868j** in 95% yield with a 1.12 g h^{-1} rate.

Allylic functionalisation. The cross-coupling of allylic compounds **870** with aryl and vinyl bromides **869** was achieved with the use of an acridinium salt and nickel catalytic strategy.[267] Under the reaction conditions, the oxidative addition of aryl bromide **869a** to Ni(0) complex gave a Ni(II) complex (Scheme 237). It was postulated that triplet–triplet energy transfer occurred between the excited photocatalyst and Ni(II) complex. A photo-induced SET process was also considered but electrode potentials (Mes-Acr-Me$^•$ $E_{red} = -0.57$ V $vs.$ SCE) suggested that this pathway was unfeasible.

9664 | Chem. Soc. Rev., 2021, **50**, 9540–9685

This journal is © The Royal Society of Chemistry 2021
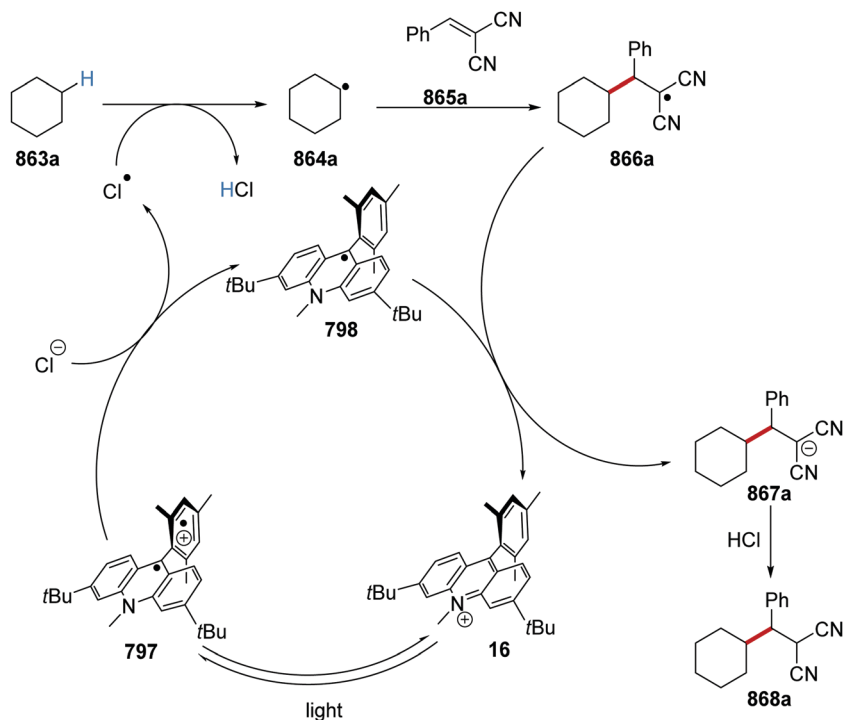
Scheme 235 C–H activation mediated with acridinium and chloride anion.
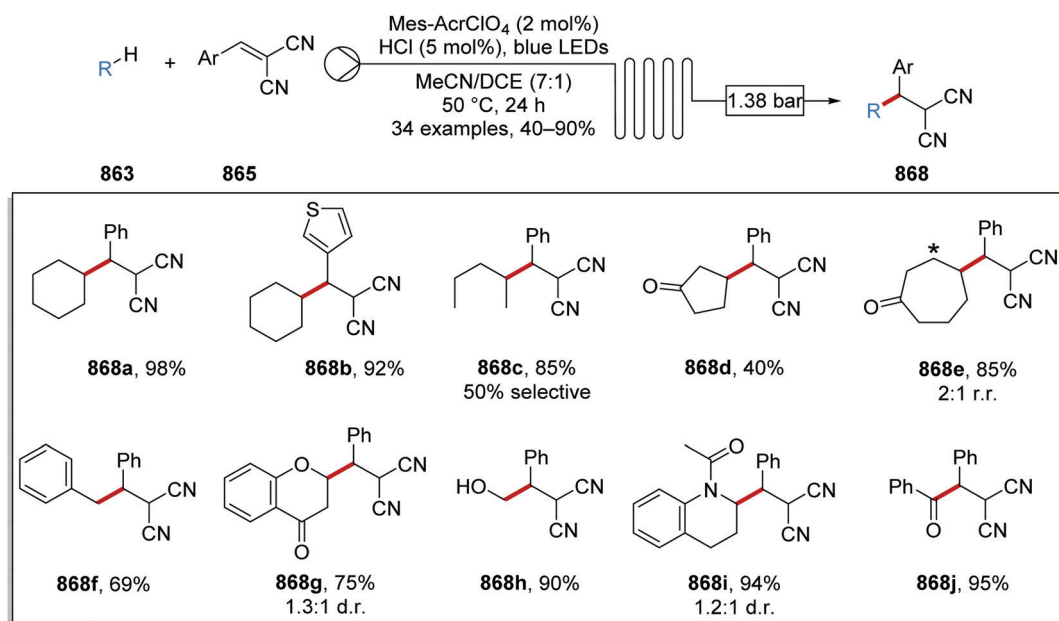
Scheme 236 Stop-flow Giese-type reaction with acridinium photocatalyst.

The triplet-excited Ni(II) complex resulted in a homolytic bond cleavage of the Br–Ni bond and this gave a bromine atom and a Ni(I) complex. The weak allylic C–H bond of alkene **870a** underwent homolytic bond cleavage via H-atom transfer to the bromine atom and this gave allylic radical **871a** and HBr. Combination of the allylic radical and Ni(I) complex gave a Ni(II) complex and this underwent reductive elimination, which resulted in the closure of

the nickel catalytic cycle and formation of coupled compound **872a** as product.

From optimisation studies, whilst both Ir[dF(CF$_3$)ppy]-(dtbbpy)PF$_6$ (gave 84% yield of **872a**) (Scheme 238) and (Mes-Acr-Me)ClO$_4$ (gave 81% yield of **872a**) resulted in successful reaction, the photocatalyst Ru(bpy)$_3$PF$_6$ gave no product. While the iridium catalyst gave a slightly increased yield of **872a**, the acridinium

This journal is © The Royal Society of Chemistry 2021

Chem. Soc. Rev., 2021, **50**, 9540–9685 | **9665**
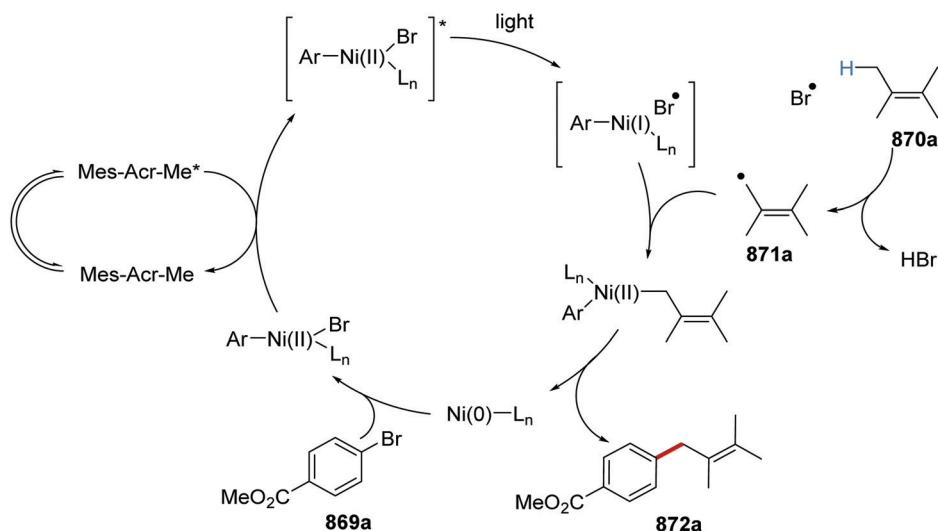
Scheme 237 Allylation of aryl bromides.
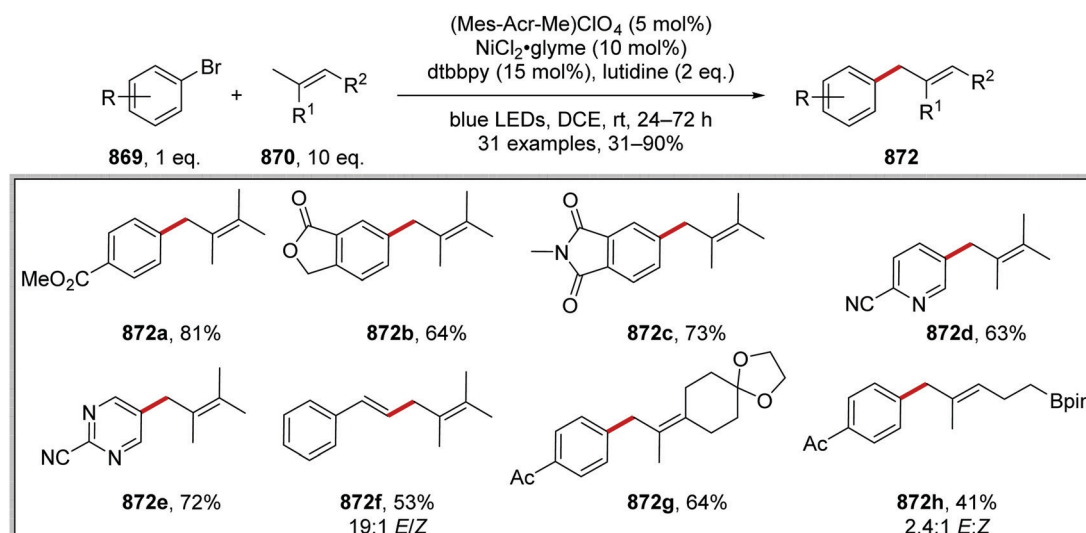
Scheme 238 Products of allylation of aryl bromides.

photocatalyst was preferred due to cost and sustainability perspectives. Further experiments found that use of the base lutidine and performing the reaction in DCE gave **872a** in maximum yield (81%). Various aryl bromides were used as substrates and gave ester **872a**, lactone **872b**, *N*-methylphthalimide **872c**, pyridine **872d** and pyrimidine **872e** products. (2-Bromovinyl)benzene also succeeded in this transformation and this gave diene **872f** in 53% yield and a 19:1 ratio of *E/Z* stereoisomers. Functionalised alkenes were tolerated under the reaction conditions giving ketal **872g** and boronic ester **872h** in 64% and 41% yield, respectively.

3.7 Excitation of radical cations and radical anions[9a]

Back in Scheme 216, the 2018 report of two quantum excitations was mentioned in relation to von Wangelin *et al.* This conPET (consecutive photoelectron transfers) was devised by König's

team in 2014[268] for reducing challenging substrates. Here the perylenediimide (PDI) **873** was first reduced to its relatively stabilised radical anion by a photo-induced reaction (Scheme 239). The radical anion was then photoexcited and, in its excited state, behaved as a powerful electron donor, reducing aryl iodides, bromides or chlorides that were slightly activated by an electron-withdrawing group in the *para*- or *ortho*-position, for example 2-chlorobenzonitrile (E_{red} = −1.91 V *vs.* SCE).[222]

Recently, the potency of such conPET donors has been extended by Miyake *et al.*, using different dyes.[269–271] Here the perylenediimide **873** was replaced by imide **878**. In the presence of NMe$_4$OH, this compound formed an adduct **879**; photoexcitation produces **880** that underwent fragmentation to the somewhat stabilised radical anion **881** (Scheme 240). This radical anion was then photoexcited to afford a very strong donor, which has been used for metal-free Birch reductions of

9666 | *Chem. Soc. Rev.*, 2021, **50**, 9540–9685

This journal is © The Royal Society of Chemistry 2021
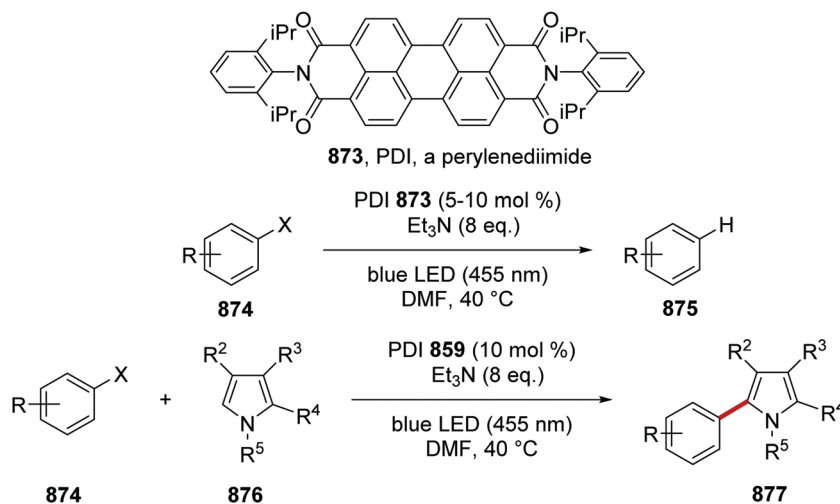
Scheme 239 ConPET (consecutive photoelectron transfers) of perylenediimide **859** in the presence of triethylamine generates a strong enough electron donor to convert aryl halides to aryl radicals.

benzenes like **883** and **885** (E_{red} = −3.42 V *vs.* SCE for benzene). To investigate this reaction calculated and experimental redox potentials were found for the photocatalyst. The ground state reduced anion **881** was unable to reduce benzene ($E_{calc}^{\bullet-}$ = −1.30 V *vs.* SCE and $E_{exp}^{\bullet-}$ = −1.24 V *vs.* SCE). Excited complex **882** had a range of different electrochemical potentials depending upon the excited state of the catalyst. Crucially, it was calculated that the first doublet state had an oxidation potential of $E_{ox}^{\bullet-*}$ = −2.43 V *vs.* SCE, (calculated value, first doublet state). Therefore, these calculations could suggest that this catalyst exhibits anti-Kasha behaviour. As previously mentioned, anti-Kasha behaviour is very rare as internal conversion to the lowest excited state is extremely. However, alternatively, the formation of a solvated electron can also occur rapidly (11 ± 1 ps).[269b] Mechanistic studies to fully elucidate the mechanism are still in progress but it was suggested by the authors that a ground-state π-stacking complex or an exciplex could be critical for the transfer of the electron. Culmination in the ability to produce Birch reductions of benzenes in the absence of redox-active metals is a remarkable achievement for the organic electron transfer chemists. Other photoredox[272a] and non-photoredox[272b] approaches to Birch reduction have also recently been published.

Inspired by the perylenes diimides work of König, alternative diimides were explored by the team of Wickens.[273] They reported in 2020 that photoactivation of the radical anion of imide **889** usefully converts aryl chlorides, some with very negative reduction potentials (E_{red} = −2.8 V *vs.* SCE for chlorobenzene), to the corresponding aryl radicals and used these radicals in heteroarylation reactions (Scheme 241) and for coupling to trialkyl phosphites. In their case, the imide is reduced to its radical anion electrochemically and this species is then photoexcited by blue LEDs to afford electron transfer.

A combination of electrochemical activation followed by photoactivation was published in 2019 by Lambert's group.[274] They prepared the trisaminocyclopropenium salt **895**, and oxidised it electrochemically to the radical dication **892**, which was then

excited by a 23 W CFL (Schemes 242 and 243). When the diradical cation was excited, it became a very strong oxidant (E_{red}^{*} = +3.33 V *vs.* SCE) and thus it was able to oxidise compounds such as benzene (E_{ox} = +2.54 V *vs.* SCE). Oxidation of arenes afforded the radical cations that were then trapped by azole nucleophiles giving products **893a–e**.

The strong oxidising power of the excited radical dication **894** was also deployed in the Minisci reactions of alkyl ethers (Scheme 243).[275] Using the same cycle as shown above, it is thought that the photoexcited radical dication has HAT properties to abstract a hydrogen atom from an ether **899** to bring about Minisci reactions with protonated pyridines and quinolines *. Additionally, the ether-derived radicals undergo Giese reactions with electron-poor alkenes and C–N coupling to azoles (not shown here).

Expanding on the repertoire, the cyclopropenium reagent **895** has been used in a study of S$_N$Ar reactions of aryl fluoride radical cations.[276] (See also the studies by Nicewicz *et al.* in this review, Scheme 226.) However, photoexcited DDQ was found to work better. This excitation of DDQ with blue LEDs afforded a highly oxidising DDQ* (E_{red}^{*} = +3.18 V *vs.* SCE) that converted aryl fluorides into their radical cations. Even *p*-difluorobenzene (E_{ox} = +2.35 V *vs.* SCE) was activated in this way to afford the derivative **904e** (63%, Scheme 244).

Triarylamine radical cations are ground state oxidants and have been used *e.g.* to oxidise DABCO to its radical cation for highly selective HAT chemistry.[38] More recently, the photoactivated radical cation of [(tri[1,1′-biphenyl]-4-yl]aminetolylaminium salt (TCPBA) has been used to oxidise arenes to their radical cations by the Barham team. The examples shown in Scheme 245 feature C–H substitution by azoles.[277] The formation of fluoroarene **904m** from fluorobenzene shows that this is a highly powerful oxidising system for arenes and competitive with those discussed above [from the teams of Nicewicz and Lambert]. The best catalyst used in this transformation, TCBPA, was calculated to be a very strong oxidant (E_{red}^{*} = +4.19 V *vs.* SCE).

This journal is © The Royal Society of Chemistry 2021

Chem. Soc. Rev., 2021, **50**, 9540–9685 | **9667**
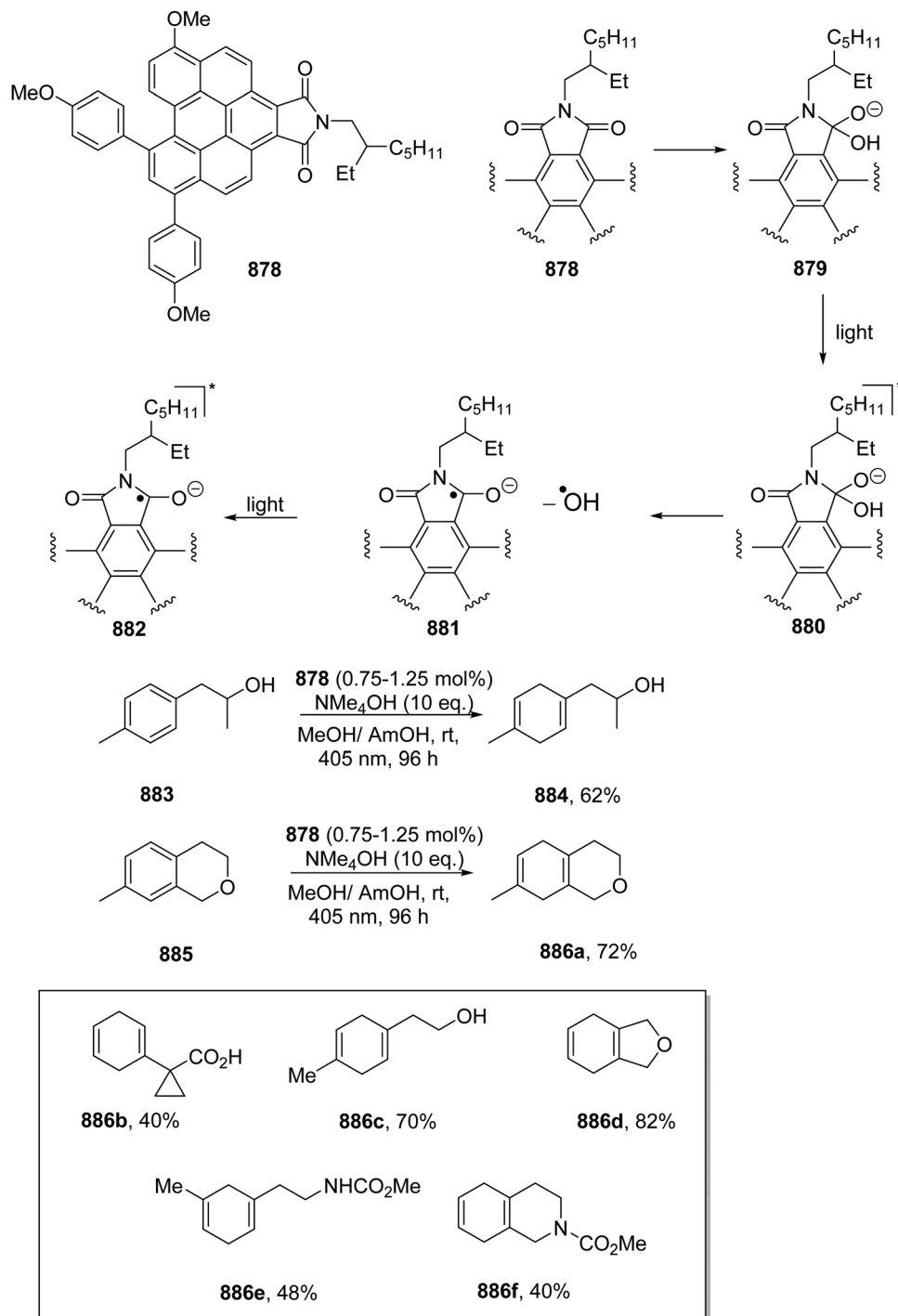
Scheme 240 Consecutive photoactivations of diimide **878** led to Birch reduction of substituted benzenes.

3.8 Selectfluor®

A Minisci coupling reaction using Selectfluor® (**22h**) as a HAT reagent precursor was reported (Schemes 246 and 247).[278,279] It was proposed, with irradiation with blue light (427 nm, 40 W) that **22h** was converted to HAT reagent, TEDA²⁺• (**22h***) *via* homolytic bond cleavage. Hydrogen atom abstraction from ether substrate **905a** with **22h*** resulted in the formation of alkyl radical **906a** and protonated species **22h⁺**. Addition of alkyl radical **906a** to protonated heterocycle **907a** resulted in the formation of a new C–C bond giving **908a**. Proton loss from **908a** gave carbon-centred radical **909a**. SET oxidation of **909a** with another equivalent of **22h** and aromatisation resulted in Minisci coupled product **910a**. From light on/off experiments, it was concluded that a radical-chain mechanism was unlikely for this process.

From the use of two different reaction conditions, a wide range of Minisci coupled products **911** was prepared (Scheme 247). It was

9668 | *Chem. Soc. Rev.*, 2021, **50**, 9540–9685

This journal is © The Royal Society of Chemistry 2021
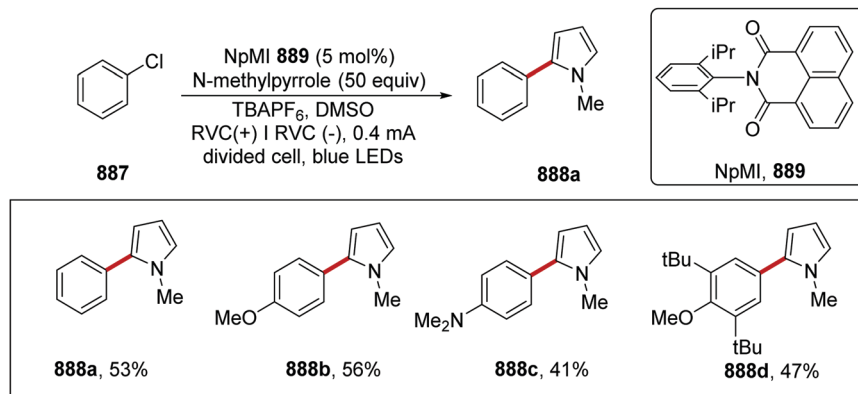
Scheme 241 Heteroarylation of aryl chlorides.
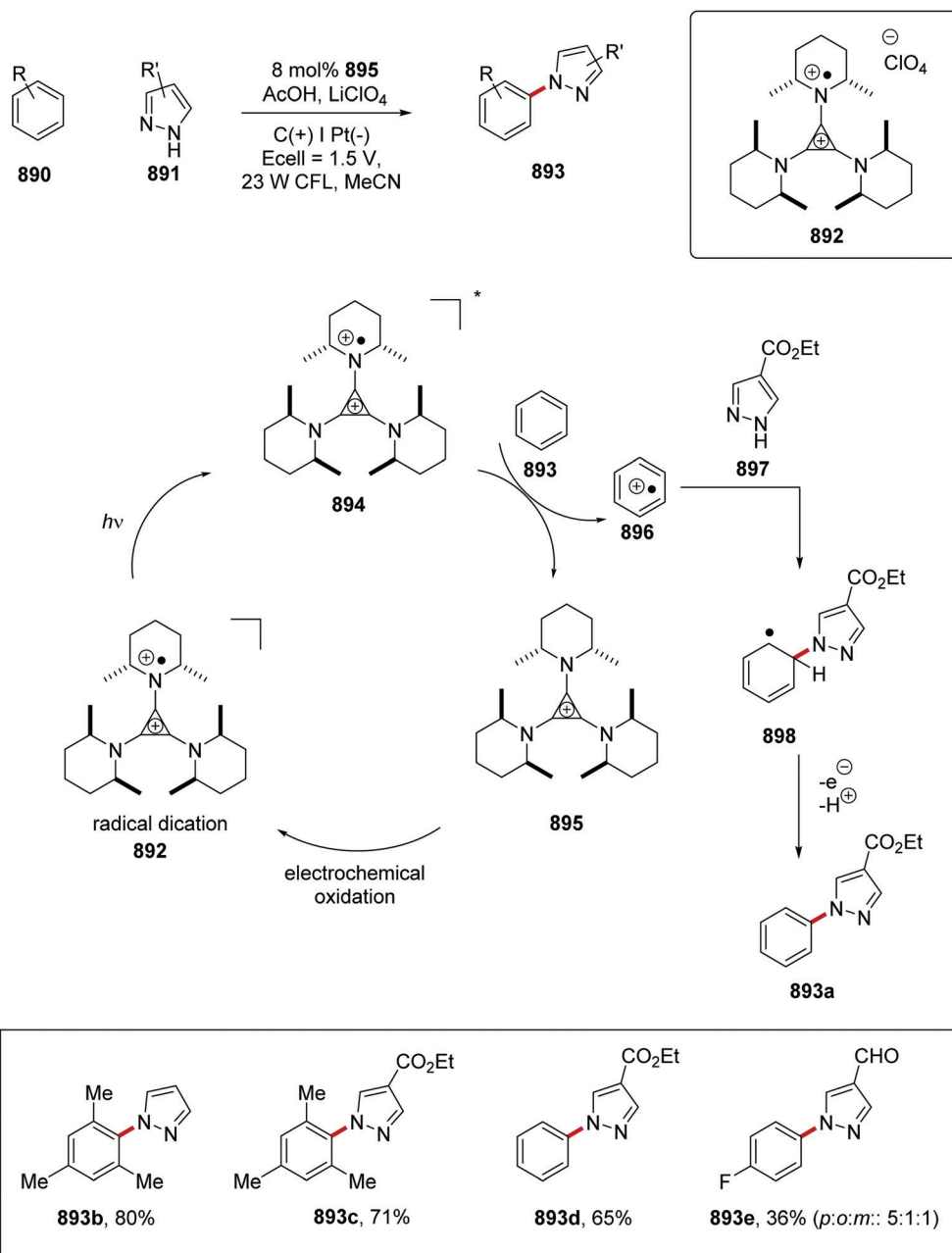
Scheme 242 C–H amination of arene radical cations with azoles.

This journal is © The Royal Society of Chemistry 2021

Chem. Soc. Rev., 2021, **50**, 9540–9685 | **9669**

895 (8 mol%)
E$_{cell}$ = 1.5 V
C(+) I Pt(-)
CFL
AcOH, TFA
LiClO$_4$, MeCN

899   900   901

901a, 80%   901b, 81%   901c, 28%   901d, 51%   901e, 62%
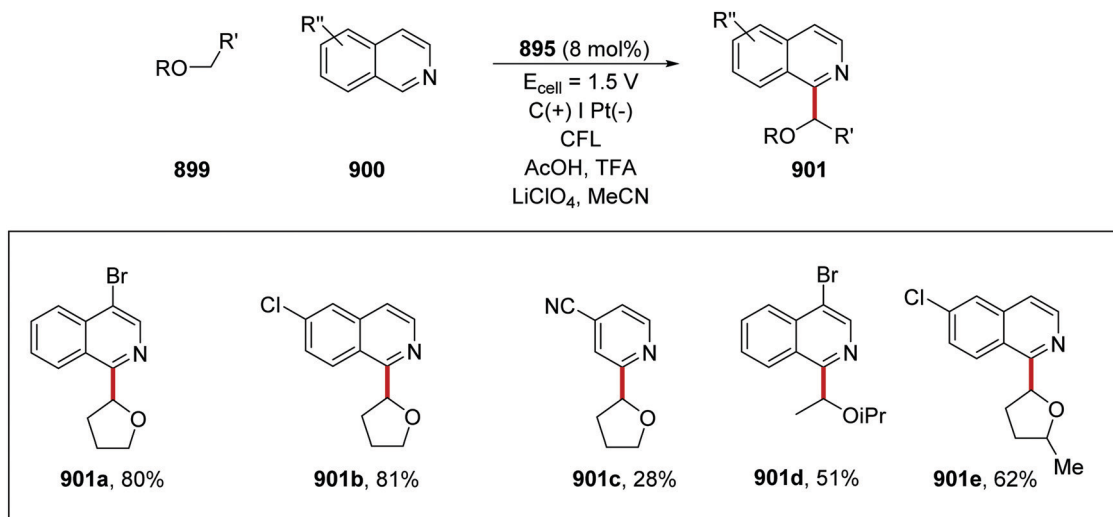
Scheme 243 Minisci reactions of ethers.

902 + Azole-H 903

DDQ (15 mol%)
E$_{cell}$ = 1.5 V
C(+) I Pt(-)
blue LED
AcOH, TBABF$_4$
LiClO$_4$, MeCN

904

904a, 73%   904b, 53%   904c, 73%   904d, 43%

904e, 63%   904f, 46%   904g, 35%
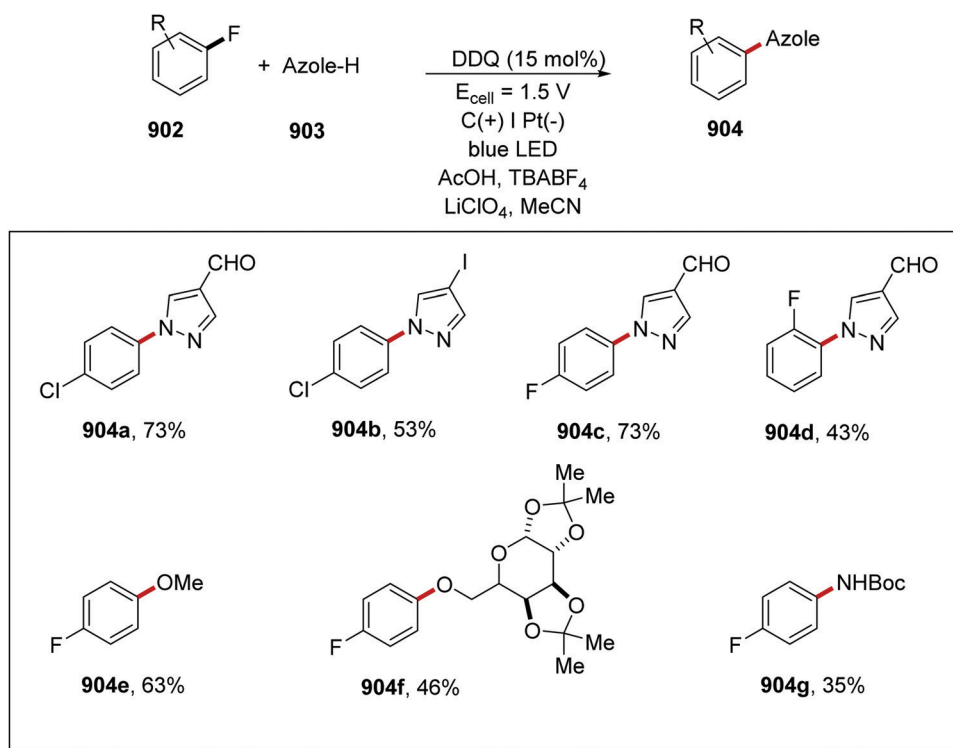
Scheme 244 Defluorinative amination of aryl fluorides.

found that alkanes, ketones, and ethers were all effective coupling partners for N-based heterocycles **907** and this allowed functionalised heterocyclic compounds **911** to be isolated efficiently. The use of cyclohexenone and 2-hexenone led to compounds **911b** and **911g** being isolated as mixtures of regioisomers. However, the use of ethers gave a highly regioselective reaction with **911c–f** being formed as single regioisomers.

From competition experiments, it was shown that the reaction propagated with a higher rate of reaction for benzylic and α-hetero C–H bonds than alkane C–H bonds (Scheme 248).[278]

Functionalisation was quicker for benzylic C–H bonds than α-heteroatom C–H bonds.

3.9 Thiocarbamate catalyst

Benzylic C–H functionalisation. Radical carbon–carbon bond formation via a Giese-type addition was achieved with a thiocarbamate nucleophilic catalyst **918** (Scheme 249).[280] This reaction was unlike previous radical coupling strategies as it did not rely upon redox potentials of substrates, BDEs or triplet energies. The use of **918** as catalyst allowed for coupling of

9670 | Chem. Soc. Rev., 2021, 50, 9540–9685

This journal is © The Royal Society of Chemistry 2021
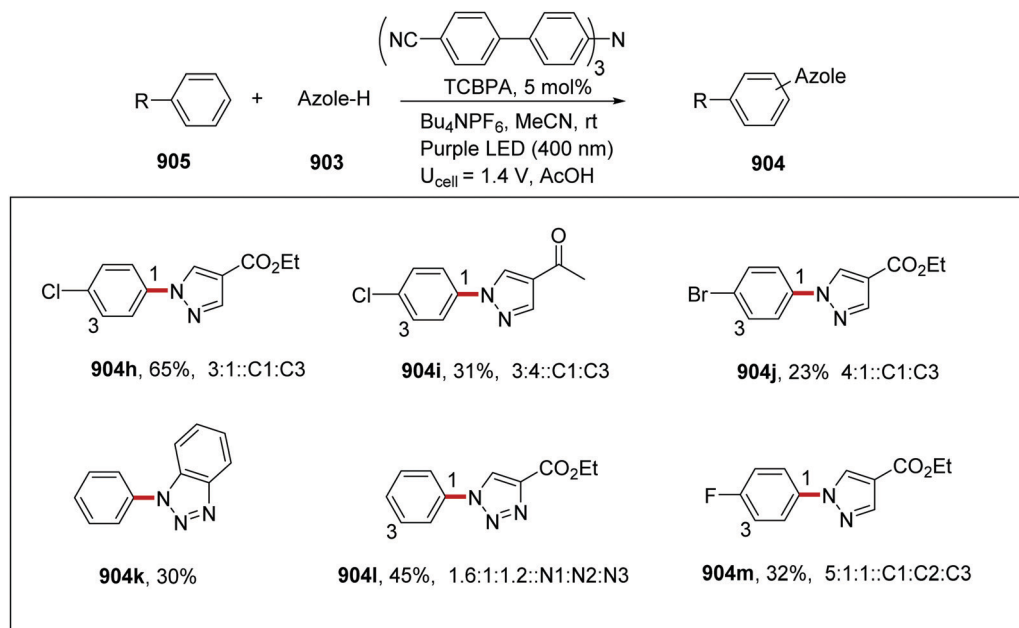
Scheme 245 Photoexcitation of triarylaminium salts affords powerful oxidants.
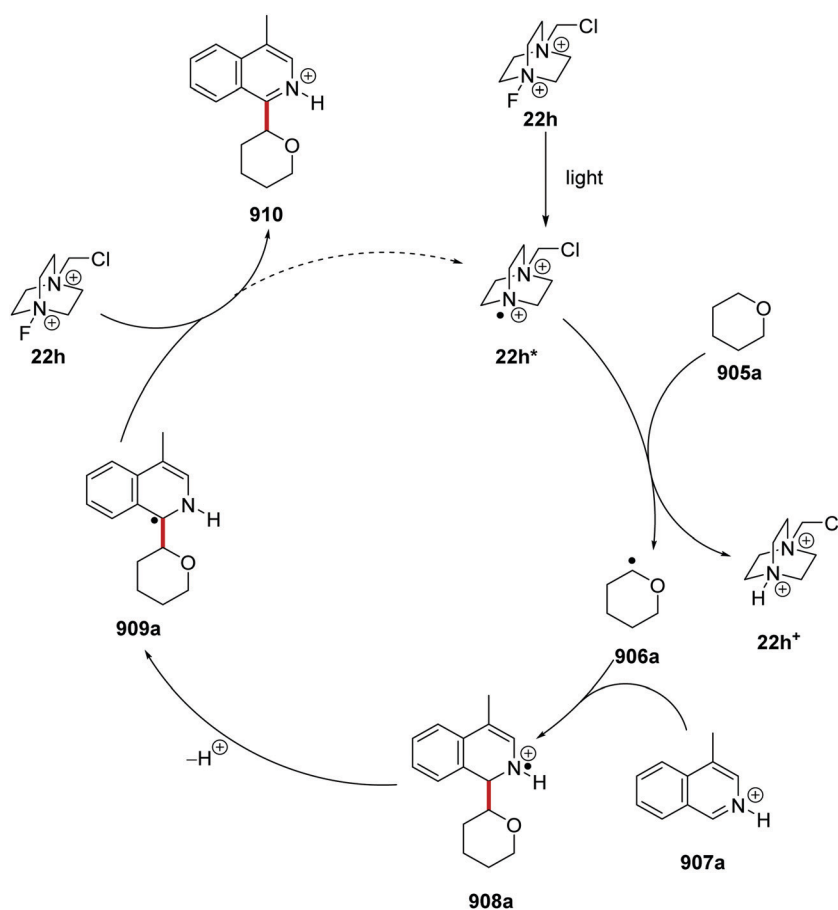
Scheme 246 Minisci reaction with Selectfluor.

compounds with suitable leaving groups, such as benzyl chloride **919a** with electron-poor alkenes such as dimethyl fumarate **920a** and this gave diester **921a**. Reaction between catalyst **918** and benzyl chloride **919a** gave indole derivative **922a**. The UV-vis

This journal is © The Royal Society of Chemistry 2021

Chem. Soc. Rev., 2021, **50**, 9540–9685 | **9671**
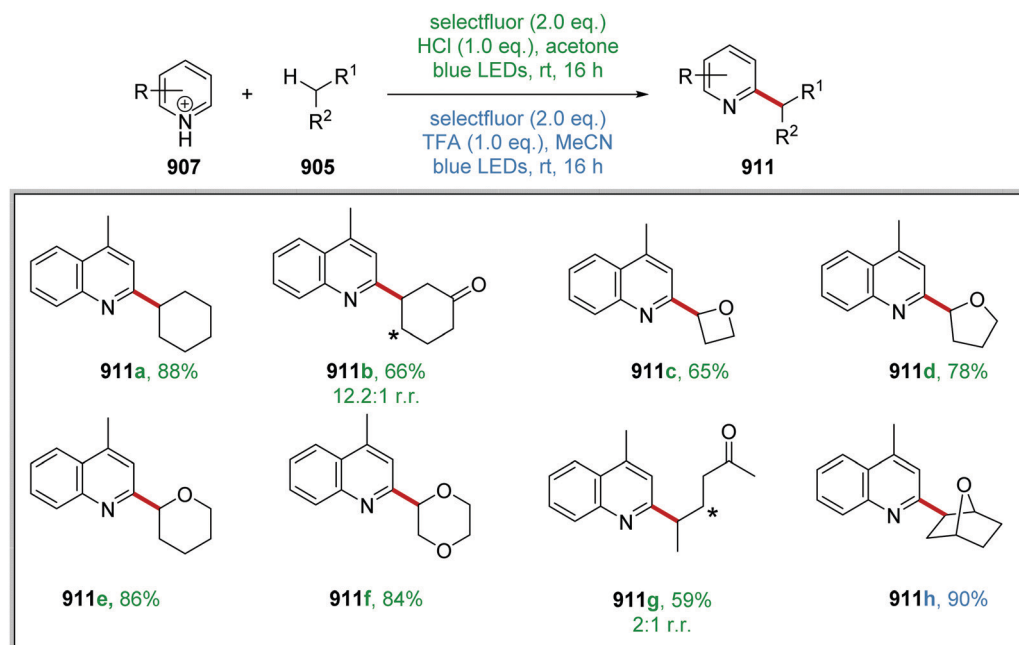
Scheme 247 Selectfluor Minisci reaction.
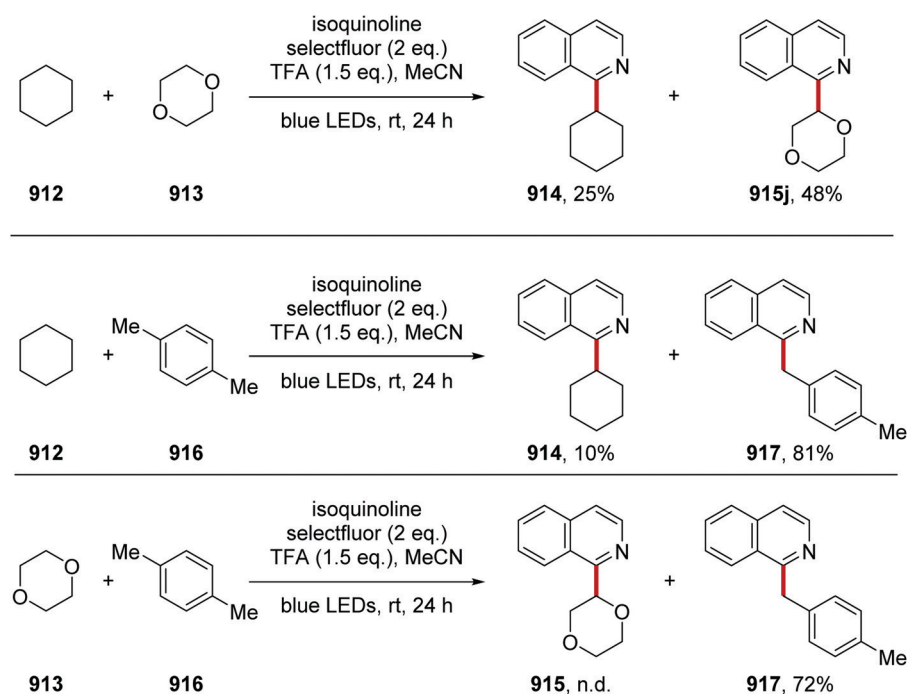
Scheme 248 Competition experiments.

absorbance of indole **922a** showed strong absorbance (λ_{max} = 344 nm, ε_{344} = 18 400 M^{-1} cm^{-1}) and could absorb light in the visible region. Irradiation of the reaction mixture with blue light (465 nm) LED led to homolytic bond cleavage of **922a** and radicals **923a** and **924** were produced. Addition of benzylic radical **923a** to alkene **920a** yielded α-ester radical **925a**. γ-Terpinene (**926**) was used as a cost-effective replacement for 1,4-cyclohexadiene as hydrogen atom source and reductant.

HAT to **925a** from **926** gave the isolated diester **921a** as product and radical **927**. The nucleophilic catalytic cycle was closed with a SET from **927** to radical **924** and reformed original catalytic species **918** and cation **928**, which, after proton loss, yielded aryl derivative **929**.

The preparation of diester **921a** from benzyl chloride **919a** and dimethyl fumarate **920a** was chosen as a model reaction in developing optimised conditions. As mentioned above, γ-terpinene

9672 | *Chem. Soc. Rev.*, 2021, **50**, 9540–9685

This journal is © The Royal Society of Chemistry 2021
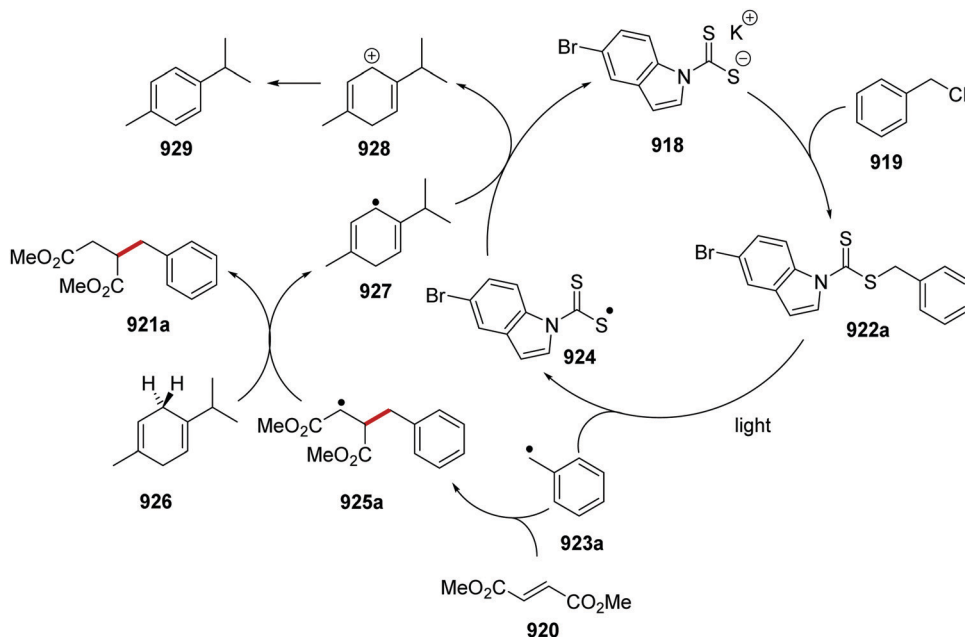
Scheme 249   The chemistry of nucleophilic catalyst **918**.
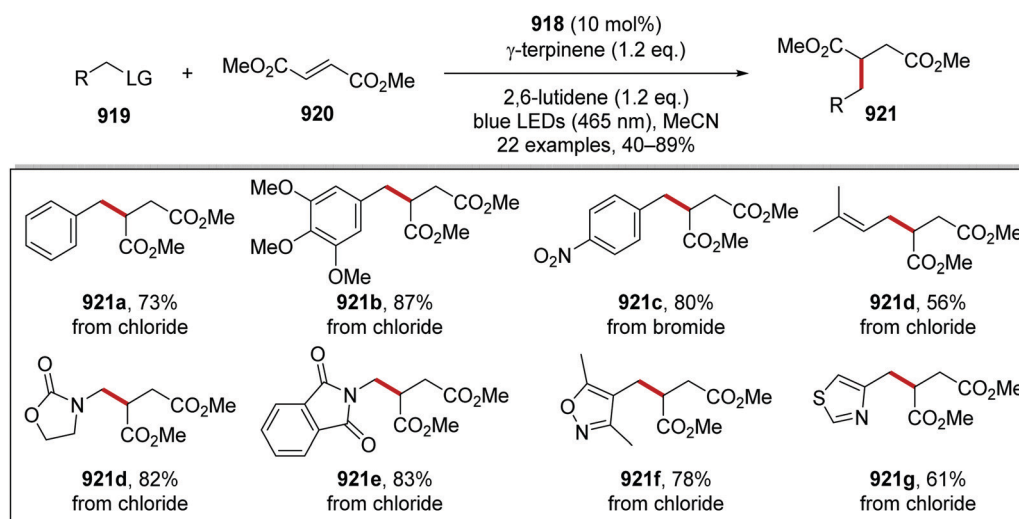
Scheme 250   Coupling products arising through use of catalyst **918**.

(1.2 eq.) **926** was chosen as 1,4-CHD replacement and 2,6-lutidine was chosen as base. Originally, potassium ethyl xanthogenate (20 mol%) was used as a nucleophilic catalyst with irradiation at 400 nm but this delivered **921a** in 19% NMR yield. When more red-shifted light was used (465 nm), no product formation was observed. It was thought that incorporation of a chromophore onto the nucleophilic catalyst would lead to greater conversion to product. Indole **922a** had far superior absorbance than the ethyl xanthogenate analogue and this did lead to greater product formation. The combination of **918** with benzyl chloride (1.5 eq.) and **920** gave **921a** in 43% NMR yield when conducted at room temperature and irradiation with 465 nm light. The yield of **921a**

was increased to 90% NMR yield (73% isolated yield, 8.6 g scale) when the temperature was increased to 60 °C (Scheme 250).

An investigation into other leaving groups was carried out. It was found when benzyl bromide was used instead of benzyl chloride, a yield of 94% was achieved for **921a**. Benzyl iodide gave 85% yield for **921a** and benzyl mesylate gave **921a** in 91% yield. Other benzylic halogens were successful substrates for this process and compounds **921b** and **921c** were prepared. When prenyl chloride was used in this transformation, this gave **921d** in 56% yield. Both aliphatic and aromatic heterocycles were used in this transformation and this gave compounds **921d–g**.

This journal is © The Royal Society of Chemistry 2021

Chem. Soc. Rev., 2021, **50**, 9540–9685 | 9673
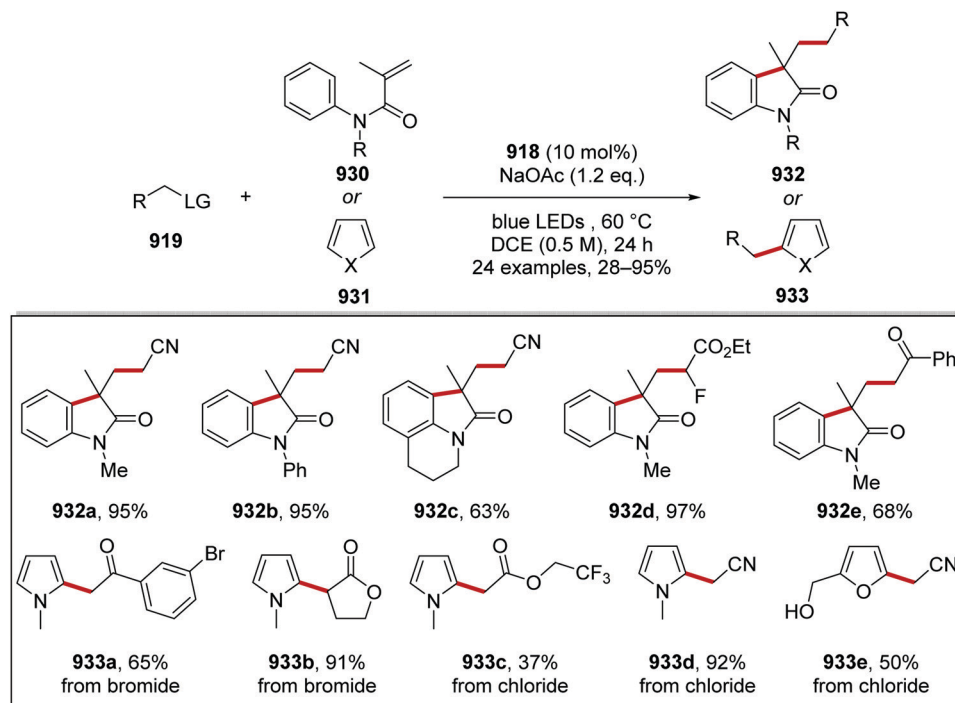
Scheme 251 Tandem reactions induced by catalyst **918**.

The use of stoichiometric sacrificial cyclohexadienyl radicals was avoided when the reactions were performed with acrylamides **930** and electron-rich heterocycles **931** (Scheme 251). When chloroacetonitrile was treated with various acrylamides under optimised reaction conditions, compounds **932a–c** were prepared. Ethyl bromofluoroacetate was an excellent substrate for this transformation and ester compound **932d** was prepared in 97% yield from it. Compound **921e** was afforded from 2-chloroacetophenone in 68% yield. When 2-bromo-1-(3′-bromophenyl)ethan-1-one was treated with *N*-methylpyrrole under the reaction conditions this yielded ketone **933a** in 65% yield. *N*-Methylpyrrole was also reacted with other alkyl halides including α-bromo-γ-butyrolactone (**933b**) and chloroacetonitrile (**933d**) and this afforded pyrrole products. Other heterocycles were also amenable to these reaction conditions; for example, furfuryl alcohol was transformed to **933e** with chloroacetonitrile in 50% yield.

3.10 Charge transfer complexes

Most of the reactions detailed so far have been accomplished by the addition of external photoredox catalysts to the reaction. However, a number of chemists, notably the group of Melchiorre, have focused on the formation of charge transfer complexes when the reactants are mixed. In these cases, photoactivation can lead to full electron transfer, thereby triggering a chemical reaction.

α-Aminosilane as radical precursor. Organic chiral catalyst **937** allowed for the coupling of enones **934** to α-silyl amines **935** which gave ketones **936** without any photocatalyst (Scheme 252). This was achieved *via* an intramolecular iminium-ion-based electron donor–acceptor complex. Condensation between enones

934 and chiral catalyst **937** under acidic conditions resulted in a chiral iminium ion that contained an electron-rich carbazole moiety and an electron-poor alkene. A light-promoted electron transfer to the alkene from the carbazole gave an intermediate that featured both an allylic radical and a carbazole radical cation. Adjacent silyl groups lower the redox potential of amines. Therefore, the use of the right α-silylamine compound would participate in inter-molecular SET with the carbazole radical cation. Dimethyl(phenyl)silyl groups (E_{ox} = +0.97 V *vs.* Ag/Ag$^+$ in MeCN for α-dimethyl(phenyl)silyl carbazole) were successful at participating in SET with the carbazole radical cation (E_{red} = +1.09 V *vs.* Ag/Ag$^+$ in MeCN), this allowed for α-aminoalkyl radical formation and propagation of the reaction. The reaction was more efficient when the catalyst had more electron-withdrawing groups present and thus, from a screen of five catalysts, catalyst **937** was the most effective. Employment of the optimal reaction conditions gave a library of nine aniline products **936a–i** in yields of 57–83%.

Even one nitrogen atom attached to an alkene gives interesting electron donating properties to enamines, notably when photoexcited. Melchiorre *et al.*[282] examined the enantioselective α-methylation and benzylation of aldehydes. (Scheme 253) Such reactions had been previously promoted by TM-based photoredox agents,[283] but Melchiorre's contribution was to bring about the reactions in their absence. Taking butyraldehyde **944** as an example, reaction with an enantiomerically pure secondary amine **952** creates the corresponding enamine **947**. When the enamine was excited, a strongly reducing species was formed (E_{ox}* = *ca.* −2.0 V *vs.* Ag/AgCl) and this was able to reduce sulfone **945** (E_{red} = −1.49 V *vs.* Ag/AgCl) to form the radical **948**. [The authors discuss the possibility of excitsation of the individual species, as well as excitation of a charge-transfer

9674 | *Chem. Soc. Rev.*, 2021, **50**, 9540–9685

This journal is © The Royal Society of Chemistry 2021
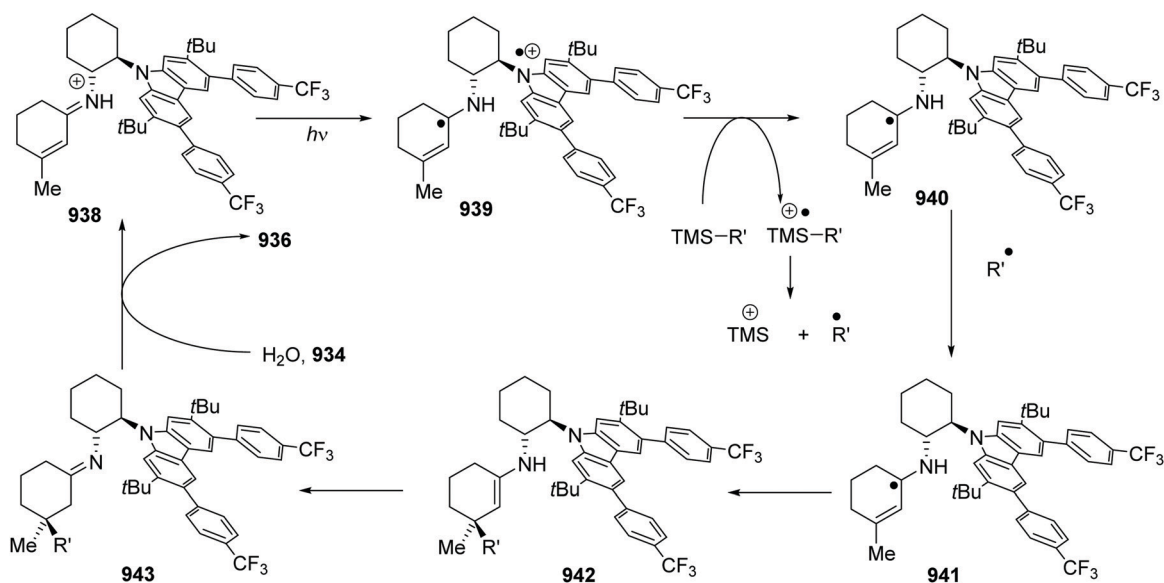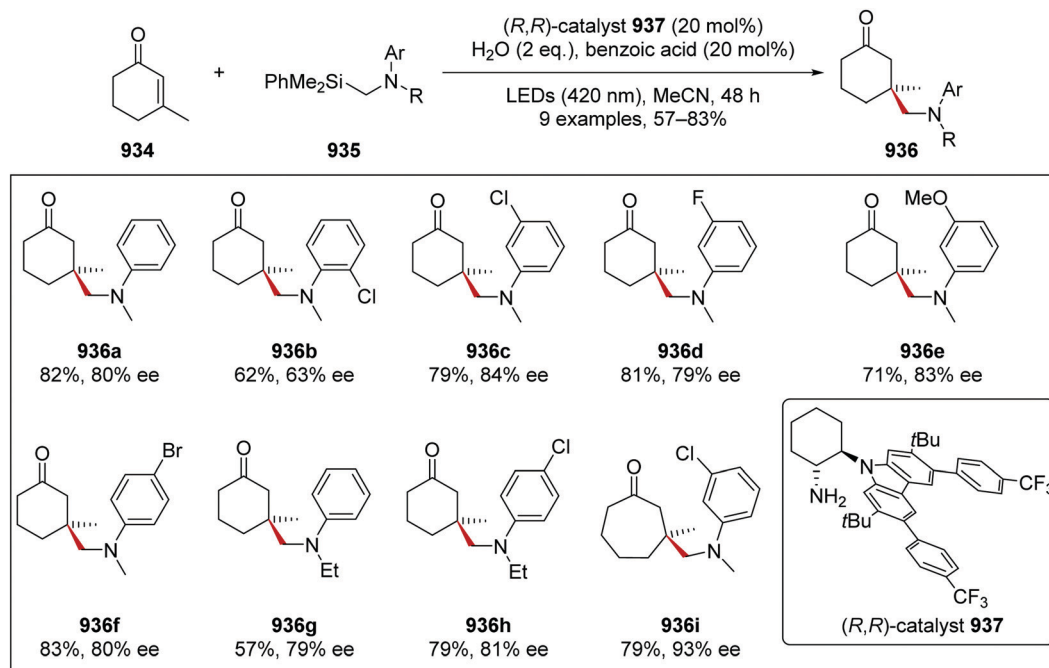
Scheme 252 Enantioselective radical addition reactions controlled by diamine **937**.

complex formed from the enamine and the iodosulfone.] The resulting radical **948** added to the enamine in a stereocontrolled manner to give α-aminoalkyl radical **949**. The reducing power of **949** (E_{ox} = −0.95 V vs. Ag/AgCl) was insufficient of reducing **945** therefore it was proposed that a halogen atom abstraction process was operative to continue the radical chain process (ϕ = 3.8). The iminium salt was hydrolysed *in situ* to provide product **951**. For ease of isolation, the product was reduced with NaBH$_4$ to the corresponding alcohol. Products **946a–d** exemplify high yields and stereoselectivity.

Melchiorre also demonstrated electron transfer properties for the dienamine (dihydropyridine) **953** (Scheme 254). Here, the excited state chromophore **956** (E_{ox}^* = ca. −1.1 V vs. SCE) should not be able to transfer an electron to compound **957** (E_{red} = −1.32 V vs. SCE).[284] Instead it was thought that electron transfer to pyridinium ion **961** (E_{red} = −1.01 V vs. SCE), which could be formed with photolysis from **953**, was more feasible. The dihydropyridine radical cation **959** underwent bond fragmentation and acyl radical **960** was delivered. Radical attack of **960** to protonated heterocycle **957** resulted in C–C bond formation. The adduct **962** easily undergoes deprotonation on carbon to give radical **963**. Protonation on oxygen affords ketyl radical **964**, which can receive an electron and a proton to give **965**, the protonated form of isolated product **955**. Hence the process

This journal is © The Royal Society of Chemistry 2021

Chem. Soc. Rev., 2021, **50**, 9540–9685 | **9675**
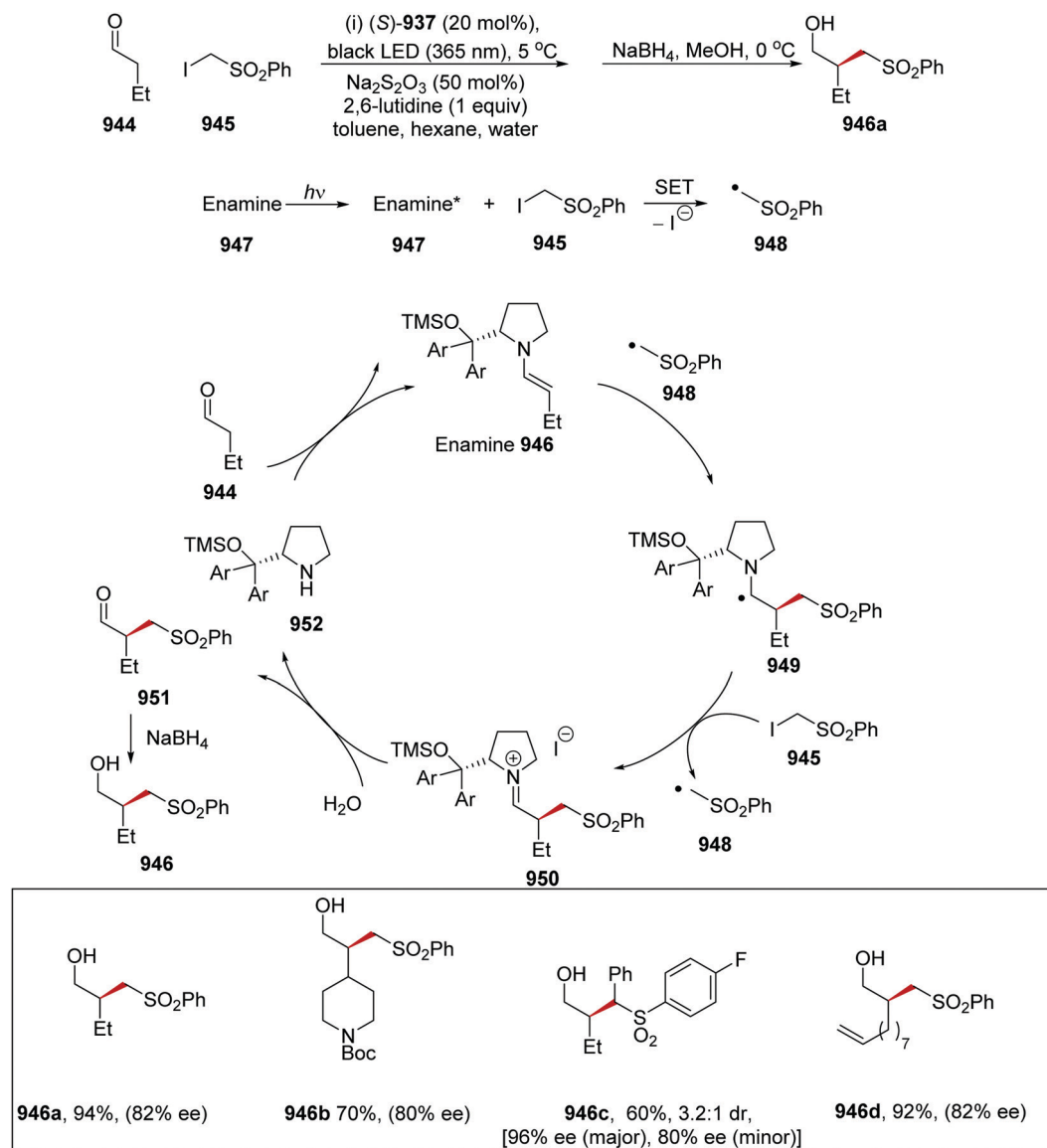
Scheme 253 Enantioselective alkylation of aldehydes.

4 Conclusions

does not follow the normal Minisci pathway, providing an hydroxyalkyl substituted heterocycle, rather than the acyl-substituted counterpart. Products **955a–c** illustrate examples of outcomes from analogous substrates.

A final example[285] illustrates the use of charge-transfer complexes for the C2 alkylation of tryptophan residues **966** (Scheme 255). Here pyridinium salts **967** act as electron-poor π-systems that can complex with the electron-rich π-system of indoles, as in tryptophan. Visible light triggers electron transfer to the charge-transfer complex, giving an indole radical cation and a pyridinyl radical that cleaves to give the parent pyridine and an alkyl radical. Under appropriate conditions, the radical reacts selectively attacking the 2-position of the indole radical cation. Subsequent proton loss affords the substituted tryptophan product **968**.

Over the past ten years considerable progress has been made in radical mediated coupling reactions exploiting PET, HAT and energy transfer processes. During that period, ruthenium and iridium photocatalysts have led the way for transition metal based redox reagents and have resulted in an astonishing number of research papers, addressing a wide variety of reactions. Perhaps because of concerns about the sustainability of supplies of some transition metals,[65] but also about management of waste-streams in pharmaceutical chemistry, organic photoredox catalysts have come to the fore, and are proving capable of attaining very challenging potentials, both reductive and oxidative. Photo-activation of cationic and anionic organic pi-systems has produced really reactive redox active molecules, and coupling of photo-activation with other methodologies, e.g. electrochemistry, has

9676 | Chem. Soc. Rev., 2021, **50**, 9540–9685

This journal is © The Royal Society of Chemistry 2021
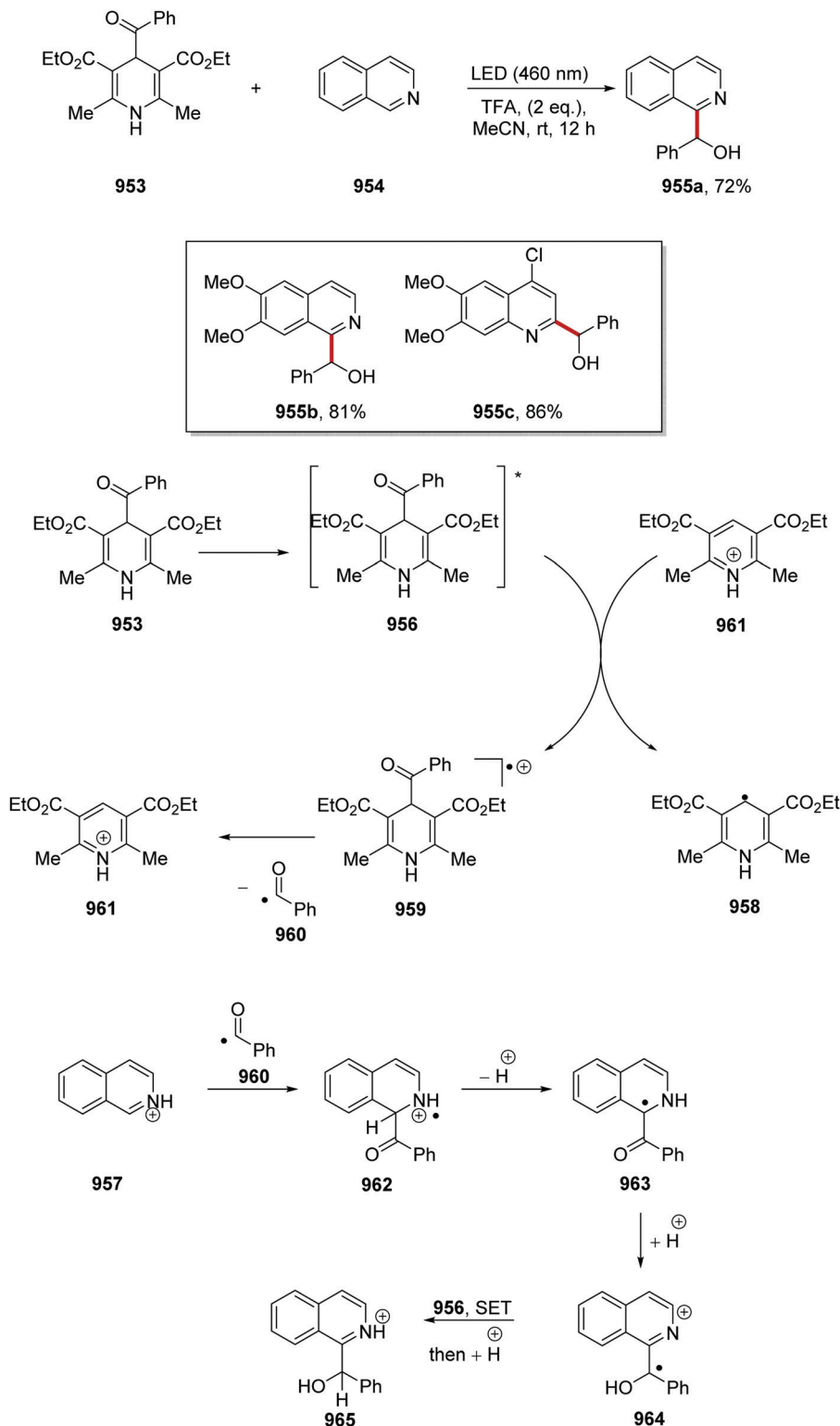
Scheme 254 A modified hydroxyalkylation Minisci process from scission of photoactivated **953**.

begun to create diverse methods of access these. The study of reactions between reagents which, although each is individually unreactive to stimulus by visible light, form a charge-transfer complex that undergoes full electron transfer upon irradiation by visible light, is another area where development is accelerating. Finally, a number of cases of photoredox catalysis that provide excellent levels of asymmetry will simulate much interest in the coming decade. The pursuit of more sustainable reagents for

This journal is © The Royal Society of Chemistry 2021

Chem. Soc. Rev., 2021, **50**, 9540–9685 | **9677**
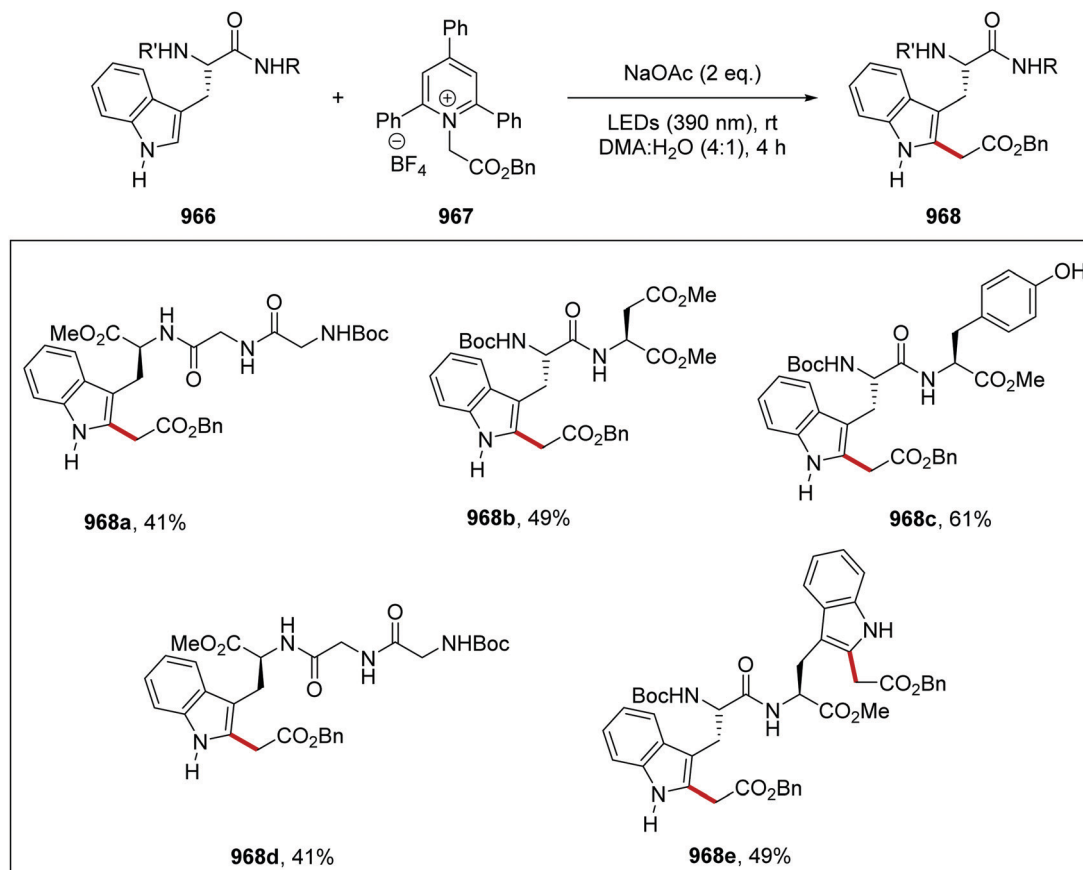
Scheme 255   Stereocontrolled alkylation at C-2 of indoles.

radical promoted coupling reactions should allow further uptake of these strategies in particular late-stage functionalisation of pharmaceutical compounds.[25]

Abbreviations

A	Pre-exponential factor
ATRE	Atom transfer radical addition–elimination
BCP	Bicyclopentane
BDC	*tert*-Butyl N,N-dimethylcarbamate
BDE	Bond dissociation energy
BDFE	Bond dissociation free energy
BET	Back electron transfer
Boc	*tert*-Butyloxycarbonyl
Bn	Benzyl
BP	Biphenyl
Bpy	Bipyridyl
Bpz	Bipyrazyl
Bz	Benzoyl
Cbz	Carboxybenzyl
ConPET	Consecutive photoelectron transfers
Cz	Carbazolyl
4CzIPN	Tetracarbazolylisophthalonitrile
DABCO	Diazabicyclooctane
DCA	9,10-Dicyanoanthracene
DCE	1,2-Dichloroethane
DFT	Density functional theory
DMA	N,N-Dimethylacetamide
DMF	N,N-Dimethylformamide
DMSO	Dimethyl sulfoxide
DIC	N,N'-Diisopropylcarbodiimide
DTA	N,N-Dimethyltrifluoroacetamide
Dtbbpy	Di-*tert*-butylbipyridyl
dr	Diastereomeric ratio
E_a	Activation energy
EDA	Electron-donor–acceptor
ee	Enantiomeric excess
er	Enantiomeric ratio
EWG	Electron-withdrawing group
FRET	Förster resonance energy transfer
Fmoc	Fluorenylmethoxycarbonyl
HAT	Hydrogen atom transfer
HFIP	Hexafluoroisopropanol
HPLC	High-performance liquid chromatography
IC	Internal conversion
ISC	Inter-system crossing
ISET	Inner-sphere electron transfer
HAT	Hydrogen atom transfer
HLF	Hofmann–Löffler–Freytag

KIE	Kinetic isotope effect
LED	Light emitting diode
MLCT	Metal–ligand charge transfer
MTBE	Methyl *tert*-butyl ether
NCS	*N*-Chlorosuccinimide
OSET	Outer-sphere electron transfer
PDI	Perylenediimide
PET	Positron emission tomography or Photoelectron transfer
Ppy	Phenylpyridyl
SCE	Saturated calomel electrode
SCS	Spin-centred-shift
SET	Single electron transfer
SOMO	Singly occupied molecular orbital
TBACl	Tetra-*n*-butylammonium chloride
TCAA	Trichloroacetic acid
Tf	Trifluoromethanesulfonyl
THIQ	Tetrahydroisoquinolinyl
TM	Transition metal
TMG	1,1,3,3-Tetramethylguanidine
TMHD	2,2,6,6-Tetramethylheptanedione
TMS	Trimethylsilyl
PCET	Proton-coupled electron transfer
PET	Photoinduced electron transfer
RCY	Radiochemical yield
RDS	Rate determining step
rr	Ratio of regioisomers
UPLC	Ultra-performance liquid chromatography

Conflicts of interest

There are no conflicts of interest to declare.

Acknowledgements

References

1 (a) M. R. Heinrich, *Chem. – Eur. J.*, 2009, **15**, 820–833; (b) S. Kindt and M. R. Heinrich, *Synthesis*, 2016, 1597–1606; (c) D. P. Hari and B. König, *Angew. Chem., Int. Ed.*, 2013, **52**, 4734–4743; (d) I. Ghosh, L. Marzo, A. Das, R. Shaikh and B. König, *Acc. Chem. Res.*, 2016, **49**, 1566–1577.

2 W. Buratti, G. P. Gardini, F. Minisci, F. Bertini, R. Galli and M. Perchinunno, *Tetrahedron*, 1971, **27**, 3655–3668.

3 F. Minisci, A. Citterio, E. Vismara and C. Giordano, *Tetrahedron*, 1985, **41**, 4157–4170.

4 (a) B. Giese, *Angew. Chem., Int. Ed. Engl.*, 1983, **22**, 753–764; (b) B. Giese, J. A. González-Gómez and T. Witzel, *Angew. Chem., Int. Ed. Engl.*, 1984, **23**, 69–70; (c) G. S. C. Srikanth and S. L. Castle, *Tetrahedron*, 2005, **61**, 10377–10441; (d) T. Kawamoto and I. Ryu, *Org. Biomol. Chem.*, 2014, **12**, 9733–9742; (e) J. Streuff and A. Gansäuer, *Angew. Chem.,*

Int. Ed., 2015, **54**, 14232–14242; (f) Q. Huang, S. R. Suravarapu and P. Renaud, *Chem. Sci.*, 2021, **12**, 2225–2230.

5 K. L. Skubi, T. R. Blum and T. P. Yoon, *Chem. Rev.*, 2016, **116**, 10035–10074.

6 B. P. Roberts and A. J. Steel, *J. Chem. Soc., Perkin Trans. 2*, 1994, 2155–2162.

7 Q.-Q. Zhou, Y.-Q. Zou, L.-Q. Lu and W.-J. Xiao, *Angew. Chem., Int. Ed.*, 2019, **58**, 1586–1604.

8 Selected reviews, general: (a) N. A. Romero and D. A. Nicewicz, *Chem. Rev.*, 2016, **116**, 10075–10166; (b) C. K. Prier, D. A. Rankic and D. W. C. MacMillan, *Chem. Rev.*, 2013, **113**, 5322–5363; (c) R. C. McAtee, E. J. McClain and C. R. J. Stephenson, *Trends Chem.*, 2019, **1**(special issue), 111–129; (d) L. Marzo, S. K. Pagire, O. Reiser and B. König, *Angew. Chem., Int. Ed.*, 2018, **57**, 10034–10072.

9 Selected recent reviews, more specific: (a) M. Schmalzbauer, M. Marcon and B. König, *Angew. Chem., Int. Ed.*, 2021, **60**, 6270–6293; (b) J. P. Barham and B. König, *Angew. Chem., Int. Ed.*, 2020, **59**, 11732–11747; (c) G. E. M. Crisenza, D. Mazzarella and P. Melchiorre, *J. Am. Chem. Soc.*, 2020, **142**, 5461–5476; (d) F. Glaser and O. S. Wenger, *Coord. Chem. Rev.*, 2020, **405**, 213129; (e) R. J. Proctor and R. J. Phipps, *Angew. Chem., Int. Ed.*, 2019, **58**, 13666–13699; (f) J. Xie, H. Jin and A. S. K. Hashmi, *Chem. Soc. Rev.*, 2017, **46**, 5193–5203; (g) D. P. Hari and B. König, *Chem. Commun.*, 2014, **50**, 6688–6699; (h) A. Péter, S. Agasti, O. Knowles, E. Pye and D. J. Procter, *Chem. Soc. Rev.*, 2021, **50**, 5349–5365; (i) X.-Y. Yu, J.-R. Chen and W.-J. Xiao, *Chem. Rev.*, 2021, **121**, 506–561; (j) N. L. Reed and T. P. Yoon, *Chem. Soc. Rev.*, 2021, **50**, 2954–2967; (k) X.-Y. Yu, Q.-Q. Zhao, J. Chen, W.-J. Xiao and J.-R. Chen, *Acc. Chem. Res.*, 2020, **53**, 1066–1083.

10 J. C. Del Valle and J. Catalán, *Phys. Chem. Chem. Phys.*, 2019, **21**, 10061–10069.

11 A. P. Demchenko, V. I. Tomin and P. T. Chou, *Chem. Rev.*, 2017, **117**, 13353–13381.

12 M. Kasha, *Discuss. Faraday Soc.*, 1950, **9**, 14–19.

13 T. J. Penfold, E. Gindensperger, C. Daniel and C. M. Marian, *Chem. Rev.*, 2018, **118**, 6975–7025.

14 M. A. El-Sayed, *J. Chem. Phys.*, 1963, **38**, 2834–2838.

15 B. Heinz, B. Schmidt, C. Root, H. Satzger, F. Milota, B. Fierz, T. Kiefhaber, W. Zinth and P. Gilch, *Phys. Chem. Chem. Phys.*, 2006, **8**, 3432–3439.

16 M. Baba, *J. Phys. Chem. A*, 2011, **115**, 9514–9519.

17 S. Yamauchi and D. W. Pratt, *Mol. Phys.*, 1979, **37**, 541–569.

18 N. Hirota, M. Baba, Y. Hirata and S. Nagaoka, *J. Phys. Chem.*, 1979, **83**, 3350–3354.

19 T. Itoh, *Chem. Phys. Lett.*, 1988, **151**, 166.

20 M. A. Theodoropoulou, N. F. Nikitas and C. G. Kokotos, *Beilstein J. Org. Chem.*, 2020, **16**, 833–857.

21 Z. S. Romanova, K. Deshayes and P. Piotrowiak, *J. Am. Chem. Soc.*, 2001, **123**, 2444–2445.

22 L. M. Hancock, E. Marchi, P. Ceroni and P. D. Beer, *Chem. – Eur. J.*, 2012, **18**, 11277–11283.

23 A. Seret, E. Gandin and A. Van De Vorst, *Chem. Phys. Lett.*, 1987, **135**, 427–431.

24 I. R. Gould and S. Farid, *Acc. Chem. Res.*, 1996, **29**, 522–528.

This journal is © The Royal Society of Chemistry 2021

Chem. Soc. Rev., 2021, **50**, 9540–9685 | **9679**

25 L. Capaldo, L. L. Quadri and D. Ravelli, *Green Chem.*, 2020, **22**, 3376–3396.

26 N. Zhang, S. R. Samanta, B. M. Rosen and V. Percec, *Chem. Rev.*, 2014, **114**, 5848–5958.

27 A. Pross, *Acc. Chem. Res.*, 1985, **18**, 212–219.

28 S. V. Rosokha and J. K. Kochi, *Acc. Chem. Res.*, 2008, **41**, 641–653.

29 *IUPAC, Compendium of Chemical Terminology*, 2nd edn (the "Gold Book"), Compiled by A. D. McNaught and A. Wilkinson, Blackwell Scientific Publications, Oxford (1997), Online version (2019-) created by S. J. Chalk, ISBN 0-9678550-9-8, DOI: 10.1351/goldbook.

30 H. G. Roth, N. A. Romero and D. Nicewicz, *Synlett*, 2016, 714–723.

31 J. Twilton, C. Le, P. Zhang, M. H. Shaw, R. W. Evans and D. W. C. MacMillan, *Nat. Rev. Chem.*, 2017, **1**, 0052.

32 A. R. White, L. Wang and D. A. Nicewicz, *Synlett*, 2019, 827–832.

33 (*a*) E. Speckmeier, T. G. Fischer and K. Zeitler, *J. Am. Chem. Soc.*, 2018, **140**, 15353–15365; (*b*) J. D. Nguyen, B. S. Matsuura and C. R. J. Stephenson, *J. Am. Chem. Soc.*, 2014, **136**, 1218–1221; (*c*) K. Chen, J. Schwarz, T. A. Karl, A. Chatterjee and B. König, *Chem. Commun.*, 2019, **55**, 13144–13147; (*d*) H. Cheng, T.-L. Lam, Y. Liu, Z. Tang and C.-M. Che, *Angew. Chem., Int. Ed.*, 2021, **60**, 1383–1389; (*e*) A. A. Isse and A. Gennaro, *Collect. Czech. Chem. Commun.*, 2003, **68**, 1379–1394; (*f*) M. Nakajima, E. Fava, S. Loescher, Z. Jiang and M. Rueping, *Angew. Chem., Int. Ed.*, 2015, **54**, 8828–8832.

34 L. Capaldo and D. Ravelli, *Eur. J. Org. Chem.*, 2017, 2056–2071.

35 J. B. McManus, N. P. R. Onuska and D. A. Nicewicz, *J. Am. Chem. Soc.*, 2018, **140**, 9056–9060.

36 I. B. Perry, T. F. Brewer, P. J. Sarver, D. M. Schultz, D. A. DiRocco and D. W. C. MacMillan, *Nature*, 2018, **560**, 70–75.

37 R. A. Aycock, C. J. Pratt and N. T. Jui, *ACS Catal.*, 2018, **8**, 9115–9119.

38 J. P. Barham, M. P. John and J. A. Murphy, *J. Am. Chem. Soc.*, 2016, **138**, 15482–15487.

39 D. D. M. Wayner, K. B. Clark, A. Rauk, D. Yu and D. A. Armstrong, *J. Am. Chem. Soc.*, 1997, **119**, 8925–8932.

40 S. J. Blanksby and G. B. Ellison, *Acc. Chem. Res.*, 2003, **36**, 255–263.

41 J. Berkowitz, G. B. Ellison and D. Gutman, *J. Phys. Chem.*, 1994, **98**, 2744–2765.

42 F. G. Bordwell, S. Zhang, X.-M. Zhang and W.-Z. Liu, *J. Am. Chem. Soc.*, 1995, **117**, 7092–7096.

43 W.-Z. Liu and F. G. Bordwell, *J. Org. Chem.*, 1996, **61**, 4778–4783.

44 J. M. Mayer, *Acc. Chem. Res.*, 2011, **44**, 36–46.

45 B. P. Roberts, *Chem. Soc. Rev.*, 1999, **28**, 25–35.

46 D. Hager and D. W. C. Macmillan, *J. Am. Chem. Soc.*, 2014, **136**, 16986–16989.

47 R. W. Alder, R. J. Arrowsmith, A. Casson, R. B. Sessions, E. Heilbronner, B. Kovač, H. Huber and M. Taagepera, *J. Am. Chem. Soc.*, 1981, **103**, 6137–6142.

48 (*a*) M. H. Shaw, V. W. Shurtleff, J. A. Terrett, J. D. Cuthbertson and D. W. C. MacMillan, *Science*, 2016, **352**,

1304–1308; (*b*) T. Toshili and N. Atsushi, *Chem. Lett.*, 2009, **38**, 160–161.

49 B. J. Shields and A. G. Doyle, *J. Am. Chem. Soc.*, 2016, **138**, 12719–12722.

50 S. Charaya, PhD thesis, New Jersey Institute of Technology, 2011.

51 C. Chatgilialoglu, D. Crich, M. Komatsu and I. Ryu, *Chem. Rev.*, 1999, **99**, 1991–2070.

52 K. Qvortrup, D. A. Rankic and D. W. C. MacMillan, *J. Am. Chem. Soc.*, 2014, **136**, 626–629.

53 (*a*) J. D. Cuthbertson and D. W. C. MacMillan, *Nature*, 2015, **519**, 74–77; (*b*) C. Zhou, T. Lei, X.-Z. Wei, C. Ye, Z. Liu, B. Chen, C.-H. Tung and L.-Z. Wu, *J. Am. Chem. Soc.*, 2020, **142**, 16805–16813.

54 E. C. Gentry and R. R. Knowles, *Acc. Chem. Res.*, 2016, **49**, 1546–1556.

55 H.-B. Yang, A. Feceu and D. B. C. Martin, *ACS Catal.*, 2019, **9**, 5708–5715.

56 J. J. Warren, T. A. Tronic and J. M. Mayer, *Chem. Rev.*, 2010, **110**, 6961–7001.

57 M. H. V. Huynh and T. J. Meyer, *Chem. Rev.*, 2007, **107**, 5004–5064.

58 H. G. Yayla, H. Wang, K. T. Tarantino, H. S. Orbe and R. R. Knowles, *J. Am. Chem. Soc.*, 2016, **138**, 10794–10797.

59 P. A. Tanner, L. Zhou, C. Duan and K.-L. Wong, *Chem. Soc. Rev.*, 2018, **47**, 5234–5265.

60 F. Strieth-Kalthoff, M. J. James, M. Teders, L. Pitzer and F. Glorius, *Chem. Soc. Rev.*, 2018, **47**, 7190–7202.

61 Z. Q. You, C. P. Hsu and G. R. Fleming, *J. Chem. Phys.*, 2006, **124**, 044506.

62 A. C. Benniston, A. Harriman, P. Li, J. P. Rostron, H. J. Van Ramesdonk, M. M. Groeneveld, H. Zhang and J. W. Verhoeven, *J. Am. Chem. Soc.*, 2005, **127**, 16054–16064.

63 E. Kumarasamy, S. K. Kandappa, R. Raghunathan, S. Jockusch and J. Sivaguru, *Angew. Chem., Int. Ed.*, 2017, **56**, 7056–7061.

64 L. M. Kammer, B. Lipp and T. Opatz, *J. Org. Chem.*, 2019, **84**, 2379–2392.

65 O. Gutierrez, J. C. Tellis, D. N. Primer, G. A. Molander and M. C. Kozlowski, *J. Am. Chem. Soc.*, 2015, **137**, 4896–4899.

66 N. A. Till, L. Tian, Z. Dong, G. D. Scholes and D. W. C. MacMillan, *J. Am. Chem. Soc.*, 2020, **142**, 15830–15841.

67 M. H. Shaw, J. Twilton and D. W. C. MacMillan, *J. Org. Chem.*, 2016, **81**, 6898–6926.

68 G. E. M. Crisenza and P. Melchiorre, *Nat. Commun.*, 2020, **11**, 803, DOI: 10.1038/s41467-019-13887-8.

69 P. J. Sarver, V. Bacauanu, D. M. Schultz, D. A. DiRocco, Y. Lam, E. C. Sherer and D. W. C. MacMillan, *Nat. Chem.*, 2020, **12**, 459–467.

70 D. Ravelli, M. Fagnoni, T. Fukuyama, T. Nishikawa and I. Ryu, *ACS Catal.*, 2018, **8**, 701–713.

71 D. Ravelli, S. Protti and M. Fagnoni, *Acc. Chem. Res.*, 2016, **49**, 2232–2242.

72 V. De Waele, O. Poizat, M. Fagnoni, A. Bagno and D. Ravelli, *ACS Catal.*, 2016, **6**, 7174–7182.

73 T. Basile, L. Capaldo, D. Ravelli and P. Quadrelli, *Eur. J. Org. Chem.*, 2020, 1443–1447.

9680 | *Chem. Soc. Rev.*, 2021, **50**, 9540–9685

This journal is © The Royal Society of Chemistry 2021

74 J. R. Clark, K. Feng, A. Sookezian and M. C. White, *Nat. Chem.*, 2018, **10**, 583–591.

75 J. Luo and J. Zhang, *ACS Catal.*, 2016, **6**, 873–877.

76 S. Fukuzumi, H. Kotani, K. Ohkubo, S. Ogo, N. V. Tkachenko and H. Lemmetyinen, *J. Am. Chem. Soc.*, 2004, **126**, 1600–1601.

77 A. Joshi-Pangu, F. Lévesque, H. G. Roth, S. F. Oliver, L. C. Campeau, D. Nicewicz and D. A. DiRocco, *J. Org. Chem.*, 2016, **81**, 7244–7249.

78 S. S. Shah, A. Paul, M. Bera, Y. Venkatesh and N. D. P. Singh, *Org. Lett.*, 2018, **20**, 5533–5536.

79 A. B. Rolka and B. König, *Org. Lett.*, 2020, **22**, 5035–5040.

80 D. Jespersen, B. Keen, J. I. Day, A. Singh, J. Briles, D. Mullins and J. D. Weaver III, *Org. Process Res. Dev.*, 2019, **23**, 1087–1095.

81 S. Blanc, T. Pigot, C. Cugnet, R. Brown and S. Lacombe, *Phys. Chem. Chem. Phys.*, 2010, **12**, 11280–11290.

82 F. A. Bell, A. Ledwith and D. C. Sherrington, *J. Chem. Soc. C*, 1969, 2719–2720.

83 N. G. Connelly and W. E. Geiger, *Chem. Rev.*, 1996, **96**, 877–910.

84 M. R. Talipov, M. M. Hossain, A. Boddeda, K. Thakur and R. Rathore, *Org. Biomol. Chem.*, 2016, **14**, 2961–2968.

85 M. Schorpp, T. Heizmann, M. Schmucker, S. Rein, S. Weber and I. Krossing, *Angew. Chem., Int. Ed.*, 2020, **59**, 9453–9459.

86 S.-i. Kato, T. Matsuoka, S. Suzuki, M. S. Asano, T. Yoshihara, S. Tobita, T. Matsumoto and C. Kitamura, *Org. Lett.*, 2020, **22**, 734–738.

87 T. A. Schaub, T. Mekelburg, P. O. Dral, M. Miehlich, F. Hampel, K. Meyer and M. Kivala, *Chem. – Eur. J.*, 2020, **26**, 3264–3269.

88 (*a*) H. Jakob, S. Leininger, T. Lehmann, S. Jacobi and S. Gutewort, *Ullmann's Encyclopedia of Industrial Chemistry*, Wiley-VCH Verlag GmbH & Co. KGaA, Weinheim, Germany, 2007, pp. 503–519; (*b*) S. Härtinger, J. Rosenmund, E. Savinova, S. Wasle and K. Doblhofer, *J. Phys. Chem. B*, 1997, **101**, 2411–2414.

89 E. J. Behrman, *Beilstein J. Org. Chem.*, 2006, **2**, 22.

90 M. T. Westwood, C. J. C. Lamb, D. R. Sutherland and A. L. Lee, *Org. Lett.*, 2019, **21**, 7119–7123.

91 C. Dai, F. Meschini, J. M. R. Narayanam and C. R. J. Stephenson, *J. Org. Chem.*, 2012, **77**, 4425–4431.

92 D. R. Sutherland, M. Veguillas, C. L. Oates and A.-L. Lee, *Org. Lett.*, 2018, **20**, 6863–6867.

93 V. Piano, B. A. Palfey and A. Mattevi, *Trends Biochem. Sci.*, 2017, **42**, 457–469.

94 J. B. Metternich, R. J. Mudd and R. Gilmour, in *Photocatalysis in Organic Synthesis*, ed. B. Koenig, Georg Thieme Verlag, Stuttgart, 2019, vol. 6, pp. 391–404.

95 (*a*) S. Bloom, C. Liu, D. K. Kölmel, J. X. Qiao, Y. Zhang, M. A. Poss, W. R. Ewing and D. W. C. MacMillan, *Nat. Chem.*, 2018, **10**, 205–211; (*b*) D. M. Schultz, J. W. Sawicki and T. P. Yoon, *Beilstein J. Org. Chem.*, 2015, **11**, 61–65.

96 A. H. Tolba, F. Vávra, J. Chudoba and R. Cibulka, *Eur. J. Org. Chem.*, 2020, 1579–1585.

97 S. L. J. Tan and R. D. Webster, *J. Am. Chem. Soc.*, 2012, **134**, 5954–5964.

98 R. Martinez-Haya, M. A. Miranda and M. L. Marin, *Eur. J. Org. Chem.*, 2017, 2164–2169.

99 B. Giese, J. A. González-Gómez and T. Witzel, *Angew. Chem., Int. Ed. Engl.*, 1984, **23**, 69–70.

100 D. B. Gerth and B. Giese, *J. Org. Chem.*, 1986, **51**, 3726–3729.

101 N. Miyamoto, D. Fukuoka, K. Utimoto and H. Nozaki, *Bull. Chem. Soc. Jpn.*, 1974, **47**, 503–504.

102 J. Xiang, W. Jiang, J. Gong and P. L. Fuchs, *J. Am. Chem. Soc.*, 1997, **119**, 4123–4129.

103 F. Le Vaillant, T. Courant and J. Waser, *Angew. Chem., Int. Ed.*, 2015, **54**, 11200–11204.

104 X. Zhang, R. T. Smith, C. Le, S. J. McCarver, B. T. Shireman, N. I. Carruthers and D. W. C. MacMillan, *Nature*, 2020, **580**, 220–226.

105 E. Tsui, H. Wang and R. R. Knowles, *Chem. Sci.*, 2020, **11**, 11124–11141.

106 M. J. Cabrera-Afonso, Z.-P. Lu, C. B. Kelly, S. B. Lang, R. Dykstra, O. Gutierrez and G. A. Molander, *Chem. Sci.*, 2018, **9**, 3186–3191.

107 M. L. Agazzi, V. A. S. Almodovar, N. S. Gsponer, S. Bertolotti, A. C. Tomé and E. N. Durantini, *Org. Biomol. Chem.*, 2020, **18**, 1449–1461.

108 J. Fischer, P. Nun and V. Coeffard, *Synthesis*, 2020, 1617–1624.

109 Y. Jiang, C. Wang, C. R. Rogers, M. S. Kodaimati and E. A. Weiss, *Nat. Chem.*, 2019, **11**, 1034–1040.

110 E. M. Sherbrook, H. Jung, D. Cho, M. H. Baik and T. P. Yoon, *Chem. Sci.*, 2020, **11**, 856–861.

111 Z. Zhang, C. R. Rogers and E. A. Weiss, *J. Am. Chem. Soc.*, 2020, **142**, 495–501.

112 A. Hossain, S. K. Pagire and O. Reiser, *Synlett*, 2017, 1707–1714.

113 (*a*) A. G. Condie, J. C. González-Gómez and C. R. J. Stephenson, *J. Am. Chem. Soc.*, 2010, **132**, 1464–1465; (*b*) Q. Yang, L. Zhang, C. Ye, S. Lou, L.-Z. Wu and C.-H. Tung, *Angew. Chem., Int. Ed.*, 2017, **56**, 3694–3698.

114 D. B. Freeman, L. Furst, A. G. Condie and C. R. J. Stephenson, *Org. Lett.*, 2012, **14**, 94–97.

115 G. Bergonzini, C. S. Schindler, C. J. Wallentin, E. N. Jacobsen and C. R. J. Stephenson, *Chem. Sci.*, 2014, **5**, 112–116.

116 L. Ruiz Espelt, I. S. McPherson, E. M. Wiensch and T. P. Yoon, *J. Am. Chem. Soc.*, 2015, **137**, 2452–2455.

117 J. Yoshida, T. Maekawa, T. Murata, S. Matsunaga and S. Isoe, *J. Am. Chem. Soc.*, 1990, **112**, 1962–1970.

118 Z.-J. Wang, S. Zheng, J. K. Matsui, Z. Lu and G. A. Molander, *Chem. Sci.*, 2019, **10**, 4389–4393.

119 M. Jouffroy, D. N. Primer and G. A. Molander, *J. Am. Chem. Soc.*, 2016, **138**, 475–478.

120 B. A. Vara, X. Li, S. Berritt, C. R. Walters, E. J. Petersson and G. A. Molander, *Chem. Sci.*, 2018, **9**, 336–344.

121 A. G. Amador, E. M. Sherbrook and T. P. Yoon, *J. Am. Chem. Soc.*, 2016, **138**, 4722–4725.

122 J. M. Tanko and R. E. Drumright, *J. Am. Chem. Soc.*, 1992, **114**, 1844–1854.

123 J. W. Tucker, J. M. R. Narayanam, S. W. Krabbe and C. R. J. Stephenson, *Org. Lett.*, 2010, **12**, 368–371.

124 L. Furst, B. S. Matsuura, J. M. R. Narayanam, J. W. Tucker and C. R. J. Stephenson, *Org. Lett.*, 2010, **12**, 3104–3107.

This journal is © The Royal Society of Chemistry 2021

Chem. Soc. Rev., 2021, **50**, 9540–9685 | **9681**

125 E. R. Welin, A. A. Warkentin, J. C. Conrad and D. W. C. MacMillan, *Angew. Chem., Int. Ed.*, 2015, **54**, 9668–9672.

126 X. Huang, R. D. Webster, K. Harms and E. Meggers, *J. Am. Chem. Soc.*, 2016, **138**, 12636–12642.

127 (*a*) A. Ruffoni, F. Juliá, T. D. Svejstrup, A. J. McMillan, J. J. Douglas and D. Leonori, *Nat. Chem.*, 2019, **11**, 426–433; (*b*) T. Xiong and Q. Zhang, *Chem. Soc. Rev.*, 2016, **45**, 3069–3087; (*c*) J.-R. Chen, X.-Q. Hu, L.-Q. Lu and W.-J. Xiao, *Chem. Soc. Rev.*, 2016, **45**, 2044–2056.

128 T. W. Greulich, C. G. Daniliuc and A. Studer, *Org. Lett.*, 2015, **17**, 254–257.

129 S. L. Rössler, B. J. Jelier, P. F. Tripet, A. Shemet, G. Jeschke, A. Togni and E. M. Carreira, *Angew. Chem., Int. Ed.*, 2019, **58**, 526–531.

130 W. S. Ham, J. Hillenbrand, J. Jacq, C. Genicot and T. Ritter, *Angew. Chem., Int. Ed.*, 2019, **58**, 532–536.

131 H. Jung, H. Keum, J. Kweon and S. Chang, *J. Am. Chem. Soc.*, 2020, **142**, 5811–5818.

132 L. Chu, C. Ohta, Z. Zuo and D. W. C. MacMillan, *J. Am. Chem. Soc.*, 2014, **136**, 10886–10889.

133 S. J. McCarver, J. X. Qiao, J. Carpenter, R. M. Borzilleri, M. A. Poss, M. D. Eastgate, M. M. Miller and D. W. C. MacMillan, *Angew. Chem., Int. Ed.*, 2017, **56**, 728–732.

134 Z. Zuo, D. T. Ahneman, L. Chu, J. A. Terrett, A. G. Doyle and D. W. C. MacMillan, *Science*, 2014, **345**, 437–440.

135 A. Noble, S. J. McCarver and D. W. C. Macmillan, *J. Am. Chem. Soc.*, 2015, **137**, 624–627.

136 N. A. Till, R. T. Smith and D. W. C. MacMillan, *J. Am. Chem. Soc.*, 2018, **140**, 5701–5705.

137 Z. Zuo, H. Cong, W. Li, J. Choi, G. C. Fu and D. W. C. MacMillan, *J. Am. Chem. Soc.*, 2016, **138**, 1832–1835.

138 C. P. Johnston, R. T. Smith, S. Allmendinger and D. W. C. MacMillan, *Nature*, 2016, **536**, 322–325.

139 L. Chu, J. M. Lipshultz and D. W. C. Macmillan, *Angew. Chem., Int. Ed.*, 2015, **54**, 7929–7933.

140 C. C. Le and D. W. C. MacMillan, *J. Am. Chem. Soc.*, 2015, **137**, 11938–11941.

141 C. C. Nawrat, C. R. Jamison, Y. Slutskyy, D. W. C. MacMillan and L. E. Overman, *J. Am. Chem. Soc.*, 2015, **137**, 11270–11273.

142 X. Zhang and D. W. C. MacMillan, *J. Am. Chem. Soc.*, 2016, **138**, 13862–13865.

143 J. H. Kim, A. Ruffoni, Y. S. S. Al-Faiyz, N. S. Sheikh and D. Leonori, *Angew. Chem., Int. Ed.*, 2020, **59**, 8225–8231.

144 (*a*) Y. Miyake, Y. Ashida, K. Nakajima and Y. Nishibayashi, *Chem. Commun.*, 2012, **48**, 6966–6968; (*b*) B. E. Cooper and W. J. Owen, *J. Organomet. Chem.*, 1971, **29**, 33–40; (*c*) S. Farid, J. P. Dinnocenzo, P. B. Merkel, R. H. Young, D. Shukla and G. Guirado, *J. Am. Chem. Soc.*, 2011, **133**, 11580–11587.

145 A. Casado-Sánchez, P. Domingo-Legarda, S. Cabrera and J. Alemán, *Chem. Commun.*, 2019, **55**, 11303–11306.

146 M. El Khatib, R. A. M. Serafim and G. A. Molander, *Angew. Chem., Int. Ed.*, 2016, **55**, 254–258.

147 D. N. Primer and G. A. Molander, *J. Am. Chem. Soc.*, 2017, **139**, 9847–9850.

148 (*a*) J. K. Matsui, Á. Gutiérrez-Bonet, M. Rotella, R. Alam, O. Gutierrez and G. A. Molander, *Angew. Chem., Int. Ed.*, 2018, **57**, 15847–15851; (*b*) Y. Nishigaichi, T. Orimi and A. Takuwa, *J. Organomet. Chem.*, 2009, **694**, 3837–3839.

149 M. W. Campbell, J. S. Compton, C. B. Kelly and G. A. Molander, *J. Am. Chem. Soc.*, 2019, **141**, 20069–20078.

150 P. Zhang, C. C. Le and D. W. C. MacMillan, *J. Am. Chem. Soc.*, 2016, **138**, 8084–8087.

151 V. Bacauanu, S. Cardinal, M. Yamauchi, M. Kondo, D. F. Fernández, R. Remy and D. W. C. MacMillan, *Angew. Chem., Int. Ed.*, 2018, **57**, 12543–12548.

152 T. Q. Chen and D. W. C. MacMillan, *Angew. Chem., Int. Ed.*, 2019, **58**, 14584–14588.

153 R. T. Smith, X. Zhang, J. A. Rincón, J. Agejas, C. Mateos, M. Barberis, S. García-Cerrada, O. de Frutos and D. W. C. MacMillan, *J. Am. Chem. Soc.*, 2018, **140**, 17433–17438.

154 C. Le, T. Q. Chen, T. Liang, P. Zhang and D. W. C. MacMillan, *Science*, 2018, **360**, 1010–1014.

155 (*a*) H. Tian, Q. Xia, Q. Wang, J. Dong, Y. Liu and Q. Wang, *Org. Lett.*, 2019, **21**, 4585–4589; (*b*) J. Xie, J. Yu, M. Rudolph, F. Rominger and A. S. K. Hashmi, *Angew. Chem., Int. Ed.*, 2016, **55**, 9416–9421.

156 C. Le, Y. Liang, R. W. Evans, X. Li and D. W. C. MacMillan, *Nature*, 2017, **547**, 79–83.

157 M. N. Hopkinson, A. Gómez-Suárez, M. Teders, B. Sahoo and F. Glorius, *Angew. Chem., Int. Ed.*, 2016, **55**, 4361–4366.

158 J. Chateauneuf, J. Lusztyk and K. U. Ingold, *J. Am. Chem. Soc.*, 1988, **110**, 2886–2893.

159 S. Mukherjee, B. Maji, A. Tlahuext-Aca and F. Glorius, *J. Am. Chem. Soc.*, 2016, **138**, 16200–16203.

160 J. C. Day, N. Govindaraj, D. S. McBain, P. S. Skell and J. M. Tanko, *J. Org. Chem.*, 1986, **51**, 4959–4963.

161 S. Rohe, A. O. Morris, T. McCallum and L. Barriault, *Angew. Chem., Int. Ed.*, 2018, **57**, 15664–15669.

162 L. Leng, Y. Fu, P. Liu and J. M. Ready, *J. Am. Chem. Soc.*, 2020, **142**, 11972–11977.

163 Y. Zhao and D. G. Truhlar, *Theor. Chem. Acc.*, 2008, **120**, 215–241.

164 M. A. Ashley, C. Yamauchi, J. C. K. Chu, S. Otsuka, H. Yorimitsu and T. Rovis, *Angew. Chem., Int. Ed.*, 2019, **58**, 4002–4006.

165 R. D. Trepka, J. W. Belisle and J. K. Harrington, *J. Org. Chem.*, 1974, **39**, 1094–1098.

166 V. K. Aggarwal, I. Emme and S. Y. Fulford, *J. Org. Chem.*, 2003, **68**, 692–700.

167 J. Ye, I. Kalvet, F. Schoenebeck and T. Rovis, *Nat. Chem.*, 2018, **10**, 1037–1041.

168 G. J. Choi, Q. Zhu, D. C. Miller, C. J. Gu and R. R. Knowles, *Nature*, 2016, **539**, 268–271.

169 A. Noble and D. W. C. MacMillan, *J. Am. Chem. Soc.*, 2014, **136**, 11602–11605.

170 C. K. Prier and D. W. C. MacMillan, *Chem. Sci.*, 2014, **5**, 4173–4178.

171 J. J. Douglas, K. P. Cole and C. R. J. Stephenson, *J. Org. Chem.*, 2014, **79**, 11631–11643.

172 S. J. Hwang, D. C. Powers, A. G. Maher, B. L. Anderson, R. G. Hadt, S.-L. Zheng, Y.-S. Chen and D. G. Nocera, *J. Am. Chem. Soc.*, 2015, **137**, 6472–6475.

9682 | *Chem. Soc. Rev.*, 2021, **50**, 9540–9685

This journal is © The Royal Society of Chemistry 2021

173 X. Zhang and D. W. C. MacMillan, *J. Am. Chem. Soc.*, 2017, **139**, 11353–11356.

174 S. Mukherjee, R. A. Garza-Sanchez, A. Tlahuext-Aca and F. Glorius, *Angew. Chem., Int. Ed.*, 2017, **56**, 14723–14726.

175 J. Twilton, M. Christensen, D. A. DiRocco, R. T. Ruck, I. W. Davies and D. W. C. MacMillan, *Angew. Chem., Int. Ed.*, 2018, **57**, 5369–5373.

176 V. Dimakos, H. Y. Su, G. E. Garrett and M. S. Taylor, *J. Am. Chem. Soc.*, 2019, **141**, 5149–5153.

177 H. Jiang and A. Studer, *Angew. Chem., Int. Ed.*, 2018, **57**, 1692–1696.

178 H. Jiang and A. Studer, *Angew. Chem., Int. Ed.*, 2017, **56**, 12273–12276.

179 S. Zheng, Á. Gutiérrez-Bonet and G. A. Molander, *Chem*, 2019, **5**, 339–352.

180 G. J. Choi and R. R. Knowles, *J. Am. Chem. Soc.*, 2015, **137**, 9226–9229.

181 H. Wang, Y. Gao, C. Zhou and G. Li, *J. Am. Chem. Soc.*, 2020, **142**, 8122–8129.

182 A. R. Gregory, K. G. Kidd and G. W. Burton, *THEOCHEM*, 1983, **104**, 9–22.

183 L. Pause, M. Robert and J.-M. Savéant, *J. Am. Chem. Soc.*, 1999, **121**, 7158–7159.

184 (*a*) R. S. J. Proctor, A. C. Colgan and R. J. Phipps, *Nat. Chem.*, 2020, **12**, 990–1004; (*b*) L. Candish, M. Teders and F. Glorius, *J. Am. Chem. Soc.*, 2017, **139**, 7440–7443.

185 R. S. J. Proctor, H. J. Davis and R. J. Phipps, *Science*, 2018, **360**, 419–422.

186 K. Ermanis, A. C. Colgan, R. S. J. Proctor, B. W. Hadrys, R. J. Phipps and J. M. Goodman, *J. Am. Chem. Soc.*, 2020, **142**, 21091–21101.

187 Z. Zuo and D. W. C. Macmillan, *J. Am. Chem. Soc.*, 2014, **136**, 5257–5260.

188 (*a*) A. McNally, C. K. Prier and D. W. C. MacMillan, *Science*, 2011, **334**, 1114–1117; (*b*) L. Wei, M. Yuan, Y. Yingwu and Z. Yufen, *Bull. Chem. Soc. Jpn.*, 2006, **79**, 577–579.

189 J. Jin and D. W. C. MacMillan, *Angew. Chem., Int. Ed.*, 2015, **54**, 1565–1569.

190 E. A. Mayeda, L. L. Miller and J. F. Wolf, *J. Am. Chem. Soc.*, 1972, **94**, 6812–6816.

191 C. Bosset, H. Beucher, G. Bretel, E. Pasquier, L. Queguiner, C. Henry, A. Vos, J. P. Edwards, L. Meerpoel and D. Berthelot, *Org. Lett.*, 2018, **20**, 6003–6006.

192 J. Jin and D. W. C. MacMillan, *Nature*, 2015, **525**, 87–90.

193 S. Escoubet, S. Gastaldi, N. Vanthuyne, G. Gil, D. Siri and M. P. Bertrand, *J. Org. Chem.*, 2006, **71**, 7288–7292.

194 P. Wessig and O. Muehling, *Eur. J. Org. Chem.*, 2007, 2219–2232.

195 T. Patra, S. Mukherjee, J. Ma, F. Strieth-Kalthoff and F. Glorius, *Angew. Chem., Int. Ed.*, 2019, **58**, 10514–10520.

196 M. R. Becker, A. D. Richardson and C. S. Schindler, *Nat. Commun.*, 2019, **10**, 5095, DOI: 10.1038/s41467-019-13072-x.

197 M. Yoshida, H. Sakuragi, T. Nishimura, S. Ishikawa and K. Tokumaru, *Chem. Lett.*, 1975, 1125–1130.

198 T. Ni, R. A. Caldwell and L. A. Melton, *J. Am. Chem. Soc.*, 1989, **111**, 457–464.

199 A. Padwa, W. Bergmark and D. Pashayan, *J. Am. Chem. Soc.*, 1969, **91**, 2653–2660.

200 D. P. Hari and B. König, *Chem. Commun.*, 2014, **50**, 6688–6699.

201 Our review has considered visible light activations of the acridinium skeleton to provide a strong oxidant. Intermediate **798** can be activated to give a powerful reductant on irradiation at 360 nm. I. A. MacKenzie, L. Wang, N. P. R. Onuska, O. F. Williams, K. Begam, A. M. Moran, B. D. Dunietz and D. A. Nicewicz, *Nature*, 2020, **580**, 76–80.

202 D. P. Hari, P. Schroll and B. Koenig, *J. Am. Chem. Soc.*, 2012, **134**, 2958–2961.

203 T. Xiao, X. Dong, Y. Tang and L. Zhou, *Adv. Synth. Catal.*, 2012, **354**, 3195–3199.

204 D. P. Hari, T. Hering and B. König, *Org. Lett.*, 2012, **14**, 5334–5337.

205 (*a*) M. Majek and A. Jacobi von Wangelin, *Angew. Chem., Int. Ed.*, 2015, **54**, 2270–2274; (*b*) J. Liu, Y. Wei and M. Shi, *Chin. J. Chem.*, 2021, **39**, 295–300.

206 W. Guo, L.-Q. Lu, Y. Wang, Y.-N. Wang, J.-R. Chen and W.-J. Xiao, *Angew. Chem., Int. Ed.*, 2015, **54**, 2265–2269.

207 L. Gu, C. Jin and J. Liu, *Green Chem.*, 2015, **54**, 3733–3736.

208 S. A. Jadhav, D. Bakshi and A. Singh, *J. Org. Chem.*, 2015, **80**, 10187–10196.

209 A. U. Meyer, T. Slanina, C.-J. Yao and B. König, *ACS Catal.*, 2016, **6**, 369–375.

210 (*a*) M. Neumann and K. Zeitler, *Chem. – Eur. J.*, 2013, **19**, 6950–6955; (*b*) Y. Roh, H.-Y. Jang, V. Lynch, N. L. Bauld and M. J. Krische, *Org. Lett.*, 2002, **4**, 611–613; (*c*) H. O. House, L. E. Huber and M. J. Umen, *J. Am. Chem. Soc.*, 1972, **94**, 8471–8475.

211 (*a*) G. Pandey and S. Hajra, *Angew. Chem., Int. Ed. Engl.*, 1994, **33**, 1169–1171; (*b*) J. Yang, G. A. N. Felton, N. L. Bauld and M. J. Krische, *J. Am. Chem. Soc.*, 2004, **126**, 1634–1635.

212 (*a*) M. A. Ischay, M. E. Anzovino, J. Du and T. P. Yoon, *J. Am. Chem. Soc.*, 2008, **130**, 12886–12887; (*b*) J. Du, L. R. Espelt, I. A. Guzei and T. P. Yoon, *Chem. Sci.*, 2011, **2**, 2115–2119.

213 J. Davies, S. G. Booth, S. Essafi, R. A. W. Dryfe and D. Leonori, *Angew. Chem., Int. Ed.*, 2015, **54**, 14017–14021.

214 (*a*) E. Yoshioka, S. Kohtani, T. Jichu, T. Fukazawa, T. Nagai, A. Kawashima, Y. Takemoto and H. Miyabe, *J. Org. Chem.*, 2016, **81**, 7217–7229; (*b*) I. N. Rozhkov, S. M. Igumnov, G. Y. Bekker, S. I. Pletnev, G. D. Rempel and L. E. Deev, *Bull. Acad. Sci. USSR, Div. Chem. Sci.*, 1989, **38**, 2041–2043.

215 E. Yoshioka, S. Kohtani, T. Jichu, T. Fukazawa, T. Nagai, Y. Takemoto and H. Miyabe, *Synlett*, 2015, 265–270.

216 (*a*) D. P. Tiwari, S. Dabral, J. Wen, J. Wiesenthal, S. Terhorst and C. Bolm, *Org. Lett.*, 2017, **19**, 4295–4298; (*b*) X.-Q. Chu, D. Ge, M.-L. Wang, W. Rao, T.-P. Loh and Z.-L. Shen, *Adv. Synth. Catal.*, 2019, **361**, 4082–4090.

217 S. P. Pitre, C. D. McTiernan, H. Ismailoi and J. C. Scaiano, *ACS Catal.*, 2014, **4**, 2530–2535.

218 (*a*) I. Ghosh and B. König, *Angew. Chem., Int. Ed.*, 2016, **55**, 7676–7679; (*b*) S. Nishimoto, T. Izukawa and T. Kagiya, *J. Chem. Soc., Perkin Trans. 2*, 1983, 1147–1152.

219 D. R. Heitz, K. Rizwan and G. A. Molander, *J. Org. Chem.*, 2016, **81**, 7308–7313.

This journal is © The Royal Society of Chemistry 2021

Chem. Soc. Rev., 2021, **50**, 9540–9685 | **9683**

220 J. Rostoll-Berenguer, G. Blay, M. C. Muñoz, J. R. Pedro and C. Vila, *Org. Lett.*, 2019, **21**, 6011–6015.

221 Y. Kuang, K. Wang, X. Shi, X. Huang, E. Meggers and J. Wu, *Angew. Chem., Int. Ed.*, 2019, **58**, 16859–16863.

222 E. H. Discekici, N. J. Treat, S. O. Poelma, K. M. Mattson, Z. M. Hudson, Y. Luo, C. J. Hawker and J. C. Read de Alaniz, *Chem. Commun.*, 2015, **51**, 11705–11708.

223 A. F. Garrido-Castro, N. Salaverri, M. C. Maestro and J. Alemán, *Org. Lett.*, 2019, **21**, 5295–5300.

224 (*a*) A. J. Boyington, C. P. Seath, A. M. Zearfoss, Z. Xu and N. Jui, *J. Am. Chem. Soc.*, 2019, **141**, 4147–4153; (*b*) S. M. Soria-Castro, D. M. Andrada, D. A. Caminos, J. E. Argüello, M. Robert and A. B. Peñéñory, *J. Org. Chem.*, 2017, **82**, 11464–11473.

225 M. H. Aukland, M. Šiaučiulis, A. West, G. J. P. Perry and D. J. Procter, *Nat. Catal.*, 2020, **3**, 163–169.

226 A. M. Martinez-Gualda, R. Cano, L. Marzo, R. Perez-Ruiz, J. Luis-Barrera, R. Mas-Balleste, A. Fraile, V. A. de la Pena O'Shea and J. Aleman, *Nat. Commun.*, 2019, **10**, 2634, DOI: 10.1038/s41467-019-10441-4.

227 D. Liu, V. Jiao, Z.-T. Feng, X.-Z. Wang, G.-Q. Xu and P.-F. Xu, *Org. Lett.*, 2018, **20**, 5700–5704.

228 F. Speck, D. Rombach and H.-A. Wagenknecht, *Beilstein J. Org. Chem.*, 2019, **15**, 52–59.

229 S. Shibutani, T. Kodo, M. Takeda, K. Nagao, N. Tokunaga, Y. Sasaki and H. Ohmiya, *J. Am. Chem. Soc.*, 2020, **142**, 1211–1216.

230 T. C. Sherwood, N. Li, A. N. Yazdani and T. G. Murali Dhar, *J. Org. Chem.*, 2018, **83**, 3000–3012.

231 M. Garreau, F. Le Vaillant and J. Waser, *Angew. Chem., Int. Ed.*, 2019, **58**, 8182–8186.

232 K. Donabauer, M. Maity, A. L. Berger, G. S. Huff, S. Crespi and B. König, *Chem. Sci.*, 2019, **10**, 5162–5166.

233 (*a*) H. Chen, W. Fan, X.-A. Yuan and S. Yu, *Nat. Commun.*, 2019, **10**, 4743, DOI: 10.1038/s41467-019-12722-4; (*b*) H. Chen, W. Jin and S. Yu, *Org. Lett.*, 2020, **22**, 5910–5914.

234 Y. Miyake, Y. Ashida, K. Nakajima and Y. Nishibayashi, *Chem. Commun.*, 2012, **48**, 6966–6968.

235 C. Lévêque, L. Cheneberg, V. Corcé, C. Ollivier and L. Fensterbank, *Chem. Commun.*, 2016, **52**, 9877–9880.

236 N. R. Patel, C. B. Kelly, A. P. Sigenfeld and G. A. Molander, *ACS Catal.*, 2017, **7**, 1766–1770.

237 M. Uygur, T. Danelzik and O. G. Mancheño, *Chem. Commun.*, 2019, **55**, 2980–2983.

238 M. K. Jackl, L. Legnani, B. Morandi and J. W. Bode, *Org. Lett.*, 2017, **19**, 4696–4699.

239 A. Cartier, E. Levernier, V. Corcé, T. Fukuyama, A.-L. Dhimane, C. Ollivier, I. Ryu and L. Fensterbank, *Angew. Chem., Int. Ed.*, 2019, **58**, 1789–1793.

240 X. Wang, G. H. M. Davies, A. Koschitzky, S. R. Wisniewski, C. B. Kelly and G. A. Molander, *Org. Lett.*, 2019, **21**, 2880–2884.

241 A. Ryder, W. Cunningham, G. Ballantyne, T. Mules, A. G. Kinsella, J. Turner-Dore, C. M. Alder, L. J. Edwards, B. S. J. McKay, M. N. Grayson and A. J. Cresswell, *Angew. Chem., Int. Ed.*, 2020, **59**, 14986–14991.

242 M. J. Pellerite, R. L. Jackson and J. I. Brauman, *J. Phys. Chem.*, 1981, **85**, 1624–1626.

243 M. J. James, J. L. Schwarz, F. Strieth-Kalthoff, B. Wibbeling and F. Glorius, *J. Am. Chem. Soc.*, 2018, **140**, 8624–8628.

244 C. Yang, J.-D. Yang, Y.-H. Li and J.-P. Cheng, *J. Org. Chem.*, 2016, **81**, 12357–12363.

245 G. Pandey and R. Laha, *Angew. Chem., Int. Ed.*, 2015, **54**, 14875–14879.

246 G. Pandey and S. Hajra, *Angew. Chem., Int. Ed. Engl.*, 1994, **33**, 1169–1171.

247 H. Kim, H. Kim, T. H. Lambert and S. Lin, *J. Am. Chem. Soc.*, 2020, **142**, 2087–2092.

248 M. Neumeier, D. Sampedro, M. Majek, V. A. de la Pena O'Shea, A. Jacobi von Wangelin and R. Peres-Ruiz, *Chem. – Eur. J.*, 2018, **24**, 105–108.

249 N. A. Romero, K. A. Margrey, N. E. Tay and D. A. Nicewicz, *Science*, 2015, **349**, 1326–1330.

250 J. B. McManus and D. A. Nicewicz, *J. Am. Chem. Soc.*, 2017, **139**, 2880–2883.

251 N. Holmberg-Douglas, N. P. R. Onuska and D. A. Nicewicz, *Angew. Chem., Int. Ed.*, 2020, **59**, 7425–7429.

252 (*a*) W. Chen, Z. Huang, N. E. S. Tay, B. Giglio, M. Wang, H. Wang, Z. Wu, D. A. Nicewicz and Z. Li, *Science*, 2019, **364**, 1170–1174; (*b*) L. Wang, A. R. White, W. Chen, Z. Wu, D. A. Nicewicz and Z. Li, *Org. Lett.*, 2020, **22**, 7971–7975.

253 N. E. S. Tay, W. Chen, A. Levens, V. A. Pistritto, Z. Huang, Z. Wu, Z. Li and D. A. Nicewicz, *Nat. Catal.*, 2020, **3**, 734–742.

254 N. Holmberg-Douglas and D. A. Nicewicz, *Org. Lett.*, 2019, **21**, 7114–7118.

255 N. J. Venditto and D. A. Nicewicz, *Org. Lett.*, 2020, **22**, 4817–4822.

256 C. A. Lawson, A. P. Dominey, G. D. Williams and J. A. Murphy, *Chem. Commun.*, 2020, **56**, 11445–11448.

257 A. J. Perkowski, C. L. Cruz and D. A. Nicewicz, *J. Am. Chem. Soc.*, 2015, **137**, 15684–15687.

258 V. A. Pistritto, M. E. Schutzbach-Horton and D. A. Nicewicz, *J. Am. Chem. Soc.*, 2020, **142**, 17187–17194.

259 J.-M. M. Grandjean and D. A. Nicewicz, *Angew. Chem., Int. Ed.*, 2013, **52**, 3967–3971.

260 N. A. Romero and D. A. Nicewicz, *J. Am. Chem. Soc.*, 2014, **136**, 17024–17035.

261 (*a*) J.-P. Goddard, C. Ollivier and L. Fensterbank, *Acc. Chem. Res.*, 2016, **49**, 1924–1936; (*b*) L. Cheneberg, C. Lévêque, V. Corcé, A. Baralle, J. P. Goddard, C. Ollivier and L. Fensterbank, *Synlett*, 2016, 731–735.

262 (*a*) F. Lima, L. Grunenberg, H. B. A. Rahman, R. Labes, J. Sedelmeier and S. V. Ley, *Chem. Commun.*, 2018, **54**, 5606–5609; (*b*) F. Lima, U. K. Sharma, L. Grunenberg, D. Saha, S. Johannsen, J. Sedelmeier, E. V. Van der Eycken and S. V. Ley, *Angew. Chem., Int. Ed.*, 2017, **56**, 15136–15140.

263 D. R. Heitz, K. Rizwan and G. A. Molander, *J. Org. Chem.*, 2016, **81**, 7308–7313.

264 J. K. Matsui and G. A. Molander, *Org. Lett.*, 2017, **19**, 950–953.

265 J. B. McManus, N. P. R. Onuska, M. S. Jeffreys, N. C. Goodwin and D. A. Nicewicz, *Org. Lett.*, 2020, **22**, 679–683.

266 H.-P. Deng, Q. Zhou and J. Wu, *Angew. Chem., Int. Ed.*, 2018, **57**, 12661–12665.

9684 | *Chem. Soc. Rev.*, 2021, **50**, 9540–9685

This journal is © The Royal Society of Chemistry 2021

267 L. Huang and M. Rueping, *Angew. Chem., Int. Ed.*, 2018, **57**, 10333–10337.

268 I. Ghosh, T. Ghosh, J. I. Bardagi and B. Koenig, *Science*, 2014, **346**, 725–728.

269 (*a*) J. P. Cole, D.-F. Chen, M. Kudisch, R. M. Pearson, C. H. Lim and G. M. Miyake, *J. Am. Chem. Soc.*, 2020, **142**, 13573–13581; (*b*) G. A. Kenny-Wallace and C. D. Jonah, *J. Phys. Chem.*, 1982, **86**, 2572–2586.

270 D. A. Corbin, C.-H. Lim and G. M. Miyake, *Aldrichimica Acta*, 2019, **52**, 7–21.

271 Y. Du, R. M. Pearson, C.-H. Lim, S.-M. Sartor, M. D. Ryan, H. Yang, N. H. Damrauer and G. M. Miyake, *Chem. – Eur. J.*, 2017, **23**, 10962–10968.

272 (*a*) A. Chatterjee and B. Koenig, *Angew. Chem., Int. Ed.*, 2019, **58**, 14289–14294; (*b*) B. K. Peters, K. X. Rodriguez, S. H. Reisberg, S. B. Beil, D. P. Hickey, Y. Kawamata, M. Collins, J. Starr, L. Chen, S. Udyavara, K. Klunder, T. J. Gorey, S. L. Anderson, M. Neurock, S. D. Minteer and P. S. Baran, *Science*, 2019, **363**, 838–845.

273 N. G. W. Cowper, C. P. Chernowsky, O. P. Williams and Z. K. Wickens, *J. Am. Chem. Soc.*, 2020, **142**, 2093–2099.

274 H. Huang, Z. M. Strater, M. Rauch, J. Shee, T. J. Sisto, C. Nuckolls and T. H. Lambert, *Angew. Chem., Int. Ed.*, 2019, **58**, 13318–13322.

275 H. Huang, Z. M. Strater and T. H. Lambert, *J. Am. Chem. Soc.*, 2020, **142**, 1698–1703.

276 H. Huang and T. H. Lambert, *Angew. Chem., Int. Ed.*, 2020, **59**, 658–662.

277 S. Wu, J. Zurauskas, M. Domanski, P. Hitzfeld, V. Butera, D. J. Scott, J. Rehbein, A. Kumar, E. Thyrhaug, J. Hauer and J. P. Barham, *Org. Chem. Front.*, 2021, **8**, 1132–1142.

278 X. A. Liang, L. Niu, S. Wang, J. Liu and A. Lei, *Org. Lett.*, 2019, **21**, 2441–2444.

279 H. Zhao and J. Jin, *Org. Lett.*, 2019, **21**, 6179–6184.

280 B. Schweitzer-Chaput, M. A. Horwitz, E. de Pedro Beato and P. Melchiorre, *Nat. Chem.*, 2019, **11**, 129–135.

281 Z. Y. Cao, T. Ghosh and P. Melchiorre, *Nat. Commun.*, 2018, **9**, 3274, DOI: 10.1038/s41467-018-05375-2.

282 (*a*) G. Filippini, M. Silvi and P. Melchiorre, *Angew. Chem., Int. Ed.*, 2017, **56**, 4447–4451; (*b*) A. Bahamonde and P. Melchiorre, *J. Am. Chem. Soc.*, 2016, **138**, 8019–8030.

283 A. G. Capacci, J. T. Malinowski, N. J. McAlpine, J. Kuhne and D. W. C. MacMillan, *Nat. Chem.*, 2017, **9**, 1073–1077, DOI: 10.1038/NCHEM.2797.

284 B. Bieszczad, L. A. Perego and P. Melchiorre, *Angew. Chem., Int. Ed.*, 2019, **58**, 16878–16883.

285 B. Laroche, X. Tang, G. Archer, R. Di Sanza and P. Melchiorre, *Org. Lett.*, 2021, **23**, 285–289.

This journal is © The Royal Society of Chemistry 2021

Chem. Soc. Rev., 2021, **50**, 9540–9685 | **9685**